Aston University

Some pages of this thesis may have been removed for copyright restrictions.

If you have discovered material in Aston Research Explorer which is unlawful e.g. breaches copyright, (either yours or that of a third party) or any other law, including but not limited to those relating to patent, trademark, confidentiality, data protection, obscenity, defamation, libel, then please read our Takedown policy and contact the service immediately (openaccess@aston.ac.uk)

THE IMMUNOCHEMICAL CHARACTERISATION, EPITOPE ANALYSIS AND DIAGNOSTIC APPLICATIONS OF NEO-ANTIGENS FORMED BY LIPOXIDATION OF HUMAN SERUM ALBUMIN

ISABEL CARDOSO ALVES DE CAMPOS PINTO

Doctor of Philosophy

ASTON UNIVERSITY

December 2019

© Isabel Cardoso Alves de Campos Pinto, 2019
Isabel Pinto asserts her moral right to be identified as the author of this thesis.

This copy of the thesis has been supplied on condition that anyone who consults it is understood to recognise that its copyright rests with its author and that no quotation from the thesis and no information derived from it may be published without appropriate permission or acknowledgement.

Aston University

THE IMMUNOCHEMICAL CHARACTERISATION, EPITOPE ANALYSIS AND DIAGNOSTIC APPLICATIONS OF NEO-ANTIGENS FORMED BY LIPOXIDATION OF HUMAN SERUM ALBUMIN

Isabel Cardoso Alves de Campos Pinto

Doctor of Philosophy

2019

THESIS SUMMARY

Lipid oxidation has long been linked to the generation of toxic products seen to trigger many different anti-inflammatory responses. Products such as 4-hydroxynonenal (HNE) and acrolein can react with nucleophilic groups in proteins to form lipoxidation adducts, that have been detected in diseases like diabetes, cancer and cardiovascular diseases and, hence, are considered powerful biomarkers of oxidative stress *in vivo*. In this work, the reactivity of HNE towards human serum albumin (HSA), the major protein of human serum, was studied and the lipoxidised protein was used as an immunogen to derive anti-HSA-HNE antibodies (Ab) for subsequent characterisation and as a basis for development of a rapid diagnostic test. Mass spectrometry (MS) analysis confirmed the formation of HNE adducts on 15 HSA peptides, and one of the HSA-HNE immunised sheep sera was shown to contain specific antibodies to these adducts. Peptide arrays covering the HSA sequence and treated post peptide synthesis with HNE were used in a novel approach to characterise the binding patterns of the in-house anti-HNE Ab, and the results were in agreement with those obtained by MS. Nevertheless, the antibody showed cross-reactivity to HSA, which suggested some of the epitopes included not only the HNE moiety of the adducts, but also regions of HSA. Despite the cross-reactivity of this generated Ab, its potential for diagnostic applications was assessed by its deployment in a lateral flow assay together with a commercial anti-HNE Ab. The assay was able to distinguish HNE-modified proteins from non-modified ones, although further optimization is required. Finally, RNA from B lymphocytes of the HSA-HNE immunized sheep was extracted for construction of recombinant Fab and scFv phage display libraries, for the selection of monoclonal antibodies, but biopanning of anti-HSA-HNE clones was shown to be challenging due to the preponderance of anti-HSA specific clones present in the libraries.

Key words: Protein lipoxidation, albumin, diagnostics, immunoassays, immunisation, antibodies, phage-display.

The real voyage of discovery consists not in seeking new landscapes, but in seeing with new eyes.

Marcel Proust, 1913

ACKNOWLEDGEMENTS

My heartfelt thank you to each and every one who contributed to my doctoral degree. You have all inspired me very much to be a better scientist and person.

Above all, I would like to acknowledge my supervisor Professor Corinne Spickett for giving me the opportunity of handling this project. Her remarkable support and trust were crucial for me and for my work. Thank you for the guidance, constructive criticism and persistence throughout these years, and for always finding time for me.

A very special thank you to my supervisor Professor Paul Davis, not only for accepting me at Mologic and making me part of its staff, but for always believing in me and in my work. His wisdom, kindness, willingness and passion for science have always encouraged me very much to work harder and be a better scientist.

I am also extremely thankful to Dr. Matthew Tyreman, from Mologic, not only for teaching me everything I know about antibody engineering and the phage display technology, but for showing me a field that I never thought I would love so much. Thank you for guiding me and my work in this terrific journey of finding monoclonal antibodies and for always being optimistic about everything. I will always be grateful for his support, motivation and (tremendous) patience.

I would also like to acknowledge Dr. John Wilkins for all his support throughout the course of this project, Dr. James Schouten for his time spent showing me the bright side of chemistry, Steve Eida for always sharing with me his knowledge in immunoassays and Josie Mensah-Kane for helping me with the statistical analysis.

A big thank you to Dr. Maria Fedorova, from Leipzig University, for giving me the possibility of doing a secondment in her group and working with amazing people, and to Professor Andrew Pitt, from Aston University, for his time spent trying to teach me mass spectrometry and for always being available to help me with chemistry issues.

I must also thank everyone who worked with me at Mologic, Aston University, and everyone involved in the MASSTRPLAN project, in particular the 13 PhD students that joined me in this adventure.

Finally, my most important thank you goes to my friends and my family, in particular my parents, sister and wonderful nieces, for always making me feel at home, even when I was not.

LIST OF CONTENTS

LIST OF PUBLICATIONS and PRESENTATIONS

Publications:

- Campos-Pinto, I. *et al.* (2019) 'Epitope mapping and characterization of 4-hydroxy-2-nonenal modified-human serum albumin using two different polyclonal antibodies ⋆', *Free Radical Biology and Medicine*. Elsevier B.V., (March), pp. 1–11. doi: 10.1016/j.freeradbiomed.2019.05.008.

Poster presentations:

- **Isabel Campos-Pinto**, John Wilkins, James Schouten, Paul Davis, Corinne Spickett; *Immunodetection of lipoxidation: epitope mapping of HNE-modified human serum albumin using two different anti-HNE pAbs.* MASSTRPLAN Final Conference: Advances in the Study of Lipid and Protein Oxidation: From Methods to Targets (Ghent, Belgium). March 2019 (Awarded best poster presentation)

- **Isabel Campos-Pinto**, John Wilkins, James Schouten, Paul Davis, Corinne Spickett; *Immuno**detection of lipoxidation: epitope mapping of HNE-modified human serum albumin using two different anti-HNE pAbs.* SFRR–19th International Biennial Meeting (Lisbon, Portugal). June 2018.

- **Isabel Campos-Pinto**, John Wilkins, James Schouten, Paul Davis, Corinne Spickett; *Detecting lipoxidation: diagnostic tools for translation and commercial application.* International HNE Club (Graz, Austria). September 2017.

Oral presentations:

- **I. Campos Pinto**, L. Méndez, J. Schouten, J. Wilkins, M. Fedorova, A. Pitt, P. Davis, C. Spickett; *Immunodetection of lipoxidation products: Epitope mapping of 4-hydroxy-2-nonenal modified-human serum albumin using two different polyclonal antibodies.* MASSTRPLAN Final Conference: Advances in the Study of Lipid and Protein Oxidation: From Methods to Targets (Ghent, Belgium). March 2019.

LIST OF ABBREVIATIONS

A1AT	Alpha-1 antitrypsin
Ab	Antibody
Abs	Absorbance
ACN	Acetonitrile
Amp	Ampicillin
ANOVA	Analysis of variance
AP-1	Activator protein 1
AuNP	Gold nanoparticle
BCR	B cell receptor
Biot	Biotinylated
BLI	Bio-layer interferometry
CAM	Carbamidomethylation
CAP	Catabolite activator protein
CAT	Catalase
cDNA	Complementary deoxyribonucleic acid
CDR	Complementarity-determining regions
C_H	Constant domain of the antibody heavy chain
C_L	Constant domain of the antibody light chain
CID	Collision induced dissociation
COPD	Chronic obstructive pulmonary disease
DCM	Dichloromethane
DIC	1,3-Diisopropylcarbodiimide
DAMPs	Damage-associated patterns
DMA	Dimethylacetal
DMF	Dimethylformamide
DMSO	Dimethyl sulfoxide
DNA	Deoxyribonucleic acid
DNP	2,4-dinitrophenylhydrazone

DNPH	2,4-dinitrophenylhydrazine
dNTP	Deoxyribose nucleoside triphosphate
dROM	Derivatives of reactive oxygen metabolites
DTT	Dithiothreitol
ECL	Enhanced chemiluminescence
EDTA	Ethylenediaminetetraacetic acid
ELISA	Enzyme-linked immunosorbent assay
ESI	Electrospray ionisation
FA	Formic acid
FASP	Filter aided sample preparation
FDC	Follicular Dendritic Cells
Fmoc	Fluorenylmethyloxycarbonyl
FR	Framework regions
FT-ICR	Fourier transform ion cyclotron resonance
GC	Gas chromatography
GPx	Glutathione peroxidase
GSH	Glutathione
HGPRT	Hypoxanthine-guanine phosphoribosyltransferase
HHE	4-hydroxy-2-hexenal
HNA	4-hydroxy-2-nonenoic acid
HNE	4-hydroxy-2-nonenal
HNE-DEA	4-hydroxy-2-nonenal-diethylacetal
HOBt	1-Hydroxybenzotriazole
HRP	Horseradish peroxidase
HPLC	High performance liquid chromatography
HSA	Human serum albumin
Ig	Immunoglobulin
IL	Interleukin
IPTG	Isopropyl β-D-1-thiogalactopyranoside
IVD	*In vitro* diagnostic

Kan	Kanamycin
K_D	Affinity constant
Kdis	Dissociation constant
Kon	Association constant
KLH	Keyhole limpet haemocyanin
LC-MS	Liquid chromatography mass spectrometry
LDL	Low-density lipoprotein
LFA	Lateral flow assay
Lox	Lipoxygenase
LPP	Lipid peroxidation product
MA	Michael adduct
mAb	Monoclonal antibody
MALDI-TOF	Matrix-assisted laser desorption/ionization time-of-flight (mass spectrometry)
MDA	Malondialdehyde (1,3-propanedial)
MHC	Major histocompatibility complex
MPBS	Milk powder phosphate-buffered saline
mRNA	Messenger ribonucleic acid
MS	Mass spectrometry
MS/MS	Tandem mass spectrometry
MW	Molecular weight
NADH	Nicotinamide adenine dinucleotide
NADPH	Nicotinamide adenine dinucleotide phosphate
NHS	N-hydroxysuccinimide
NFkB	Nuclear factor kappa B
NMP	1-methyl 2-pyrrolidinone
NO	Nitric oxide
NOD	Nucleotide-binding oligomerisation receptors
NOX	NADPH oxidase
Nrf2	Nuclear factor erythroid 2

OD	Optical density
ONE	4-oxo-2-nonenal
OSE	Oxidative stress epitope
OVA	Ovalbumin
oxPL	Oxidised phospholipid
oxPTM	Oxidative post-translational modification
pAb	Polyclonal antibody
PAMPs	Pathogen-associated molecular patterns
PAN	Panning
PBL	Peripheral blood lymphocytes
PBS	Phosphate-buffered saline
PBST	Phosphate-buffered saline containing 1% (v/v) of Tween 20
PC	Phosphatidylcholine
PCR	Polymerase chain reaction
PE	Phosphatidylethanolamine
PEG	Polyethylene glycol
PL	Phospholipid
pNPP	p-Nitrophenylphosphate
PoC	Point-of-care
PRR	Pattern recognition receptors
PTM	Post-translation modification
PUFA	Polyunsaturated fatty acid
PVDF	Polyvinylidene fluoride
rAb	Recombinant antibody
RAGE	Receptor for advanced glycation end products
RBS	Reactive bromine species
RCS	Reactive chlorine species
ROS	Reactive oxygen species
RNA	Ribonucleic acid
RNS	Reactive nitrogen species

RT	Room temperature
SB	Schiff's base (adduct)
scFv	Single chain Fv
sdAb	Single domain antibody
SDS-PAGE	Sodium dodecyl sulfate-polyacrylamide gel electrophoresis
SHM	Somatic hypermutation
SLE	Systemic lupus erythematosus
SOD	Superoxide dismutase
SR	Scavenger receptor
TAE	Tris buffered solution containing acetic acid and EDTA
TBST	Tris buffered saline tween containing 0.1% (v/v) Tween 20
TFA	Trifluoracetic acid
TIC	Total ion chromatogram
TIPS	Triisopropylsilane
TMB	3,3',5,5'-tetramethylbenzidine
TLR	Toll-like receptor
TOF	Time-of-flight
t_R	Retention time
TNF-α	Tumour necrosis factor alpha
UPLC	Ultra-performance liquid chromatography
UV	Ultraviolet
V_H	Variable domain of the antibody heavy chain
V_L	Variable domain of the antibody light chain
V_λ	Variable domain of the antibody lambda chain
WB	Western blotting

LIST OF FIGURES

LIST OF TABLES

CHAPTER I

INTRODUCTION

1.1. Scope

The work reported in this thesis is concerned with the chemistry of oxidised lipids and the adducts they form with proteins in blood. In particular, it is focused on the capability of these adducts to behave as self-damage-associated patterns and to trigger the immune system to produce specific antibodies. These antibodies have a promising role as diagnostic reagents for the detection of lipid-protein adducts, and therefore, their deployment in point-of-care tests is of great interest. In order to set the scene for the thesis, this chapter consists of a review of these topics, which are essential areas of knowledge needed to understand the significance and relevance of the research.

1.2. Oxidative Stress, Reactive Species and Antioxidants

The term oxidative stress was first coined in 1985 as the disturbance in the balance between the production of oxidant species and antioxidant defences, in favour of the former (Sies, 1985). Since then, it has been a very controversial topic as the oxidative damage that arises from the excessive concentration of oxidant molecules seems to be linked to the onset of several pathologies (Surh & Packer, 2005). This damage can be manifested directly on the structure of biomolecules such as proteins, lipids and DNA, leading to organ and tissue damage, or indirectly by affecting gene expression and consequent disturbance of cell signalling pathways that are sensitive to changes in the cellular redox status (Birben et al., 2012; Surh & Packer, 2005). Nevertheless, oxidant species also have a beneficial role for living systems as they are also involved in the defence against infectious agents and in the regulation of a number of cellular signalling systems and pathways. For example, the Keap1/Nrf2 pathway is triggered by the presence of ROS and it is believed to play a major role in the regulation of the expression of antioxidant related genes, such as those involved in the synthesis of the antioxidants NAD(P)H quinone oxidoreductase 1, heme oxygenase 1, glutamate-cysteine ligase and glutathione S transferases (A. C. Wild, Moinova, & Mulcahy, 1999). Nrf2 is a nuclear factor that binds to the antioxidant response element (ARE) in the regulatory regions of target genes and Keap1 (Kelch ECH associating protein 1) is a repressor protein that binds to Nrf2 and promotes its degradation by the ubiquitin proteasome pathway (Kansanen, Kuosmanen, Leinonen, & Levonenn, 2013). In oxidative stress conditions, ROS are seen to oxidize cysteine residues in Keap1, which changes its conformation and leads the translocation of Nrf2 to the nucleus and consequently activates gene expression. This delicate balance between the beneficial and the harmful effects of oxidant molecules achieved by redox signalling pathways is responsible for re-establishing

the state of redox homeostasis of a cell, which is how, in fact, diseases are prevented or cured (Dröge, 2002; Ursini, Maiorino, & Forman, 2016).

Amongst oxidant species are the reactive oxygen species (ROS) such as the superoxide radical ($O_2^{\bullet-}$), the hydroxyl radical ($OH^{\bullet}$) and the hydrogen peroxide (H_2O_2), produced enzymatically by the action of nicotine adenine dinucleotide phosphate (NADPH) oxidases or xanthine oxidases, and reactive nitrogen species (RNS), like nitric oxide ($NO^{\bullet}$), generated in biological tissues by specific nitric oxide synthases. Although less reported, there are also oxidant species derived from the halogens chlorine and bromine, that are commonly classified as reactive chlorine species (RCS) and reactive bromine species (RBS), respectively (Halliwell & Gutteridge, 2015; Sies, 1985). Regardless of their origin, oxidant molecules can also be classified as free radical species or non-radical species, depending on whether their atomic or molecular orbitals have, or have not, unpaired electrons (Phaniendra, Jestadi, & Periyasamy, 2015). Free radicals are generally more reactive, as the absence of paired electrons makes them to react with other molecules to become stable. (Halliwell & Gutteridge, 2015; Pham-Huy, He, & Pham-Huy, 2008). An extensive list of free radical and non-radical ROS, RNS, RCS and RBS can be found in **Appendix 1.**

The main endogenous source of ROS is the electron transport chain in the mitochondria, where 90% of the cellular oxygen is consumed (Khansari, Shakiba, & Mahmoudi, 2009). During the electron transfer needed for reduction of oxygen to water, approximately 1 to 3% of all electrons leak from the complex I and III to produce superoxide ($O_2^{\bullet-}$), hydrogen peroxide (H_2O_2) and hydroxyl radical ($OH^{\bullet}$) instead of water (Birben et al., 2012). Additional endogenous sources of ROS include cytochrome p450, endoplasmic reticulum and peroxisomes, through the action of NADPH and xanthine oxidases, and phagocytic cells like neutrophils and macrophages that, during their encounter with pathogens release superoxide radicals ($O_2^{\bullet-}$) and hydrogen peroxide (H_2O_2) through the action of the enzyme NADPH oxidase, and hypochlorite (ClO^-) via myeloperoxidases (Birben et al., 2012; Dahlgren & Karlsson, 1999). Among these sources of ROS, it is important to highlight NADPH oxidase enzymes (NOX) as they are the only enzymes that produce ROS as their primary function. NOX enzymes are transmembrane proteins expressed by a wide variety of cell types and include different isoforms. The mammalian NOX family includes seven isoforms and all of these isoforms are composed the catalytic subunit gp91phox (known as NOX2) together with the regulatory subunits p22phox, p47phox, p40phox, p67phox and the RAC and RAP1A GTPases (Touyz, Briones, Sedeek, Burger, & Montezano, 2011). Isoforms NOX1, NOX2, NOX4, and NOX5 have been identified in vascular tissue and NOX3, expressed in the inner ear (Lambeth, 2004).

Moreover, hydroxyl radicals (HO•) can also be generated by Fenton-type reactions, which involve the reaction of Iron (II) with hydrogen peroxide (Höhn, König, & Grune, 2013).

Oxidants can also be produced exogenously from xenobiotics like pollutants, smoke, or radiation, that *per se* contain components that stimulate the production of ROS. For example, industrial pollutants such as phthalate and nonylphenol, that are found in plastics and cosmetic products and are seen to interfere with the hormonal system of numerous organisms, have been also reported to be linked to the production of O_2^- and H_2O_2 in male testicular tissue. Cigarette smoke, which contains alkaloids, inorganic molecules, and nitrosamines, was also seen to increase the number of leukocytes in plasma, and consequent production of ROS (Pandey & Rizvi, 2011; Shamim i. Ahmad, 2016).

To balance the levels of oxidative species *in vivo*, organisms have developed defence mechanisms based on antioxidant species, that are stable enough to donate electrons to a free radical, neutralising it, and thus delaying and preventing its capacity for oxidation (Sies, 1993). Examples of antioxidants include the enzymes superoxide dismutase (SOD), catalase (CAT), and glutathione peroxidase (GPx), which are synthesized *in vivo*, and vitamin E (α-tocopherol), vitamin C (ascorbic acid), carotenoids, and other phenols, considered to be "antioxidant nutrients", as they can only be up taken through the diet (Aruoma, 1998).

The interaction between oxidants and antioxidants is, therefore, critical for the prevention of oxidative damage and promotion of the cellular redox homeostasis (**Figure I.1**), as the signal damage triggers appropriate modulation mechanisms necessary for either cell survival or apoptosis (Wojciech & Agnieszka, 2017).

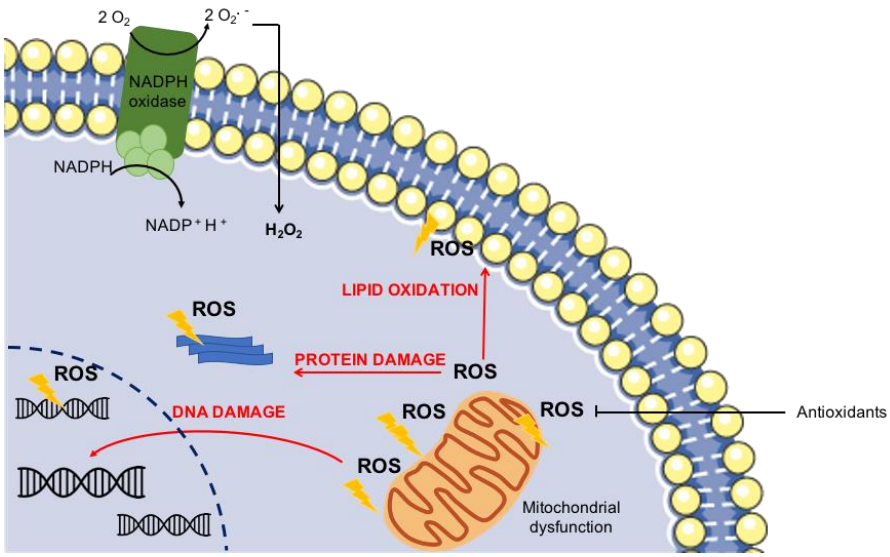

Figure I.1. Schematic representation of some of the biological implications of ROS in the cell. ROS produced either by mitochondrial dysfunction and/or NADPH oxidases can bind to proteins and lipids affecting its conformation and trigger redox pathways involved the expression of oxidative stress-related genes.

1.3. Lipid Peroxidation

Lipids, especially the unsaturated ones, are very susceptible to oxidative attack under oxidative stress conditions and undergo a process of lipid peroxidation (**Figure I.2**) to generate lipid peroxyl radicals and hydroperoxides, which can be further rearranged or fragmented to yield a wide variety of esterified and non-esterified lipid oxidation products (Ayala et al., 2014). The term lipid peroxidation is commonly used to define the oxidative deterioration of polyunsaturated lipids (lipids that contain at least one double bond (C=C) within the fatty acid chain) to yield lipid peroxides. Examples of polyunsaturated lipids are 9,12-octadecadienoic and 5,8,11,14-eicosatetraenoic acids, also known as linoleic and arachidonic acids, respectively, and docosahexaenoic acids, all essential constituents of cell membranes. Hence, lipid peroxidation causes damage to the membrane of lipids and, therefore is responsible for destructive cytotoxicity in the affected cells (Halliwell & Gutteridge, 2015).

The mechanism of lipid peroxidation starts with the abstraction of a hydrogen atom from a methylene group (CH_2) of the fatty acid, by the attack of a reactive specie – the **initiation stage**. The presence of a double bond weakens the C-H bonds on the adjacent carbon atom, and so the H removal gets easier. From this, a carbon radical (C-H•) is formed, which tends to stabilize to a conjugated diene (hydrocarbon that contains two carbon double bonds) by a molecular rearrangement. By further reaction with an oxygen molecule, a peroxyl radical, R-OO• is formed. The hydroxyl and peroxyl radicals generated can further abstract a hydrogen atom from adjacent fatty-acid side-chains and yield new carbonyl radicals that can react with O_2 to form new peroxyl radicals, leading, therefore, to a chain reaction phenomenon – the **propagation stage**. When two radicals encounter and react with each other, they form a new bond between themselves and produce a non-radical specie, ending the propagation chain – **termination stage** (Halliwell & Gutteridge, 2015).

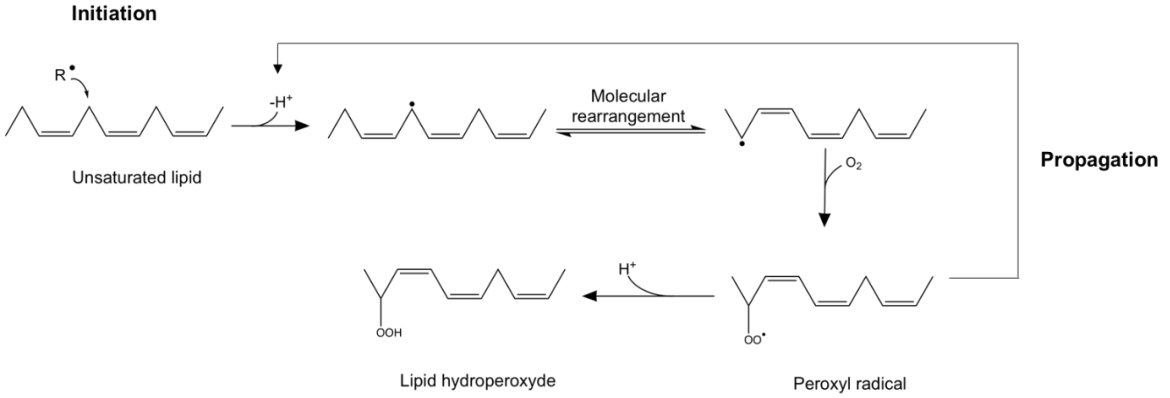

Figure I.2. Representation of the mechanism of free radical-mediated lipid peroxidation. Oxidation of unsaturated fatty acids such as linoleic acid starts with the abstraction of a hydrogen atom from the unsaturated chain to form a CH• radical, which rearranges to form a peroxyl radical. Due to its instability, peroxyl radicals react with other free fatty acids, to produce new radicals, in a chain reaction that only stops when two radical species react with each other to form a non-radical species. Examples of hydroperoxides formed from linoleic acid are the 9-hydroperoxyoctadecadienoate and the 13-hydroperoxyoctadecadienoate and these can further originate intermediate products such as 9-Peroxyoctadecadienoate, 9,10-Dioxetaneoctadecadienoate or 13-Peroxy-9,10- Dioxetaneoctadecadienoate.

1.3.1. Lipid Peroxidation Products

A key feature of lipid peroxidation is the breakdown of polyunsaturated fatty acids (PUFAs) to yield a variety of electrophilic short-chain aldehydes that are thought to have a major role on human health and lifespan (Uchida, 2007). These lipid peroxidation products (LPP) can react covalently with macromolecules to form adducts, through which they mediate the activation of redox-sensitive signalling pathways involved in diverse aspects of cellular responses, such as detoxification and proinflammatory and anti-inflammatory responses (Reis & Spickett, 2012; Uchida, 2007). Examples of redox-sensitive pathways include the keap1/Nrf2 pathway, the nuclear factor kB (NF-kB) signalling pathway and the tyrosine and MAP kinases pathways , all critical in gene regulation during inflammatory and immune responses (Deen et al., 2018; Leonarduzzi, Robbesyn, & Poli, 2004).

Depending on the profile of the oxidised lipid (i.e. its length, and number and position of the double bonds) and the type of oxidant molecule, the generated LPPs can be classified into five different categories **(Table I.1**): (1) Alkanals, when only containing a single aldehyde group; (2) alkenals, when, besides the aldehyde group, they also contain a double bond in the hydrocarbon chain; (3) γ-substituted alkenals, when the aldehyde contains additional functional groups; (4) keto-aldehydes when the aldehyde contains a keto group; and (5)

alkanedials, when the molecules contain two terminal carbonyl groups (Domingues et al., 2013; Sousa, Pitt, & Spickett, 2017; Uchida, 2007).

Table I.1. Classes of aldehydes formed by lipid peroxidation of polyunsaturated acids and corresponding examples. Nomenclature is based on the length, and number and position of the double bonds.

Alkanals	Alkenals	γ-substituted Alkenals	Ketoaldehydes	Alkanedials
2-hydroxybutanal	Acrolein	4-hydro-2-hexenal	4-Oxononemal	Glyoxal
2-hydroxyheptanal	Crotonaldehyde	4-hydroxy-2-nonenal	Methyl glyoxal	Malondialdehyde
Pentanal	2-Pentanal	4-hydroxy-2,6-nonadienal	-	-
Hexanal	2-Hexenal	4-hydroxy-2,6-dodecadienal	-	-

Alkanals, when compared to the other classes of oxidised lipids, are fairly simple molecules. Because they only present a single carbonyl functional group, these molecules can only react with one amine group, yielding a single adduct. Butanal, hexanal and nonanal are listed as the major alkanals generated by lipid peroxidation (Sousa et al., 2017). Alkenals, on the other hand, due to the presence of the two electrophilic reaction centres, are much more reactive molecules, and this bi-reactivity is particularly interesting as it enables the formation of cross-link adducts, which are likely to have a bigger impact on the normal functioning of a cell. γ-substituted alkenals, such as the ones containing the functional groups hydroperoxyl (-OOH), epoxy, hydroxyl (4-hydroxyalkenals), or keto (4-oxo-alkenals), at the C4 position, are considered to be the most prominent class of lipid peroxidation-specific aldehydes (Sousa et al., 2017). Belonging to γ-substituted alkenals there is the very well-studied aldehyde 4-hydroxy-2-nonenal, considered to be one the most cytotoxic LPPs (Benedetti, Comporti, & Esterbauer, 1980). Ketoaldehydes, including ketoalkanals and ketoalkenals, are another important class of reactive aldehydes, of which 4-oxo-2-nonenal (ONE) is part. ONE is originated from the peroxidation of n-6 PUFAs and is able to form three possible crosslink molecules as it contains a ketone, a carbonyl group and a double bond in its structure (Uchida, 2003b). Alkanedials, or di-aldehydes, are molecules containing two terminal carbonyl groups and, like γ-substituted alkenals, are bifunctional and able to crosslink proteins and DNA (Sousa et al., 2017).

1.3.1.1. 4-Hydroxynonenal (HNE), the Most Toxic Lipid Peroxidation Product

4-hydroxy-*trans*-2-nonenal, or hydroxynonenal, usually abbreviated to HNE, deserves special attention as it has been reported to be the most toxic, reactive and abundant LPP (Castro, Jung, Grune, & Siems, 2017). This product was first discovered and detected in the 1960s by Schauenstein et al., but it was only recognised as a cytotoxic product 20 years later (Ayala et al., 2014; Benedetti et al., 1980). This compound falls into the category of γ-substituted alkenals and it is a major product of the decomposition of ω-6 polyunsaturated fatty acids, such as linoleic and arachidonic acid, through either enzymatic or non-enzymatic pathways (Spickett, 2013). By the enzymatic process, HNE can result from 13-hydroperoxyoctadecadienoic acid (13-HPODE), which is a product of oxidation of linoleic acid, via the action of 15-lipoxygenase 1 (15-LOX-1) or from 15-hydroperoxyeicosatetraenoic acid (15-HPETE), a product of oxidation of arachidonic acid, by the action of 15-lipoxygenase 2 (15-LOX-2) (Wojciech & Agnieszka, 2017). In the non-enzymatic process, the production of HNE involves several oxygen radical-dependent reactions involving hydroperoxides, alkoxyl radicals, epoxides and fatty acyl groups. The main reaction is believed to be the beta-cleavage reaction of lipid peroxyl radicals, which leads to the cyclization of peroxyl radicals to form dioxetane, for subsequent chain cleavage (Ayala et al., 2014; Wojciech & Agnieszka, 2017).

The levels of HNE generated during lipid peroxidation depend primarily on the availability of endogenous PUFAs, but exogenous PUFAs, derived from food, can also play a major role. In fact, a study revealed that in western diets, where the ratio of ω-6: ω-3 fatty acids is around 15:1, the levels of HNE were increased and so did the onset of several chronic inflammatory diseases (Patterson, Wall, Fitzgerald, Ross, & Stanton, 2012). Values reported for plasmas, cells, and subcellular fractions showed that in physiological conditions (0.1-1 μM), HNE is thought to be beneficial to cells, as it can act as a signalling molecule stimulating the synthesis of detoxifying enzymes and cell resistance to oxidative stress (Hermann Esterbauer, Schaur, & Zollner, 1991). Conversely, at higher concentrations (10-60 μM), it has been reported that this aldehyde starts promoting organelle and protein damage, which leads to induction of autophagy, senescence, or cell cycle arrest; nevertheless, cells can subsist. At concentrations above 100 μM, HNE was seen to induce cell dysfunction and apoptosis by inhibiting glycolytic enzymes, mitochondrial respiration and even DNA and protein synthesis (Barrera et al., 2014; Hermann Esterbauer et al., 1991; Schaur, 2003; Shoeb, Ansari, Srivastava, & Ramana, 2013; Wojciech & Agnieszka, 2017; Zhang & Forman, 2017).

When HNE is present at high concentrations, it can react with proteins and/or DNA to form adducts, which, therefore, results in a variety of cytotoxic and genotoxic consequences. This reactivity is due to the presence of the hydroxy group, the C=C double bond and the C=O carbonyl group, all electrophilic centres for nucleophilic attack. HNE can form Schiff's base adducts between its carbonyl group and the free amino groups of Lys and Arg residues, and/or Michael adducts between its β carbon and the nitrogen lone pair of the His and Lys residues, or the sulfhydryl group of Cys residues (**Figure I.3**) (Domingues et al., 2013). HNE can also contribute to protein crosslinking due to its bi-reactivity, and according to the literature, it is estimated that 1-8% of the HNE formed in cells ends up covalently bound to proteins (Zhong & Yin, 2015).

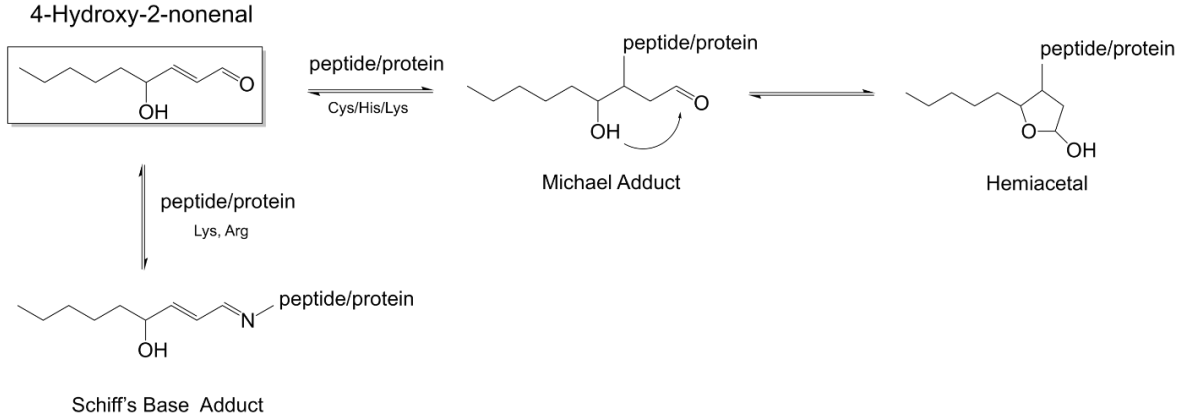

Figure I.3. Chemical structure of 4-hydroxy-2-nonenal (HNE) and reaction mechanisms involved in the formation of Michael and Schiff's base adducts. This aldehyde contains functional groups with a very high reactivity towards nucleophilic residues of peptides/proteins, namely the C=C double bond and the C=O carbonyl group, allowing HNE to form Michael adducts with cysteine, lysine or histidine residues and/or Schiff's base adducts with lysine amino acids.

Due to its amphiphilic nature, HNE is able to diffuse across cell and organelle membranes and covalently modify cytoplasmic or nuclear compounds far from the site of its generation. If formed outside the cells (i.e., in an inflammatory site or in the plasma), HNE can react with stromal proteins or proteins belonging to adjacent cells, that do not undergo lipid peroxidation. HNE has also been reported to mediate several pathological events in humans, including cellular growth inhibition and apoptosis induction (Barrera et al., 2014; Nakashima et al., 2003; Xiao, Zhong, Xia, Tao, & Yin, 2017).

Regarding its metabolism, HNE has a half-life of less than 2 min in physiological conditions and can be metabolized by glutathione-S-transferase (GST), alcohol dehydrogenase (ADH) and aldehyde dehydrogenase (ALDH), depending on the stress level, to its corresponding alcohol, 1,4-dihydroxy-2-nonene (DHN), corresponding acid, 4-hydroxy-2-nonenoic acid

(HNA), or to an HNE-glutathione conjugate product (Ayala et al., 2014; Chapple, Cheng, & Mann, 2013).

Elevated levels of HNE adducts have been found in chronic liver diseases (Poli, Biasi, & Leonarduzzi, 2008), Alzheimer's disease (Reed, Pierce, Markesbery, & Butterfield, 2009), systemic lupus erythematosus (Khan, Moinuddin, Mir, Isalma, & Alam, Khursheed, Ali, 2016), cancer (Zhong & Yin, 2015), cardiovascular diseases, diabetes, and Parkinson's disease (Ayala et al., 2014; Csala et al., 2015; Shoeb et al., 2013), providing evidence that HNE is highly present in cells and tissue and may contribute to the progression of many diseases. A very succinct table showing the concentration of different aldehydes in the serum of healthy individuals and individuals with diabetes, rheumatoid arthritis and lung cancer can be found in **Table I.2**.

Table I.2. Concentration of different aldehydes in serum or plasma collected from healthy and diseased individuals (adapted from Sousa et al., 2017).

Aldehyde	Condition				Detection Method [a]
	Healthy	Diabetes	Rheumatoid arthritis	Lung cancer	
Glyoxal	1.04 μM	2.75 μM	1.34 μM	-	A
Methylglyoxal	146.5 nM	299 nM	145 nM	-	B
Acetaldehyde	1279 nM			-	C
Propionaldehyde	135 nM			-	C
Acrolein	42.2 nM	68.7 nM	76.3 nM	-	B
	1.26 μM	6.35 μM	2.92 μM		A
Malondialdehyde	5.54–6.56 μM			-	D
	0.36–1.24 μM			-	E
	15.1 μM	25.6 μM	37 μM	-	A
	0.44–0.89 μM				E
Crotonaldehyde	61.3 nM			-	B
Valeraldehyde	7 nM			-	C
Hexanal	17 nM			-	C
	1.04-2.06 μM			2.28–25.3 μM	F
2-Hexanal	59.5 nM	59.2 nM	61.7 nM	-	B
Heptanal	0.02–0.91 μM			0.16–3.91 μM	F
Hydroxynonenal	0.96 μM	1.27 μM	1.78 μM		A
	82 nM				G
	68.9-107 nM				H
	0.65 μM				I

[a] Detection methods: A – HPLC–fluorescence detection of difurylimidazole derivatives; B – LC-MS with peroxyoxalate chemiluminescence detection after fluorescence labelling with 4-(N,N-dimethylaminosulfonyl)-7-hydrazino-2,1,3-benzoxadiazole; C – HPLC of fluorescent decahydroacridine derivatives; D – HPLC-DAD, HPLC-fluorescence, LC-DAD or LC/MS-SIM; E - HPLC analysis of the thiobarbituric acid (TBA) derivative; F - Derivatization with 2,4-dinitrophenylhydrazine (DNPH), extraction with DLLME-SFO, analysis by HPLC; G – HPLC of the oxime-bis-tert-butyldimethylsilyl derivative; H – Derivatization with dinitrophenylhydrazine (DNPH), analysis by LC; I – DNPH derivitization, SPE of hydrazine and HPLC with detection at 370 nm.

Therefore, as biomarkers of oxidative stress *in vivo,* HNE-protein adducts may deserve a place in medical diagnostic testing (Requena et al., 1996).

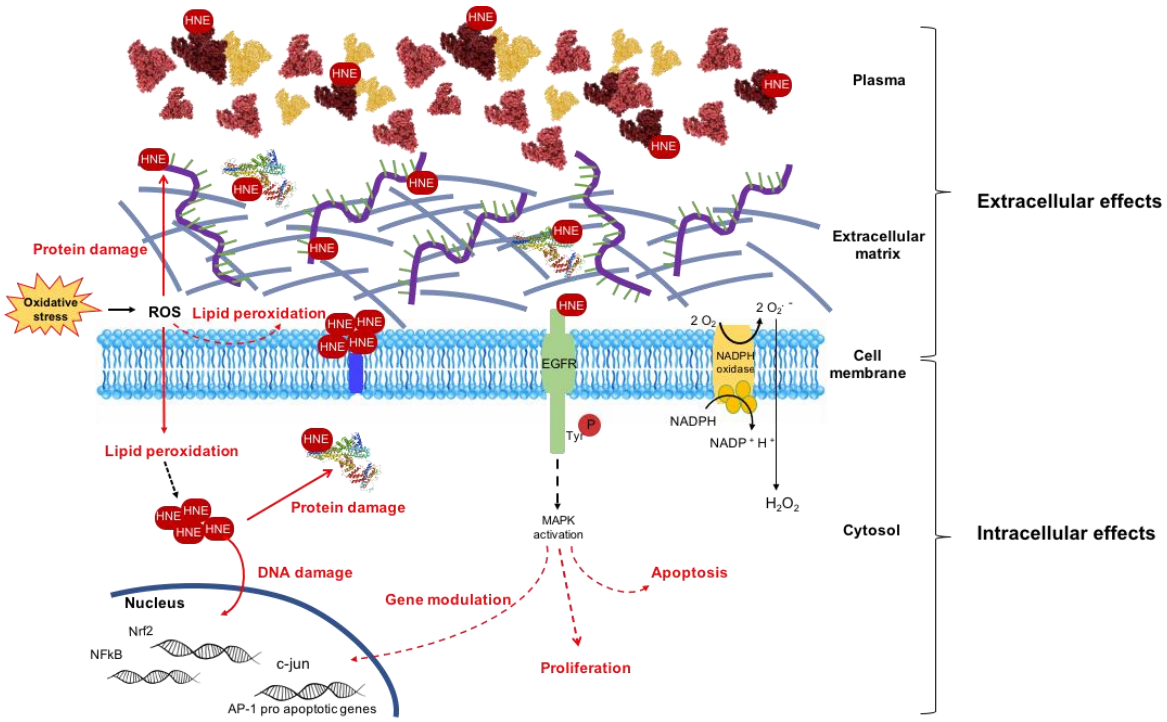

Figure I.4. Schematic illustration of the effects of HNE inside and outside the cell. HNE mediates cell signaling pathways like Nrf2/keap1 involved in processes such as autophagy, proliferation and apoptosis, and can react with protein and/or lipids leading to conformational changes and, therefore, protein and lipid damage.

1.4. Protein Lipoxidation

Proteins can undergo a wide variety of oxidative post-translational modifications (oxPTM), by reaction with the LLPs above mentioned. This phenomenon is known as protein lipoxidation, and the protein-lipid adducts therefrom are called lipoxidation products (Domingues et al., 2013). The mechanism through which these adducts are formed depends on both the functional groups of the LPPs and the availability of specific amino acids but, generally, LPPs are seen to react most frequently with four chemical groups: the free amine group (NH_2-) of lysine residues, the imidazole group of histidine residues, the guanidine group of arginine residues and the thiol (SH-) group of cysteine residues. The order of reactivity of nucleophilic amino acids towards electrophilic compounds is reported to be Cys>>His>Lys; however, factors including solvent accessibility and nucleophilicity can also affect their reactivity (Aldini et al., 2015). Michael adducts, generated by Michael addition, are formed by reaction of the electrophilic carbon located in the β position with

respect to the α, β unsaturated carbonyl group with the nitrogen lone pair of the histidine/lysine or the thiol group of cysteines (**Figure I.5**) (Domingues et al., 2013).

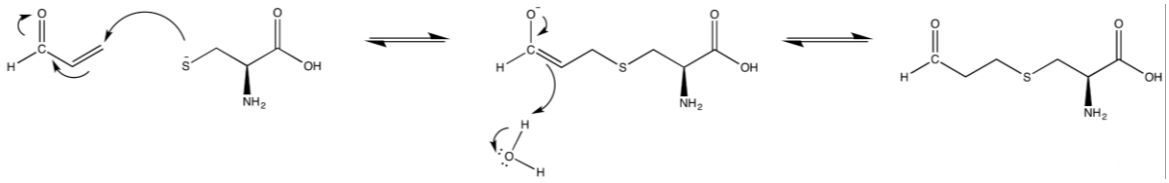

Figure I.5. Mechanism of Michael adduct formation between an aldehyde and a cysteine residue. The Michael reaction starts with the attack of the nucleophile (in this case a cysteine residue) to the aldehyde (in this case the LPP acrolein) at the electrophilic alkene carbon, yielding an enolate ion. The enolate then deprotonates a water molecule recreating hydroxide and the energetically more favourable carbonyl group.

Although Michael adducts are theoretically reversible, Michael addition to cysteine and histidine residues is seen almost as irreversible, as the rate of the reverse reaction is considerably lower when compared to the rate for the formation of the adduct. However, for Michael adducts to Lys residues the same is not observed, meaning that for its stabilization, a reduction reaction with $NaBH_4$ is needed (Domingues et al., 2013).

Schiff's base adducts, on the other hand, are formed by condensation of an aldehyde or a ketone with the primary amine of Arg or Lys residues. In more detail, the reaction starts with the formation of a carbinolamine intermediate that rearranges and loses water to yield a Schiff base (**Figure I.6**). Like Michael adducts, Schiff's base adducts are reversible and can always be hydrolysed back to their aldehydes or ketones and amines by aqueous acid or base conditions (Vistoli et al., 2013).

Bi-functional lipid peroxidation products, as mentioned before, have the capability of reacting via the two different functional groups and can therefore form Michael and Schiff's base adducts, promoting protein cross-linking (Aldini et al., 2015).

The importance of lipoxidation has attracted a great deal of attention in the recent years, due its recognition as a mechanism for regulating protein function in health and disease, especially as lipoxidation adducts may interact or compete with other modifications, including oxidative modifications or adduct formation with drugs in therapeutic regimes of patients (Aldini et al., 2015).

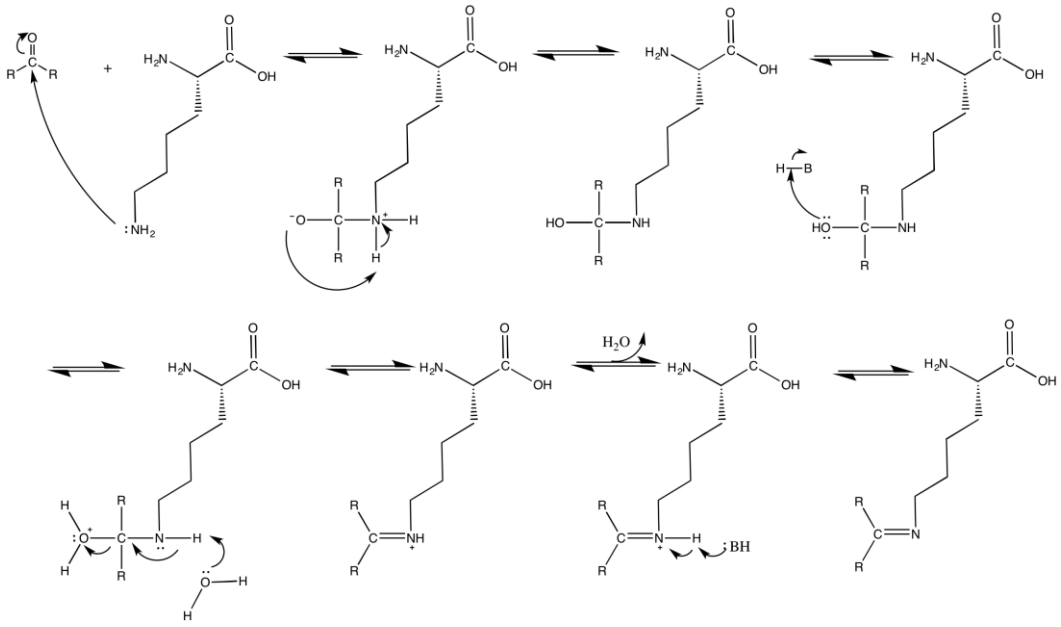

Figure I.6. Mechanism of Schiff base adduct formation between a ketone and a lysine residue. The Schiff base formation mechanism involves an initial attack from a nucleophile ((in this case a lysine residue) to the carbonyl group, followed by transfer of a proton from a weak acid to a strong base. After protonation of the -OH group, a molecule of water is released, allowing the formation of a double bond.

1.4.1. Biological Occurrence of Lipoxidation Adducts

The accumulation of lipoxidation products in tissues has been reported to increase the level of inflammation in the body through the activation of specific cell receptors called RAGE (receptor for advanced glycation end products), seen to be involved in modulation of proinflammatory signals (Bengmark, 2007). In particular, RAGE binds to proinflammatory cytokine-like mediators of the S100/calgranulin family, which encompasses polypeptides released by inflammatory cells, and to the nuclear protein amphoterin, that when released exerts proinflammatory activities (Hofmann et al., 1999; Hori et al., 1995). Moreover, the binding of RAGE to glycated and lipoxidation products in vascular cells, such as endothelial cells and neuronal cells, and inflammatory cells like monocytes, may activate the signalling pathways of erk1/2 (p44/p42), p38 and SAPK/JNK MAP kinases, rho GTPases, phosphoinositol-3 kinase and of NF-κB, all linked to inflammation status (Chavakis, Bierhaus, & Nawroth, 2004). Tyrosine kinase receptors, such as the epidermal growth factor receptor (EGFR) and the platelet-derived growth factor receptor (PDGFR), have also been recognized as targets of electrophilic oxidised lipids (Leonarduzzi et al., 2004). LPPs like acrolein and 4-HNE elicit PDGFRβ modification and subsequent dysfunction, leading to the defective proliferation of smooth muscle cells, which could be implicated in the pathogenesis of fibroatheroma and vulnerable plaque (Uchida, 2007). However,

lipoxidation has also been reported to occur in healthy individuals, where the formation of lipoxidation products can even induce gain of protein function or activity, leading to beneficial effects (Levonen et al., 2004; Martín-Sierra, Laranjeira, Domingues, & Paiva, 2019). Bacterial proteins SoxR and OxyR are transcriptional activators that respond to superoxide and H_2O_2, respectively, and by getting oxidized activate directly the transcription of several genes including catalase (katG), alkyl hydroperoxide reductase (ahpCF) genes, glutathione reductase (gorA), glutaredoxin 1, and a ferric uptake regulator (Halliwell & Gutteridge, 2015).

Lipoxidation products are particularly associated with ageing and age-related diseases such as cancer, atherosclerosis, diabetes, chronic obstructive pulmonary disease, systemic lupus erythematosus and neurodegenerative diseases (including Huntington's, Parkinson's and Alzheimer's diseases) (Baraibar & Friguet, 2013).

In diabetes mellitus, the high level of glycoxidation and lipoxidation products in plasma and tissue proteins suggests that oxidative stress is increased, however, it is still not clear whether oxidative stress has a primary role in diabetic complications or it is a secondary indicator of end-stage tissue damage in diabetes (Baynes & Thorpe, 1996; Dröge, 2002). Superoxide was seen to be generated by the process of glucose autoxidation, and furthermore, in hyperglycaemia conditions, low-density lipoprotein (LDL) peroxidation was reported to occur in endothelial cells and account for the generation of LPPs (Afonso & Spickett, 2018; Dröge, 2002). Lipoxidation adducts to apolipoprotein B of LDL (lysine-MDA, the cross-link lysine-MDA-lysine, lysine-HNE, and histidine-HNE) were already reported, as well as a significant increment in the levels of HNE-modified human serum albumin (HNE-HSA) in sera of patients with type 2 diabetes (Jakus, Bauerova, Michalkova, & Carsky, 2000; Lyons & Jenkins, 1997; Toyokuni et al., 2000)

Regarding cancer, the role of lipid peroxidation and lipoxidation is still not completely understood, as lipid composition can differ between each type of cancer cell. Nevertheless, increased incidence of HNE-protein adducts has been observed in human liver, kidney and colon cancer tissues (Zhong & Yin, 2015). Moreover, studies in astrocytic and ependymal glial tumours showed the incidence of HNE-positive tumour cells was directly related to increasing grades of malignancy (Martín-Sierra et al., 2019).

In atherosclerosis, one of the first events that occurs is the invasion of the artery wall by monocytes and macrophages, cells that possess the scavenger receptor to oxidised LDL (oxLDL) and that, by binding to oxLDL, become activated and stimulated to produce even more ROS. HNE, MDA, methylglyoxal and glyoxal have been reported to directly modify the structure of LDL, changing its metabolism towards macrophages. In particular, protein

carbonyls, MDA and HNE-adducts on Lys were detected in atherosclerotic plaque, but the total extent of lysine modification by these compounds was less than 1% of the lysine residues in plaque proteins (Baynes & Thorpe, 2000).

In autoimmune diseases, the presence of lipoxidation adducts was also observed, namely in systemic lupus erythematosus (SLE), where catalase and HSA were reported to be modified by HNE. However the actual site of modification was not reported (D'souza et al., 2008; Grune et al., 1997; Khan et al., 2016). SLE patients were also seen to have elevated levels of anti-oxLDL autoantibodies that cross-react with phospholipids, which suggests the antigen might be oxidised on both the protein and lipid structures of LDL (Kurien, Hensley, Bachmann, & Scofield, 2006). Regarding neurological diseases, increased levels of modified proteins were found in neuronal cytoplasmin disease compared to age-matched control samples. Carbonyls were confirmed in creatine kinase BB, glutamine synthase, ubiquitin carboxy-terminal hydrolase L-1, α-enolase and dihydropyrimidinase-related protein 2, although the nature of the carbonyl formation was not confirmed (Domingues et al., 2013).

While it can be seen that there is abundant evidence of protein lipoxidation in the pathology of several diseases, they are in most of the cases focused on HNE and MDA adducts, as most of the detection methods (at least antibody-based ones) are directly targeted to these products. Development of improved methods to identify and characterize electrophilic lipid–protein adducts are still in great demand, as well as the need to understand the exact relation between redox status and protein lipoxidation in the triggering of antioxidant and adaptive response (Vasil'ev, Tzeng, Huang, & Maier, 2014).

1.4.2. Detection of Lipoxidation Adducts

Given the importance of lipoxidation products in the pathology of human disease, there has been a great effort to develop technologies to specifically detect lipid-protein adducts in biological and clinical samples. Mass spectrometry (MS) is one of the techniques that has been used for many years for the study of proteins-lipid adduct. As MS analysis is based on determining the mass-to-charge (*m/z*) ratio of ionized analytes, and oxPTMs change the *m/z* ratio of the intact proteins, MS is seen as a powerful method not only for detecting but to characterize lipoxidation products (Verrastro, Pasha, Jensen, Pitt, & Spickett, 2015). When operated in tandem mode (MS/MS), MS not only provides detailed structural information of the protein-lipid adduct, it can also be used to confirm the location of the oxidative post-translational modification in the peptide backbone (oxPTM) (Aldini et al., 2015). Adducts can be detected by MS analysis with either matrix assisted laser

desorption/ionization (MALDI), or electrospray (ESI), often coupled to liquid chromatography (LC–MS), in positive ion mode (Bollineni, Hoffmann, & Fedorova, 2011). Modified peptides are typically recognized in the MS spectrum based on the mass shift versus the native peptide: if it is Michael adduct the mass shift caused by the modification is equal to the molecular weight of the LPP, if it is a Schiff's base adduct the difference is then equal to the molecular weight of the LPP minus 18 amu, owing to loss of H_2O during adduct formation (Aldini et al., 2015). The characterization of the adducts can be performed by following either a top-down strategy, that involves analysis of intact proteins and fragmentation within the mass spectrometer, or a bottom-up proteomic approaches that consist of enzymatically digesting the protein (usually using trypsin) to a peptide mixture, before MS analysis (Loizides-Mangold, 2013).

Several studies following these approaches for the detection of HNE, MDA and acrolein adducts have already been published and there has been extensive characterization of these adducts *in vitro* and *in vivo* (Domingues et al., 2013). Nevertheless, for the identification of protein lipoxidation adducts in more complex samples, such as cells, tissues or even biological fluids, untargeted approaches are not always appropriate, and label-dependent methods (involving chemical probes) are required (Domingues et al., 2013). Because most of the existing derivatization methods exploit the high reactivity of the free carbonyl groups of the adducts, carbonyl-reactive reagents such as 2,4-dinitrophenylhydrazine (DNPH) are commonly used. DNPH has been extensively used due to its convenience, low expense and relative simplicity, however this method is not completely specific to lipoxidation products, as other carbonyls formed by direct oxidative attack on the protein will be detected as well (Domingues et al., 2013). Other labelling reagents have been reported for detecting carbonyls, like fluorescein derivatives or biotin-based hydroxylamine-functionalized reagents (Vasil'ev et al., 2014); nevertheless it is important to note that these labelling methods cannot be used to identify lipoxidised proteins *in vivo* in humans, as they require the presence of an artificially labelled lipid in the tissue of interest.

It is essential to understand the requirements and limitations of the techniques used and select appropriate approaches to address the research question. Although MS approaches are being developed and applied (Afonso & Spickett, 2018; Aldini et al., 2006; Shibata et al., 2017), they have the limitation of requiring expensive specialist equipment and being challenging to perform. Moreover, their translation for early diagnostic screening tools in clinical settings continues to be difficult, owing to factors such as lack of well-established validation protocols for oxPTMs, the wide variety of methodologies, and complex data analysis (Verrastro et al., 2015).

Therefore, antibody-based techniques remain attractive in the field of oxidative stress, as immunoassays have the advantage of combining high sensitivity, relative simplicity, accessibility and rapidity in one single platform, which is the ultimate goal in terms of healthcare diagnostics. Antibodies specific to HNE, HHE, MDA, acrolein, crotonaldehyde and methylglyoxal have been used both in enzyme-linked immunosorbent assays (ELISA) and immunohistochemistry methods, and the identification and detection of LPPs and lipoxidation adducts has seen to be successful (Zarkovic, Jakovcevic, & Zarkovic, 2017). Regarding HNE, the first generated antibodies against this lipid peroxidation oxidation product were in the late 1980s, when Palinski *et al* (1989) and Jurgens *et al* (1990) produced antibodies against HNE-treated LDL (Jurgens, Ashy, & Esterbauer, 1990; Palinski et al., 1989). Subsequently other groups adopted different approaches and raised antibodies against alternative immunogens, such as HNE-treated keyhole limpet haemocyanin (KLH) (Hartley, Kroll, & Petersen, 1997; Toyokuni et al., 1995; Uchida, Szweda, Chae, & Stadtman, 1993; Waeg, Dimsity, & Esterbauer, 1996), a synthetic peptide Gly_3-His-HNE-Gly_3 conjugated to KLH (Uchida, Itakura, et al., 1995), or HNE-modified HSA (Khan et al., 2016; Khatoon, Moinuddin, Alam, & Ali, 2012).The majority of these were polyclonal sera able to recognize HNE adducts on a variety of proteins but some monoclonal antibodies were also produced (Toyokuni et al., 1995; Waeg et al., 1996). In some cases, specificity for a specific modified residue or adduct was reported, as is the case of antibodies specific to histidine (Toyokuni et al., 1995; Waeg et al., 1996) or cysteine adducts (Hartley et al., 1997), while other antisera showed broader specificity. Monoclonal antibodies to MDA–lysine adducts of LDL and polyclonal antibodies to MDA–lysine adducts of KLH were also developed for ELISA immunohistochemistry protocols and similar approaches were used for acrolein and HHE-adducts (Haberland, Fong, & Cheng, 1988; Uchida et al., 1998; Yamada et al., 2004). Another interesting antibody available in the field is the mAb EO6 autoantibody, found in apoE-deficient mice, that has been shown to be specific to oxidised phospholipids (oxPL) and low-density lipoprotein-oxPL adducts (Hörkkö et al., 1999). Currently, there is a vast offer of commercial anti-HNE antibodies, from several companies, that derive in most cases from the original clones listed below in **Table I.3**.

However, even though all these antibodies have been found to detect different kinds of lipoxidation adducts, one of the limitations of immunoassays is the dependence on the antibody specificity. Some of the reagents are polyclonal and likely to have cross-reactivity to similar adducts (Sousa et al., 2017). Moreover, none of the immunoassays are able to provide information about precise site of modification within the protein, or on the kind of protein that is modified.

Table I.3. List of the first antibodies generated against the lipid peroxidation product 4-HNE.

Immunogen	Animal	Clonality	Reference	Year
4-HNE-LDL	Guinea Pig	Polyclonal	Palinski *et al*	1989
4-HNE-LDL	Rabbit	Polyclonal	Jurgens *et al*	1990
$4\text{-HNE}_{reduced}$-LDL	Guinea Pig	Polyclonal	Palinski *et al*	1990
4-HNE-KLH	Rabbit	Polyclonal	Uchida et al	1993
Gly_3-His-HNE-Gly_3	Rabbit	Polyclonal	Uchida et al	1995
4-HNE-KLH	Mouse	Monoclonal	Toyokuni et al	1995
4-HNE-KLH	Mouse	Monoclonal	Waeg et al	1996
4-HNE-KLH	Rabbit	Polyclonal	Hartley et al	1997
4-HNE-HSA	Rabbit	Polyclonal	Khatoon et al	2012

1.5. Oxidation and Immunity

Recent hypotheses have indicated that oxidative stress and oxidised biomolecules are involved in a process of sterile inflammation (i.e., inflammation in the absence of pathogens), activating the innate and adaptive immune responses. The modification of "self" biomolecules by oxidised lipids is seen to generate oxidation-specific epitopes (OSEs) that share a molecular identity with both pathogen-associated molecular patterns (PAMPs) on microbial pathogens, and damaged-associated molecular patterns (DAMPs) on apoptotic cells, making them to be recognized by a variety of pattern recognition receptors (PRR), that trigger signalling pathways to induce the secretion of inflammatory chemokines and cytokines. OSEs have a crucial role in physiological processes, as they target oxidatively modified endogenous molecules as damaged by oxidative stress, allowing the host to identify dangerous biological waste and maintain homeostasis (Uchida, 2013). OSEs including OxPLs and MDA-protein adducts have been reported on the surface of apoptotic cells, microvesicles and damaged structures such as OxLDLs (Leibundgut, Witztum, & Tsimikas, 2013).

PPRs for OSEs encompass a wide set of molecules such as toll-like receptors (TLRs), nucleotide-binding oligomerization receptors domain-like receptors (NODs), scavenger receptors (SR; e.g., CD36 and SR-A1), RAGEs, and many others. They are mostly cell-associated, located at the surface of antigen presenting cells, but soluble PPRs like components of the complement system, lectins, and pentaxins have also been reported (Foell, Wittkowski, & Roth, 2007). Detailed studies have shown that CD36 is the major SR for OxLDL and accounts for most of the binding and uptake of OxLDL by macrophages, and LOX1 to mediate MDA-induced nitric oxide (NO) production and binding to HNE adducts with ApoB100 protein in oxLDL (Binder, Papac-Milicevic, & Witztum, 2016). Toll-

like receptors (TLR) have also been reported to recognize and respond to OSEs, namely TLR1, TLR2 and TLR4-6 heterodimer. Sensing of oxidised phosphatidylcholine (oxPC) seems to be important for the TLR4-mediated effects, OxPLs were seen to stimulate macrophages via a TLR2 pathways, chemokine secretion by macrophages stimulated with oxLDL was shown to require the cooperation of CD36 with a TLR4-TLR6 heterodimer and oxidised cholesteryl esters (OxCEs) were seen to trigger pro-inflammatory macrophage responses via TLR4. TLRs have not, however, been seen to be directly implicated in chemokine secretion induced by MDA or HNE (Weismann & Binder, 2012).
Regarding soluble PPRs, C-reactive protein and complement factor H have been seen to bind to PC and PC-OxPL found in oxLDL, and MDA-epitopes, respectively, and more recently, milk fat globule-epidermal growth factor 8 (MFG-E8) has been shown to specifically recognize oxPC and oxidised phosphatidylethanolamine (oxPE) (Miller et al., 2012).

OSEs have also been identified as major targets of natural IgM antibodies (Binder et al., 2016; Miller et al., 2012). Levels of IgMs specific for oxLDL and MDA-LDL were found to be higher in cord blood samples when in comparison with matched maternal blood samples. Studies have also reported several OSEs, including PC-oxPL, MDA and HNE adducts to be bound to up 30% of all natural IgM found in the plasma of wild-type mice (Grönwall et al., 2016). Furthermore, several natural monoclonal IgM antibodies with specificity to OSEs have been characterized, as is the case for the E06 mAb that was originally cloned from the spleens of atherosclerosis-prone apolipoprotein E ($Apoe^{-/-}$) mice and showed specificity to PC-oxPL (Hörkkö et al., 1999).

Despite the clear evidence that lipoxidation adducts are linked to the main inflammatory mechanisms, the exact biological consequences of lipoxidation adducts in pathology is still far from being understood. Undoubtedly, interdisciplinary studies combining different analytical techniques, cell biology, and immunology could help clarify the role of lipid-derived DAMPs in disease aetiology.

1.6. Antibodies

As aforementioned, OSEs represent an important class of endogenous “danger signals” likely to exert positive selection pressure for natural antibody-producing B cells, and antibodies to these epitopes could present a promising strategy to target therapeutic molecules to active sites of inflammation. For better understanding how the immune system responds to these structures and how anti-HSA-HNE antibodies were generated in this

project, the following topics of this introduction are focused on immune responses that lead to the development of such specific molecules and how can these be generated and further refined for commercial application.

1.6.1. Innate and Adaptive Immunity

Upon infection by foreign pathogens, the immune system has the capability of triggering two different kinds of responses. Up to 12 hours after infection, the immune responses are based on the action of physical and chemical barriers, such as epithelial and antimicrobial substances, phagocytic cells such as neutrophils and macrophages, blood proteins, and cytokines, in what is known as innate immunity. After a day, and up to a week after infection, the immune responses start to develop specificity and memory capacity, via the production of antibodies that bind specifically to extracellular pathogens, so subsequent infections with the same pathogen can be easily fought. This delayed response is what constitutes adaptive immunity (Abbas, Lichtman, & Pillai, 2007).

For a B lymphocyte to start producing antibodies it needs first to be activated via interaction with the antigen/OSEs and helper T cells (T_H cells), and this activation takes place in peripheral lymphoid organs (lymph nodes and the spleen). When the antigen binds to the B cell receptor (BCR) it gets internalized through receptor-mediated endocytosis and is degraded and presented to T cells as peptides in a complex with major histocompatibility complex (MHC) class II molecules. Upon recognition of these peptide:MHC complexes by the T_H cell, several signals such as the activation of CD40 on B cells and production of various cytokines by T_H cells (IL-21, IL-6, TGF-β, IFN-γ, and IL-4) will cause B cells to migrate to different areas of the lymph nodes (**Figure I.7**), and proliferate and differentiate into antibody-secreting plasma cells that secrete different classes of antibodies with different functions (Murphy & Weaver, 2017).

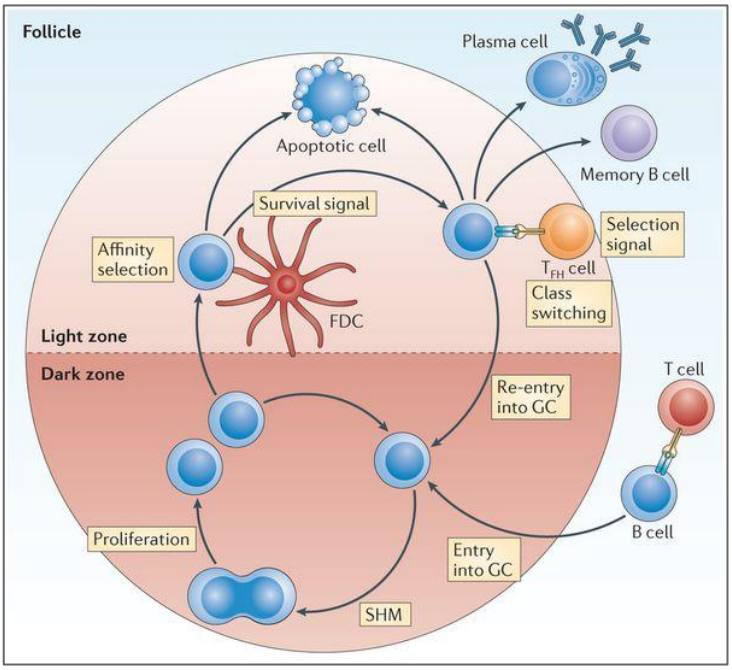

Figure I.7. Illustration of the B cell affinity maturation process in a lymph node. Once B cells present the antigen to T helper cells and these receive co-stimulatory signals the selected B cells enter the dark zone of the follicle and undergo somatic hypermutation (SHM). After one or possibly more cycles of proliferation, B cells migrate to the light zone and, in the light zone, the mutated B cell receptors (BCR) are now exposed to antigens that are incorporated into immune complexes on the follicular dendritic cells (FDC). If the affinity of the BCR is very low, the B cell will not receive survival signals and will undergo apoptosis, and the surviving B cells can either re-enter the dark zone and undergo further proliferation and SHM, exit the follicle as plasma cells or they can exit as memory B cells. Adapted from: Heesters, Myers, & Carroll, 2014

1.6.2. Molecular Structure and Functional Features

All human antibody molecules share the same basic structural characteristics but display remarkable variability in the regions where the antigen binds. They are all Y-shaped molecules with a symmetric core structure containing two identical light chains and two identical heavy chains, covalently linked by disulphide bonds (**Figure I.8**). Each heavy and light chain has a molecular weight of approximately 50 kDa and 25 kDa, respectively, making an antibody of 150 kDa. Each antibody molecule has two antigen binding sites located at the amino terminal variable regions (known as V_H and V_L, respectively for variable regions located on heavy and light chains), where sets of complementarity-determining regions (CDRs) exists. These CDRs constitute a paratope, i.e., the antibody sequence that recognises antigen. The region on the antigen to which the paratope binds is called epitope (Schroeder Jr & Cavacini, 2010).

Figure I.8. General representation of the antibody structure. 3D structure of an IgG antibody (PDB: 1IGT) illustrated as a ribbon diagram of the backbones of the polypeptide chains, where the heavy chains are depicted in green and the light chains in blue (A). Each heavy chain consists of three constant regions (C_H) and one variable region (V_H) while each light chain is composed of one constant (C_L) and one variable region (V_L). The two antigen-binding sites are formed by the juxtaposition of V_L and V_H domains. The bottom section of the antibody is the Fc region to which two arms, the Fab regions, are attached. The two heavy chains are linked to each other by disulphide bonds, and each heavy chain is linked to a light chain by a disulphide bond (B). The structure in panel B was taken from https://bxcell.com/antibody-structure/.

The carboxy-terminal constant regions (C_H and C_L respectively for heavy and light chains), are, as the name states, constant, and only the C_H regions are seen to mediate effector functions. There are 5 different classes of antibodies: IgG, IgM, IgD, IgE and IgA, being IgG by far the most abundant Ig in serum. It is also important to note that there are two types of light chains, known as lambda (λ) and kappa (κ), and they can be found in any of these five major classes of antibodies (Abbas et al., 2007; Murphy & Weaver, 2017). No functional difference has been found between these two chains, however the ratio of κ to λ seems to be different from species to species: for mice it is 20:1, for humans 2:1 and for cattle 1:20 (Sun et al., 2012).

1.6.3. Antibody Variability

The diversity of antibody repertoires arises mainly from two genetic events that involve recombination and mutation of the immunoglobulin genes. In a first instance, variability is generated by gene rearrangement mechanisms that occur due to the fact that, unlike most genes, the complete DNA sequence of the variable-region exon is encoded by two separate DNA fragments; then, upon rearrangement, the diversity is further enhanced by somatic

hypermutation processes, that introduce point mutations into those same V-regions genes (Murphy & Weaver, 2017).

The rearrangement that produce the complete Ig light chain and heavy chain genes, also known as V(D)J recombination is depicted in **Figure I.9**, and occurs during B cell's maturation. For the light chain, the rearrangement encompasses the variable (V) and joining (J) gene segments; whereas for the heavy chain there is a third gene segment involved called the diversity, of D gene segment. Because there are multiple copies of the V, D and J gene segments and each of which can be rearranged in many different formulas, several millions of immunoglobulin V regions can actually be formed; and this is the principle in which all the *in vitro* cloning techniques are based on for the generation of recombinant antibodies libraries (Abbas et al., 2007).

Somatic hypermutation, on the other hand, occurs only in activated B cells, after the initiation of an immune response has been triggered, as a mechanism of affinity maturation for production of antibodies with greater affinity. Somatic hypermutation introduces mutations in the V regions via an enzyme called activation-induced cytidine deaminase, that might change from one to a few amino acids, leading to the formation of closely related B cell clones that only differ subtly in specificity and antigen affinity (Reynaud, Garcia, Hein, & Weill, 1995).

In humans, the Ig variable regions accumulate mutations at a rate of about one base pair change per 10^3 base pairs per cell division, which is known to be 1 million-fold higher that the spontaneous rate of mutations in most of other genes (Z. Li, Woo, Iglesias-Ussel, Ronai, & Scharff, 2004). Although these mutations may be both transitions (e.g., C to T, G to A) and transversions (e.g., C to A or G; G to C or T), there seem to be preferentially targeted motifs like the WRCY (W = A or T, R = A or G, C, Y = T or C) and WA, that are referred to as hot spots (Peled et al., 2008). Nevertheless, nucleotide changes tend to be clustered in the CDRs of the V-regions, whereas silent or neutral mutations, that do not alter the amino acid sequence seem to occur in frame work regions (Jenne, Kennedy, & Reynolds, 2006).

Figure I.9. Somatic DNA recombination of the V-region genes. Light-chain V region genes are constructed from the variable (V) and joining (J) gene segments of the genomic DNA to form a complete light-chain V-region exon. The light-chain constant region (C) is encoded in a separate exon and is joined to the V-region exon by splicing of the light-chain RNA to remove the V-to-J and the J-to-C introns. Heavy-chain V regions are first constructed from the diversity (D) and the J gene segments, and then the V gene segment joins to the combined DJ sequence, forming a complete V_H exon. A heavy-chain C region gene is encoded by several exons, that together with the leader sequence, are spliced to the V-domain sequence during processing of the heavy-chain RNA transcript. The leader sequence is later removed after translation, and the disulphide bonds that link the polypeptide chains are formed. The hinge region is shown in purple. From *Murphy, K., Travers, P., Walport, M., & Janeway, C. (2008). Janeway's immunobiology. New York: Garland Science.*

1.6.4. Polyclonal, Monoclonal and Recombinant Antibodies: Distinguishing characteristics and applications

When considering the use of antibodies for a certain application, whether it is biomedical research, diagnostics, therapy or even medicine, the first choice to be made is the type of antibody to use. There are polyclonal antibodies (pAbs), a mixture of antibodies that recognize different epitopes on the same antigen, monoclonal antibodies (mAbs), that only recognize a single epitope per antigen, and even recombinant antibodies (rAbs), that are tailor-made mAbs generated *in vitro* from a unique set of genes. Each type comes with their

own unique advantages and disadvantages and is produced by very different methods, making them suitable for different applications.

pAbs are a heterogeneous mixture of antibodies, meaning each antibody recognizes a different epitope on the same antigen. Therefore, pAbs are more suitable for detection methods, namely detection of low concentration antigens, as the target antigen will bind to more than one antibody molecule on its multiple epitopes, so that its signal is effectively amplified. This is, however, a disadvantage for quantification studies. Another characteristic of pAbs is their tolerance for changes in the antigens, i.e. polymorphisms, heterogeneity of glycosylation, or slight denaturation. Minor changes in the structure of the antigen will not drastically affect their binding to the antibodies, and for this reason pAbs are often preferred over mAbs for detection of denatured proteins. pAbs are also known for being more robust and more stable over a broader range of pH and buffer compositions than mAbs (Lipman, Jackson, Trudel, & Weis-Garcia, 2005). However, pAbs have a great degree of batch-to-batch variability, as their production depends always on the immunisation of an animal, and often present cross-reactivity to other serum proteins (Leenaars & Hendriksen, 2005).

mAbs, on the other hand, are generated from a single B-cell clone and therefore only recognize a single epitope per antigen, which makes them highly monospecific and very suitable for quantification applications (Lipman et al., 2005). They are also less likely to cross-react with other proteins and present a high degree of homogeneity, which means they provide higher reproducibility, not only between batches but also between experiments. However, traditional methods for developing mAbs are dependent on animal immunisation, as for pAbs, and on creation or screening of immortalized hybridoma cell lines, which can cause a bottleneck in mAb production. Moreover, traditional mAbs are mostly limited to murine sources because the myeloma cell lines required for immortalization are not commonly available for other species. MAbs are less flexible in terms of epitope recognition, which might be an inconvenience when the target is not shared across a range of species (Baird et al., 2009; Laffly & Sodoyer, 2005).

Recombinant antibodies, as opposed to the two other types aforementioned, are generated *in vitro* and were developed with the aim of overcoming the disadvantages of the pAbs and combining the advantages of the mAbs. RAbs are selected from antibody synthetic libraries of generally 10^8 antibodies clones whose DNA variability is induced *in vitro*, which increases the chances of producing a highly specific, sensitive and stable antibody. Moreover, production of rAbs *in vitro*, despite being very challenging, is robust and can overcome the batch-to-batch variability of the pAb. rAbs can be very useful for analysing the proteome of a cell, as they can give a very sensitive readout of the relative abundance of a given protein in a cell lysate (Holt, Enever, Wildt, & Tomlinson, 2000; Laffly & Sodoyer, 2005).

1.6.5. Production of Antibodies

1.6.5.1. Generation of Polyclonal Antibodies by Immunising Animals

Immunising and bleeding animals to produce polyclonal sera is a technically straightforward procedure, but one needs to remember that animals must always be injected and bled as safely and painlessly as possible. All immune systems of living species display the property of self-tolerance, i.e., the immune system of an animal is normally not triggered by a self-antigen/protein, in order to protect the animal from autoimmune damage. Therefore, immunisations should always be done in animals that are as far in evolutionary distance from the source of the antigen as possible. Immunisation of closely related species might result in a predominant IgM response due to the lack of T cell recruitment (Lipman et al., 2005).

The choice of animal is usually based on how much serum will be needed, the species from which the target antigen is isolated, whether mAbs will be further needed and how much antigen is available. Rabbits, mice, rats, hamsters and guinea pigs are commonly used in the laboratory because of their small size, and they usually yield bleeds of 100-200 μL (for mouse) to 25 mL (for rabbits). Nevertheless, for most of the commercial applications, larger animals like pigs, horses, sheep and donkeys are used, because larger volumes of serum can be obtained. In case of shortage of antigens, small rodents are preferred because they generally respond better to low doses than larger animals.

Before proceeding to the immunisation, the form and dosage of the antigen needs also to be considered. Particulate antigens, like cells bacteria and virus, are usually much better immunogens than soluble molecules due to their mechanism of phagocytosis. Nevertheless, most soluble antigens can be made more immunogenic by coupling them chemically to larger biomolecules, beads or even cells. The valency of an antigen has a strong impact on its immunogenicity as phagocytosis is triggered by particles> 0.5 μm (Martínez-Riaño et al., 2018) .

Regarding the dose, the optimum amount to achieve the strongest response will vary from host to host. For example, for a sheep, an initial dose of 0.5 to 1 mg of a pure soluble protein antigen in adjuvant (stimulators of the immune response usually injected together with the target antigen) is applied and for further injections this amount can be lowered or kept the same (Harlow & Lane, 1988).

Usually, antibodies start to be detected in the serum 5 to 7 days after the immunisation and persist at low levels for a few days, reaching a peak titre around day 10 (Harlow & Lane, 1988). However, the primary responses are generally very weak, requiring a secondary

immunisation, 2 to 3 weeks later, from which the response is usually different. The number of B cells expressing surface antibodies increases exponentially, reaching a peak between days 3 and 4, and antibodies in the serum reach a peak around days 10-14. Typically, high levels of antibody persist for about 2- 4 weeks after the second injection. After a third immunisation, the immune response appears to be very similar to the one obtained with the previous injection, but the quality of the antibodies in the serum is improved due the maturation process of the B cells (Harlow & Lane, 1988). Further boosts might be administrated but extended intervals are needed so the circulating level of antibody drops enough to prevent rapid clearance of the newly injected antigen (Harlow & Lane, 1988).

Serum samples, taken 7-14 days after each injection, can be assessed by ELISA or another immunoassay technique, against the immunogen, and by comparing the different antibody titres of the different immunisations, the immune response of an animal over time can inferred.

1.6.5.2. Generation of Monoclonal Antibodies by Hybridoma Technology

More than four decades ago César Milstein and Georges J. F. Köhler described the hybridoma technology for generating monoclonal antibodies (mAbs), revolutionising not only biomedical research and diagnostics but also the generation of an arsenal of therapies for many diseases (Köhler & Milstein, 1975). mAbs were first recognized in sera of patients with multiple myeloma in which clonal expansion of malignant plasma cells produced high levels of an identical antibody resulting in a monoclonal gammopathy. The hybridoma technology was then based on fusing B cells from an immunized animal (typically a mouse) with a myeloma cell line and growing the hybrid cells under conditions where unfused normal and tumour cells cannot survive. Hybrid cells are then grown as single cell clones and tested for the secretion of the antibody of interest.

The selection of the hybrid clones is done by using a medium containing hypoxanthine, aminopterin and thymidine (HAT medium), compounds known to be related to biosynthesis of nucleotides. In the presence of aminopterin, tetrahydrofolate cannot be produced, which results in a defect in *de novo* purine synthesis; however, the myeloma cells used for this protocol lack the gene for expressing the enzyme hypoxanthine-guanine phosphoribosyltransferase (HGPRT), which allows them to survive using *de novo* purine synthesis, and therefore only the hybrid cells expressing the HGPRT gene from the myeloma cells will survive in medium containing aminopterin (Milstein, 1999).

1.6.5.3. Generation of Recombinant Antibodies by Phage Display Technology

The phage display technique, created by George Smith in 1985 for displaying polypeptides, is based on the direct linkage between phage phenotype and its encapsulated genotype, which allows the display of molecule libraries on the surface of phage (Smith, 1985). DNA encoding millions of variants of peptides, proteins or fragments can be cloned into the phage genome, as a fusion to the gene encoding one of the phage coat proteins, and upon expression, the coat protein fusion will be incorporated into new phage particles that are assembled in the bacterium, as illustrated in **Figure I.10** (Brien, Aitken, Chames, Hoogenboom, & Henderikx, 2002).

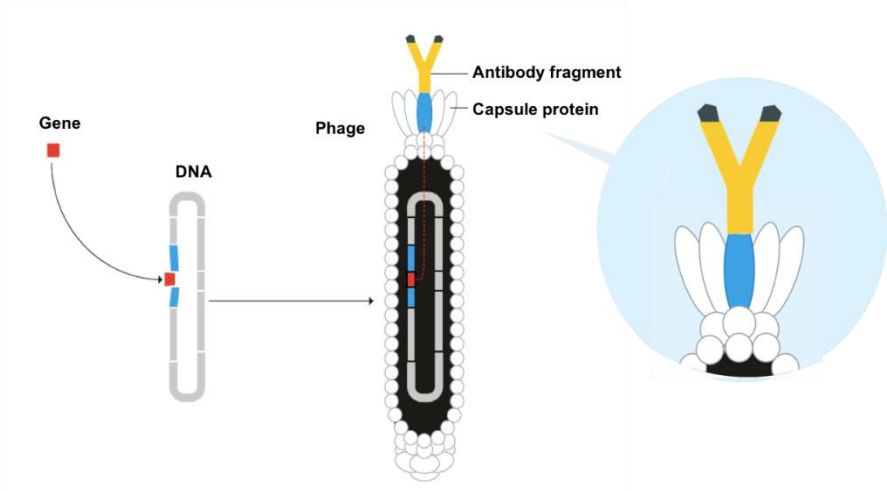

Figure I.10. Principle of phage display technology. The genetic information of the desired antibody is inserted into the phage DNA and ends up being expressed as part of the capsule protein on the surface of the phage, where it is displayed. Adapted from https://www.nobelprize.org/prizes/chemistry/2018/popular-information/.

Phages expressing the desired molecules can be retained by interaction with the target (while unbound phages are washed away) and be recuperated for further infection of a new batch of bacteria for replication and enrichment of those same clones from the library. This selection process, commonly referred to as biopanning, illustrated in **Figure I.11**, is usually repeated 2-4 times, depending on the antibody fragment format and on the type of phage display library (Teixeira & Gonzalez-Pajuelo, 2018). In the end each pool of enriched phages collected after each round of panning can be subjected to affinity analysis by immunoassays, so the enrichment can be confirmed, and individual clones can be selected for expression.

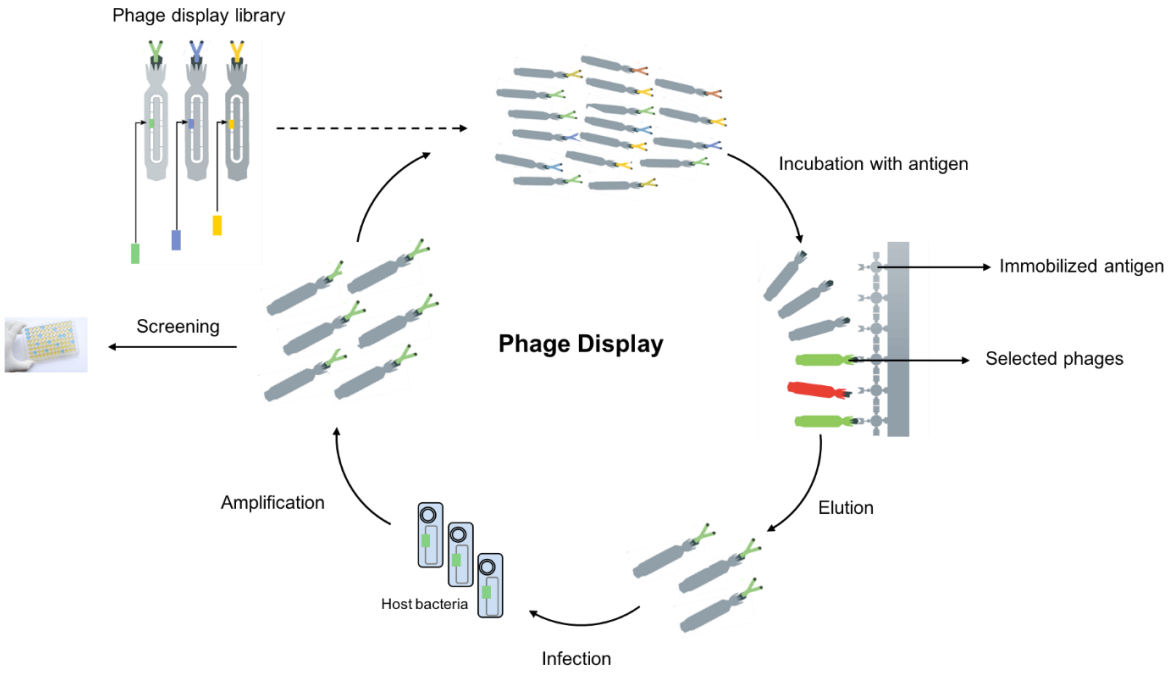

Figure I.11. Schematic representation of the phage display process. Once the antibody library is generated, phages expressing the different clones are incubated with the target antigen for positive selection, in a process called biopanning. After elution from the antigen, the phages are recovered, used to infect new bacteria for amplified and the generation of a more enriched library. This process is usually performed 2-4 times to allow a sufficient enrichment of the specific phages.

Phage display was not only a key stepping stone for the development of tailor-made antibodies, bypassing the classical approach of the hybridoma technology, but also a valuable tool to target novel antigens, and therefore characterize human immune libraries and to study autoimmune diseases (Brien et al., 2002). Synthetic libraries, in particular, because they are not constrained by the immune system, avoid bias caused by any tolerance mechanisms, and therefore screening synthetic peptide phage-libraries is a great approach for obtaining a range of affinity-selected phage clones specific to autoantibodies and to target unique self-epitopes (Hust & Lim, 2002).

1.7. Antibodies Specific to Lipoxidation Products as Promising Diagnostic Tools

Given the very low concentrations and short half-lives of reactive species (half-life for $O_2^{\bullet-}$ and H_2O_2 were reported to be 200 ns in cells (Schmitt et al., 2014)), the *in vivo* oxidative stress levels can only be determined indirectly mainly via the measurement of metabolites

of ROS/RNS, levels of antioxidants, and biomarkers of oxidative damage, such as DNA damage, protein carboxylation, and LPPs, that are more stable than free radicals (Kumar Maurya & Chandra, 2017). In detail, clinically tested biomarkers so far include MDA, HNE and acrolein-lysine adducts, F2-isoprostane (markers of lipid peroxidation), 8-oxo-7,8-dihydro-2′-deoxyguanosine (8-oxodG, a marker of oxidative DNA damage), carboxymethyl-lysine, pentosidine (markers of glycol-oxidation), nitrotyrosine, nitrite/nitrate (markers of nitro-oxidation), and bilirubin oxidative metabolites (a marker of haem oxygenase activity) (Tsukahara & Kaneko, 2014). Studies reporting the detection of these biomarkers use mainly analytical techniques like HPLC, GC and MS, but a recent growth in the use of ELISA assays for the detection of oxidative modified molecules has also been gaining attention (Hsieh, Dantzler, & Weigl, 2017; Noiri & Tsukahara, 2005; Satoh et al., 1999; Uchida, Osawa, Hiai, & Toyokuni, 1995; Weber et al., 2013). Nevertheless, these techniques are still too time consuming for diagnostic or even clinical use, posing the need for the development of easier, more rapid and sensitive assays, such as point-of-care (PoC) tests. PoC testing is one way of dealing with decreasing healthcare budgets by reduce the expensive care in hospitals and encouraging more patients to be assessed and treated in primary care or the community. The total *in vitro* diagnostics (IVD) market is estimated to be worth in excess of US$ 51 billion annually (2011 data) with growth estimated at 7% per annum, of which approximately US$15 billion was PoC testing. Of the total PoC testing market in 2011, 55% of it was in the US, 30% in Europe and 12% in Asia, largely dominated by glucose testing and home pregnancy tests (St John & Price, 2014).

As regards oxidative stress diagnostics, there are four assays that bring laboratory testing to the near-patient testing fields: the FORD (Free Oxygen Radicals Defense) test that measures the presence of antioxidants based on a colorimetric reaction, the FORT (Free Oxygen Radicals Testing) test for measuring hydroperoxyl molecules, also based on a colorimetric reaction, the BAP (biological antioxidant potential) test for measuring the reducing/antioxidant balance on blood samples based on the reduction of Fe^{3+} ions, and lastly, the dROMs (derivatives of reactive oxygen metabolites) test for measurement of hydroperoxides present in blood, through the formation of alkoxyl ($RO^{\cdot}$) and peroxyl ($ROO^{\cdot}$) radicals (Palmieri & Sblendorio, 2007). According to data from 2007, FORT's manufacturers have full IVD certification and CE mark, FORD's has both the IVD and Self Testing Certification, BAP's has the CE mark, while dROMs had still its patent pending. Both FORD and FORT were tested in blood from patients with newly diagnosed type 2 diabetes, where FORT and FORD levels were seen to be increased and decreased, respectively, in diabetic patients, with interassay coefficients of variation of 6.2% and 6.6%, respectively for the FORT and FORD (Pavlatou, Papastamataki, Apostolakou, Papassotiriou, & Tentolouris, 2009).

Apart from these four assays, another reported, yet non-patented, PoC test developed is a rapid lateral flow assay (LFA) that combines electrochemical and colorimetric detection for the measurement of 8-hydroxy-2′-deoxyguanosine (8-OHdG), a DNA oxidative damage biomarker (Kaneko et al., 1970). Nevertheless, despite the substantial number of antibodies specific to lipoxidation products and the very optimistic growth potential for POC testing, so far, no rapid diagnostic tools have been developed for the detection of these oxPTMs. LFA technology, that detect analytes via the use of specific antibodies in only a few minutes, can therefore be a promising approach for the assessment of oxidative stress levels *in vivo*. Information on the functioning of LFAs can be found in the introduction in **CHAPTER IV**.

1.8. Aims of the Project

The strong association between lipoxidation adducts and the development of inflammation responses identifies these adducts as powerful biomarkers for oxidative stress-related pathologies. However, although there is a vast diversity of antibodies specific to many lipid peroxidation products, no attempt has been made, so far, to apply these molecules to the development of rapid diagnostic tests. The overall aim of this project was to understand the immunogenic impact of lipoxidation adducts, as immunogenic, to determine the neo-antigenic epitopes formed when self-proteins are made, and to make antibodies suitable for the deployment in a prototype diagnostic test. To meet this aim, the work was divided in four main tasks, which are detailed in four chapters:

- Chapter II describes the development of synthetic methods for the preparation of lipoxidised proteins and peptides, and the subsequent characterisation and validation of the adducts via mass spectrometry and immunoassays.

- Chapter III reports the application of the lipoxidation adducts (neo antigens) generated in the work described in Chapter II for the generation of polyclonal antibodies through the immunisation of different animals. The immunogenicity of different types of adducts was investigated, and the general structure of the adduct-based epitopes recognised by the generated antibodies was characterised.

- Chapter IV describes the work performed for the development of a lateral flow assay for the detection of HNE adducts, in order to evaluate the diagnostic utility of the in-house generated antibodies.

- Chapter V describes the use of phage display technology for the generation of monoclonal antibody fragments through the construction of Fab and scFv libraries based on RNA extracted from one of the animals immunised with HSA-HNE adducts.

CHAPTER II

GENERATION, DETECTION AND CHARACTERIZATION OF HNE ADDUCTS ON INTACT HUMAN SERUM ALBUMIN AND HUMAN SERUM ALBUMIN SEQUENCE PEPTIDES

2.1. Introduction

2.1.1. Principles of Mass Spectrometry and Instrumentation

Mass spectrometry (MS) is an analytical technique that measures the mass-to-charge ratio (*m/z*) of ionized analytes, and, consequently can be used to measure the molecular mass of proteins/polypeptides and detect the presence of PTMs. Conventionally, a mass spectrometer is composed of an ion source used to ionise the sample, a mass analyser to measure the *m/z* ratio, and a detector that is responsible for converting the ions into electrical signals (Aebersold & Domon, 2006). Regarding the ion sources, electrospray ionisation (ESI) and matrix-assisted laser desorption/ionization (MALDI) are, possibly, the two most commonly used methods (Aebersold & Mann, 2003). In ESI, the ionisation occurs through the use of a strong electric field that converts the macromolecules into small droplets, which later, by application of a direct flow of dry gas, desolvate and create the molecular ions; in MALDI, the sample is ionised by being mixed with matrix first, and then fixed to a metal plate, that upon receiving a pulsed laser radiation, causes the ablation of the sample from the matrix due to the action of a hot plume of gases, creating the molecular ions. As both ESI and MALDI are soft ionisation methods, they can be used to generate molecular ions, which facilitates the analysis of biomolecules such as proteins (Pitt, 1998).

Once the ions have been generated, they are transferred to the mass analyser where they are separated according to their *m/z*, through the action of an electrical or sometimes magnetic field, depending on the type of mass analyser. MALDI is usually coupled to time-of-flight (TOF) analysers that measure the *m/z* of intact peptides, whereas ESI is usually coupled to a combination of ion traps and triple quadrupole instruments, in what is denoted as tandem mass spectrometry (MS/MS). The use of two or more mass analysers is typically applied when structural information is required, something that is achieved by the generation of fragmentation patterns. In a simple manner, tandem MS relies on the first analyser to select specific molecules (the precursor/parent ions), which while moving through a collision cell, get fragmented by the collision with an inert gas (usually nitrogen or argon), and then proceed to the second mass analyser for further analysis. Depending on the collision energy applied, the breakage of the peptide bonds may occur closer to the N terminus or the C terminus of the peptide, producing characteristic fragment ions (Verrastro et al., 2015). Tandem MS has, therefore, been an extremely useful tool for the identification and localisation of lipoxidation sites in peptides, as reported in the literature (Annibal et al., 2016; Milic et al., 2015; Vasil'ev et al., 2014).

2.1.2. Human Serum Albumin: The Most Abundant Protein of the Human Sera

Human serum albumin (HSA) is a monomeric multi-domain macromolecule present in the human plasma. It is known to regulate plasma osmotic pressure, modulate fluid distribution between different body compartments, serve as carrier for endogenous and exogenous substances in plasma, such as bilirubin and fatty acids, and to act as free radical scavenger (Anraku, Chuang, Maruyama, & Otagiri, 2013; Fanali et al., 2012; Petersen, Ha, Harohalli, Feix, & Bhagavan, 2000; Rippe, Kamiva, & Folkow, 1979). HSA is also the most abundant protein in human plasma, accounting for 55-60% of the total protein content, at a typical concentration of approximately 3.5–5.0 g/dL (Turell, Radi, & Alvarez, 2013).

HSA is synthesized in the hepatic cells as preproalbumin, which has an N-terminal peptide that is removed before the nascent protein is released from the rough endoplasmic reticulum. The product, also called proalbumin, is in turn cleaved in the Golgi vesicles to produce the secreted albumin, which is composed of 585 amino acids with a molecular weight of 66,700 Da (Fanali et al., 2012). Structurally, HSA resembles a globular heart-shaped protein composed of approximately 67% α-helices, 23% extended chains, and 10% β-turns, characterized by having no carbohydrate moiety, a scarcity of Trp, Gly, Ile and Met residues and an abundance of charged amino acids such as Cys, Leu, Glu, and Lys (Anguizola et al., 2013).

Because HSA is a negative acute-phase protein, in stressful conditions or acute infections the concentration of the hepatic HSA mRNA is depressed, and HSA is only synthesized in a suitable nutritional, hormonal, and osmotic environment (Fanali et al., 2012). Hepatic cytokines such as interleukin-6 (IL-6) and tumour necrosis factor alpha (TFN-α) appear to be the main regulatory agents, but hormones such as insulin and amino acid deficiencies can also play an important role in HSA synthesis. Studies have shown that levels of HSA may decrease to around 1.5 g/L (Fanali et al., 2012).

Because of its abundance and because it is subject to post-translational modifications, this protein is also considered a very valuable biomarker for diagnosis of many diseases and for the assessment of therapeutic responses (Gundry, Fu, Jelinek, Van Eyk, & Cotter, 2007; Otagiri & Giam Chuang, 2016). Particularly in oxidative stress-related conditions such as chronic liver and kidney diseases and diabetes, the formation of oxPTMs on HSA has been reported (Boisvert, Koski, & Skinner, 2010; Musante et al., 2007; Oettl et al., 2013). However, the determination of the HSA levels *per se* in blood can also constitute a method for assessing in cancer patients the severity and progression of the tumour, and their prognosis (Lam, Leung, & Tse, 2007).

2.1.3. HSA Modifications

HSA has been reported to undergo many different types of modifications, including acetylation, namely on Lys199, Lys402, Lys519 and Lys 545 (Liyasova, Schopfer, & Lockridge, 2010), glycation on Arg410 and Arg525 via a Schiff's base reaction (Ahmed, Dobler, Dean, & Thornalley, 2005), nitration and nitrosylation at Trp and Tyr residues, and oxidation on Cys, Met and Lys residues (Fanali et al., 2012). In fact, oxidation of HSA is a feature in many pathological conditions characterized by oxidative stress, as aforementioned, and it is believed to be an age-related consequence (Era, Kuwata, Imai, Hayashi, & Masaru, 1995). Moreover, HSA has the interesting feature of only containing a single free cysteine in its structure, Cys34, which represents the largest fraction of free thiol in human plasma (Turell et al., 2013). In 70-80% of healthy individuals, this residue is seen in the form of free sulfhydryl group, while in 25-30% it forms a mixed disulphide bond either with cysteine/homocysteine or glutathione. Cys34 can also be oxidized to either sulfonic acid or sulfinic acid, irreversible modifications that have seen augmented in several pathologies (Turell, Botti, Carballal, Radi, & Alvarez, 2009; Turell et al., 2013).

HSA has also been implicated in the formation of protein carbonyls, when subjected to oxidative stress conditions (Aćimović, Jovanović, Srećković, Penezić Romanjuk, & Mandić, 2013; Temple, Yen, & Gronert, 2006). A study has identified HSA as the major carbonylated protein in bronchoalveolar lavage fluid of older smokers, reporting HSA adducts to acrolein and crotonaldehyde at Cys34, His39, Lys351, Lys525, Lys541 and Lys545 (Rossi, Colombo, Carini, Milzani, & Dalle-donne, 2010). The reactivity of HSA to HNE and HHE has also been extensively characterized with adducts being identified at Cys34, His146, Lys199, His242 and His288 (Aldini et al., 2006; Q. Liu, Simpson, & Gronert, 2012).

2.1.4. Chapter II Aims

The aim of the work described in this chapter was to generate, detect and characterize HNE adducts in both intact HSA protein and HSA sequence peptides, for later use as antigen for generation of anti-HSA-HNE antibodies. For this purpose, both the intact protein and the synthesized peptides were treated with HNE at different molar ratios on aqueous solutions to mimic physiological conditions and analysed by immunoassays and mass spectrometric methodologies.

2.2. Reagents

Human serum albumin (product code: A1653) and albumin from chicken egg white (product code; A5503) were obtained from Sigma-Aldrich. Alpha-1 antitrypsin (A1AT) from human plasma (≥95% (SDS-PAGE)) was purchased from Merck (Germany). 4-hydroxynonenal-diethylacetal (HNE-DEA) was generously supplied by Prof. Giancarlo Aldini from University of Milan. HNE was prepared from HNE-DEA by 1mM aqueous HCl hydrolysis (1 h at room temperature) and quantified by UV spectroscopy (λ_{max}=224 nm; ε=13,750 L mol-1cm- 1). Fluorenylmethyloxycarbonyl (Fmoc) protected amino acids were purchased from Intavis (20×1 cartridge of 0.5 mmol of Fmoc-Ala-OH, Fmoc-Arg (Pbf)-OH, Fmoc-Asn(Trt)-OH, Fmoc-Asp(OtBu) OH, Fmoc-Cys (Trt)-OH, Fmoc-Gln (Trt)-OH, Fmoc-Glu (tBu)-OH, Fmoc-Gly-OH, Fmoc-His (Trt)-OH, Fmoc-Ile-OH, Fmoc-Leu-OH, Fmoc-Lys (Boc)-OH, Fmoc-Met-OH, Fmoc-Phe-OH, Fmoc-Pro-OH, Fmoc-Ser(OtBu)-OH, Fmoc-Thr (tBu)-OH, Fmoc-Val-OH). Fmoc-PAL-PEG-PS resin was acquired from Thermo Fisher Scientific (UK) and 1-methyl 2-pyrrolidinone (NMP), dimethylformamide (DMF), 1,3-diisopropylcarbodiimide (DIC), 1-hydroxybenzotriazole (HOBt), acetonitrile, formic acid, dichloromethane (DCM), and ethanol were purchased from Rathburn chemicals Ltd (Walkerburn, Scotland). Trifluoracetic acid (TFA), triisopropylsilane (TIPS) and piperidine were obtained from Sigma. Commercial goat polyclonal antibody anti-HNE (Ab46544) was purchased from Abcam, and 3,3′,5,5′-tetramethylbenzidine (TMB) and HRP-labelled anti-goat IgG were purchased from Sigma Aldrich (UK). All solvents were of LC-MS grade and all solutions were prepared using ultra-pure Milli-Q water. All other reagents were of analytical grade.

2.3. Materials and Methods

2.3.1. Solid-Phase Peptide Synthesis

Synthetic peptides were synthesized by fluorenylmethyloxycarbonyl (Fmoc) chemistry on a Liberty Automated Synthesizer controlled by Pepdriver software. The Fmoc-PAL-PEG-PS resin was loaded into the reaction vessel at final concentration of 0.1 mM and the Fmoc protected amino acid derivatives were individually added into flasks at final concentrations of 0.2 M in dimethylformamide (DMF).

The peptide synthesis was performed by cycles of coupling, deprotection and washes. Once the resin was swollen in DMF, the first amino acid was added in the presence of 1,3-diisopropylcarbodiimide (DIC) and 1-hydroxybenzotriazole (HOBt), for activation of the carboxylic group (coupling step) and then 20% v/v piperidine in DMF was added for removal of the Fmoc group (deprotection step). The resin was drained and washed with DMF at the

end of each step to remove excess reagents. This process was repeated sequentially for each peptide sequence and the list of specific reagents and corresponding volumes used for each synthesized peptide is in **Appendix 2**, **Appendix 3** and **Appendix 4**.

Once the synthesis was finished, the resin was transferred to a 25-mL fritted filtration column (Fisher Scientific, UK) and washed twice with dichloromethane (DCM) and twice with ethanol and then freeze-dried for 1-2h. The resin-bound peptides were cleaved from the resin with a trifluoracetic acid (TFA) containing mixture (0.5 mL of H_2O, 0.5 mL of TIPS and 20 mL of TFA) at room temperature for 2 h. TFA and solvents were further removed on the rotary evaporator to leave a crude residue. Solid crude peptides were then precipitated in cold diethyl ether, dried under a stream of air, dissolved in 50:50 (v/v) H_2O/Acetonitrile (ACN) and freeze-dried overnight to yield a white solid.

For synthesis of biotinylated peptides, the same protocol was applied but the resin used was the Fmoc-PEG Biotin NOVATag™ from Merck Millipore (Darmstadt, Germany).

2.3.2. Peptide Purification by High Performance Liquid Chromatography

Crude peptides were purified on a Kinetix® C18 HPLC column, pore size 100 Å, dimensions 250 x 4.6 mm (Phenomenex) in a Dionex Ultimate 3000 HPLC system (Thermo Fisher, UK) , using a linear gradient from 95% solvent A (5% v/v acetonitrile, 95% v/v water, plus 0.1% TFA) to 100% of solvent B (100% acetonitrile plus 0.1% TFA) for approximately 30 min at a flow rate of 2.5 ml/min.

After column equilibration for 5 min, the crude peptide was dissolved in solvent A at a concentration of 1 mg/mL and aliquots of 200 μL were injected using the automated HPLC injector. The absorbance (Abs) was monitored at 230 nm and 280 nm. The main HPLC peaks were collected for further assessment by MS. Once the identity of the desired peptide was confirmed, an automated sequence of injections was set up and executed to purify all the peptide solution. The HPLC fractions of interest were collected, combined and freeze-dried overnight, and peptides were stored at -20°C until further use.

2.3.3. Liquid Chromatography-Electrospray Mass Spectrometry Analysis to Confirm Synthetic Peptide Identity

To confirm the molecular mass of the synthesized peptides, 0.1-0.5 μg of the dried peptide stock was dissolved in 200 μL of solvent A (5% v/v acetonitrile, 95% v/v water plus 0.1% formic acid) and analysed by LC-ESI-MS in positive ion mode, using a Waters 2690XE HPLC coupled to a ZMD2000 Quadrupole Mass Spectrometer (MS). Separations were carried out on a reversed-phase elution with a Kinetex® C18 column (pore size: 100 Å; dimensions: 100 x 2.10 mm), using a 21-min linear gradient from 95% of Solvent A (5% v/v acetonitrile, 95% v/v water, plus 0.1% formic acid) to 90% of Solvent B (100% acetonitrile plus 0.1% formic acid), followed by a 7-min equilibration period. Samples were injected in volumes of 100 μL, and a flow rate of 0.3 mL/min was used.

ESI-MS analyses were carried out by setting the ESI source to positive-ion mode and using capillary temperature of 150C, capillary potential of +2.5-4.0 kV, cone at 70 V, extractor at 1-5 V and RF lens at 0.5 V. The flow rate of the nebulizer gas (nitrogen) was 5 L/min and acquisition was performed using 1-minute scans within the *m/z* of 200-2000 Da.

2.3.4. Generation of HNE Adducts on HSA, HSA Peptides, OVA and A1AT

For the generation of HNE adducts, 0.1 mL aliquots of each protein/peptide (at a concentration of 10 mg/mL in PBS) were reacted with HNE (stock concentration of 5.2 mg/mL in 1 mM HCl) at a molar ratio of 1:1, 1:5 or 1:10 for 2 h at 37°C. The concentration of each reaction was then adjusted to 1 mg/mL by addition of 0.9 mL of PBS. All the reactions performed in this chapter were all done using the same batch of HNE and each of these HNE reactions was performed in triplicate (n=3).

2.3.5. Identification of HNE Modifications on Synthetic HSA Peptides by LC-MS/MS

Peptides were individually analysed using an Ultimate 3000 HPLC system (Thermo Scientific, UK) coupled to a 5600 TripleTOF MS (ABSciex, Warrington, UK). Briefly, each purified peptide was resuspended in 2% v/v acetonitrile 0.5% v/v formic acid and loaded onto a C18 trap column (C18 PepMap™, 5 μm, 0.5 x 5 mm, Thermo Scientific, UK) at 30 μL/min in 2% v/v acetonitrile 0.5% v/v formic acid followed by a 4 minute wash, before

separation on a nano-HPLC column (C18 PepMap™, 5 µm, 0.075 x 150mm, Thermo Scientific, UK) at 300 nL/min using a gradient elution running from 2% to 45% aqueous acetonitrile, 0.1% v/v formic acid over 45 minutes. Ionization of the peptides was achieved by electrospray using a voltage of 2.4 kV, a source temperature of 150°C, declustering potential of 100V, nebulizer gas flow of 15 L/min and a curtain gas setting of 25 psi. Survey scans were collected in positive mode from *m/z* 350 to 2000 Da using high-sensitivity TOF-MS mode. All the LC-MS/MS experiments ware performed in triplicate (n=3).

2.3.6. Identification of HNE Modifications on HSA by Matrix-Assisted Laser Desorption/Ionization Time-of-Flight (MALDI-TOF) MS

The analysis of native HSA and HNE modified HSA samples by MALDI-TOF MS was performed on a Bruker Autoflex Speed MS (Bruker, MA, USA) using a sinapinic acid matrix (10 mg/mL in 70:30 (v/v) water/acetonitrile with 0.1% TFA) as the matrix in positive ion mode. A 20 µL aliquot of each sample was desalted using a mixed bed ion exchange resin (Amberlite MB-9L from Sigma-Aldrich), and 1 µL of desalted sample was spotted onto the MALDI plate and allowed to dry naturally. Finally, 1 µL of matrix solution was spotted onto the dry sample and allowed to dry at room temperature before analysis. MALDI-TOF analysis were only performed once (n=1).

2.3.7. Identification of HNE Modifications on HSA by LC-MS/MS of Tryptic Digested HSA Peptides Modified by HNE

HNE-modified HSA samples (50 µg) were digested with trypsin according to the Filter Aided Sample Preparation (FASP) protocol. Briefly, proteins were reduced with dithiothreitol (DTT) (100 mM, 1 h, at room temperature), transferred onto a Microcon centrifugal filter (30 KDa cut-off) by centrifugation at 14 000 × g, alkylated in situ with iodoacetamide (50 mM, 20 min in the dark), washed twice with urea buffer (8 M Urea, 100 mM Tris-HCl, pH 8.5) and two times with ammonium bi-carbonate buffer (50 mM) before digestion with trypsin (1:25 enzyme to protein ratio w/w) overnight at 37°C in a humidified environment. Peptides were recovered in ammonium bicarbonate buffer (50 mM), dissolved at 250 ng/µL in 3% (v/v) acetonitrile in water and used for LC-MS analysis using a nano-ACQUITY UPLC system (Waters GmbH, Eschborn, Germany) coupled online to an LTQ Orbitrap XL ETD mass spectrometer equipped with a nano-ESI source (Thermo Fischer Scientific, Bremen, Germany). Eluent A was formic acid (0.1% v/v) in water and Eluent B was formic acid (0.1%

v/v) in acetonitrile. Samples (10 µL injection) were diluted in Eluent A and loaded onto the trap column (nano Acquity Symmetry C18; internal diameter 180 µm, length 20 mm, particle diameter 5 µm) at a flow rate of 10 µL/min. The separation was performed using a BEH 130 column (C18 column, internal diameter 75 µm, length 100 mm, particle diameter 1.7 µm) at a flow rate of 0.4 µL/ min, with a linear gradient from 3% to 30% of eluent B over 18 min and then to 85% of eluent B over 1 min. The transfer capillary temperature was set to 200°C and the tube lens voltage to 110 V. An ion spray voltage of 1.6 kV was applied to a PicoTip online nano-ESI emitter (New Objective, Berlin, Germany). The precursor ion survey scans were acquired on an Orbitrap MS with resolution of 60,000 at *m/z* 400 across a range from *m/z* 400 to 2000. CID tandem mass spectra (isolation width 2.00, activation Q 0.250, normalized collision energy 35.0%, activation time 30.0 ms) were recorded in the linear ion trap by data-dependent acquisition (DDA) for the top six most abundant ions in each survey scan with a dynamic exclusion of 60 s using Xcalibur software 3.0 (Thermo Fischer Scientific, Bremen, Germany). All LC-MS/MS experiments were performed in triplicate (n=3).

2.3.8. Identification of Tryptic Peptides of HSA Modified by HNE Using Sequest Search Engine

HNE modifications were identified using the Sequest search engine (Proteome Discoverer 1.4, Thermo Scientific) against *Homo sapiens* (Human) database, allowing up to two missed cleavages and a mass tolerance of 10 ppm for precursor ions and 0.8 Da for product ions. Oxidation of methionine and cysteine, carbamidomethylation (CAM) of cysteine, HNE Michael adducts (on cysteine, lysine and histidine) and Schiff's base adducts (on lysine) were used as variable modifications and results were filtered for rank 1 peptides and score vs. charge states corresponding to Xcorr/z 2.0/2, 2.25/3, 2.5/4, 2.75/5.

2.3.9. Identification of HNE Modifications on HSA, OVA and A1AT by direct ELISA

96-well microtiter plates (Corning, MA, USA) were coated with 100 µL of both HNE treated and non-treated proteins in a concentration range from 0 to 1 µg/mL, overnight at 4°C. Following aspiration of the antigen solution, the plates were washed three times with tris-buffered saline, 0.1% Tween 20 (TBST), and the wells were blocked with 120 µL of 1% (w/v) BSA/PBS for 1 h at room temperature. After another three-wash step with TBST, 100

µL of the anti-HNE pAb (Ab46544; Abcam) was added to each well and the plate was left to incubate for 1 h with shaking at room temperature. The wells were once again washed three times with TBST and the plate was further incubated with 100 µL of mouse anti-goat IgG (AP labelled) in 1% (w/v) BSA/ PBST, for 1 h with shaking at room temperature. The detection was done using pNPP (Thermo Fisher Scientific, USA) and the absorbance was read at 405 nm using a microplate reader. The assay was performed in duplicate (n=2), with technical triplicates.

2.3.10. Statistical Analysis

Data depicted in **Figure II.14** were analysed in two different ways as the assay was only performed in duplicate (n=2). Firstly, data was analysed individually using o one-way analysis of variance (ANOVA) tests with Microsoft Excel to assess significative differences between the three HNE molar ratios used on each individual set of proteins. Secondly, combined data was analysed with software R using the non-parametric Kruskal-Wallis rank sum test (non-parametric alternative to one-way ANOVA test) as the data did not meet the criteria required for one-way ANOVA tests. For the combined data Post hoc Dunn tests was further performed for multiple comparison of groups and a significance threshold was set to 0.0083 – Bonferroni Correction –, since six different tests were performed.

2.3.11. SDS-PAGE of HNE Modified Proteins

Sodium dodecyl sulfate–polyacrylamide gel electrophoresis (SDS–PAGE) was performed to evaluate the profile of the modified and non-modified proteins. Samples were prepared in Laemmli buffer 4% SDS, 20% glycerol, 10% 2-mercaptoethanol, 0.004% bromophenol blue and 0.125 M Tris HCl, pH 6.8) and heated at 100◦C for 5 min. Samples were loaded onto a 12% acrylamide gel, prepared using 40% acrylamide/bis (29:1), 10% ammonium persulfate and 10% SDS stock solutions (following the standardized Bio-Rad protocol), and run at 100 mV using as running buffer 192 mM glycine, 25 mM Tris-HCl and 0.1% SDS, pH 8.3. Gels were stained with Coomassie Brilliant Blue (Pharmacia, Uppsala, Sweden). Images were acquired with the Gel Doc EZ System from Bio-Rad (CA, USA).

2.3.12. Western Blotting of HNE Modified Proteins

For the western blot analysis, HNE treated proteins were run on 12% SDS-PAGE gels and separated following the conditions described before. Proteins were transferred from the gel

to polyvinylidene fluoride (PVDF) membranes using the Trans-Blot Turbo Transfer System (Bio-Rad, CA, USA). The membranes were blocked overnight at 4°C with AdvanBlock-PF blocking solution (Advansta, Inc, CA, USA) and then incubated with the primary antibody (Abcam anti-HNE, dilution 1:10000), for 1h at room temperature. The membranes were then washed with AdvanWash washing solution (Advansta, Inc, CA, USA) three times for 10 min and incubated with the secondary antibody (HRP-labelled anti-sheep and anti-goat, dilution 1:10000). The detection was carried out with WesternBright Sirius ECL (Amersham, UK), using the ChemiDoc™ XRS+ System (Bio-Rad, CA, USA). The results were interpreted by densitometry analysis using the software ImageJ, Version 1.48.

2.3.13. Bio-layer Interferometry

OctetRED96 (FortéBio Inc.) was used to measure the association and dissociation rates of the commercial antibody anti-HNE to the modified HNE-modified biotinylated ^{31}LQQCPFE^{37} peptide through bio-layer interferometry. The binding assay was performed in a 96-well plate using Dip and Read™ Streptavidin coated biosensors. The peptide ^{31}LQQCPFE^{37} was resynthesized with a biotin tag at the C-terminal for immobilization to the streptavidin biosensors. The biotinylated peptide was reacted with HNE as mentioned before, and the HNE-peptide adduct was purified by reverse-phase HPLC. The ligand concentration used for the assay was 2 µg/mL, and all the steps were performed at 30°C with the plate shaking speed set at 1000 rpm. The antibody and antigens solutions were diluted in a Kinetics Buffer from FortéBio Inc, containing PBS + 0.1% w/v BSA, 0.02% v/v Tween20 and 0.05% w/v sodium azide, at pH 7.4 and used as a ligand for the anti-HNE commercial pAb.

Eight Dip and Read™ Streptavidin coated biosensors were dipped into the biotinylated ^{31}LQQCPFE^{37}-HNE adduct solution for 10 min, and the association data was acquired for 15 min from solutions of pAb anti-HNE where the concentration was varied between 64 nM to 1 nM by 1:2 serial dilution. After the equilibrium was reached, the dissociation step was carried out over 20 min in Kinetics Buffer (provided from ForteBio). The assay data were processed using Data Analysis (version 6.3, ForteBio) to obtain kinetic values. Briefly, a buffer blank was used as a reference cell subtraction and the data series was evaluated using a global fit algorithm for 1:1 binding interaction, assuming that an immobilized ligand protein and analyte bind to each other with an association rate constant (K_{on}) and dissociate with a dissociation rate constant (K_{dis}). The association rate = K_{on} [ligand][analyte] and the dissociation rate = K_{dis} [ligand-analyte]. At equilibrium, forward and reverse rates are equal. Hence, the equilibrium dissociation (or affinity) constant, K_D, is equal to K_{dis}/K_{on} = [ligand][analyte]/[ligand-analyte].

2.4. Results

2.4.1. Design of Key Model HSA Sequence Peptides

The use of synthetic peptides as a means to generate antibody reagents is a very common procedure when specific targeted antibodies are desired. By immunizing with a particular sequence of a protein, antibodies can be raised against unique regions such as highly conserved regions, active sites or even regions of post translation modification.

As stated before, one of the aims this chapter was to synthesize key peptides from HSA which can be, in theory, highly subjected to HNE modifications, and identify and characterize those same HNE adducts. According to the literature, Cys34, His146 and Lys199 were reported to be the three most reactive HNE-adduction sites on HSA (Aldini et al., 2006), and therefore, peptide sequences containing these three residues were synthesized for further assessment. The red, blue and purple peptide chains highlighted in both panels A and B of **Figure II.1** represent the peptide sequences containing the residues Cys34, His146 and Lys199, respectively, which are located on the surface of the protein, making the amino acids prone to be attacked and consequently more easily modifiable by HNE. Cys34 and the adjacent amino acids (red sequence) are rearranged in a β-pleated sheet, while His146 and Lys199 together with its respective adjacent amino acids (light blue and purple, respectively) are part of α-turns. These characteristics are important when considering the generation of antibodies as the response of the immunity system is dictated by the structural differences between the antigen and the host's self-proteins (Benjamin et al., 1984). According to Aldini *et al,* HNE forms Michael adducts with Cys34 and His146, while with Lys199 yields a Schiff's base adduct (Aldini et al., 2006). HSA sequences containing these three amino acid residues were therefore synthesized for assessment of HNE-adducts formation.

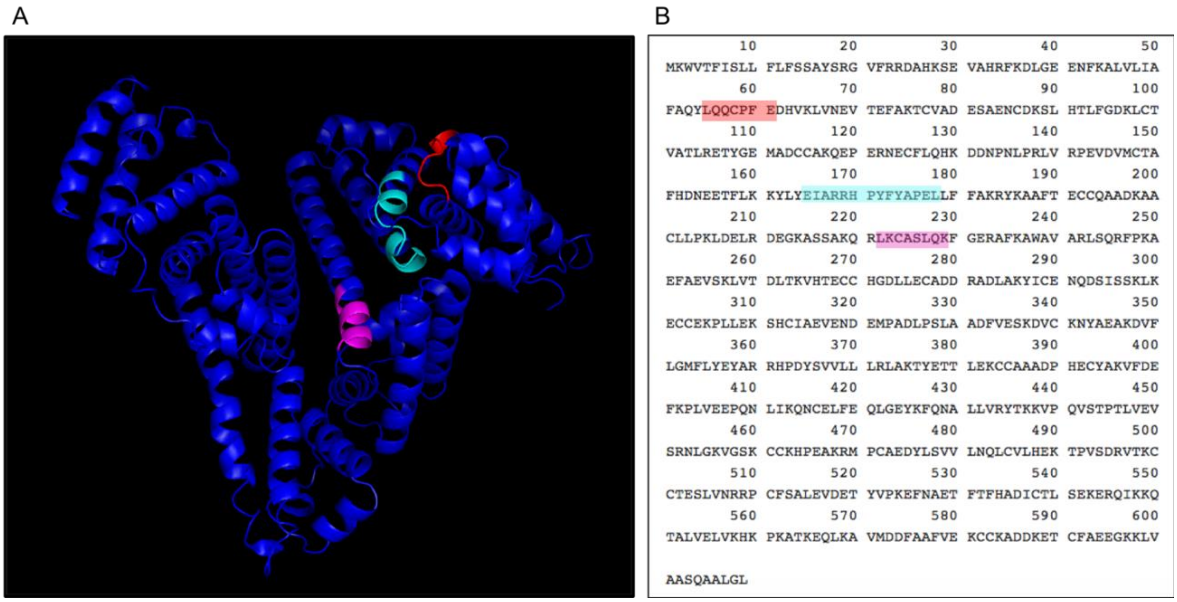

Figure II.1. Location of Cys34 (red), His146 (light blue) and Lys199 (purple) residues in the 3D molecular structure of human serum albumin (**PBD FILE: 1AO6) (A) and in the amino acid sequence (B).** Peptides ^{31}LQQCPFE^{37}, ^{141}EIARRHPYFYAPEL^{154}, ^{198}LKCASLQK^{205} containing these three key amino acids were selected for chemical synthesis and HNE treatment.

2.4.2. Synthesis of HSA Peptide Sequences

Three HSA peptide sequences containing the three most reactive HNE-adduction sites were synthesized by FMOC chemistry using a solid phase peptide synthesis method according to well-established methods (Behrendt, White, & Offer, 2016). The amino acid sequences, chemical formulas and monoisotopic masses of each individual peptide and respective HNE adduct are presented in **Table II.1**. Due to the resin used, all the synthesised peptides have an amide group at the C-terminal, and both the ^{41}EIARRHPYFYAPEL^{154} and ^{198}LKCASLQK^{205} peptides have as well an acetyl group at the N-terminal to avoid reaction between the HNE and the common free amine at the free peptide N-termini. Each peptide purified by reverse-phase liquid chromatography and their masses were confirmed by ESI-MS.

Table II.1. List of key HSA peptides synthesized based on a study where the residues Cys34, Lys199 and His146 were identified as the most reactive HNE-adduction sites of HSA (Aldini et al., 2006)**.** For each peptide, their corresponding amino acid sequence, chemical formula, average molecular weight and monoisotopic mass is presented, together with the monoisotopic mass of the expected HNE adduct (MA for Michael adduct and SB for Schiff's base). Both the ^{41}EIARRHPYFYAPEL^{154} and ^{198}LKCASLQK^{205} peptides have an amide group at the C-terminus and an acetyl group at the N- terminus, while the ^{31}LQQCPFE^{37} has only the amide group at the C-terminus.

Peptide Sequence and Chemical Formula	Average MW (g/mol)	Monoisotopic Mass	Monoisotopic mass of peptide-HNE* Adduct
NH_2-^{31}LQQCPFE^{37}-$CONH_2$ $C_{38}H_{58}N_{10}O_{11}S$	862.99	862.3994	1018.5144 (Single MA) 1174.6295 (Double MA)
$AcNH_2$-^{141}EIARRHPYFYAPEL^{154}-$CONH_2$ $C_{85}H_{123}N_{23}O_{28}$	1803.02	1801.9237	1958.0387 (Single MA)
$AcNH_2$-^{198}LKCASLQK^{205}-$CONH_2$ $C_{40}H_{74}N_{12}O_{11}S$	931.15	930.5305	1086.6455 (Single MA) 1242.7606 (Double MA) 1068.6305 (Single SB)

*Monoisotopic mass of HNE: 156.1150

The HSA peptide sequence ^{31}LQQCPFE^{37} was selected based on the presence of Cys34, the only free cysteine present in the whole protein. Upon completion of the synthesis of the peptide, the crude solution was loaded on a reverse-phase chromatography column for peptide purification (**Figure II.2 A**) and its mass was confirmed by ESI-MS (**Figure II.2 B**).

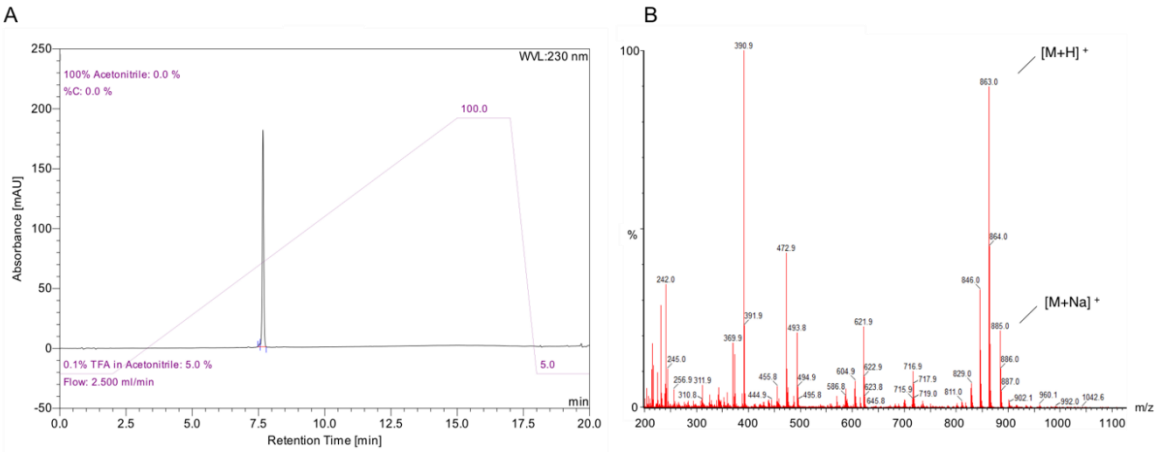

Figure II.2. HPLC chromatogram (A) and MS spectra (B) obtained for purified ^{31}LQQCPFE^{37} HSA peptide (monoisotopic mass: 862.40). The crude peptide was initially dissolved in 5% v/v acetonitrile, 95% v/v water, plus 0.1% TFA, to a concentration of 1 mg/mL, all eluted peaks were collected for MS analysis and once the peak corresponding to the HSA peptide was identified further HPLC runs were set up for purification of that single product. In the end all the fractions were combined, the peptide was freeze dried, and analytical runs by HPLC (A) and ESI-MS (B) were performed for confirmation of purity.

The mass spectrum (MS) depicted in **Figure II.2 B** exhibits a peak at *m/z* 863.0 which corresponds to the protonated pseudo molecular ion, $[M+H]^+$, suggesting that the peptide was successfully synthesized. The peak at *m/z* 885.0 was identified as the sodiated molecular ion, $[M+Na]^+$ and the other minor peaks observed at lowers *m/z* correspond to impurities that co-eluted with the peptide.

The HSA peptide sequence ^{141}EIARRHPYFYAPEL^{154} was selected based on the presence of His146, considered to be one of the most HNE-reactive sites. Again, once the synthesis of the peptide was completed, the crude solution was loaded on a reverse-phase chromatography column for peptide purification (**Figure II.3 A**) and its mass was confirmed by ESI-MS (**Figure II.3 B**).

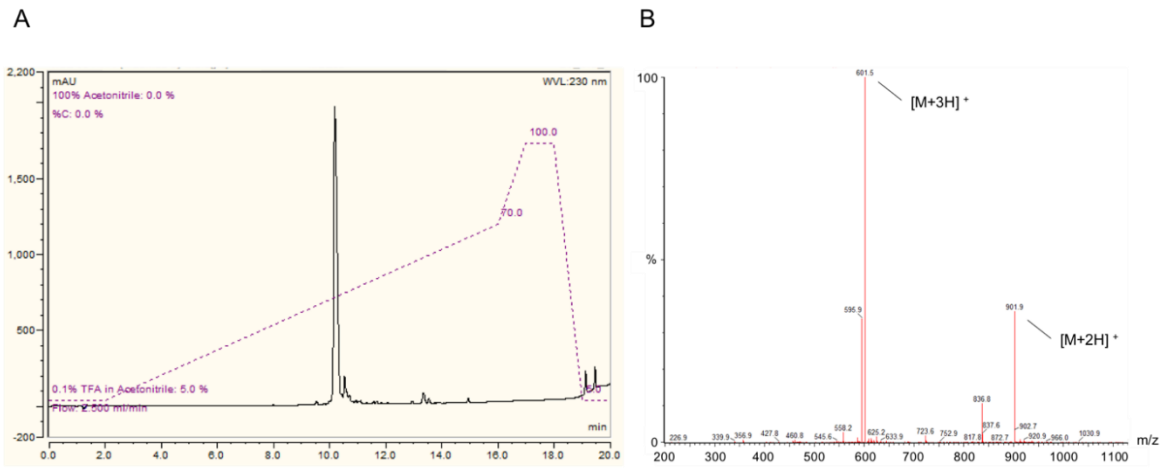

Figure II.3. HPLC chromatogram (A) and MS spectra (B) obtained for purified ^{141}EIARRHPYFYAPEL^{154} HSA peptide (monoisotopic mass:1801.93). The crude peptide was initially dissolved in 5% v/v acetonitrile, 95% v/v water, plus 0.1% TFA, to a concentration of 1 mg/mL, all eluted peaks were collected for MS analysis and once the peak corresponding to the HSA peptide was identified further HPLC runs were set up for purification of that single product. In the end all the fractions were combined, the peptide was freeze dried, and analytical runs by HPLC (A) and ESI-MS (B) were performed for confirmation of purity.

The MS in **Figure II.3 B** shows two main peaks at m/z 601.5 and 901.9, corresponding to the ion $[M+2H]^{2+}$ and $[M+3H]^{3+}$, respectively, confirming the correct synthesis of the peptide. The peaks at m/z 595.9 and 620.2 are again thought to be impurities or peptide fragments.

The peptide sequence ^{98}LKCASLQK^{205}, was selected for synthesis due the presence of the residue Lys199, another amino acid considered to be one of the most HNE-reactive sites. The peptide was purified by reverse phase liquid chromatography (**Figure II.4 A**) and the mass was confirmed by ESI-MS (**Figure II.4 B**).

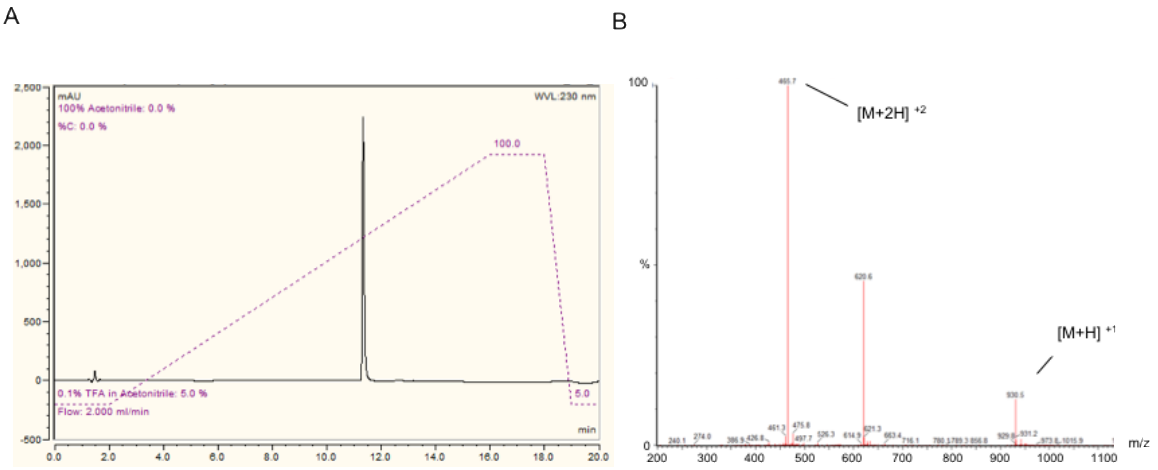

Figure II.4. HPLC chromatogram (A) and MS spectra (B) obtained for purified ^{198}LKCASLQK^{205} HSA peptide (monoisotopic mass: 930.53). The crude peptide was initially dissolved in 5% v/v acetonitrile, 95% v/v water, plus 0.1% TFA, to a concentration of 1 mg/mL, all eluted peaks were collected for MS analysis and once the peak corresponding to the HSA peptide was identified further HPLC runs were set up for purification of that single product. In the end all the fractions were combined, the peptide was freeze dried, and analytical runs by HPLC (A) and ESI-MS (B) were performed for confirmation of purity.

The peptide ^{198}LKCASLQK^{205} was identified on the MS spectra (**Figure II.4 B**) by the peaks observed at *m/z* 930.6 and 465.7 corresponding to the ions $[M+H]^+$ and $[M+2H]^{2+}$, respectively. The ion peak observed at *m/z* 620.6 is an impurity co-eluted with peptide of interest.

2.4.3. Detection of HNE Modifications on HSA Peptides by LC-MS

Purified peptides ^{31}LQQCPFE^{37}, ^{141}EIARRHPYFYAPEL^{154} and ^{198}LKCASLQK^{205} were individually incubated with HNE at a 1:10 protein:HNE molar ratio and the reaction products were analysed by ESI-MS.

The total ion chromatogram (TIC) obtained for the HNE-treated ^{31}LQQCPFE^{37} peptide depicted in **Figure II.5 A** shows the presence of one main peak (retention time (RT): 35 min) followed by four other minor peaks with longer RTs. As seen in the extracted-ion chromatogram (XIC) in **Figure II.5 B**, the main peak (RT: 35 min) corresponds to the elution of the non-modified peptide (*m/z* 863.413) but comprises as well the elution of an HNE-modified form of the peptide with an *m/z* = 1019.534 (**Figure II.5 C**), that corresponds to the formation of an HNE Michael adduct. The peaks with longer RTs relates to the formation of a double HNE-modified peptide (**Figure II.5 D**) as seen by the presence of a product with an *m/z* = 1175.656, that corresponds to the formation of two HNE Michael adducts. It is

worth noting that the addition of a single HNE molecule to the peptide seemed to not affect the elution time of the peptide, as it eluted at a very similar time to the non-modified peptide, but the addition of two HNE molecules makes the peptide to bind more strongly to the column and to only elute 5-7 s later.

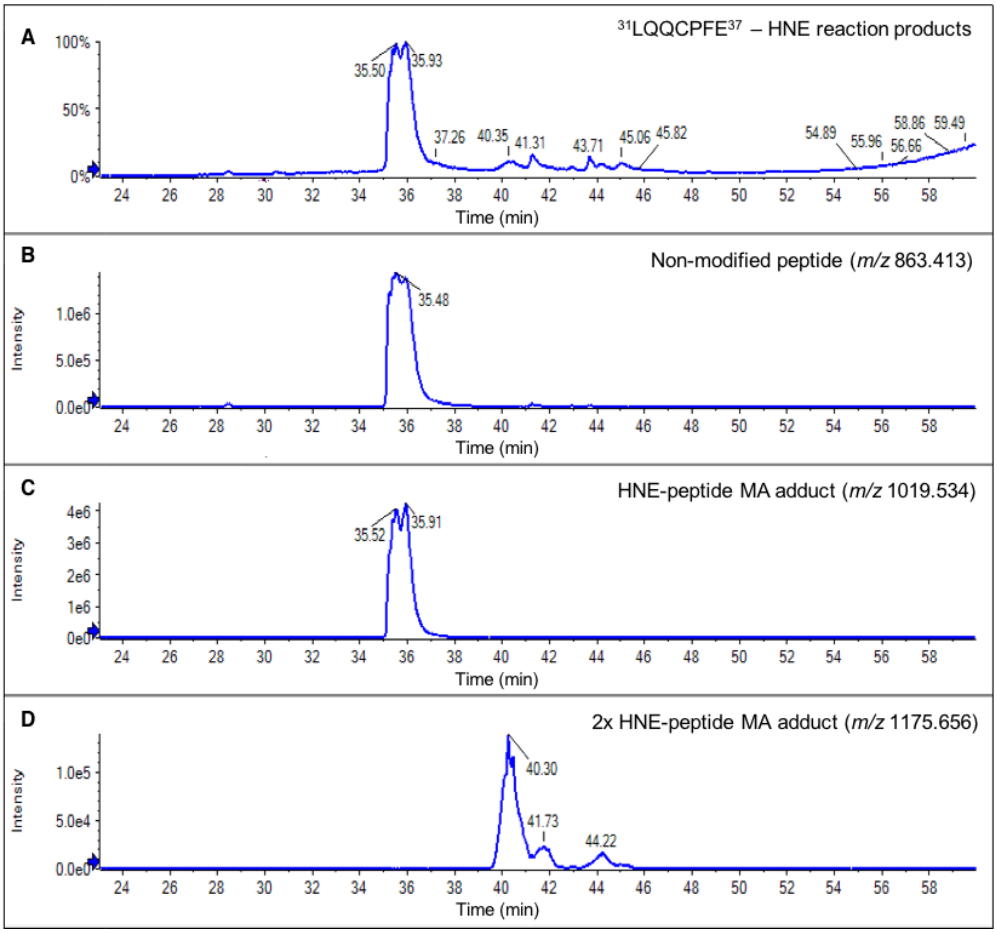

Figure II.5. Identification of the products formed by reacting peptide ^{31}LQQCPFE^{37} with HNE at a peptide-HNE molar ratio of 1:10; and their respective difference in the retention time. The TIC chromatogram of the total reaction products (A) show a main peak at R_t 35 min corresponding to the prediction of the non-modified peptide (*m/z* 863) (B) and one HNE Michael adduct (*m/z* 1019), and a few other peaks with longer RT corresponding to a two HNE Michael adduct (*m/z* 1175). The experiment was performed in triplicate (n=3).

Regarding the peak at RT 35.736 min, the spectrum in **Figure II.6 A** confirms the co-elution of both non-modified peptide and one Michael Adduct (MA)-HNE-peptide species in the same elution peak. The formation of a MA-HNE-peptide adduct is confirmed by the presence of the ions peak at *m/z* 1019.5 (corresponding to the protonated molecular ion $[M+HNE+H]^+$), while the presence of the non-modified ^{31}LQQCPFE^{37} peptide is confirmed by the presence of the ions peaks $[M+H]^+$ *m/z* 863.4 and $[M+2H]^{2+}$ *m/z* 432.19, which correspond to the predicted mass of the native peptide.

The formation of a double MA-HNE-peptide adduct (predicted *m/z* 1174) is shown in the MS spectrum relative to the peak at RT 40.397 min (**Figure II.6 B**). The ion peaks at *m/z* 1175.65 and 579.31 correspond to the protonated molecular ion $[M+2HNE+H]^+$ and to the double charged molecular ion $[M+2HNE-18+2H]^{2+}$, respectively. This last molecular ion suggests that one of the MA adducts suffered a rearrangement to a Schiff's Base adduct due to the loss of 18 amu (equivalent to a molecule of water). The presence of the ion peaks at *m/z* 863 ($[M+H]^+$), *m/z* 1019.5 ($[M+HNE+H]^+$) and *m/z* 510.24 ($[M+HNE+2H]^{2+}$) show that the non-modified peptide and the single MA-HNE-peptide adduct are also co-eluting with the double- MA-HNE-peptide adduct.

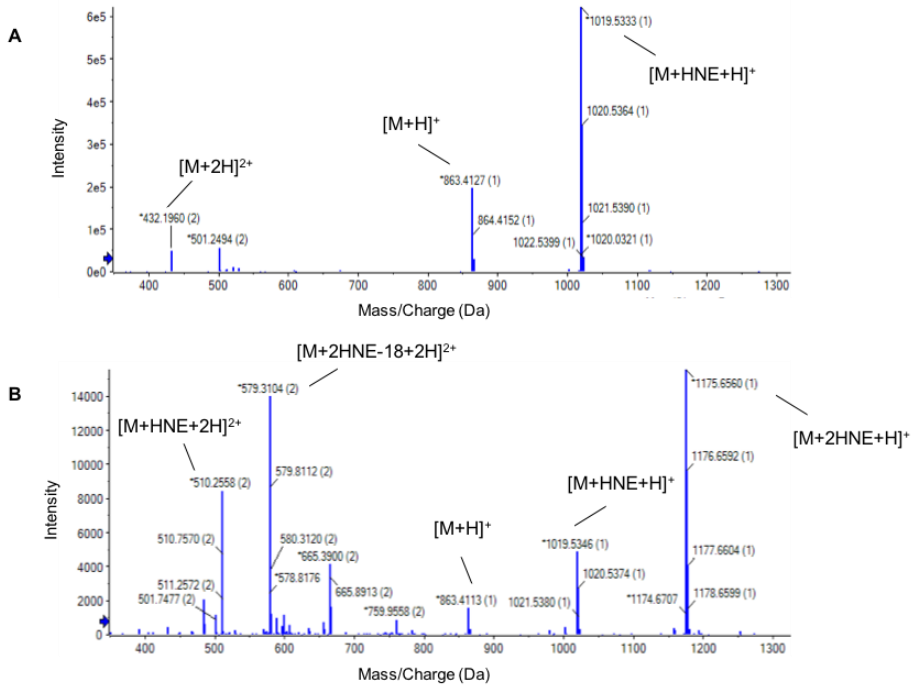

Figure II.6. Identification of HNE Michael adducts on peptide ^{31}LQQCPFE^{37} by MS, following a 2 h reaction with HNE at a peptide-HNE molar ratio of 1:10. The formation of a single MA-HNE-peptide adduct was confirmed by the ion peak at *m/z* 1019.5 ($[M+HNE+H]^+$), and by the ion peak at *m/z* 501.24 ($[M+HNE+2H]^{2+}$) (A). The ions peaks at *m/z* 1175.6 and *m/z* 579 correspond to the protonated molecular ion $[M+2HNE+H]^+$) and to the double charged molecular ion $[M+2HNE+2H]^{2+}$, respectively, confirming the formation of a double MA-HNE-peptide adduct (B). The experiment was performed in triplicate (n=3).

A Schiff's base (SB)-HNE-peptide adduct was also identified in the MS data (**Figure II.7 A**), by the observation of an ion peak with a RT of 43.817 min relative to the ions $[M+HNE-18+H]^+$ *m/z* 1001.5 and the $[M+HNE-18+2H]^{2+}$ *m/z* 501.2. Again, the ion peak regarding the non-modified peptide (*m/z* 863.4) is observed. Moreover, a Michael and Schiff's base adducts within the same peptide was also identified by MS spectrum in **Figure II.7 B**, by observation of a peak with a RT of 44.240 min with *m/z* 579.3102 corresponding to the double protonated ion $[M+2HNE-18+2H]^{2+}$. This species is; however, co-eluting with the

Schiff's base adduct (*m/z* 1001.522), the double MA adduct (*m/z* 1175.65) and the non-modified peptide (*m/z* 863.41).

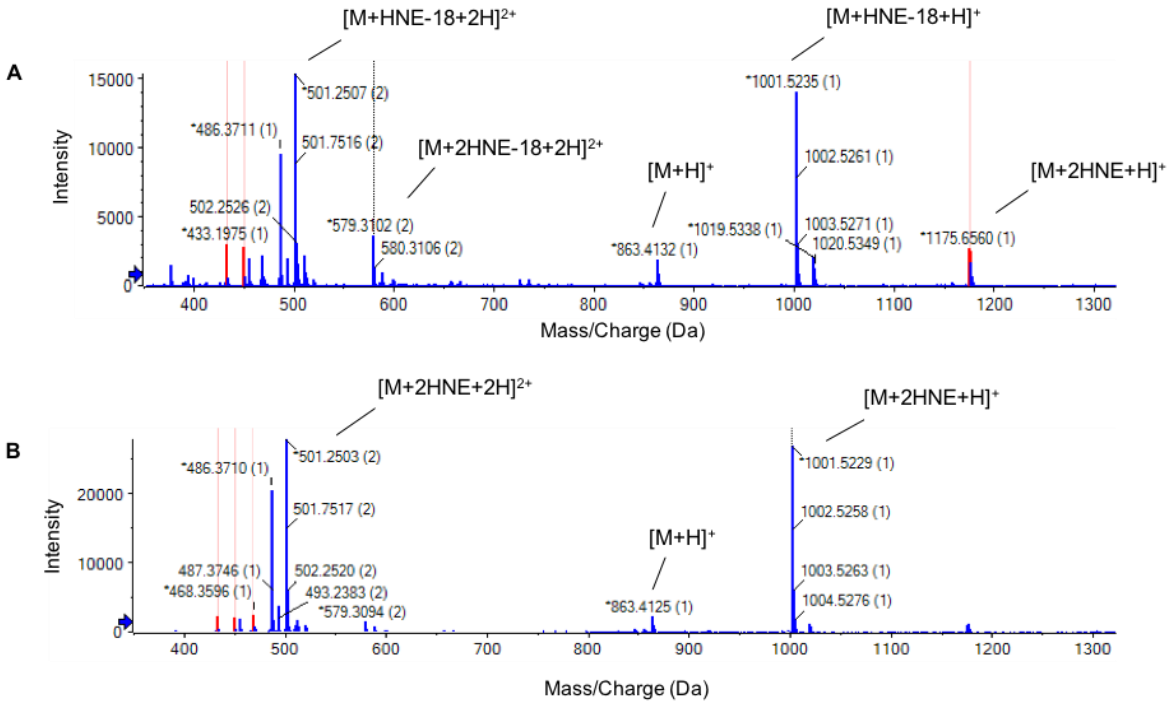

Figure II.7. Identification by LC-MS of a Schiff's base (A) and a double MA (B) adducts formed on peptide ^{31}LQQCPFE^{37}, followed reaction with HNE at peptide-HNE molar ratio of 1:10. The MS spectrum of the peak with an RT of 43.817 shows the ion peaks with *m/z* 1001.5 and *m/z* 501.2, which correspond to the single ([M+HNE-18+H]$^+$) and double ([M+HNE-18+2H]$^{2+}$) protonated ions relative to the predicted mass of a Schiff's base adduct, and the MS spectrum of the peak with a RT of 44.240 depicts the molecular ion *m/z* 579.3102 relative to the predicted mass of both a Michael and Schiff's base adducts [M+2HNE-18+2H]$^{2+}$. The ion peaks with *m/z* 1175.6560, 1001.5235 and 863.4132 suggest the co-elution of this adduct with other products, namely the non-modified peptide, the MA-HNE and SB-HNE peptide adducts. The experiment was performed in triplicate (n=3).

Regarding the ^{141}EIARRHPYFYAPEL^{154} peptide, the TIC obtained for the HNE-peptide reaction products (**Figure II.8 A**) shows the presence of two main peaks with RTs of 32 (**Figure II.8 B**) and 37 min (**Figure II.8 C**) corresponding to the non-modified peptide (predicted m/z 1801.9) and to a Michael adduct (predicted m/z 1957), respectively. **Figure II.8** shows the deviations in the elution patterns between the non-modified peptide (Panel B) and the HNE-peptide adduct (Panel C), suggesting that the addition of an HNE molecule changes the hydrophobicity of the peptide, and consequently its retention time.

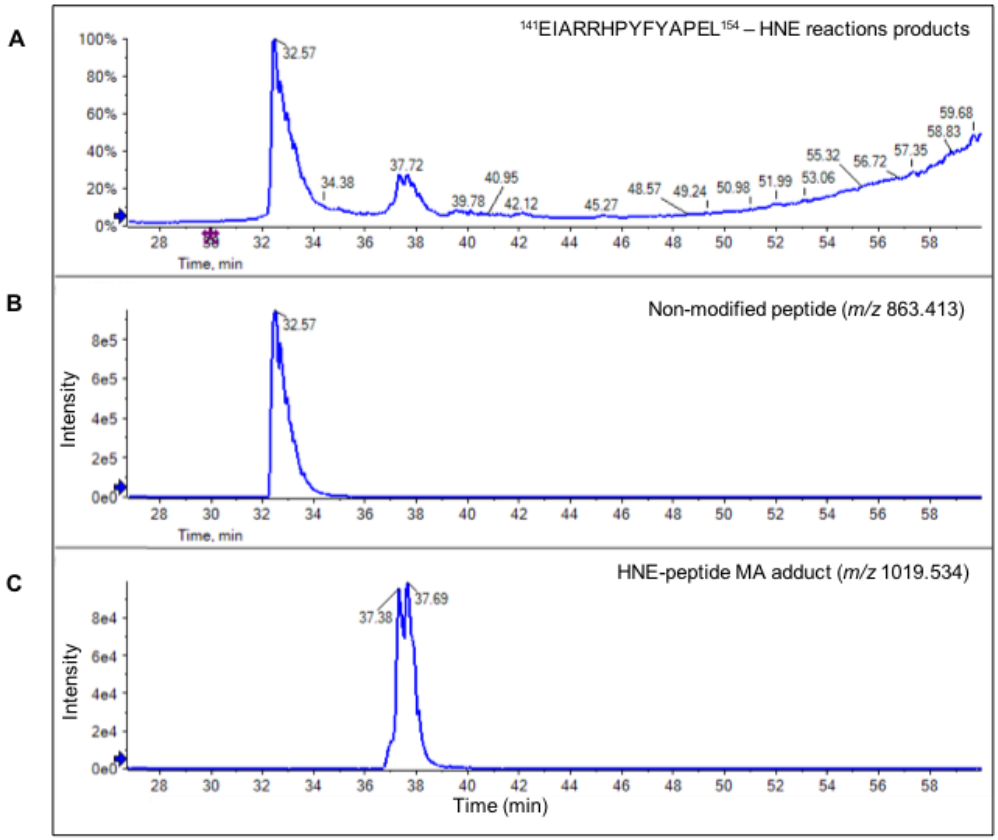

Figure II.8. Identification by LC-MS of the products formed by reacting peptide ^{141}EIARRHPYFYAPEL^{154} with HNE at a peptide-HNE molar ratio of 1:10; and their respective difference in the retention time. Panel A shows the total ion chromatogram of the total reaction products and panels B and C show the TICs relative to the prediction mass of the non-modified peptide and MA-HNE-peptide adduct, respectively. The experiment was performed in triplicate (n=3).

The MS spectrum depicted in **Figure II.9** shows two main ions peaks at m/z 980.5313 and 653.6792, which correspond to the predicted mass of a double charged molecular ion ($[M+HNE+2H]^{2+}$) and the triple charged molecular ions ($[M+HNE+3H]^{3+}$), respectively, confirming the formation of a MA-HNE-peptide adduct.

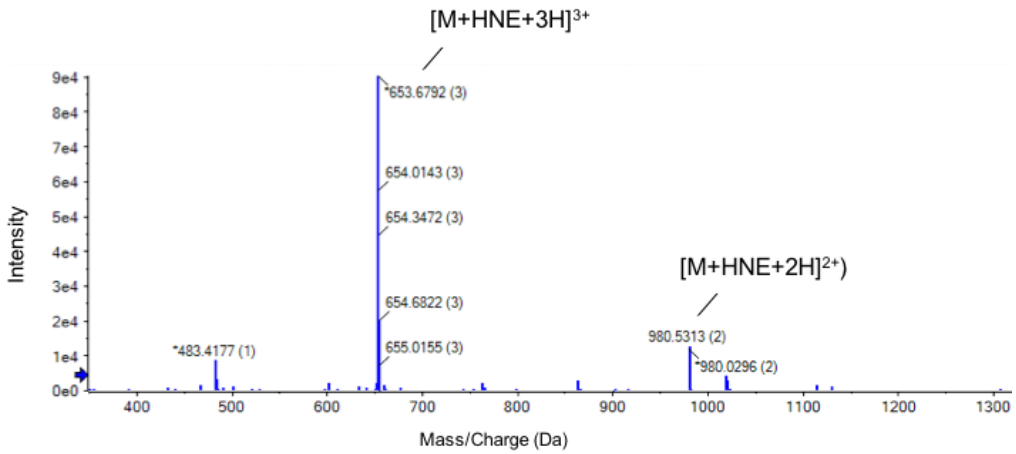

Figure II.9. Identification by LC-MS of a Michael adduct formed on the peptide ^{141}EIARRHPYFYAPEL^{154} followed reaction with HNE at a peptide-HNE molar ratio of 1:10. MS spectrum relative to the peak with an RT of 37.740 min reveals the ions peaks at m/z 980.5313 and 653.6792, which correspond to the double ($[M+HNE+2H]^{2+}$) and triple ($[M+HNE+3H]^{3+}$) charged ions regarding the predicted mass of the an MA-HNE-peptide adduct (m/z = 980.53). The experiment was performed in triplicate (n=3).

Regarding peptide ^{198}LKCASLQK^{205} , the MS of its reaction products with HNE (**Figure II.10**), shows three molecular ion peaks of m/z 1008.5941, m/z 1087.1615 and m/z 1165.2288 (present in the panels A, B and C, respectively), which correspond to the three different Michael adducts. These appear to be doubly charged molecular ions, which suggests that the peptide may have dimerized in the solution. Nevertheless, the peaks of m/z 1859.06, m/z 672.72 and m/z 504.79 observed in **Figure II.10 A**, correspond to the double, triple and quadruple protonated molecular ions, respectively, which are consistent with the presence of a dimerized peptide containing a single HNE-MA-peptide adduct. The same is observed for the double HNE-MA- adduct to the dimerized peptide (in **Figure II.10 B**) by the presence of the peaks of *m/z* 1087.1615, *m/z* 724.7648 and *m/z* 543.8180, which correspond the double, triple and quadruple protonated molecular ions, respectively. In **Figure II.10 C** the observed peaks at *m/z* 1165.2288, *m/z* 777.1412 and *m/z* 583.0994 are consistent with the triple HNE-MA adduct of the dimerized peptide. In the same panel a peak at *m/z* 622.39 is also observed, which was not identified.

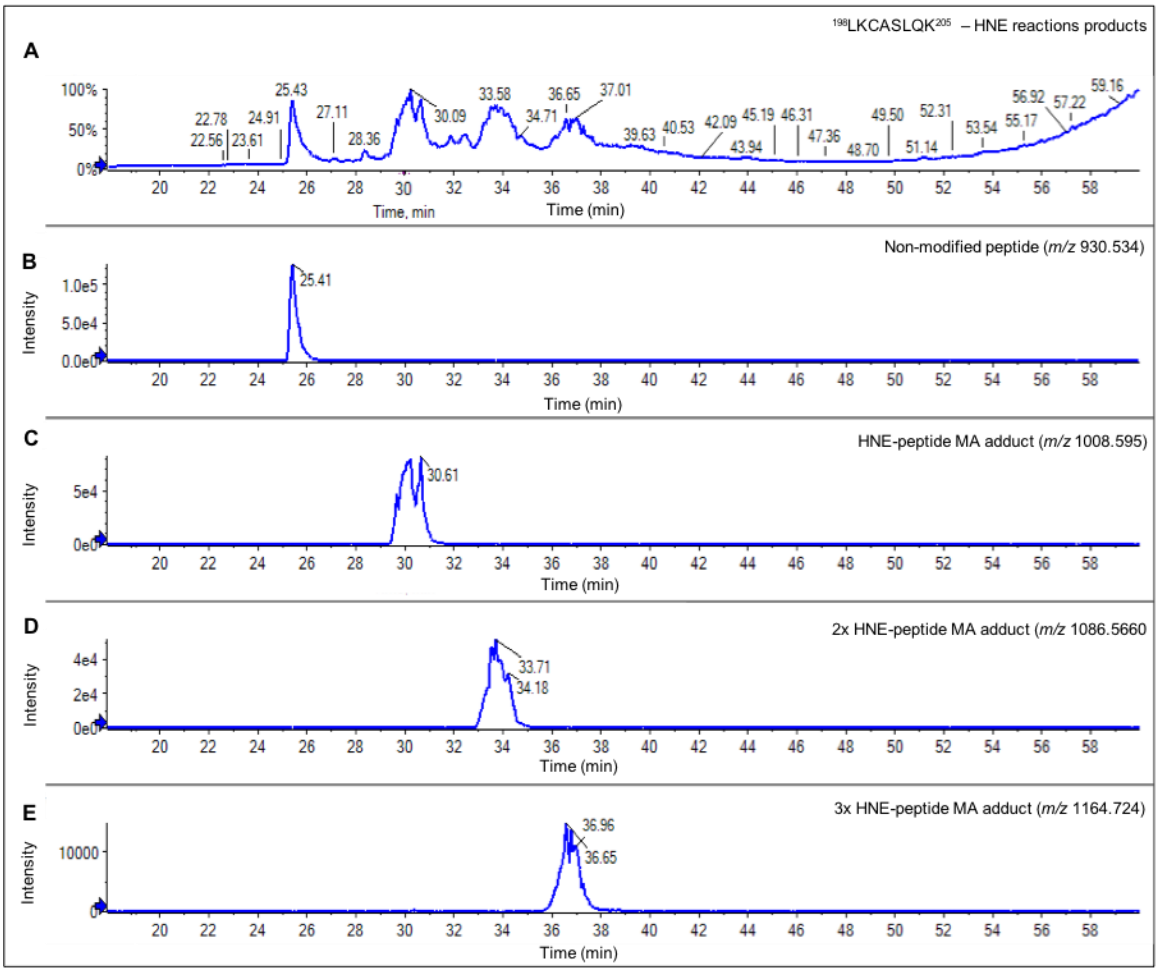

Figure II.10. Identification by LC-MS of the products formed by reacting peptide ^{198}LKCASLQK^{205} with HNE at a peptide-HNE molar ratio of 1:10; and their respective difference in the retention time. TIC in panel A represents the total elution profile of all the reaction products formed and the XICs regarding peaks at RT 25 min (B), 30 min (C), 33 min (D) and 36 min (E) correspond to the prediction of the non-modified peptide (*m/z* 930.534), the single MA-HNE-peptide adduct (*m/z* 1008.595), the double MA-HNE-peptide adduct (m/z 1086.660) and the triple MA-HNE-peptide adduct (*m/z* 1164.724), respectively. The experiment was performed in triplicate (n=3).

When analysing the MS spectra of each MA adduct (**Figure II.11**), the molecular ion peaks of m/z 1008.5941, m/z 1087.16.15 and m/z 1165.2288 (present in the panels A, B and C, respectively), that corresponds, respectively, to the three different Michael adducts, appear to be doubled charged molecular ions, which suggest that the peptide has dimerized in the solution. Nevertheless, the peaks of m/z 1859.06, m/z 672.72 and m/z 504.79 observed in **Figure II.11 A**, correspond to the double, triple and quadruple protonated molecular ions, respectively, which are consistent with the presence of a dimerized peptide containing a single HNE-MA-peptide adduct. The same is observed for the double HNE-MA-adduct to the dimerized peptide (**Figure II.11 B**) by the presence of the peaks of *m/z* 1087.1615, *m/z* 724.7648 and *m/z* 543.8180, which correspond to the double, triple and quadruple protonated molecular ions, respectively, and for the triple HNE-MA-adduct to the dimerized

peptide (in **Figure II.11 C)** by the presence of peaks *m/z* 1165.2288, *m/z* 777.1412 and *m/z* 583.0994 that correspond to the double, triple and quadruple protonated molecular ions.

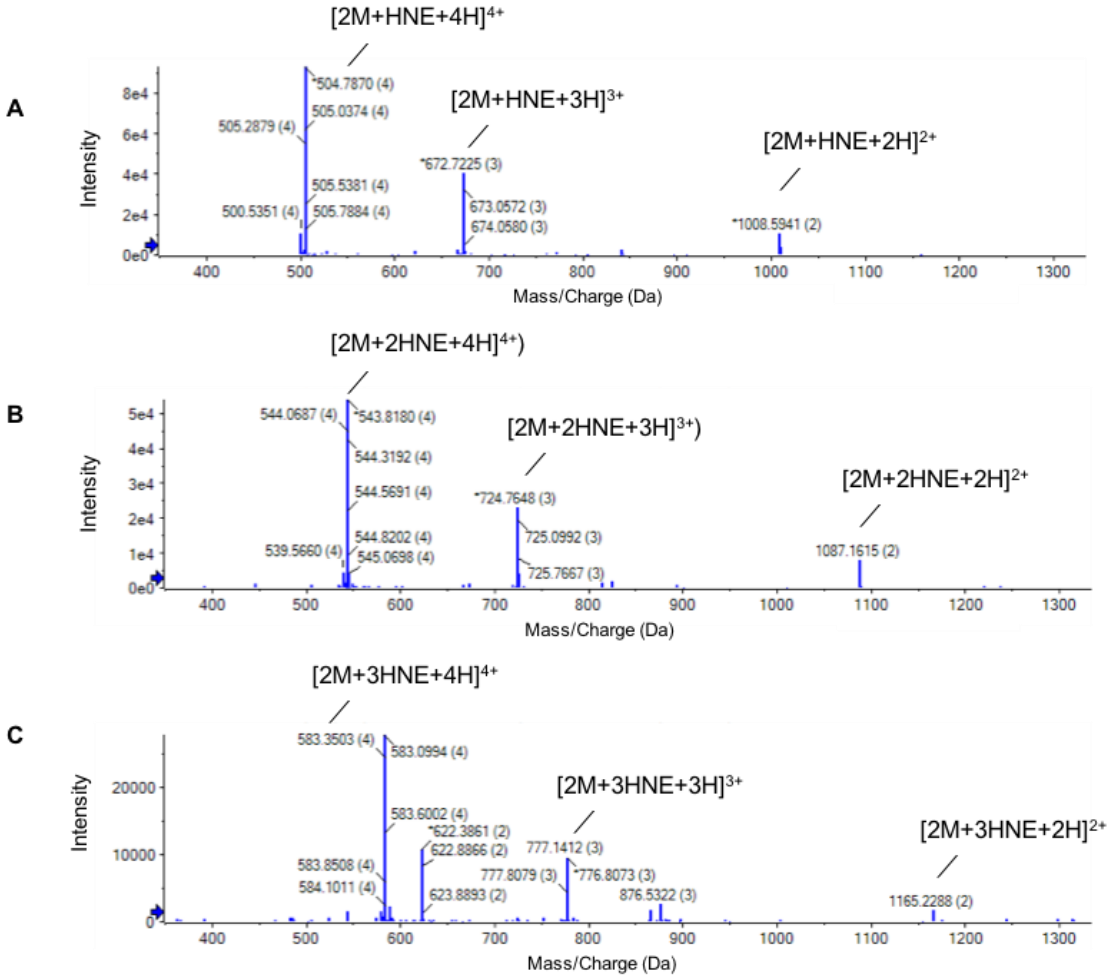

Figure II.11. Identification by LC-MS of Michael adducts formed on peptide ^{198}LKCASLQK^{205} followed reaction with HNE at peptide-HNE molar ratio of 1:10. Panel A shows the MS spectrum relative to the peak with an R.T. of 29.944 showing the ion peak relative to the predicted single Michael adduct (*m/z* = 1087.1615); Panel B shows the MS spectrum relative to the peak with an R.T. of 33.707 showing the ion peak relative to the predicted double Michael adduct (*m/z* = 1165.2288); Panel C shows the MS spectrum relative to the peak with an R.T. of 36.848 showing the ion peak relative to the predicted triple Michael adduct (*m/z* = 1165.2288). The experiment was performed in triplicate (n=3).

2.4.4. Detection of HNE Modifications on Intact HSA by LC-MS/MS

The structural modifications of HSA by HNE were also characterized digesting the native HSA and HNE-modified (1:10) HSA samples with trypsin and analysing the generated peptides by LC-MS/MS. The Sequest search engine provided 81% protein sequence coverage, from which 15 peptides containing HNE adducts were identified, of which 8 were

Michael adducts and 3 were Schiff's Bases (**Table II.2**). The HNE-modified peptides were identified based on their *m/z*, which were determined with mass accuracy ≤5 ppm, and an increase of the retention times over the unmodified peptides. Since after trypsinization, the generated peptides were treated with iodoacetamide to block the thiols groups of cysteine residues, most of the unmodified cysteine-containing peptides were identified as carbamidomethylated (CAM), and the exact location of some of the identified HNE modifications could not be determined because of the neutral loss of the HNE moiety during MS/MS fragmentation. Examples of this are His105 and Lys106 from peptide ^{99}NECFLQHKDDNPNLPR^{114} and His67 and Lys73 from peptide ^{52}TCVADESAENCDKSLHTLFGDKLCTVATLR^{81}; however, the manual annotation of the MS spectra, the *m/z* of the modified peptides and the differences observed in the retention times between the modified and equivalent unmodified peptides allowed the confirmation of HNE modification on peptides (**Table II.2**). As the covalent adduction of HNE molecules to peptides is typically seen to increase the overall hydrophobicity of the peptides, changes in their retention time on a HPLC column can usually be used to confirm the modifications. It should be noted that the LC-MS/MS data report on the total variety of modifications detected, and that any individual protein molecule is likely to contain a subset of these adducts.

Table II.2. Tryptic peptides of HNE-modified HSA identified using the Sequest database search engine (Proteome Discoverer 1.4, Thermo Scientific). Oxidation of methionine and cysteine, carbamidomethylation (CAM) of cysteine, HNE Michael adducts (on cysteine, lysine and histidine) and Schiff's base adducts (on lysine) were used as variable modifications and results were filtered for rank 1 peptides and score vs. charge states corresponding to Xcorr/z 2.0/2, 2.25/3, 2.5/4, 2.75/5.

HSA Peptide Sequence	*Modifications* [a]	*Theo. MH^+ [Da]* [b]	*z*	*m/z [Da]*	*Δ ppm*	*t_R (min)*
^{52}*TCVADESAENCDKSLHTLFGD*^{73}	2xCAM C53; C62; 1xHNE MA H67	2653.2120	3	885.0750	0.37	35.0
	2xCAM C53; C62	2497.0970	3	833.0372	-0.28	27.4
^{65}*SLHTLFGDK*^{73}	1xHNE MA H67	1173.6514	2	587.3284	1.42	35.3
	-	1017.5364	2	509.2706	2.08	22.6
^{52}*TCVADESAENCDKSLHTLFGDKLCTVATLR*^{81}	3xCAM C53; C62; C75; 1xHNE MA H67/K73	3567.7128	4	892.6862	-3.04	39.2
	3xCAM C53; C62; C75;	3411.5978	3	1137.8713	-0.67	33.8
^{94}*QEPERNECFLQHKDDNPNLPR*^{114}	1xCAM C101; 1xHNE MA H105	2792.3421	3	931.4533	-1.39	27.8
	1xCAM C101	2636.2270	3	879.4126	1.22	20.2
^{99}*NECFLQHKDDNPNLPR*^{114}	1xCAM C101; 1xHNE MA H105/K106	2153.0444	3	718.3517	1.57	28.8
	1xCAM C101	1996.9294	2	998.9680	0.17	20.9
^{115}*LVRPEVDVMCTAFHDNEETFLK*^{136}	1xCAM C124; 1xHNE MA H128	2806.3790	3	936.1309	0.15	40.5
	1xCAM C124	2650.2640	3	884.0940	-1.51	35.3
^{115}*LVRPEVDVMCTAFHDNEETFLKK*^{137}	1xCAM C124; 1xHNE MA H128	2934.4740	4	734.3732	0.70	38.3
	1xCAM C124	2778.3590	3	926.7914	-0.43	33.1
^{226}*AEFAEVSKLVTDLTK*^{240}	1xHNE SB K233	1788.9993	2	895.0037	-0.55	47.3
	-	1650.8949	2	825.9522	-1.54	39.3
^{241}*VHTECCHGDLLECADDR*^{257}	3xCAM C245; C246; C253; 1xHNE MA H242	2242.9526	3	748.3223	-0.11	26.1
	3xCAM C269; C270; C277	2086.8375	3	696.2834	0.65	19.2
^{241}*VHTECCHGDLLECADDRADLAK*^{262}	3xCAM C245; C246; C253; 1xHNE MA H242	2741.2328	3	914.4163	-0.74	26.7
	3xCAM C245; C246; C253	2585.1177	3	862.3770	0.27	22.7
^{241}*VHTECCHGDLLECADDRADLAKYICENQDSISSK*^{274}	2xCAM C245; C246; 1xOxidation C265; 1xHNE MA H247	4067.8089	4	1017.7064	1.05	27.0
	2xCAM C245; C246; 1xOxidation C265	3911.6939	4	978.6787	0.02	23.5
^{373}*VFDEFKPLVEEPQNLIK*^{389}	1xHNE SB K378	2183.1998	2	1092.1036	-0.21	48.4
	-	2045.0954	2	1023.0520	-0.80	38.3
^{501}*EFNAETFTFHADICTLSEK*^{519}	1xCAM C514; 1xHNE MA H510	2416.1377	2	1208.5740	-1.34	42.1
	1xCAM C514	2260.0227	2	1130.5161	-1.13	35.7
^{501}*EFNAETFTFHADICTLSEKER*^{521}	1xCAM C514; 1xHNE MA H510	2701.2814	3	901.1012	-3.03	39.8
	1xCAM C514	2545.1664	2	1273.0881	-1.13	33.7
^{542}*EQLKAVMDDFAAFVEK*^{557}	1xHNE SB K545	1979.0194	2	990.0121	1.15	47.3
	-	1840.9150	2	920.9618	-0.88	41.7

[a] For each peptide, top line (white background) corresponds to the modified peptide, and the bottom line (grey background) to the non-modified peptide.

[b] Theoretical mass

2.4.5. Detection of HNE Modifications on Intact HSA by Direct Infusion ESI-MS

Native and HNE treated (1:10) HSA samples were analysed by direct infusion on a quadrupole mass spectrometer equipped with an electrospray ionization source to evaluate changes in the protein mass and assess the number of HNE adducts formed on intact protein. Positive-ion ESI mass spectra of native and HNE-modified HSA are depicted in **Figure II.12 A** and **D**, respectively. Both spectra were smoothed (panels B and E, respectively for native and HNE modified HSA) and the peaks were centred (panels C and F, respectively for native and HNE modified HSA).

The spectrum of the native HSA (**Figure II.12 A**) shows multiply charged peaks ranging from *m/z* 1075 to *m/z* 1858, which corresponds to the addition of 62 to 36 protons, respectively; and for the modified protein (**Figure II.12 D**), even though ion peaks are quite broad, the spectrum shows multiply charged peaks ranging from *m/z* 1164 to *m/z* 1877, which correspond to the addition of 58 to 36 protons. By deconvoluting the spectra, the molecular weights of the non-modified and modified species were calculated to be 66749.11 Da and 67481.26 Da, respectively, meaning that the HNE-modified HSA is 732.15 Da bigger. Because HNE contains three functional groups – aldehyde, C=C double bond and one hydroxyl group – it can react with more than one amino acid, either via Michael or Schiff base mechanisms. If the adducts were all formed via Michael addition, this result suggests the presence of 4.69 molecules of HNE per molecule of HSA. If the adducts, or some of them, were formed via Schiff base addition, which involves a loss of 18 Da (loss of H_2O) in the reaction, this would increase the number of HNE molecules added up to 5.3. Nevertheless, the mass increment between the two forms shows the generation of HNE adducts on HSA was possible under these conditions.

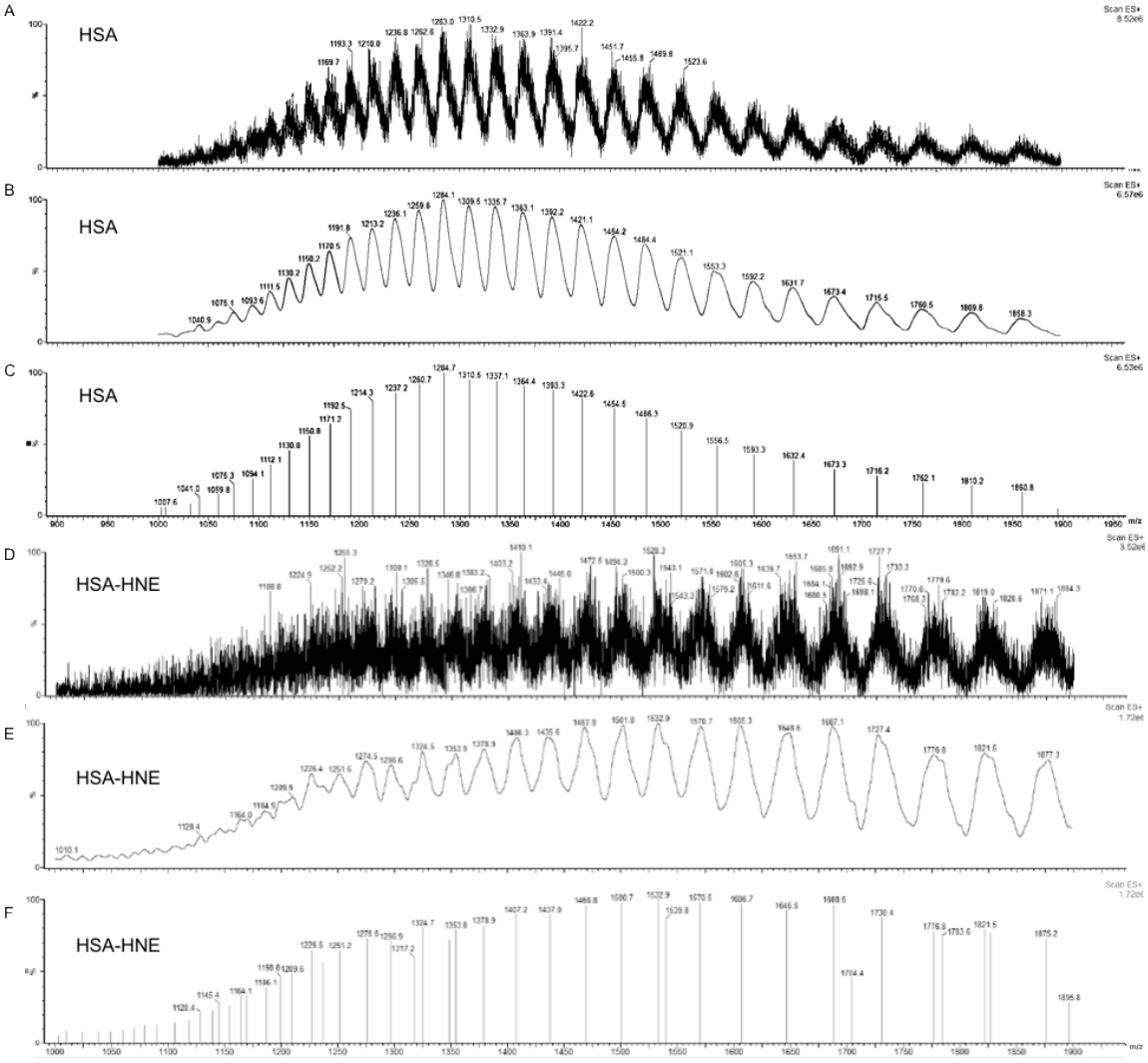

Figure II.12. Direct infusion ESI-MS analysis of native HSA (A) and HNE-modified HSA (D). Both spectra were smoothed (Panels B and E, respectively for native HSA and HNE-modified HSA) and the peaks were centred (Panels C and F, respective for native HSA and HNE-modified HSA). ESI-MS spectrum of the native HSA shows multiply charged peaks ranging from *m/z* 1075-1858 and the spectrum of the modified HSA shows multiply charged peaks ranging from *m/z* 1164 to m/z 1877.

2.4.6. Detection of HNE Modifications on Intact HSA by MALDI-TOF-MS

As MALDI-TOF-MS allows the analysis of large proteins, the formation of HNE adducts on HSA (sample treated with HNE at a protein:HNE molar ratio of 1:10) could also be confirmed by this method. The data in **Figure II.13 A** shows that the HNE-modified HSA was shifted by +477 Da compared to native HSA (**Figure II.13 B**), which corresponds approximately to the addition of 3 molecules of HNE per HSA molecule on average, assuming the adducts were formed via Michael addition (+156.1 Da). Nevertheless, this number could be slightly

higher if there were a mixture of different adducts being formed on HSA, as suggested by the MS/MS data described above.

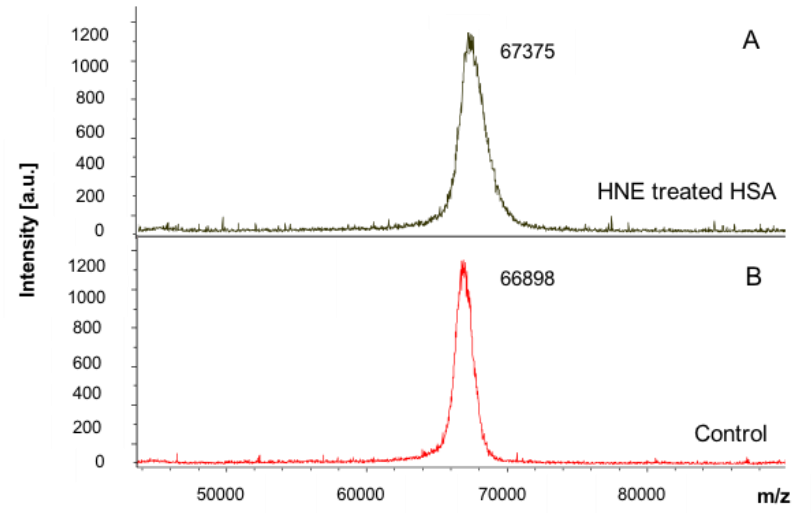

Figure II.13. MALDI-TOF-MS spectra of HSA treated with HNE at a protein:HNE molar ratio of 1:10 (A) and native HSA (B). The difference in mass between the peak representing the modified protein and the peak representing the native form correspond to the addition of ~3 molecules of HNE per HSA.

2.4.7. Detection of HNE Modifications on Intact Proteins by Direct ELISA Assay

Prior to initiating the immunization protocol, the reactivity of HNE towards three different proteins was assessed by direct ELISA using a commercial polyclonal antibody (pAb) anti-HNE. This commercial antibody was generated by immunization of HNE-treated keyhole limpet hemocyanin (KLH), a protein found in the haemolymph of the giant keyhole limpet *Megathura crenulata*, to avoid cross-reactivity to human or mammalian proteins, which was thought to make the results more reliable by limiting false positives.

HSA, A1AT and OVA were treated individually with the aldehyde at a protein:HNE molar ratios of 1:1, 1:5 and 1:10, before being coated onto the immunoassay plate.

The plot depicted in **Figure II.14** shows HNE adducts were formed in all three proteins when treated with HNE at protein:HNE molar ratios of 1:5 and 1:10, but when observing the data regarding the 1:1 molar ratio, only A1AT seems to have been modified.

Comparing the three proteins, A1AT appears to be the protein with a higher number of HNE adducts whilst HSA the one with the lowest number of HNE modifications. When looking in detail to the data gathered when the antigen was plated at the concentration of 1 µg/mL,

A1AT appears to be three times more modified than HSA, as seen by the absorbance values acquired when both proteins as treated at a 1:10 protein-HNE molar ratio.

Statistical data obtained from both individual sets of experiments – as this assay was only performed in duplicate – showed there was statistical difference between all the three modified and respective non-modified proteins (**Appendix 8 A**); however, as the combined data did not meet the criteria of normal distribution and equal variance, which are needed for performing a single way ANOVA analysis, the non-parametric Kruskal-Wallis rank sum test was used (**Appendix 8 B**). The *p* values obtained by this test indicate only A1AT-HNE and OVA-HNE are significatively different from A1AT and OVA, respectively, as opposed to HAS-HNE and HSA. Using the Dunn test to determine where exactly the statistical difference occurs within the HNE modified A1AT and OVA, it was possible to infer that the significant difference occurs between non-modified A1AT and A1AT-HNE (1:10) and OVA-HNE (1:1) and OVA-HNE (1:10) – *p* values of 0.0024 and 0.0049, respectively (**Appendix 8 C)**.

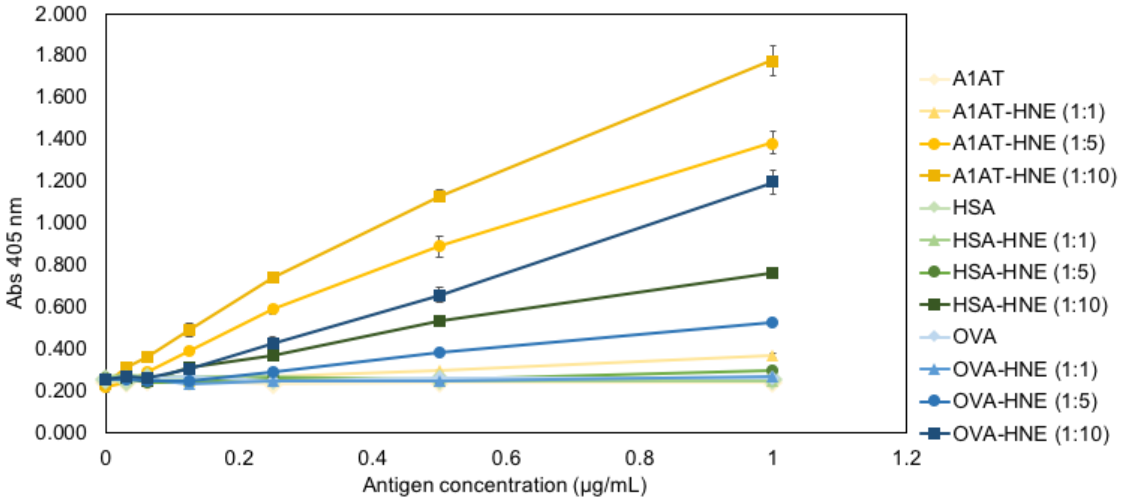

Figure II.14. Identification of HNE adducts on A1AT, HSA and OVA by direct ELISA using the commercial anti-HNE polyclonal antibody from Abcam. Each protein was individually incubated with HNE at three different protein-HNE molar ratios (1:1, 1:5 and 1:10) for 2h at 37°C, and different concentrations from these batches, ranging from 0 to 1 µg/mL, were adsorbed onto an ELISA plate (A). The data obtained when using 1 µg/mL of each modified and non-modified antigen was isolated and represented in a graph bar for ease of understanding (B). The assay was performed in duplicate (n=2), with SEM of technical triplicates; * p<0.0125.

Nonetheless, the ELISA assay confirms the aldehyde is able to modify the proteins regardless of their origin or size, which is in agreement with several studies found in the literature. The protein:HNE molar ratio of 1:10 was chosen for further experiments since statistically significant differences were observed for all these three batches of modified proteins.

2.4.8. Detection of HNE Modifications on Intact Proteins by SDS-PAGE and Western Blotting

To complement the results obtained by ELISA, the same three proteins, non-modified (**Figure II.15 A**) and HNE-modified at the same molar ratios (**Figure II.15 B**), were subjected to SDS-PAGE gel and western blotting analysis with the same commercial anti-HNE pAb (**Figure II.15 C**).

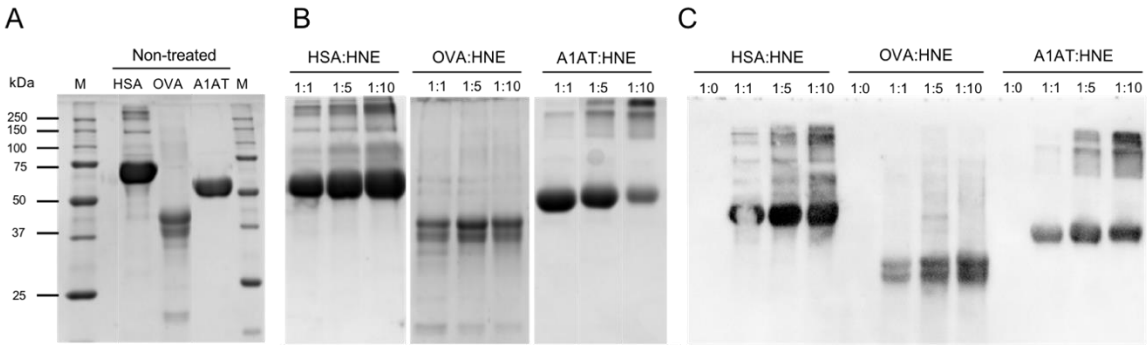

Figure II.15. SDS-PAGE (A and B) and western blotting analysis (C) of non-modified and HNE modified HSA, OVA and A1AT. Non-modified proteins are represented in panel A whereas HNE modified HSA, OVA and A1AT at three different molar ratios (1:1, 1:5 and 1:10) are depicted in panel B. The HNE modifications on the three proteins were also confirmed by western blotting analysis using the Abcam anti-HNE (C). The experiment was only performed once (n=1).

Visual interpretation of the SDS-PAGE gel depicted in **Figure II.15 B** shows that, regarding HSA (MW: 66.5 kDa), there is an increment of the molecular weight of the protein band as the protein-HNE molar ratio is increased, suggesting HNE is forming adducts on the protein. For OVA (MW: 45 kDa), no major changes can be observed in the protein bands; however, for the 1:5 molar ratio, the protein band detected seems to be stronger than the bands observed for 1:1 and 1:10 molar ratios. For A1AT (54 kDa), the protein band seems to decrease its intensity with increasing concentration of HNE, but the onset of high molecular weight bands can be seen. This phenomenon was also observed for HSA, which suggests in the presence of high concentrations of HNE induced the formation of protein crosslinks and aggregation.

The formation of HNE adducts on HSA, OVA and A1AT, in all the three protein:HNE molar ratios tested, was further confirmed by western blotting using a commercial antibody specific to HNE (**Figure II.15 C).** The blot shows as well increasing intensities of the bands with increasing protein:HNE molar ratios, suggesting, as expected, the formation of a greater number of HNE modifications with increasing concentrations of HNE. Regarding HSA and OVA, the detection top bands by the anti-HNE pAb confirms the formation of HNE-

crosslinks with more than one molecule of HSA or OVA, as the SDS-PAGE implied. Although quantitative studies were not done for this western blot, densitometry analysis will be shown later for this and other western blot experiments in *3.4.4. Enrichment and Characterization of SA269 anti-HSA-HNE Antibodies using Protein G and KLH-HNE Conjugated Resins.*

2.4.9. Kinetic and Affinity Characterization of anti-HNE pAb to HNE treated ^{31}LQQCPFE^{37} Peptide

The development of a lateral flow assays relies mainly on the sensitivity of the antibodies used for the capture and detection of the target analyte; therefore, target binding characterization is an essential analytical step for the selection of high affinity (K_D < 1 nM) and highly specific antibody molecules. As preliminary experiment, the kinetic parameters of the commercial anti-HNE antibody were tested with the HNE-modified biotinylated ^{31}LQQCPFE^{37} peptide using FortéBio Octet assay with "Dip and Read™ Streptavidin Biosensors". For this purpose, the peptide ^{31}LQQCPFE^{37} was re-synthesized with a biotin tag in the C-terminal (MW: 1291.63), purified by reverse-phase chromatography and its mass was confirmed by LC-MS (**Figure II.16**). The peaks at *m/z* 1262.6338 and 646.8129, which correspond to the single and double charged ions ($[M+H]^+$) and ($[M+2H]^{+2}$) of the peptide, confirmed the correct synthesis and purification of the peptide.

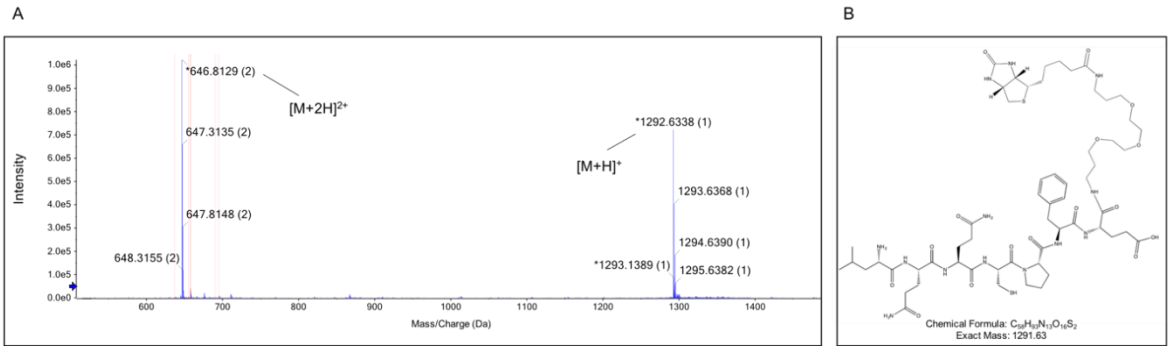

Figure II.16. MS analysis of synthetic biotinylated ^{31}LQQCPFE^{37} peptide (A) and corresponding structure (B). Ion peaks at *m/z* 1292.6338 and 646.8129 correspond to the single and double charged ions ($[M+H]^+$) and ($[M+2H]^{+2}$), respectively, of the peptide. The experiment was performed in triplicate (n=3).

The biotinylated ^{31}LQQCPFE^{37} (biot-^{31}LQQCPFE^{37}) peptide was further reacted with HNE under the same conditions, for generation of HNE adducts, and its corresponding reaction products were analysed by LC-MS. **Figure II.17 A** and **B** show, respectively, the formation of one MA and one SB.

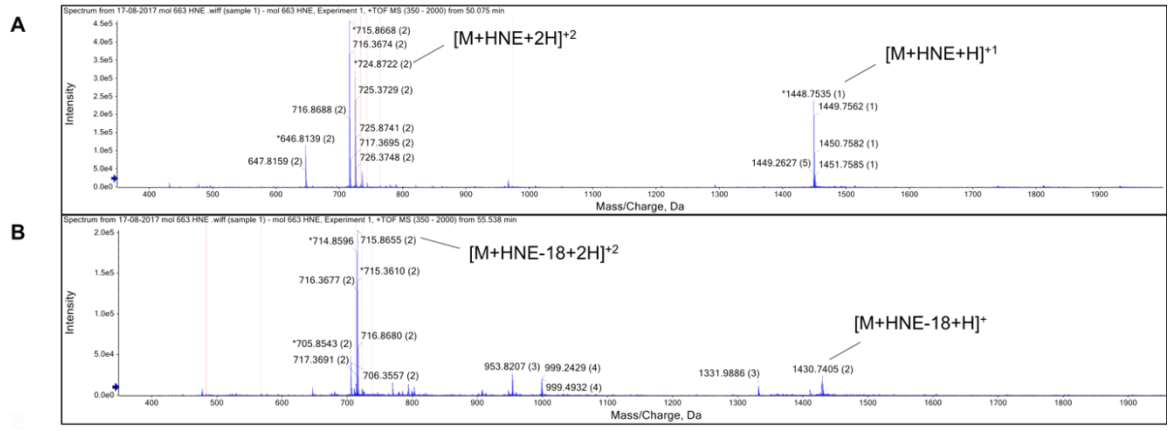

Figure II.17. Identification by LC-MS of HNE adducts formed on biotinylated 31LQQCPFE37 peptide followed reaction with HNE at peptide-HNE molar ratio of 1:10. An HNE-MA-peptide adduct was confirmed by the presence of the ion peaks m/z 1448.7535 and 724.8722, that correspond to the single and double ion species, respectively (A), and a Schiff's base adduct was confirmed by the ion peaks m/z 1430.7405 and 715.8655, which correspond as well the single and double ion species, respectively (B). The experiment was performed in triplicate (n=3).

Once the formation of HNE adducts was confirmed, the purified HNE-adducted form of the biot-^{31}LQQCPFE^{37} peptide (HNE-biot-^{31}LQQCPFE^{37}) was immobilized onto a streptavidin plate for calculation of association and dissociation constants of the Abcam anti-HNE pAb, by bio-layer interferometry. The traces depicted in **Figure II.18** show the interference in the wave light caused by the association and dissociation of HNE-biot-^{31}LQQCPFE^{37} peptide when using different antibody concentrations. The higher the concentration of antibody, the faster the association and dissociation steps.

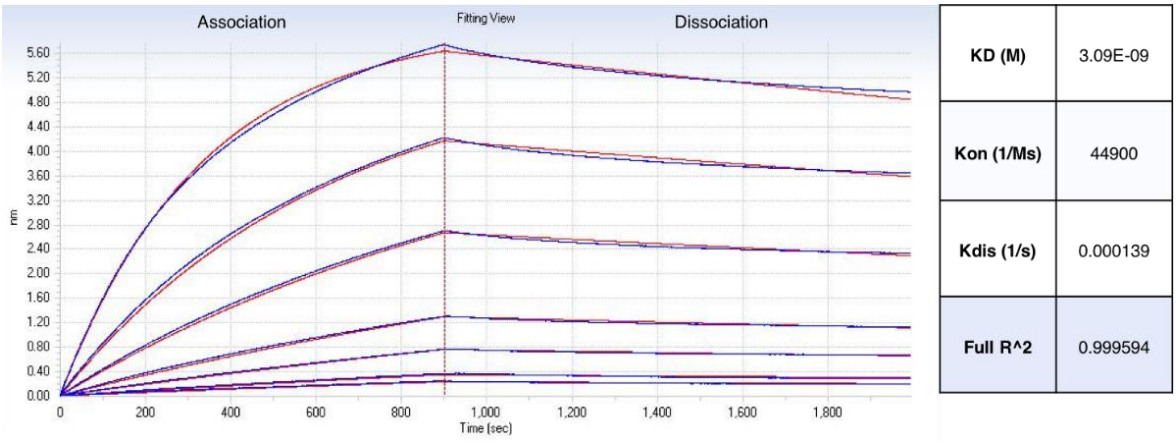

KD (M)	3.09E-09
Kon (1/Ms)	44900
Kdis (1/s)	0.000139
Full R^2	0.999594

Figure II.18. Kinetic and affinity analysis of Abcam anti-HNE pAb to immobilized HNE-biotinylated-^{31}LQQCPFE^{37} peptide. Kinetic constants were calculated testing eight different antibody concentrations (64, 32, 16, 8, 4, 2 and 1 nM) and the the binding curves (red lines) were fit using a global fit algorithm for 1:1 binding interaction in the Octet Data Analysis software v. 7.0. The assay was performed only once (n=1).

The assay data was processed using Data Analysis (ForteBio) to obtain the kinetic values, using a global fit algorithm for 1:1 binding interaction, which fits multiple concentrations to one set of constants. The K_D obtained for interaction between the Abcam anti-HNE pAb and the HNE-biot-^{31}LQQCPFE^{37} peptide was 3.09 x10^{-9} M (10 nM), which is considered a high affinity binding.

2.5. Chapter II Discussion, Conclusions and Future Work

When evidence for a correlation between oxidative stress and the onset of several chronic diseases began to emerge, the need to develop novel detection and identification strategies for oxidation products became more crucial. It is now clear that lipid oxidation products in particular can react and form covalent adducts with different molecules, altering their structure and modifying their function in a process called lipoxidation, and emphasizing the need to detect not only free radicals and antioxidants, but also oxidized lipid-protein-adduction products. HSA-HNE adducts, in particular, are of very great interest as they can serve as blood markers of oxidative stress *in vivo.*

High resolution MS approaches led the identification of 11 HNE modifications on intact HSA, from which 8 were formed via Michael addition and 3 via Schiff's base reaction, confirming the *in vitro* reactivity of this lipid peroxidation product towards HSA. Apart from the HNE modification on peptide ^{115}LVRPEVDVMCTAFHDNEETFLK^{136} (possibly localised at His128), all the other HNE modifications identified in this study had already been reported by *Aldini et al* (Aldini et al., 2006), Liu *et al* (Q. Liu et al., 2012)*,* and Szapacs *et al* (Szapacs, Riggins, Zimmerman, & Liebler, 2006), reinforcing not only the veracity of this study, but also the accuracy of MS strategies in the detection of lipoxidation products. However, in all three studies, the residue Cys34, known to be the only free cysteine of HSA, was also identified as HNE-modified, that was not observed in this study. This residue is as well known to be the largest fraction of thiol in blood serum (~80%) (Rossi et al., 2010) and therefore is commonly used as an indicator of the oxidative stress in serum; however, because the HSA used in our studies comes from a commercial source and had probably been extensively exposed to the atmospheric oxygen, this might have caused the possible oxidation of Cys34, biasing the formation of HNE adducts. Another possible explanation for the non-identification of the HNE-Cys34 adduct relies on the 81% of protein sequence coverage achieved by the search engine used, which could have missed the protein sequence including the Cys34 residue. Apart from the HNE modifications identified in the work described in this chapter, *Liu et al* has also identified HNE adducts on residues

Lys162, Lys199, Lys212, Lys262, His288, Lys351, His367, Lys414 and Lys525, possibly due to the longer HNE reaction times used in these experiments (3h) (Q. Liu et al., 2012).

In addition to MS, antibody-based techniques confirmed the formation of HNE adducts on HSA, and as well on OVA and A1AT (as control), either by ELISA and western blotting, suggesting different intact proteins are susceptible to HNE modifications and can be used directly as immunogens. However, the use of specific peptide sequences as immunogens is also a strategy very much applied for the generation of antibodies, namely for generating "highly-specific" polyclonal antibodies (Burdon & van Knippenberg, 1988) – which in this case might be translated as specificity to a particular HNE adduct on HSA. Therefore, the formation of HNE adducts on peptides containing target amino acids was well assessed in this work. In all the three synthesised peptides HNE adducts were identified, but their exact location was, unfortunately, not achieved. Regarding peptides ^{31}LQQCPFE^{37} and ^{98}LKCASLQK^{205} in particular, more than one adduct was identified (in each sequence), suggesting the excess of HNE used allowed the modification of other nucleophilic amino acids as well. In fact, in ^{31}LQQCPFE^{37} we believe the second HNE adduct identified might be located on the NH_2 group of the N-terminus of the peptide, as this was not acetylated, and there are no other potentially reactive amino acids in the peptide sequence.

The affinity of the anti-HNE commercial pAb towards one of the synthesised peptides was then measured via a bio-layer interferometry (BLI) assay, as the adsorption of single peptides to ELISA plates is not viable. The peptide ^{31}LQQCPFE^{37} was biotinylated and reacted with HNE, and then linked to a streptavidin plate for the kinetic measurements. The affinity of an antibody is commonly measured by its equilibrium dissociation constant (K_D), that is a ratio of k_{dis}/k_{on}, between the antibody and its antigen, and therefore, the lower the K_D value, the higher is the affinity of the antibody for its target, and the less antibody is required in an immunoassay for detection of the analyte. The commercial antibody presented a K_D of 3.09 x10^{-9} M towards the modified peptide, which makes this antibody a high affinity antibody. High affinity antibodies generally a K_D in the low nanomolar range (10^{-9}) and very high affinity antibodies a K_D in the picomolar (10^{-12}) range. However, this kinetic measurement was not performed for the neither of the other two peptides, not allowing to establish any type of correlation between affinity antibody and specific adducts. It would be of great interest for future work to compare the K_Ds of different commercial anti-HNE antibodies towards His, Cys and Lys-HNE specific adducts and understand if the immunization methodology applied influences the affinity/specificity of the antibody.

Another possible idea for future work regarding the MS approaches followed in this work would be to test a gentler collision energy on the mass analyser, like electron capture dissociation, in order to identify the exact location of the HNE adducts within the HSA amino

acid sequence, and equally important, to compare this study using freshly purified HSA to assess the differences in HNE modifications.

Nevertheless, either by using the intact protein or by chemically synthesising peptides, the formation of HNE adducts on HSA was confirmed, opening the possibility of using these adducts as immunogens to trigger the production of polyclonal antibodies.

CHAPTER III

GENERATION AND CHARACTERIZATION OF ANTI-HSA-HNE POLYCLONAL ANTIBODIES AND IMMUNOASSAY DEVELOPMENT

3.1. Introduction

3.1.1. Generation of anti-HNE Antibodies by Immunisation

Antibodies have undoubtedly become one of the most desirable classes of biomolecules for several industries, due to their high sensitivity and specificity towards specific targets. Particularly in the last 20-30 years, with the development of hybridoma and phage display technologies for generation of monoclonal antibodies, these molecules have been highly produced for application in scientific research, namely for laboratory assays such as radioimmunoassays and enzyme-linked immunosorbent assays (ELISA), in diagnostics, and even for immunotherapy (Sifniotis, Cruz, Eroglu, & Kayser, 2019). Regarding diagnostics and what concerns oxidative stress-related disorders, there has been a great interest in developing antibodies specific to lipid oxidation products such as HNE (Toyokuni et al., 1995), ACR (Uchida et al., 1998), MDA (Sevilla et al., 1997) and HHE (Yamada et al., 2004) for scientific purposes, but further deployment of these reagents in diagnostic assays for commercial application has not been accomplished yet.

With the exception of synthetic recombinant antibody production methods, virtually all antibodies are derived from active immunization of animals with an immunogen; however, not all molecules are considered immunogenic. In order to induce a good antibody response in a host animal, immunogens need to be bigger than 3000-5000 Da, so they can simultaneously bind to antibodies on the surface of B cells and to class II-T cell receptors (Harlow & Lane, 1988). Since most of the lipid oxidation products, including HNE, are of very small molecular weight, the generation of specific antibodies towards these products is considerably more challenging. To overcome this issue, these small molecules must be coupled to bigger molecules, also known as carrier proteins, which can elicit a much better immune response. Another very common strategy to trigger the immune system to produce antibodies, quite often used when working with lipid peroxidation products, is to chemically synthesize peptide sequences of proteins of interest, react them with the lipid oxidation product, and couple the modified the lipoxidised peptide to a carrier protein, so antibodies can be generated specifically against a certain peptide sequence. This strategy can be particularly useful when studying lipoxidation adducts, as the immunization of HNE-modified peptide sequences containing single and known nucleophilic residue may lead to the generation of antibodies specific to a certain type of lipoxidation adduct. For example, Uchida *et al* in 1995 generated an anti-HNE-His antibody by immunizing rabbits with HNE-conjugated to the heptapeptide Gly_3-His-Gly_3 covalently bound to a carrier protein (Uchida, Itakura, et al., 1995).

Equally important to the size of the antigen is its source, as animals develop immunological tolerance to self-molecules (Burdon & van Knippenberg, 1988). If antigens are very similar to host molecules, animals might not respond as B and T cells that display receptors specific to self-proteins have been previously eliminated from the system. Therefore, for the best immune response, antigens should be different from host molecules, ideally from a different animal species, so the immune cells recognize it. Non-human carrier proteins like keyhole limpet haemocyanin (KLH) and bovine serum albumin (BSA) are very often used in immunization protocols has they are very large proteins and do not cross-react to human proteins.

Once the immunization protocol is finished, antisera are relatively quick and inexpensive to produce, but the specificity and affinity of the desired antibodies entirely depend on further processing of the antiserum (Harlow & Lane, 1988). The whole IgG fraction is usually obtained from the serum by affinity chromatography, which is based on specific and reversible binding of the Fc regions of the IgG to lectins, such as Protein A or Protein G. However, if only a specific population of IgG is desired, then their capture requires immobilization of the immunogen onto a solid support to allow the specific antibodies to bind to the antigen. For both strategies, after extensive washing of the solid phase, which removes everything that does not bind to the antigen, specific antibodies can be eluted by disruption of immunological binding by either low pH or high concentrations of a competitor molecule (H. F. Liu, Ma, Winter, & Bayer, 2010).

The first anti-HNE antibody generated was raised by immunization of rabbits with HNE-treated KLH (Uchida et al., 1993) but other anti-HNE pAbs have been raised by coupling HNE to bovine serum albumin (BSA) (Satoh et al., 1999; Uchida, Itakura, et al., 1995). As regards the application of anti-HNE antibodies to immunoassays for detection of HNE-protein adducts, ELISAs have been by far the most developed assay. They are fairly easy and inexpensive to develop, rapid to perform, and can be designed in different ways; however, the accuracy of the test entirely relies on the sensitivity and specificity of the antibodies, which is not always consistent due to the complexity of the tested matrices. For example, a comparative study of two different anti-HNE primary antibodies in serum samples of obese patients have showed differences in the quantification range of HNE-protein adducts in plasma/serum between both direct ELISAs, even when both antibodies were stated to be specific to the HNE-His epitope (Weber et al., 2013). Nevertheless, Uchida *et al* in 1999 reported the development of a rapid competitive ELISA assay for quantification of acrolein and HNE modified proteins by using mAbs specific for the acrolein-modified FDP-lysine (N^{α}-(3-formyl-3,4-dehydropiperidino)-L-lysine) residue (mAb5F6) and the HNE-modified histidine residue (mAb HNEJ-2), and the results were very consistent.

Another direct ELISA developed for the detection of HNE adducts using the same anti-HNE-His mAb was tested in human osteosarcoma cell cultures and was shown to be able to determine HNE-His conjugates when cells were treated with less than 3 nmol of HNE/10^5 cells: however, the assay showed elevated background values due to the presence of several cell contaminants (Borovic, Rabuzin, Waeg, & Zarkovic, 2006). Regardless of the background, the authors stated that the assay had a sensitivity of 8.1 pmol HNE–His/mg of protein and an inter-assay precision of 12%, when tested with human osteosarcoma cell cultures (Borovic et al., 2006).

As none of these anti-HNE antibodies seem to be fully characterized in terms of epitope binding and even results obtained with monoclonal antibodies seem to be variable, there is still a very big window open for research and development in this field.

3.1.2. Chapter III Aims

As HSA was found to be one of the major nucleophilic target of HNE in the human sera (Aldini, Vistoli, et al., 2008), the aim of this section of the project was to generate antibodies with specificity to only HNE adducts on HSA and deploy these molecules in a immunoassay for rapid detection of HNE-HSA adducts.

To accomplish this aim, the HNE adducts formed on intact HSA and on ^{31}LQQCPFE^{37} peptide, confirmed in Chapter II, were prepared for immunization and administrated, separately, on different animals. After each vaccination, polyclonal sera were collected for screening by ELISA against different HNE-modified and non-modified target proteins, and subsequently, the potential anti-HSA-HNE antibodies were purified by different strategies. After epitope characterization, purified anti-HSA-HNE antibodies were applied on a sandwich immunoassay for assessment of specificity and sensitivity.

3.2. Reagents

Human serum albumin (A1653) and albumin from chicken egg white (A5503) were obtained from Sigma-Aldrich. Imject™ mcKLH (in PBS) and CarboxyLink™ coupling resin were purchased from Thermo Fischer Scientific (UK). 4-hydroxynonenal diethylacetal (HNE-DEA) was generously supplied by Prof. Giancarlo Aldini from University of Milan. HNE was prepared from HNE-DEA as stated before in **2.2 Reagents**. Commercial goat polyclonal antibody anti-HNE (Ab46544) was purchased from Abcam, and 3, 3′, 5, 5′-tetramethylbenzidine (TMB) and HRP-labelled anti-goat IgG were purchased from Sigma

Aldrich (UK). NHS-Activated Sepharose 4 Fast Flow columns and HiTrap Protein G HP columns were purchased by GE Healthcare (UK). Fluorenylmethyloxycarbonyl (Fmoc) protected amino acids were purchased from Intavis (20×1 cartridge of 0.5 mmol of Fmoc-Ala-OH, Fmoc-Arg (Pbf)-OH, Fmoc-Asn(Trt)-OH, Fmoc-Asp(OtBu) OH, Fmoc- Cys (Trt)-OH, Fmoc-Gln (Trt)-OH, Fmoc-Glu (tBu)-OH, Fmoc-Gly-OH, Fmoc-His (Trt)-OH, Fmoc-Ile-OH, Fmoc-Leu-OH, Fmoc-Lys (Boc)-OH, Fmoc-Met-OH, Fmoc-Phe-OH, Fmoc-Pro-OH, Fmoc-Ser(OtBu)-OH, Fmoc-Thr (tBu)-OH, Fmoc-Val-OH). 1-methyl 2-pyrrolidinone (NMP), dimethylformamide (DMF), 1,3-diisopropylcarbodiimide (DIC), 1-hy- droxybenzotriazole (HOBt) acetonitrile, formic acid, dichloromethane (DCM), and ethanol, were purchased from Rathburn chemicals Ltd (Walkerburn, Scotland). Trifluoracetic acid (TFA), triisopropylsilane (TIPS) and piperidine ≥99.5% was obtained from Sigma (UK). Sodium chloride (NaCl), Sodium Phosphate (Na_2HPO_4), potassium phosphate (KH_2PO_4), Glycine, Tween 20 and Trizma® (TRIS base) were purchased from Sigma Aldrich (UK). All solutions were prepared using ultra-pure Milli-Q water.

3.3. Materials and Methods

3.3.1. Preparation of HSA-HNE Adducts for Immunization

For the generation of HNE adducts, 5 mg of HSA were reacted with HNE (stock concentration of 5.2 mg/mL in 1 mM HCl) at a molar ratio of 1:10 in 1 mL of phosphate buffer saline buffer (PBS; 137 mM NaCl, 2.7 mM KCl, 10 mM Na_2HPO_4, 1.8mM KH_2PO_4, pH 7.4) for 2 h at 37°C. Once the 2 h were completed, the concentration of the reaction mix was adjusted to 1 mg/mL by addition of 4 mL of PBS.

3.3.2. Preparation of KLH-peptide-HNE Conjugate for Immunization

HNE-modified ^{31}LQQCPFE^{37} peptide was conjugated to KLH before sheep immunization, according to the protocol recommended by the manufacturer (Thermo-Scientific). The carrier protein, KLH, was activated with maleimide and reconstituted to 10 mg/mL in distilled water. It was then incubated with an equal volume of 10 mM sulfosuccinimidyl-4 -[N-maleimidomethyl] cyclohexane-1- carboxylate at room temperature for 1 h, with gentle periodic mixing. After equilibrating the PD-10 column (Thermo Scientific, UK) with conjugation buffer (100 mM ethylenediaminetetraacetic acid, 83 mM sodium phosphate, 100 mM sorbitol and 900 mM NaCl, pH 7.2), the excess cross-linker was removed by desalting. To ensure efficient conjugation, the peptide was prepared in a 10-molar excess

to KLH, by adding the molecular weight equivalents of the peptide and protein. The peptide was reconstituted to 1 mg/mL in conjugation buffer and incubated for 2 h with the collected column eluate. Again, PD-10 columns were equilibrated with conjugation buffer, and the conjugated peptide-KLH mixture was filtered through the column to remove any excess unconjugated peptide.

3.3.3. Generation of anti-HSA-HNE Polyclonal Antibodies

The immunization protocol was performed by the subcontracted company Orygen in Edinburgh, UK, that was responsible for administrating the initial immunization with 1 mg/mL of immunogen and further three (or, in some cases, four) boosts (one 28 days days) with 0.25 or 0.50 mg/mL of the immunogen, in each respective animal.

For generation of anti-HSA-HNE polyclonal sera, the effect of the stability of the adducts was tested by immunizing two sheep (SA350 and SA369) with non-reduced HSA-HNE adducts and two other sheep (SA351 and SA352) with $NaBH_4$-reduced HSA-HNE adducts. For generation of anti-HNE-modified ^{31}LQQCPFE^{37} conjugated peptide, two sheep (SA414 and SA415) and two rabbits were used (rabbits RA511 and RA512). Before the start of each immunization protocol, a pre-immune bleed was collected for further control analysis. Seven days after each injection a bleed (~300 mL) was collected.

Table III.1. List of the immunizations performed for the generation of anti-HSA-HNE antibodies.

Immunogen	Animals immunised
HSA-HNE (reduced addct)	2 sheep (SA351 and SA352)
HSA-HNE (non-reduced adduct)	2 sheep (SA350 and SA369)
HNE- modified ^{31}LQQCPFE^{37}	2 sheep (SA414 and SA415) and 2 rabbits (RA511 and RA512)

3.3.4. Polyclonal Sera Screening by Direct ELISA

The collected bleeds were screened for antibody binding by direct ELISA by coating 96-well microtiter plates (Corning, MA, USA) with 100 µL of the target antigen at 1 µg/mL, overnight at 4°C. Following aspiration of the antigen solution, the plates were washed three times with tris-buffered saline, 0.1% Tween 20 (TBST), and the wells were blocked with 120 µL of 1% (w/v) BSA/PBS for 1 h at room temperature. After another three-wash step with TBST, 100 µL aliquots of each bleed were added to the wells in 4-fold dilution factors in 1% (w/v) BSA/PBST (1/400, 1/1600, 1/6400, 1/25,600, 1:102,400 and 1/409,600) and the plate was incubated for 1 h with shaking at room temperature. The wells were once again washed three times with TBST and the plate was further incubated with 100 µL of 1:25,000 dilution

of mouse anti-sheep IgG or mouse anti-rabbit conjugated to alkaline phosphatase in 1% (w/v) BSA/ PBST, for 1 h with shaking at room temperature. The detection was done using pNPP (Thermo Fisher Scientific, USA) and the absorbance was read at 405 nm using a microplate reader. A schematic illustration of the assay is depicted below in **Figure III.1**.

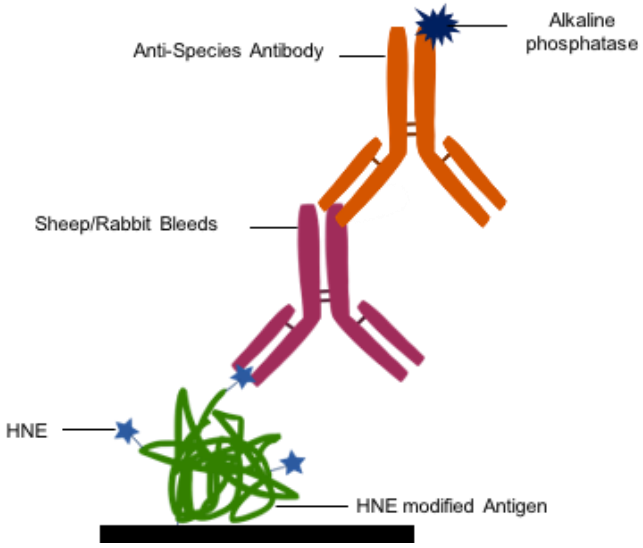

Figure III.1. Illustration of the direct ELISA assay performed for the detection of anti-HNE antibodies generated by animal immunization. The HNE-modified antigen was coated on a 96 well plate, to which the sera was added (after blocking). The detection was performed using an alkaline phosphatase labeled antibody anti-species.

3.3.5. Selective Capture of anti-HSA-HNE Antibodies

Selective enrichment of anti-HSA-HNE antibodies from crude serum of sheep SA369 was carried out by following two different affinity purification approaches. The first approach involved a first affinity chromatographic step using a HiTrap™ NHS-activated column modified with HNE-treated HSA (1 mL) for purification of the mixture of anti-HSA and anti-HSA-HNE antibodies, and a second affinity purification with a HiTrap™ NHS activated column modified with HSA (1 mL) for depletion of the anti-HSA antibodies. Anti-HSA-HNE pAbs were collected from the unbound fraction of the second purification run.

The second approach consisted of a first purification step with a HiTrap™ Protein G column (1 mL) for purification of the whole population of antibodies, and later, for the specific purification of anti- HNE antibodies a HiTrap™ NHS activated column modified with HNE-treated KLH was used. For both approaches, the columns were equilibrated with 5 column volumes of PBS pH 7.4, prior to loading of 10 mL of crude serum (previously centrifuged and filtered). Washing for removal of non-specific binding compounds was achieved by increasing the salt concentration to 1M NaCl for 2 column volumes. After re- equilibration

into PBS, the elution of bound antibodies was triggered by decreasing the pH to 2.5, using a 0.1M Glycine-HCl aqueous buffer. Column flow through and eluate were continuously collected as 5 and 2 mL fractions, respectively, in a FRAC 950 fraction collector from GE Healthcare. The collected samples containing the antibody of interest were combined neutralized by adding 60 µL of 1M Tris-HCl pH 9.0, per each 5 mL, and then placed in dialysis tubing overnight in 2 L of PBS. After dialysis, samples were loaded onto the second NHS modified column (KLH-HNE or HSA-modified) for depletion of anti-HSA anti- bodies. The same elution and dialysis methods were applied. The chromatographic runs with both columns were performed on an Äkta™ Purifier 10 system from GE Healthcare. The data collection and processing were accomplished using Unicorn 5.1 software. Chromatographic parameters such as conductivity and UV absorbance at 280 nm were measured continuously. The concentration of the eluate samples from both columns was calculated by measuring the absorbance at 280 nm using a spectrophotometer, and then dividing that value by 1.4 (extinction coefficient of IgG).

3.3.6. SDS-PAGE

Sodium dodecyl sulfate–polyacrylamide gel electrophoresis (SDS–PAGE) was performed to characterise the SA369 polyclonal serum and the different enriched populations of anti-HSA-HNE pAbs. Samples were prepared in Laemmli loading buffer, heated at 100°C for 5 min, and loaded onto a 12% acrylamide gel, prepared from 40% acrylamide/bis stock solution (29:1) (Bio-Rad, UK) and run at 100mV using 192mM glycine, 25mM Tris–HCl and 0.1% SDS, pH 8.3. Gels were stained with Coomassie Brilliant Blue (Pharmacia, Uppsala, Sweden). Images were acquired with the Gel Doc EZ System from Bio-Rad (CA, USA).

3.3.7. Western Blotting using the SA369 anti-HSA-HNE Polyclonal Antibody

For the Western blot analysis, samples were separated on 12% SDS-PAGE gels according to the conditions described before. Proteins were transferred from the gel to PVDF membranes using the Trans-Blot Turbo Transfer System (Bio-Rad, CA, USA). The membranes were blocked overnight at 4 °C with AdvanBlock-PF blocking solution (Advansta, Inc, CA, USA) and then incubated with the primary antibodies (either the in-house enriched anti-HNE pAb or the Abcam anti- HNE pAb, dilution 1:10,000), for 1 h at RT. The membranes were washed with AdvanWash washing solution (Advansta, Inc, CA, USA) three times for 10 min and incubated with the secondary antibody (HRP-labelled anti-

sheep and anti-goat, dilution 1:10,000). Detection was performed using the WesternBright Sirius ECL reagent (Amersham, UK), and images acquired using the ChemiDoc™ XRS + System (Bio- Rad, CA, USA). The results were interpreted by densitometry analysis using the software ImageJ, Version 1.48.

3.3.8. Sandwich ELISA for Detection of HNE adducts

A sandwich ELISA using the SA369 pAb as capture antibody and the Abcam anti-HNE pAb as detection antibody was developed for the detection of HNE adducts (**Figure III.2**). 96-well ELISA plates were coated overnight at 4 °C with 100 µL per well of the capture antibody (SA396 anti-HSA-HNE pAb) solution at 1 µg/mL. Plates were washed three times with TBST (20mM Tris, 137mM NaCl 0.05% Tween-20 pH 7.6) and blocked with 120 µL of 1% (w/v) BSA/PBS (137 mM sodium chloride, 2.7mM potassium chloride, 8mM disodium hydrogen phosphate, 1.5 mM potassium dihydrogen phosphate, pH 7.4), for 1 h at room temperature. Plates were once again washed three times with TBST, and then incubated with 100 µL of the antigen (KLH, HSA or OVA previously treated with HNE at a protein:HNE 1:10M ratio for 2 h at 37 °C and prepared in 1% (w/v) BSA/PBST at a range of 0–20 µg/mL) for 1 h with shaking. After another three wash steps with TBST, the plates were incubated with 100 µL of the detection pAb (Abcam anti-HNE HRP-la- belled (dilution: 1/2000)) for 1 h. TMB substrate solution (100 µL) was used for detection and its reaction was stopped after 15–30 min by addition of 50 µL of stopping solution (1M HCl). Absorbance was read at 450 nm.

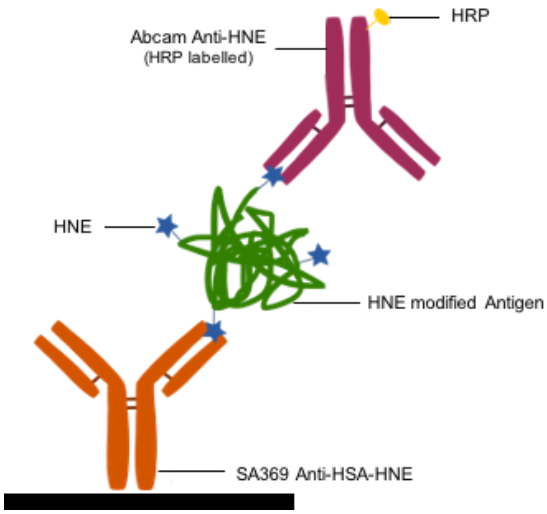

Figure III.2. Illustration of the sandwich ELISA assay developed for the detection of HNE adducts on proteins. The in-house sheep SA369 pAb was used as capture antibody and the Abcam anti-HNE pAb as detection antibody.

3.3.9. Statistical Analysis

Data from the ELISA assays shown in **Figure III.14 A** and **B** were both analysed with Microsoft Excel program, using a Student's t-Test: Paired Two Sample for Means for comparing individual concentrations of non-modified vs modified antigen in **Figure III.14 A**, and one-way ANOVA tests to assess in **Figure III.14 B** significative differences between HNE modified and non-modified HSA.

3.3.10. HRP-Labelling of Antibodies

Enriched anti-HSA-HNE pAbs and commercial anti-HNE pAb were labelled separately with horseradish peroxidase (HRP), for direct detection on the membrane immunoassays, using a commercial labelling kit from Innova Biosciences. The conjugation was performed according the manufacturer's instructions, by mixing the 10 µl of antibody solution (2 mg/mL) with 1 µl of LL-modifier reagent. After a 3 h incubation at room temperature with the Lightning-Link® mix, 1 µl of LL-quencher reagent was added. The conjugate was stored at 4ºC.

3.3.11. Design and Synthesis of Peptide Arrays

The sequence of HSA, including the 18-residue signal peptide and 6-residue pro-peptide (accession number P02768) and ovalbumin (OVA) (accession number P01012) was divided into 15-mer peptides with sequential peptides overlapping by 13 amino acids, and each peptide was synthesised on commercially available derivative membranes (amino-PEG500-UC540 Sheets) based on conventional Fmoc chemistry, using the Intavis ResPep SL peptide synthesiser (INTAVIS, Köln, Germany). Peptides were cellulose-coupled to the C-termini and the principle of the peptide arrays is depicted in **Figure III.3**.

The membranes were initially washed with DMF and ethanol, the coupling of the amino acids was achieved by pre-activation in 0.5M amino acid (in NMP), 1.1M activator (HOBt) and 1.1M of DIC in DMF. Any unreacted free amino groups were blocked by washing the membranes with 10% acetic anhydride in DMF (capping solution). The peptides were built one amino acid at a time, starting from the C-terminus to the N-terminus. In the last coupling cycle, the capping step was omitted and the final Fmoc-deprotection was carried out with 20% piperidine in DMF. The HSA and OVA sequences of each synthesised peptide and their localization on the peptide array are shown in **Appendix 5** and **Appendix 6**, respectively. Once the synthesis was completed, the membrane was treated with a mixture

of TFA/TIPS/H2O (18:1:1) for 1–2 h for final sidechain deprotection, and then washed with DCM for 30 min. Finally, the membranes were washed with ethanol and water, in cycles of 5 min and once dried they were stored in a sealed container at RT. In the text, HSA residues are numbered from the start of the mature protein sequence, without the signal and pro-peptides.

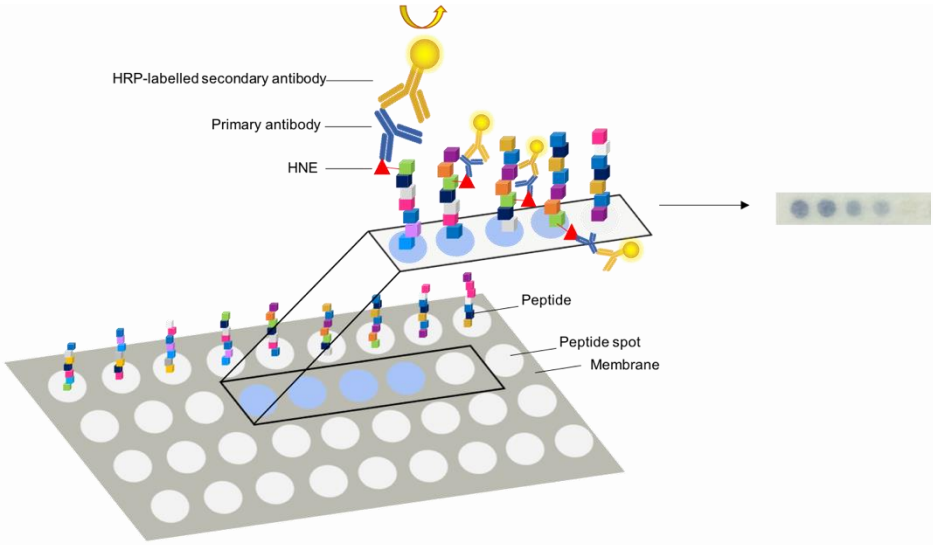

Figure III.3. Schematic representation of a peptide array. The membrane is firstly incubated with HNE and subsequently with the primary and the HRP-labelled secondary antibody. After incubation with the substrate, the peptide spots to which the antibody is bound develop a blue colour.

3.3.12. Epitope Mapping on Peptide Arrays

The cellulose membranes were initially washed 3 times for 10 min with PBS for rehydration and for the HNE adduct formation, the membranes were then incubated with 0.02 mM HNE in PBS for 2 h at 37 °C (for negative controls this step was omitted). Subsequently, membranes were washed twice with PBS containing 0.1% (v/v) Tween 20 (PBST) for 30 min and blocked with 20 mL of blocking solution (5% skimmed milk powder in PBST) for 1 h. The blocking reagent was discarded and a 20 mL aliquot of 100 ng/mL of HRP-conjugated anti-HNE antibody in blocking agent was added. After a 1 h incubation the membranes were washed with 3 volumes of PBST (3×5 min) and incubated with 5 mL of TMB for 15–30 min, until color is observed and the signal was completely developed. The membranes were washed with two volumes of water, allowed to drip dry and then scanned using a GS-800TM Calibrated Densitometer from Bio-Rad (CA, USA). The regeneration of the membranes was accomplished by incubation with 20 mL of 1% SDS in 100 mM Tris-HCl, pH 6 + 140 µl of β-mercaptoethanol.

3.4. Results

3.4.1. ELISA Screening of anti-HSA-HNE Polyclonal Sera

For the generation of anti-HSA-HNE polyclonal antibodies two sheep were immunized with non-reduced HSA-HNE adducts (sheep SA350 and SA369) and two other sheep were immunized with $NaBH_4$-reduced HSA-HNE adducts (sheep SA351 and SA352). Sera collected every month (7 days after an immunization) from the four immunized sheep, together with their respective pre-immune bleeds, were tested by ELISA against HSA-HNE and OVA-HNE coated microwell plates (**Figure III.4**). As seen in **Figure III.4 A**, all the four sheep responded well to the immunization by producing sera specific to HSA-HNE. In general, the three bleeds show increased binding to the antigen over time and no binding is observed for the pre-immune bleeds. For sheep SA350 and SA369, for the 1/1600 dilution, the Abs values start to decrease, which is due to a phenomenon known as “the hook effect” (D. Wild, John, & Sheehan, 2013). This suggests that, for the dilution in question, the concentration of antibodies and other proteins is so high that the binding of the antibodies to the antigen cannot be established. The higher concentration of antibodies produced by these two sheep might be related to the absence of adducts reduction, as it is the only existing difference between the two immunized immunogens.

As HNE is a very small molecule (MW: 156.1 Da) located on the surface of a very large protein (HSA MW: 66.5 kDa), the majority of the antibodies are likely to be generated against HSA. Therefore, the screening performed against HSA-HNE does not necessarily indicate the production of antibodies specific to HNE adducts on HSA. Thus, to discriminate the anti-hapten-specific antibodies (anti-HNE) from the anti-carrier specific antibodies (anti-HSA), all the bleeds collected from the four sheep were tested again by ELISA this time against HNE-modified (OVA) (**Figure III.4 B**). OVA was chosen as the carrier protein because, despite its name, it does not have any sequence similarity to HSA, but it has a similar molecular weight. The data shows that, in fact, only sheep SA369 exhibits a good immune response against HNE, as revealed by antibody titers >1/20,000 achieved by direct binding ELISA.

Regarding sheep SA350, which as well immunized with non-reduced HSA-HNE adducts, a small response to OVA-HNE was registered, different from the binding of the pre-immune bleed, however the titer of anti-HNE antibodies is very low. About sheep SA351 and SA352, none of the post-immunization collected bleeds showed binding to HNE adducts on OVA, being the absorbances values acquired the same level as the one obtained for the pre-immune bleeds.

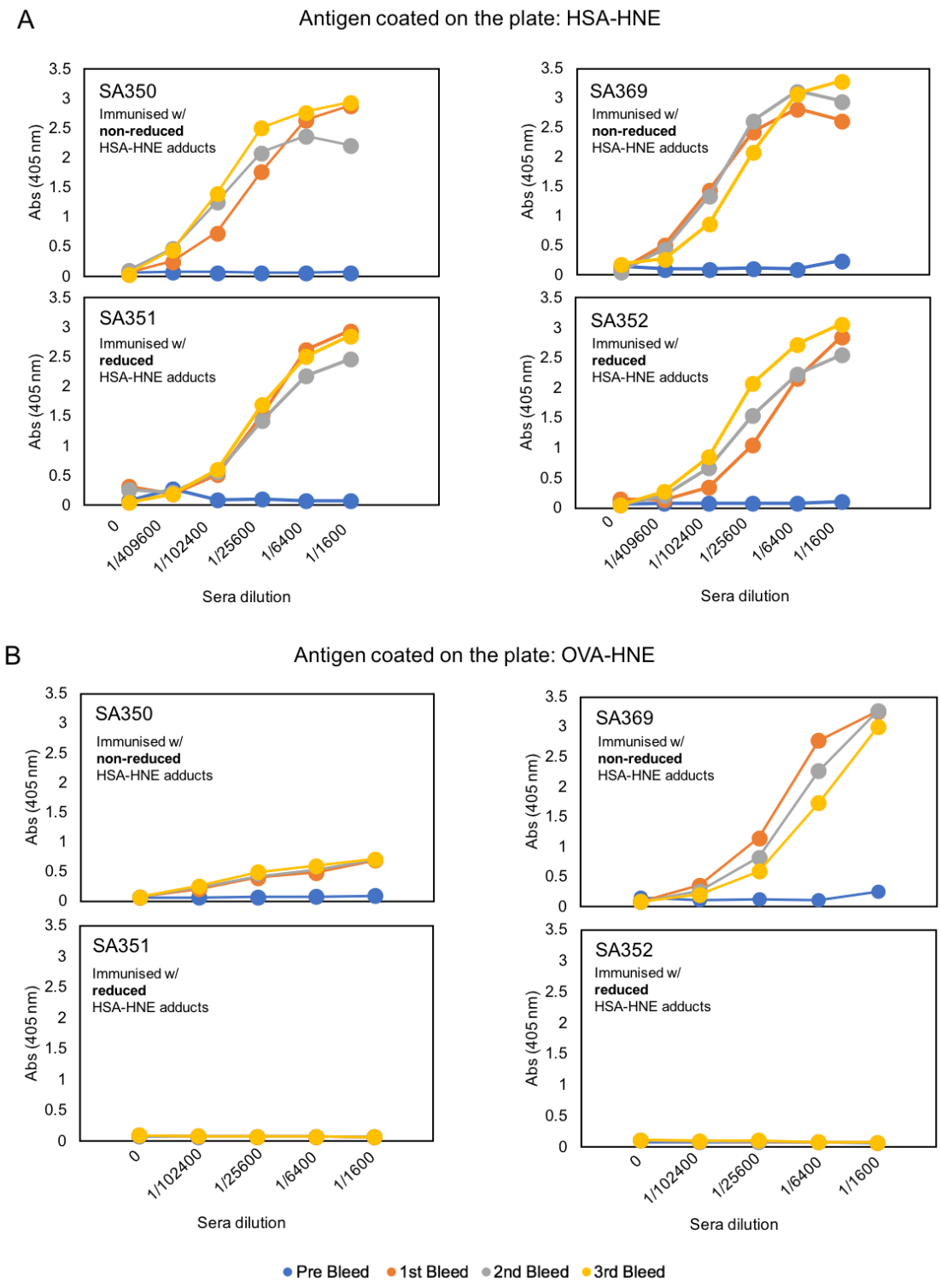

Figure III.4. Screening of anti-HSA-HNE polyclonal sera collected from sheep SA350, SA369, SA351 and SA352, by ELISA against HSA-HNE (A) and OVA-HNE (B). Sheep SA350, SA369 were immunized non-reduced HSA-HNE adducts and sheep SA351 and SA352 were immunized with $NaBH_4$-reduced HSA-HNE adducts. All the three post-immunization bleeds were screened against their respective pre-immunization collected bleed, as a control. The assays were only performed once (n=1), as the aim of this assay was to only assess the presence of target antibodies, in order to proceed to their purification.

3.4.2. ELISA Screening of anti-KLH-^{31}LQQCPFE^{37}-HNE Polyclonal Sera Screening

A second more targeted strategy for the generation of antibodies specific to HNE adducts on HSA involved the immunization of two sheep (SA414 and SA415) and two rabbits (RA511 and RA512) with HNE-modified ^{31}LQQCPFE^{37} peptide, which is the HSA sequence that contains the only free cysteine on the protein, and therefore has an enormous potential of being HNE modified *in vivo*. Because the modified peptide has a considerably low size (MW of 1019 Da for an HNE-MA adduct), in order to trigger a good immune response, the peptide was coupled to a carrier protein, KLH, before being used for immunization.

As for the previous reported immunization process, three post-immunization bleeds were collected and tested together with the pre-immune bleed, by ELISA against HNE-modified biotinylated ^{31}LQQCPFE^{37} peptide (**Figure III.5**).

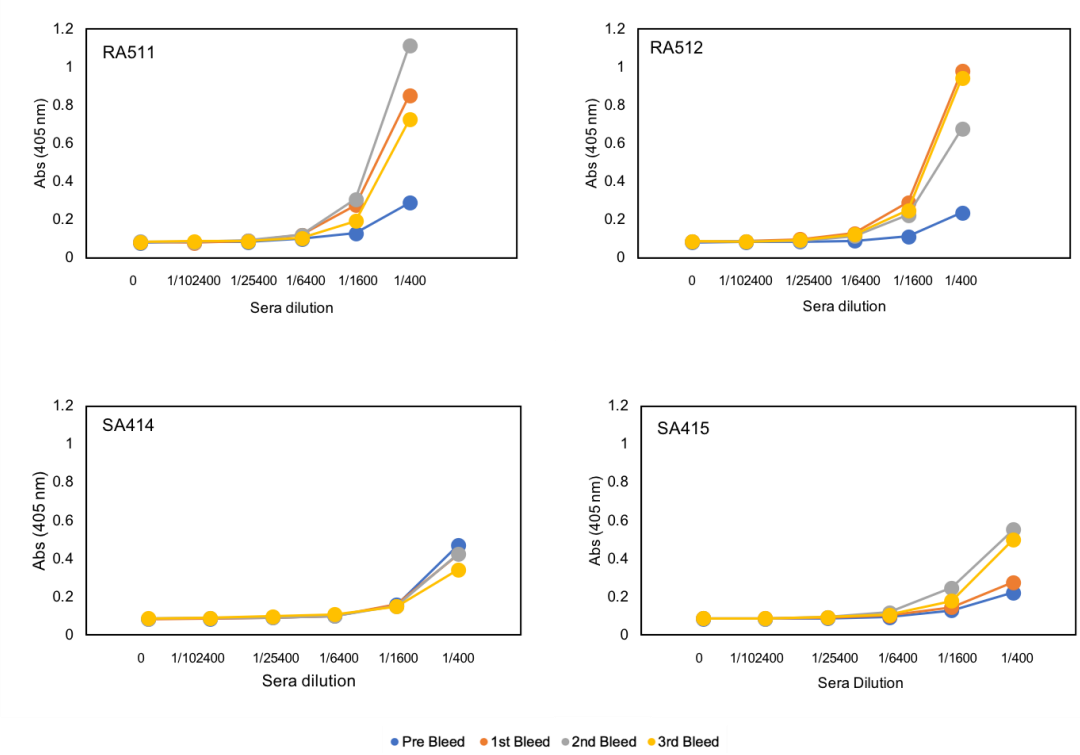

Figure III.5. Screening of the antibodies present in the pre-immune bleed and in three post-immunization bleeds collected from rabbit RA511 and RA512 and sheep SA414 and 415 immunized with KLH-^{31}LQQCPFE^{37}-HNE. The binding to Biotinylated-^{31}LQQCPFE^{37}-HNE modified HSA was accessed by ELISA assay. The assays were only performed once (n=1), as the aim of this assay was to only assess the presence of target antibodies, in order to proceed to their purification.

The ELISA data show a very weak response to the HNE-modified peptide for all of the bleeds collected either from the rabbits or sheep. Nevertheless, when comparing both species, rabbits seemed to have responded better, as seen by the higher absorbance values obtained for the smallest dilution of 1/400.

Sheep SA414's post-immunization bleeds do not reveal any binding to the modified peptide, as their absorbance values are of the same order of magnitude as the pre-immune bleed, and for SA514, even though a small increase in the binding is observed after the second boost, the titers appear to constant after the third and last immunization.

Consequently, as the antibody titers obtained from this peptide immunization are very low, both sheep SA414 and SA415 and rabbits RA511 and RA512 were terminated, and further work was carried out using only bleeds collected from sheep SA369, immunized with non-reduced HSA-HNE adducts, whose sera samples showed a much higher antibody titer to work with.

3.4.3. Enrichment and Characterization of SA369 anti-HSA-HNE Antibodies using HSA and HSA-HNE-conjugated Resins

In order to purify from the SA369 serum only the polyclonal antibody population specific to HSA-HNE and, possibly HNE only, a two-step chromatography purification was executed. This strategy involved an initial chromatography step using an HSA-HNE coupled resin for recovery of all anti-HSA and anti-HSA-HNE antibodies (**Figure III.6 A**), followed by a second chromatographic step with an HSA-coupled resin, for the depletion of antibodies with affinity for unmodified HSA (**Figure III.6 B**). The enrichment of anti-HNE/HSA-HNE antibodies with the first chromatographic run yielded a very tall and sharp elution peak around minute 37 (**Figure III.6 A**), which corresponds to all the antibody population that was bound to immobilized HNE-modified HSA. However, from the second chromatographic run with the HSA-coupled resin, one can see that the majority of the antibodies collected was specific to HSA, as seen by the very tall peak around minute 20 (**Figure III.6 B**). The antibody fraction that did not bind to this second resin was collect and tested by ELISA for binding assessment (**Figure III.6 C**).

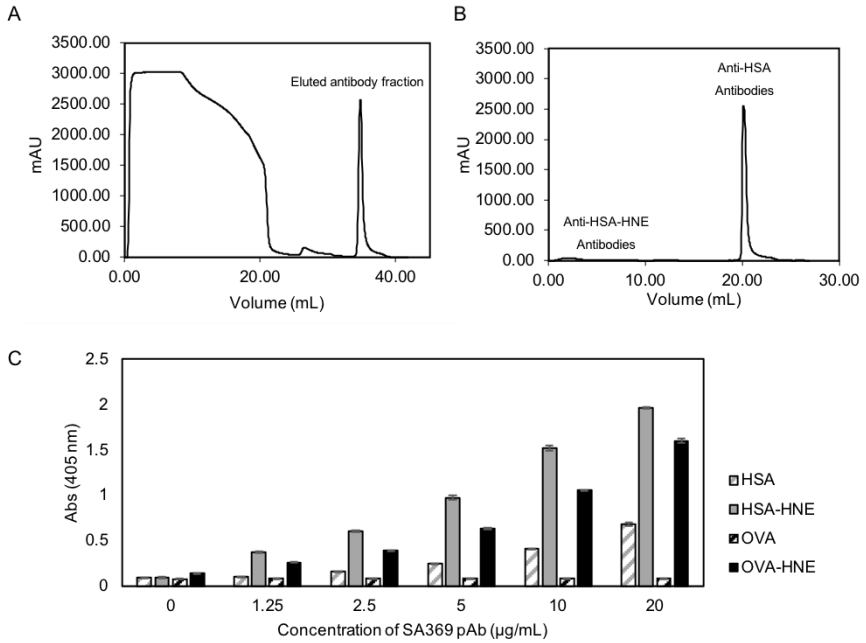

Figure III.6. Affinity purification chromatograms for purification of SA369 anti-HSA-HNE pAb using an HSA-HNE-coupled resin to recover the mixture of anti-HNE and anti-HSA-HNE antibodies (A) and an HSA-coupled resin for depletion of anti-HSA antibodies (B). The bound pooled fraction of the antibodies obtained in (A) was loaded into the second column, where the enriched pooled fraction of anti-HSA-HNE was collected from the unbound fraction. Binding assessment of the enriched pAbs to HSA, HSA-HNE, OVA and OVA-HNE was performed by direct ELISA (C) by immobilizing the antigens at 1.25 µg/mL and testing with the antibody concentrations indicated on the graph. This assay was performed in duplicate (n=1), showing average of 3 technical replicates ± SD.

The enriched SA369 antibodies collected the flow through of the chromatographic run with the HSA-couple resin appeared to have stronger affinity to HNE-modified HSA and HNE-modified OVA, as expected, but cross-reactivity to native HSA was observed. The fact that the pAbs recognized OVA-HNE and not non-modified OVA suggests that the fraction collected contains antibodies that recognize HNE modifications, regardless of the protein they are on. As cross-reactivity to unmodified HSA was observed and the yield and concentration of the enriched antibodies achieved was not high enough for further experiments, an alternative strategy was tested.

3.4.4. Enrichment and Characterization of SA269 anti-HSA-HNE Antibodies using Protein G and KLH-HNE Conjugated Resins

The second purification strategy applied for the enrichment of anti-HNE/HSA-HNE antibodies involved a first purification of all the IgG content from the sera, using a protein G resin, followed by a second purification with an NHS-activated sepharose column coupled to HNE-modified KLH for recovery of all the anti-HNE and, potentially anti-HSA-HNE antibodies, and depletion of the anti-HSA antibodies. KLH was chosen as carrier protein as it is a large protein (390 kDa) and has a high content of histidine and lysine residues (219 and 151, respectively), and is therefore a good target for HNE modifications.

The enrichment of IgGs using the Protein G resin (**Figure III.7 A**) yielded a very tall and sharp elution peak, which was collected and loaded on the KLH-HNE coupled resin (**Figure III.7 B**). A big fraction of the antibodies was depleted by this column (the unbound Ab fraction) and a small sharp elution peak corresponding to anti-HNE/HSA-HNE antibodies was collected (bound Ab fraction). The antibodies collected on both these fractions were tested by ELISA against HSA, HSA-HNE, KLH and KLH-HNE (**Figure III.7 C** and **D**). It was expected that this alternative enrichment strategy would select antibodies that recognized HNE with less cross-reactivity to HSA. **Figure III.7 C** shows that the unbound fraction (containing the antibodies that did not bind to the KLH-HNE modified resin) had a very high binding towards both HSA and HSA-HNE but showed little reactivity to KLH or HNE-treated KLH, indicating that substantial depletion of the anti-HSA antibodies was achieved with the second chromatography step. However, in **Figure III.7 D** it is seen that the bound fraction had similar binding to HSA, HSA-HNE, and HNE-modified KLH, but low affinity for native KLH. The cross-reactivity to native HSA suggests that some of the epitopes recognized by the SA369 enriched antibodies include not only the HNE moiety of the adducts on HSA or KLH, but also regions of the HSA, to which they can bind even in the absence of HNE.

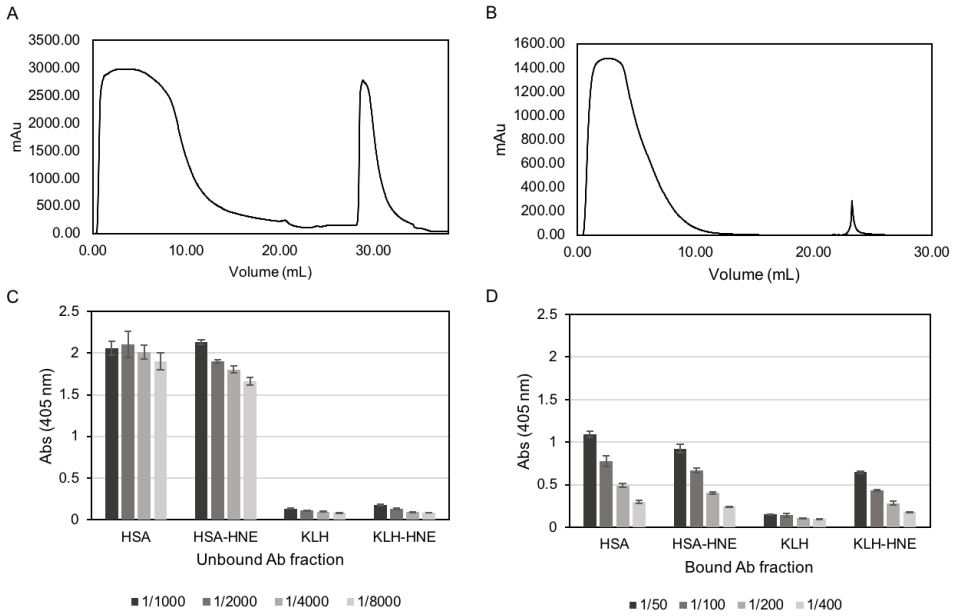

Figure III.7. Purification of anti-HNE/HSA-HNE antibodies from SA369 crude serum. IgGs were first were enriched by affinity chromatography using a Protein G resin (A) and later a KLH-HNE-coupled resin was used for capture of anti-HNE pAbs (B). The IgG eluted fraction obtained in (A) was loaded into the second column, where the enriched pooled fraction of anti-HNE pAbs was collected (eluted peak) (B). Binding assessment of the both pAb populations (unbound (C) and bound (D) from KLH-HNE resin) were tested against HSA, HSA-HNE, OVA and OVA-HNE by direct ELISA by immobilizing the antigens at 1.25 μg/mL and testing with the antibody concentrations indicated on the graph. This assay was performed in duplicate (n=1), showing average of 3 technical replicates ± SD.

The purity of the enriched SA369 anti-HNE pAb fraction was assessed by SDS-PAGE electrophoresis (**Figure III.8**)**,** under reduced and non-reduced conditions**.** As traces of serum albumin and immunoglobulins of higher molecular weight (possibly IgM) were observed in the lanes 2 and 5 of **Figure III.8**, so the SA369 anti-HNE antibody cannot be considered to be completely purified, but rather enriched.

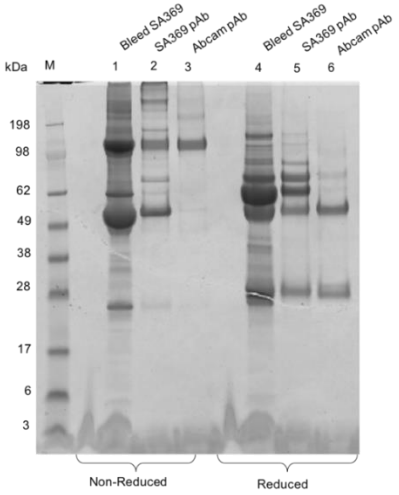

Figure III.8. SDS-PAGE gel analysis of the purified anti-HNE/HSA-HNE SA369 pAbs using a KLH-HNE covalently bound a sepharose resin. The collected pooled fractions contain still a trace of serum albumin as observed by a band corresponding to the weight of 65 kDa and some other immunoglobulins of higher molecular weight, possibly IgM. Samples in lanes 1, 2 and 3 were run under non-reducing conditions, while samples in lanes 4, 5 and 6 were run under reducing conditions. In lanes 5 and 6 bands corresponding to the weight of the heavy (50 kDa) and light chains (25 kDa) of the pAbs are seen. Proteins were separated by SDS- PAGE and stained with Coomassie blue.

In order to investigate further the specificity of the SA369 enriched antibodies, HSA, OVA or alpha-1 anti-trypsin (A1AT) were incubated with HNE in three different molar ratios, and the binding of the pAb preparation to these different HNE-modified proteins was assessed by Western blotting (**Figure III.9**). A1AT was tested as an additional plasma protein of comparable size with clinical relevance. The same Western blot was also performed with a commercial anti-HNE pAb (**Figure III.9 A**), as a positive control, which demonstrated treatment concentration-dependent binding to all three HNE-modified proteins but not to the unmodified controls, reflecting the recognition of HNE adducts regardless of the protein carrier. The enriched SA369 anti-HNE pAb showed strong concentration-dependent binding to HSA-HNE, but also bound weakly to unmodified HSA (**Figure III.9 B**), confirming the results obtained by the ELISA assay. In contrast, the OVA-HNE and A1AT-HNE were weakly recognized, both in comparison to the HSA-HNE and the binding of the commercial antibody, and there was little detection of native OVA or A1AT. This suggests there is additional combined specificity to the carrier (HSA) in the purified SA369 pAb preparation. The decrease in signal at the MW corresponding to the native proteins with increasing HNE:protein molar ratio in both blots may be explained by the formation of higher molecular weight forms and aggregates seen in the gels.

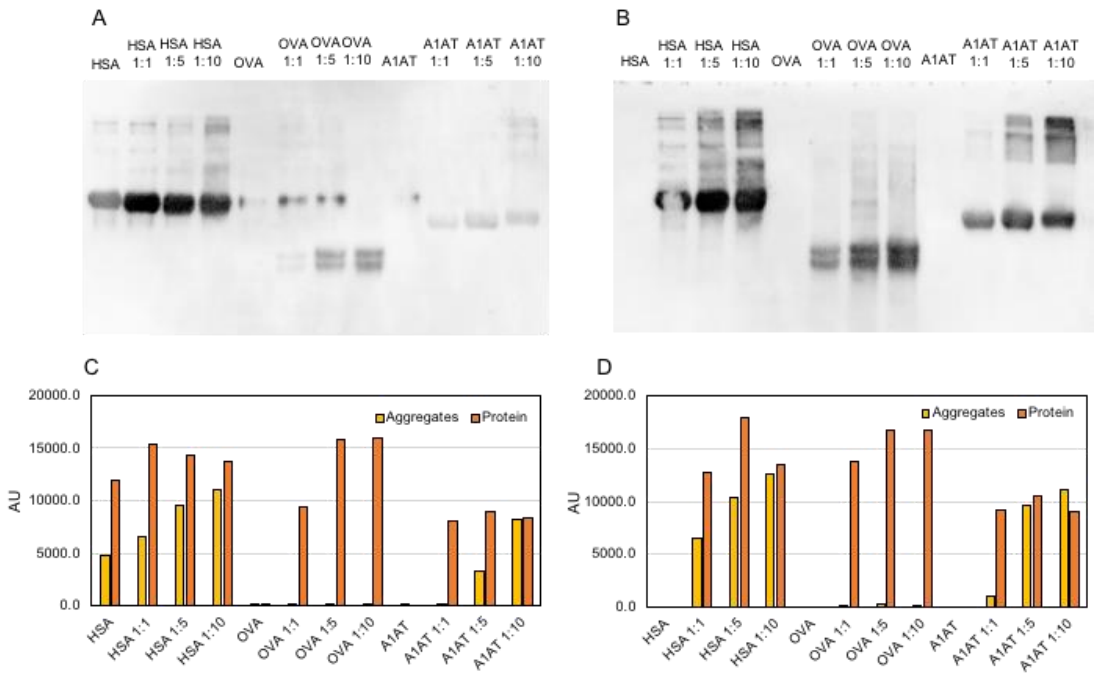

Figure III.9. Western blotting analysis of the SA369 anti-HNE enriched pAb. Human serum albumin (HSA), ovalbumin (OVA) and alpha 1-antitrypsin (A1AT) were treated with HNE at protein:HNE molar ratios of 1:1, 1:5 and 1:10, and their detection by the SA369 anti-HNE enriched pAb (A) and by the Abcam anti-HNE (B) was determined by western blotting. Both membranes were visualized under identical conditions, so the binding strength would be comparable, and densitometry analysis of both the aggregates formed post-modification and the protein were generated for the blots detected with SA369 anti-HNE pAb (C) and Abcam anti-HNE pAb (D). The experiment was only performed once (n=1).

3.4.5. Epitope Mapping

In view of the apparent recognition of both HNE and HSA epitopes from the SA369 pAb preparation, further epitope investigation using peptide arrays was performed. SPOT peptide array technology was used to identify and compare the binding sites of the commercial anti-HNE pAb (generated against HNE-modified KLH), and the in-house SA369 enriched pAb (generated against HNE-modified HSA), using peptide arrays designed with 15-mer peptides covering the whole sequence of HSA and OVA. One set of arrays was incubated with HNE prior to the incubation with each individual antibody, and the analysis was performed with control replicate membranes that were not treated with HNE. **Figure III.10** shows that both antibodies are able to recognize many epitopes in the HNE-treated arrays, as indicated by the darker spots. For the commercial pAb, twelve main peptides on the array stand out in terms of the intensity of signal: A27–29, C1-3, C16, D2-4, E11-16, E21–24, F2–F7, F16-20, G12-17, G25-28, I1-4 and I26-29 (**Figure III.10 A** and **Appendix 5** for peptide sequences), but binding to HSA control membrane was very weak (**Figure III.10 C**). There was substantial overlap in the set of HNE-modified peptides recognized by the in-house SA369 pAb (**Figure III.10 B**), indicated by the red boxes, but there was also binding to a number of other peptides, and it can be seen that the background binding to the control HSA membrane (**Figure III.10 D**) was substantially stronger than that of the commercial pAb. Similarities between the SA369 pAb binding to the HSA-HNE and HSA control membranes are indicated by yellow boxes. The OVA-HNE arrays showed clear similarities between the binding of the commercial pAb (**Figure III.10 E**) and the SA369 pAb preparation (**Figure III.10 F**), although the non-specific background staining was higher for the latter. Five regions were recognized by both pAbs (A5-9, B5-9, B26–30, F8-16 and G3), while the peptides D8-11 were only recognized by SA369 pAb and only the commercial pAb bound to C1.

One of the peptides to which both anti-HNE antibodies showed particular strong binding was the HNE-modified ^{365}DPHECYAKVFDEFKPLV^{381} peptide sequence (located in the **Figure III.10 A** and **B** at positions G16 and G17). Although never seen reported in the literature as a potential target of HNE adduction on HSA, this peptide contains in its sequence one His, one Cys and two Lys residues, which when displayed in a linear probably suffer an HNE modification and yield a tetra-HNE peptide adduct. It is not clear, however, why adjacent peptides G18 and G19 are not recognized by the commercial anti-HNE pAb, or G14 and G15 by the SA369 anti-HNE pAb with similar intensities, nonetheless, both anti-HNE antibodies have recognized this peptide very strongly in the membranes.

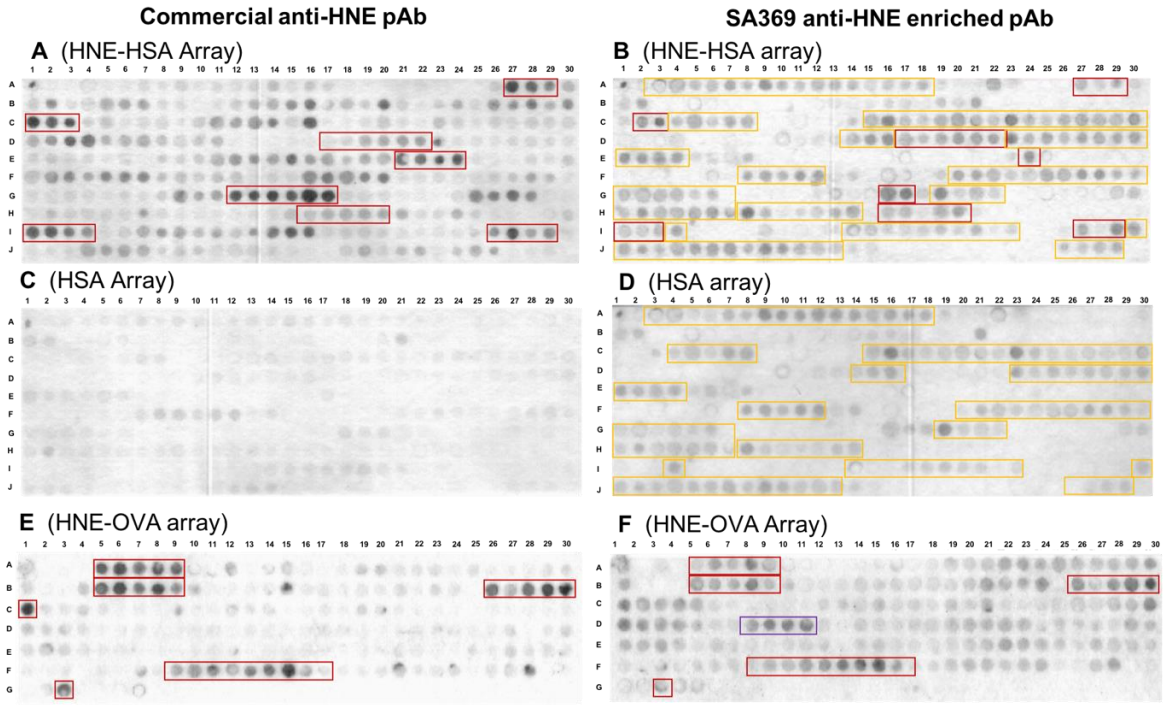

Figure III.10. Epitope mapping analysis for the SA369 enriched pAb using HNE-treated and untreated peptide arrays. A and B are arrays of HSA peptides (15-mer) treated with HNE; C and D are the equivalent arrays without HNE treatment; E and F are arrays of ovalbumin (OVA) peptides (15-mers) treated with HNE. Binding of the commercial Abcam anti-HNE pAb is shown in the left-hand column (panels A, C, E) and binding of the SA369 enriched pAb is shown in the righthand column (panels B, D, F). Peptides recognized by both polyclonal antibodies are boxed in red and cross-reactivity to HSA peptides recognized by the SA369 enriched pAb are boxed in yellow. The single purple peptide represents an OVA peptide recognized by the in-house pAb but not by the commercial pAb. All experiments were carried in duplicate and representative blots are shown. The list of all peptide sequences can be found in **Appendix 5** and **Appendix 6**, respectively for the HSA and OVA arrays. The arrays were synthesised in duplicate (n=2) and the immunoblot analysis performed in triplicate (n=3).

3.4.6. Synthesis of ^{365}DPHECYACVFDEFKPLV^{381} Peptide

As stated before, as the HNE-modified peptide ^{365}DPHECYAKVFDEFKPLV^{381} was reported as one of the epitopes recognized by both anti-HNE antibodies with highest affinity, this peptide was thought be a good capture sequence to be used for selection of high affinity anti-HNE antibodies and exclusion of the anti-HSA cross-reactive antibodies.

The peptide sequence ^{365}DPHECYAKVFDEFKPLV^{381} was chemically synthesized by the Fmoc chemistry (**Appendix 7** for reagents used), as previously for other HSA peptides, purified by reverse-phase chromatography (**Figure III.11 A)** and analysed by ESI-MS for mass confirmation (**Figure III.11 B**).

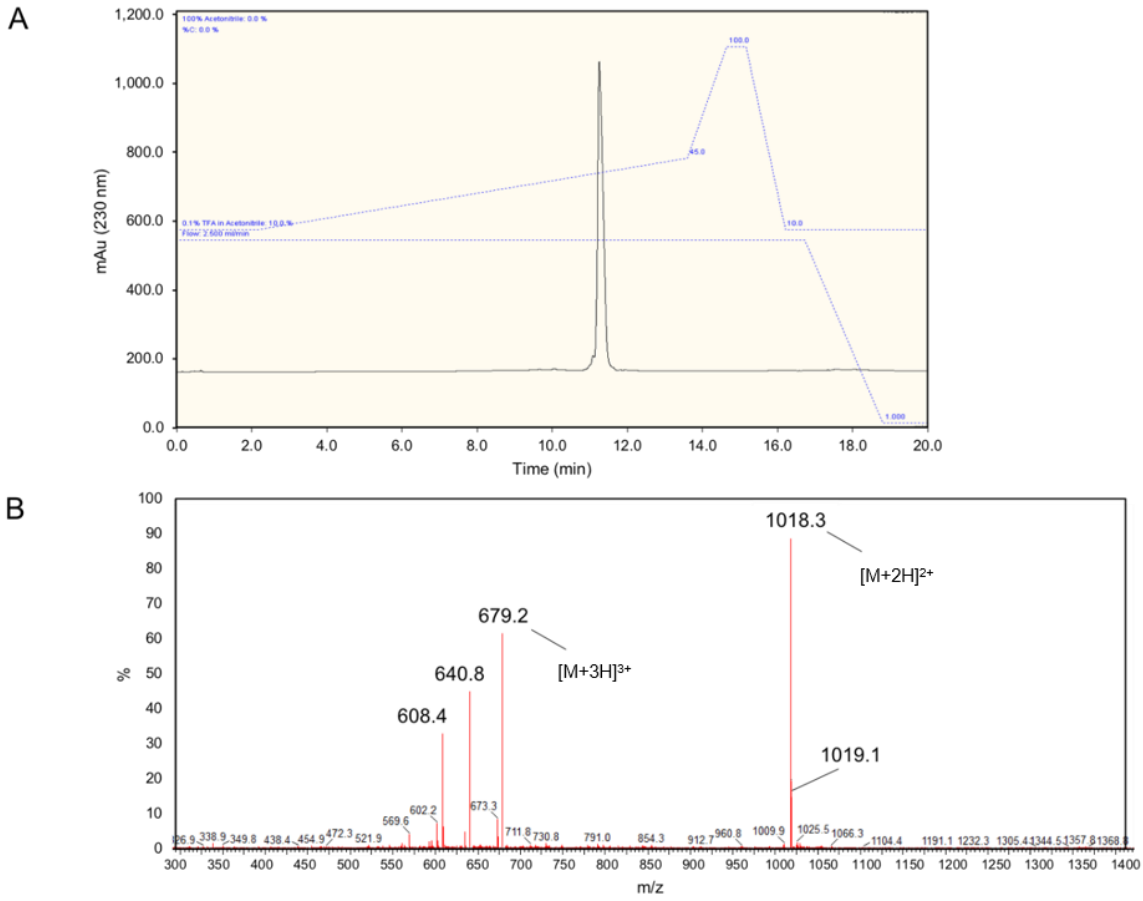

Figure III.11. HPLC chromatogram (A) and MS spectra (B) of the synthetic purified HSA peptide ^{365}DPHECYAKVFDEFKPLV^{381} (theoretical monoisotopic mass: 2034.99) identified by epitope mapping experiments as the strongest epitope for the enriched SA369 anti-HSA-HNE pAb. The crude peptide was initially dissolved in 5% v/v acetonitrile, 95% v/v water, plus 0.1% TFA, to a concentration of 1 mg/mL, all eluted peaks were collected for MS analysis and once the peak corresponding to the ^{365}DPHECYAKVFDEFKPLV^{381} peptide was identified further HPLC runs were set up for purification of that single product. In the end all the fractions were combined, the peptide was freeze dried, and analytical runs by HPLC (A) and ESI-MS (B) were performed for confirmation of purity.

The peptide of average molecular weight 2036.34 and theoretical exact mass of 2034.99 was confirmed by MS by the presence of the ion peaks at *m/z* 1018.3 and *m/z* 679.2, which correspond to the double protonated ($[M+2]^{2+}$) and triple protonated ($[M+3]^{3+}$) molecular ion species, respectively.

Once purified, the peptide was reacted with HNE *in vitro* in a molar ratio peptide:HNE of 1:10 for generation of HNE adducts. The formation of a single MA-HNE-peptide adduct was confirmed by the peak at *m/z* 1096.3, which corresponds to the protonated molecular ion $[M+HNE+H]^{1+}$ (**Figure III.12 A**) and the formation of a double MA-HNE adduct was confirmed by the peak at *m/z* 1174.3, which corresponds to the protonated molecular ion $[M+2HNE+H]^{1+}$(**Figure III.12 B**).

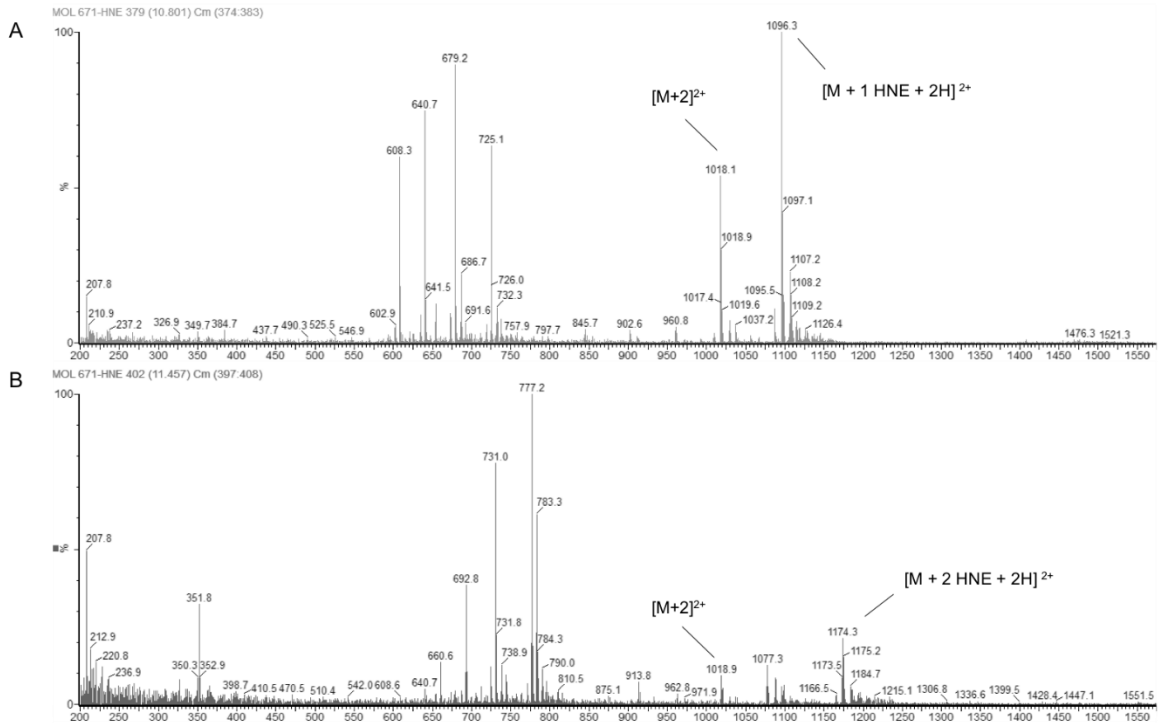

Figure III.12. Identification of HNE Michael adducts on peptide ^{365}DPHECYAKVFDEFKPLV^{381} (m/z 2034.99) by MS, following a 2 h reaction with HNE at a peptide-HNE molar ratio of 1:10. The formation of a single MA-HNE-peptide adduct was confirmed by the ion peak at *m/z* 1096.3, that corresponds to the double charged molecular ion $[M+HNE+2H]^{2+}$ (A). The ions peak at *m/z* 1173.3 that corresponds to the protonated molecular ion $[M+2HNE+H]^{+}$) confirms the formation of a double MA-HNE-peptide adduct (B). This MS analysis was performed in triplicate (n=3).

3.4.7. Enrichment and Characterization of SA369 anti-HSA-HNE Antibodies using a ^{365}DPHECYACVFDEFKPLV^{381} Conjugated Resin

The HNE-modified ^{365}DPHECYAKVFDEFKPLV^{381} peptide was immobilized on a carboxyLink resin, which is composed of crosslinked agarose beads pre-activated with diamino-dipropylamine for coupling of carboxyl-containing molecules, for purification of anti-HSA-HNE antibodies from the SA369 anti-sera.

The chromatogram in **Figure III.13 A** shows a very large depletion of proteins that did not bind to resin, followed by an unexpected large peak of proteins that were eluted with 1M NaCl, and therefore were only non-specifically bound to the resin, followed by a small elution peak of antibodies specifically bound to the modified resin. The unbound fraction collected from the flow through and both the bound fractions eluted with NaCl and glycine

were further analysed by ELISA and SDS-PAGE for binding and purification assessment, respectively.

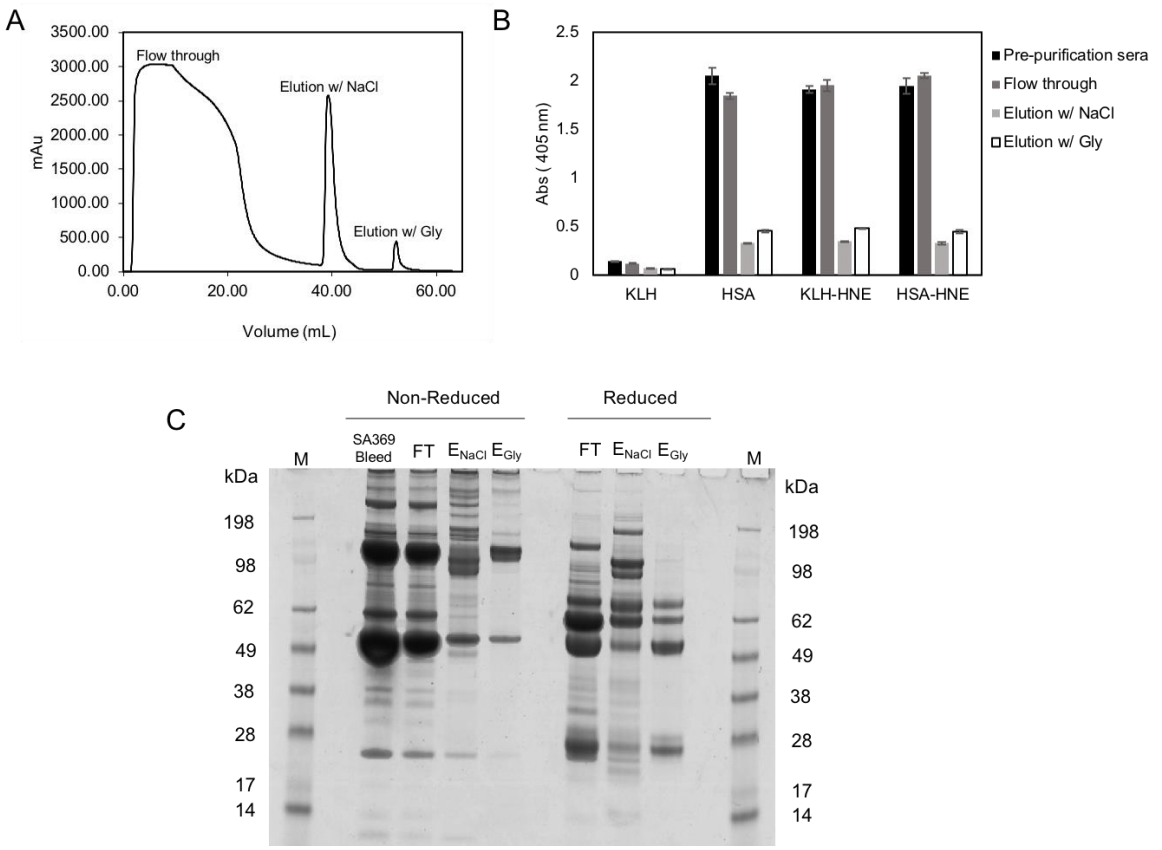

Figure III.13. Characterisation of SA369 anti-HNE/HSA-HNE antibodies after affinity purification using an agarose resin conjugated to the HNE-modified ^{365}DPHECYAKVFDEFKPLV^{381} peptide. Proteins detected in the chromatogram (follow-through and both the eluted fractions after washes with 1M NaCl and 0.1M Glycine-HCl) were collected and analysed by ELISA against HSA, KLH, HSA-HNE and KLH-HNE (B) and the purification pattern was assessed by SDS-Page gel (C). The experiment was done in duplicate (n=2), showing average of 3 technical replicates.

When analysing the ELISA results depicted in **Figure III.13 B**, no significant enrichment toward HNE-modified proteins is observed, as all the three collected fractions show similar level of binding (relative to each other) towards HSA, HSA-HNE and KLH-HNE. The unbound antibodies from the flow through fraction showed a very high binding towards non-modified HSA and both HSA-HNE and KLH-HNE, as the original loaded sera, which implies that the binding capacity of the column was surpassed, leading to the loss of anti-HSA-HNE/anti-HNE antibodies on the flow-through fraction.

Regarding the SDS-Page gel in **Figure III.13 C**, it is possible to see that the protein composition of the flow-through fraction (FT) is very similar to the original loaded bleed, being both characterized by two strong bands of molecular weight ~150 and 50 kDa (regarding non-reduced conditions) that correspond to the size of IgG and albumin,

respectively. Proteins eluted after the NaCl wash show a significant decrease in the binding towards the same antigens, with no difference being noted between HSA, HSA-HNE or KLH-HNE, which again confirms the loss of most of the target antibodies on the flow-through fraction. The separation of the proteins collected in this fraction by SDS-Page shows the presence of many bands of high molecular weight and a very low content of IgG, which supports the low binding observed by ELISA. Regarding the glycine-eluted fraction, the gel shows an almost pure IgG band (only with some traces of albumin), but the ELISA shows that once again the cross-reactivity to HSA was not eliminated.

3.4.8. Anti-HNE Sandwich ELISA Assay

Since both the commercial antibody anti-HNE and the SA369 enriched pAb anti-HSA-HNE are polyclonal, they are naturally a mixture of clones with individual characteristics and, therefore, recognise distinct epitopes. However, although there is a clear epitope diversity observed in the experiment with HSA peptide arrays, it is also clear that both these pAbs contain clones that are able to recognize HNE adducts in different proteins (HSA, OVA, KLH), and therefore, from the translational point of view, these could be valuable for immunoassay application (either a sandwich ELISA or a lateral flow assay) for analysis of biological, or even clinical samples.

Therefore, a sandwich ELISA assay was developed by pairing both antibodies, using the enriched SA369 pAb as a capture Ab and the Abcam anti-HNE pAb as detection Ab (previously labelled to horseradish peroxidase (HRP)). The ELISA was tested for its ability to recognize HNE adducts on different HNE-treated proteins – KLH, HSA and OVA –, using as negative control the respective non-modified proteins (**Figure III.14**). The plot shows that the detection signal increases for HNE-modified proteins, with increasing concentrations of the capture pAb, reaching a plateau at approximately 2 µg/mL of HNE-modified protein, whereas the signal for non-modified proteins seems to be kept low. Statistical analysis (**Appendix 9**) confirm significative differences, with *p*-values below 0.05 for the all the proteins when using concentrations of capture antibody $\geq$ 2.5 µg/mL.

For equivalent protein antigen concentrations, KLH-HNE showed by far the strongest intensity of signal, followed by OVA-HNE, and with HSA-HNE giving the weakest signal. In fact, the same ANOVA analysis show that for OVA and KLH, even when using capture antibody concentrations below 2.5 µg/mL there is statistical significative differences (*p*-values below 0.01). The strong KLH response may be justified by the its higher number of nucleophilic amino acids (52 Cys, 219 His and 151 Lys), when compared with the number

of nucleophilic amino acids of HSA and OVA, which possibly yield a higher the number of potential adducts. Subsequently, the standard capture antibody concentration of 2 µg/mL was selected and the analysis of HSA-HNE adducts was investigated in more depth by testing a range of concentrations from 0 to 5 µg/mL. A strong specificity for HSA-HNE over unmodified HSA is seen in **Figure III.14**, with some negligible cross-reactivity to HSA. Statistical analysis based on the t-test formula (**Appendix 10**) confirms significative differences (*p* value = 9.25E-05) between HSA and HSA-HNE samples.

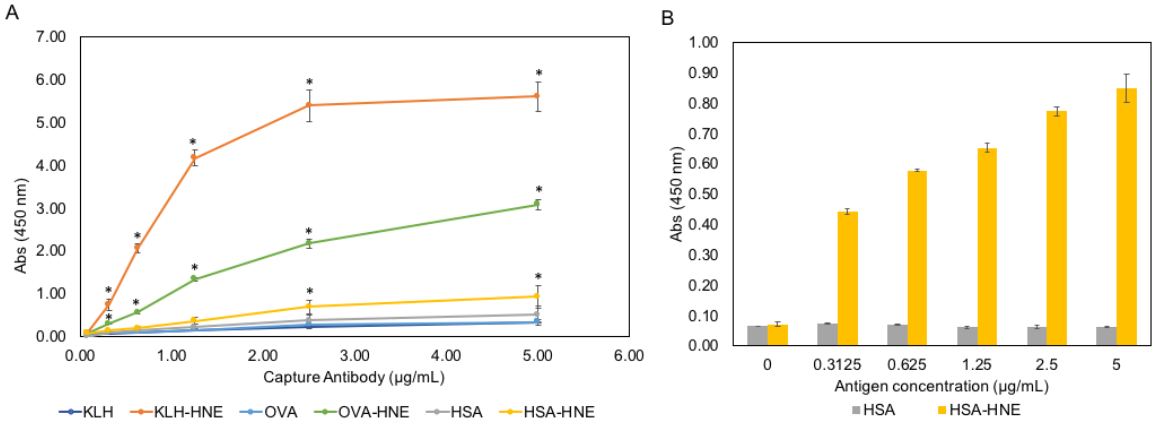

Figure III.14. Sandwich ELISA combining the enriched SA369 pAb as the capture Ab with HRP-linked Abcam anti-KLH-HNE at the detection Ab for analysis of HNE adducts. (A) Analysis of HNE-treated KLH, HSA and OVA by direct ELISA using the enriched SA369 pAb. Proteins were incubated individually with HNE at a 1:10 protein-HNE molar ratio, and non-HNE-treated protein tested as negative control. (B) Anti-HNE ELISA using a fixed concentration of the capture antibody (2 µg/mL) and a fixed concentration of the detection pAb (0.5 µg/mL). The antigen was added in a range of concentrations from 0 to 20 µg/mL. The assays were performed in triplicate (n=3) and data is presented as mean ± SEM, * p<0.01.

3.5. Chapter III Discussion, Conclusions and Future Work

The work presented in this chapter describes the generation of two different polyclonal antisera using as immunogens the neo-antigens of lipoxidised HSA. The antisera generated against HNE-modified HSA yielded some specific antibodies, but cross-reactivity to non-modified HSA was always observed regardless of the enrichment method applied for the purification of the HNE-specific antibodies. The data suggest that the enriched antibody fraction obtained by purification with an HSA-HNE resin and depletion with an HSA resin contains a mixture of different antibody clones that recognise both the HNE molecule and HSA peptide backbone, which causes the cross-reactivity observed.

The use of human albumin rather than any other species of albumin, for the immunization process, relied on the fact that the final application of the antibodies is to be for human diagnostics, and therefore recognition of human serum albumin is required, but also because the immune response is typically better triggered when antigen molecules are different from host molecules (Harlow & Lane, 1988). Rabbit (UniProt ID: P49065) and sheep (UniProt ID: P14639) albumin proteins share, respectively, 75.33% and 75.66 % of their amino acid sequence with the human (UniProt ID: P02768) albumin, which shows small amino acid differences of 20-30% may in fact make a difference in the immune response. In addition, the great interest and, consequently, great challenge of this project was to find if, rather than just the HNE molecules itself, the immune system could induce the synthesis of antibodies specific to HSA-HNE adducts only, which selectivity is much needed in diagnostic assays.

Immunisations with non-reduced and $NaBH_4$-reduced HSA-HNE adducts were performed in order to evaluate potential effects of stability over the immune system action and, interestingly, only sheep SA369, immunised with non-reduced HSA-HNE adducts, responded to the antigen properly and produced antibodies able to recognise HNE-modified proteins. Moreover, the immunization of sheep and rabbits with HNE modified ^{31}LQQCPFE^{37}-KLH-conjugated peptide, showed to not be successful either, as the ELISA assays performed with the collected sera did not show any recognition of HNE-treated proteins. The reversibility of the adduct, in this particular case, may have been critical for the immune response as, from the formation of the peptide adduct until the vaccination process, the peptide had to undergo several processing steps such as KLH conjugation, HPLC purification and freeze drying, that could have caused the disruption of the HNE from the target residues. Nevertheless, the work proceeded with the anti-sera generated from sheep SA369, which from the application point of view is in fact more appealing, as the reduction of adducts does not occur *in vivo*, and so the antibodies generated should recognize the structure of the HNE adducts that are likely to be formed.

The population of anti-HSA-HNE and anti-HNE antibodies was purified/enriched from the SA369 antiserum by three different affinity purification strategies, and the eluted fractions showed binding to different HNE-modified proteins but also to unmodified HSA in direct ELISAs and western blotting. Direct ELISAs showed relatively poor ability of the SA369 enriched pAb to discriminate between native and modified HSA, whereas western blotting indicated a substantially stronger binding to HSA-HNE.

The inability to separate clones that recognise only HSA from the ones that recognize only HNE suggested that polyclonal mixture of antibodies generated includes a significant fraction of antibodies that recognize epitopes containing structural features of both HSA

and HNE. An alternative explanation could be that, as the commercial HSA used for the majority of this study was purified from plasma, it may already contain some oxidative modifications, as has been described previously (Aldini, Vistoli, et al., 2008). However, ELISA testing of the reactivity of the SA369 pAb against recombinant HSA expressed in *Saccharomyces cerevisiae*, showed the pAb binding to both plasma purified and recombinant HSA, whereas the commercial anti-HNE pAb from Abcam showed no binding (**Appendix 8**). This suggests there is recognition of both protein and modification in the epitope. It is also possible that reactivity of the SA369 pAb to HNE on other proteins such as A1AT might result from reversibility of HNE-adducts, especially Schiff's bases, leading to transfer of HNE to other proteins within the host. In two previous studies where anti-HNE antibodies were raised against HNE-treated HSA samples, antibodies were purified from the crude sera only with a protein A resin and the authors reported strong binding to the immunogen (i.e., HSA-HNE) and almost negligible reactivity to unmodified HSA, which is surprising in the absence of a relevant depletion step (Khan et al., 2016; Khatoon et al., 2012). This discrepancy emphasizes the need to understand in more detail which peptide epitopes of HNE-modified HSA triggered B-cell clonal expansion during immunization and are recognized by the resulting immunoglobulins.

The use of HNE-treated peptide arrays provided detailed information on the linear epitopes recognized by the in-house SA369 pAb raised against HSA-HNE, and supported the idea that the diversity of antibodies include clones that recognise specifically the HNE part of the adduct (e.g. on OVA-HNE), while others seem to recognise the HNE structure combined with residues from HSA. Examination of the peptides recognized strongly by both pAbs indicated that they contain at least two to three nucleophilic amino acids in the sequence that are susceptible to attack by HNE (Cys, His or Lys) (Domingues et al., 2013), although for HSA it is well established that only Cys34 is in the thiol form and susceptible to attack by HNE; all other cysteines are disulphides (Aldini et al., 2006; Aldini, Regazzoni, et al., 2008; Nagumo et al., 2014). It was clear that the profile of peptide recognition by the two pAbs was similar for OVA, with relatively few reactive peptides, but distinct for HSA. One limitation that is important to note is that peptide array screening is not a quantitative assay; rather, it is semi-quantitative as the amount of peptide in each spot on the array may vary due to differences in the synthetic yield and peptide purity (Hilpert, Winkler, & Hancock, 2007). However, arrays were prepared in duplicate and gave comparable results, suggesting that this was not a major issue.

To understand the relationship between the HSA-HNE epitopes detected and the structure of the protein, peptides found to be HNE-modified by LC-MS/MS on chapter II were mapped onto the crystal structure of HSA and compared with those identified in the peptide arrays

(**Figure III.15**). As the epitope arrays only indicate which peptide sequences were recognized by the antibodies, the exact location of the HNE modification could not be pinpointed and therefore the possible modified residue was only labelled for the cases where the peptide detected matched the peptide identified by MS/MS. It can be seen that several peptides identified as HNE-modified by LC-MS/MS (**Figure III.15 A**) corresponded with epitopes detected in the arrays (**Figure III.15 B**). In particular, three HNE-modified peptides/residues detected by both pAbs (His105, His367 and His510), and two others detected only by the commercial pAb (His128 and His288), were found to be contain HNE adducts. It is notable that the majority of epitopes contained histidine residues, reflecting the higher stability of this adduct despite the greater reactivity of cysteine (Negre-Salvayre, Coatrieux, Ingueneau, & Salvayre, 2008; Uchida, 2003a).

The peptide that showed the highest binding intensity for both pAbs had the sequence ^{365}DPHECYAKVFDEFKPLV^{381}, and contained the potential target amino acids His367, Lys372 and Lys378. It is worth noting the residue numbering does not include the signal peptide (1–18) and pro-peptide (19–24) of HSA. These are part of an alpha helix and a loop located at the surface of the protein, which might play an important role in immunogenicity (Benjamin et al., 1984). The amino acid position within the peptide sequence seemed to be critical for the modification and/or the binding of the pAbs, as some peptides differing only by two neutral amino acids at one end of the peptide were consistently not recognized. Steric hindrance might explain this absence of binding, as adjacent bulky amino acids can hinder the access of HNE to the target amino acid, and thus slowing the chemical reaction. Alternatively, it is important to note that the isoelectric point, and consequently charge state of a peptide, as well as neighbouring-group participation effects, have a significant effect on the chemical reactivity of functional groups of individual amino acids. These are likely to be different even between adjacent, overlapping peptides on the array and may also account for the differences in modification observed for the same residue in different peptides. Another possible explanation is that synthetic linear peptides are not always authentic structural mimics of epitopes on globular proteins, where protein folding gives a distinct 3-dimensional structure (Forsström et al., 2014). This can lead to underestimation of affinity of the antibody binding. Detailed examination of the three-dimensional structure of HSA indicated that most of the epitopes recognized by the pAbs are alpha helix-containing loops, which might suggest that certain secondary structures and loops, in particular, might be more immunogenic (Hermeling, Crommelin, Schellekens, & Jiskoot, 2004).

Regarding the development of a diagnostic assays for lipoxidation of HSA by HNE, using antibodies that cross-react to non-modified HSA would be a major drawback. However, the

sandwich ELISA assay herein developed, which pairs the in-house pAb as capture antibody and the commercial pAb as the detection antibody, was shown to be able to discriminate between HSA-HNE and native HSA, and presented sensitivity to concentrations as low as 1 µg/mL of antigen. The availability of a supply of enriched SA369 pAb would make economically viable further development and testing of assays, including lateral flow assays, to analyse HSA-HNE and investigate its potential as an inflammatory marker. Alternatively, hybridoma technology or phage display for selection of single clones might offer a promising approach for the future to overcome cross-reactivity issues and improve specificity.

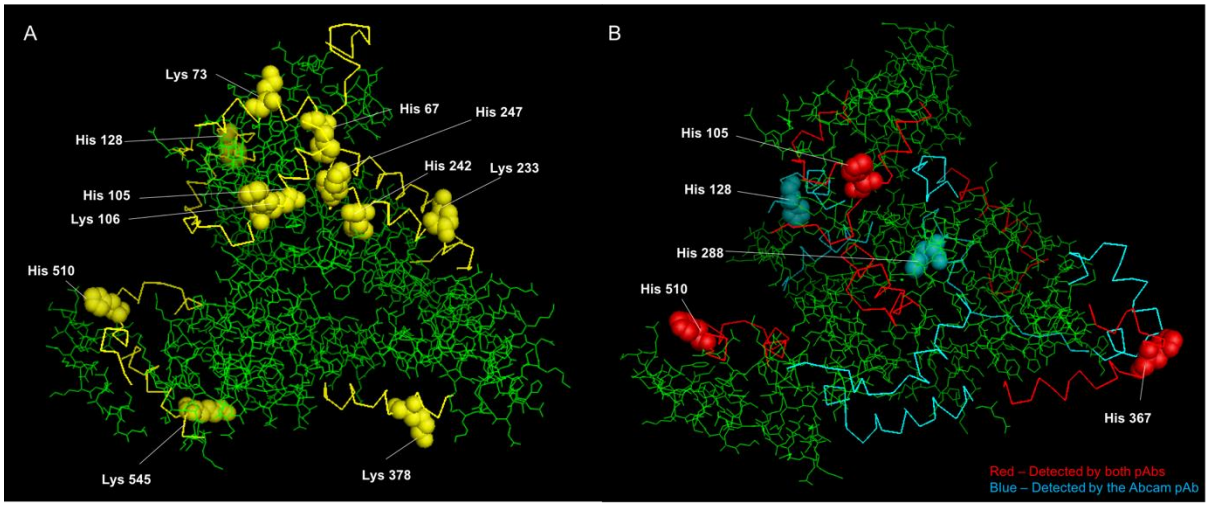

Figure III.15. 3D structure of HSA (PDB:1AO6) depicting HNE-modified peptides identified using the Sequest database search (A), and HNE-modified peptides detected by the commercial anti-HNE pAb (blue) and the in-house SA369 enriched pAb (red) on the HNE-treated HSA peptide arrays (B). The peptides recognized are indicated by backbone structure unless the nucleophilic residue likely to be responsible within the peptide could be identified. The residue numbering does not include the signal peptide (1-18) and pro-peptide (19-24) of HSA, in contrast to the arrays which did include these peptides.

Nevertheless, the enriched SA369 antibody and the commercial anti-HNE antibody were used as capture and detection antibodies, respectively, on a sandwich ELISA assay for the detection of HNE adducts on different proteins, and the assay succeeded in the distinction between HNE-modified and non-modified proteins with a sensitivity as low as 1 µg/mL of antigen.

With regards to future work, it would have been interesting to follow the animal's immunizations for a longer period. As the size of the aldehyde is very small and it is attached to large proteins like HSA and KLH, the host's immune response might have needed extra immunizations and longer time for the B cells to develop memory and make their immune response stronger.

It would have been important to test, as well, how freshly prepared HNE adducts would affect the immune response, as opposed as preparing all immunogens at the same time and shipping them to the company responsible for the immunization protocol. It is possible that the aliquot administrated by the end of month 3 did not have the same number of HNE adducts as the first administrated aliquot had, affecting therefore the specificity of the antibodies produced.

CHAPTER IV

DEVELOPMENT OF A DIAGNOSTIC LATERAL FLOW ASSAY FOR DETECTION OF LIPOXIDATION IN HUMAN MATRICES

4.1. Introduction

4.1.1. The Importance of Lateral Flow Assays

Lateral flow assays (LFA), also known as immunochromatographic assays or lateral flow strip tests, are immunoassays designed to operate along a single axis that can be used as diagnostic devices to confirm the presence or absence of a specific analyte. LFAs can be used to test a plethora of biological and physiological samples, such as urine, saliva, sweat, whole blood, serum, plasma and other body fluids, and are very well established in the fields of human diagnostics, veterinary medicine, environmental testing and pharmaceutical manufacturing (Wong & Tse, 2008). The most well-known type of LFA is the pregnancy test, developed to detect the pregnancy hormone, human chorionic gonadotrophin, in urine.

LFA technology has gained great popularity in the diagnostics field mainly for overcoming the two biggest pitfalls of the ELISA assays: the long operational time and the high number of steps. Furthermore, these devices are considerably small and portable, have a long shelf life, are robust and are simple to use as, typically, little or no sample preparation is required. Also, because this technology employs inexpensive materials, the low development cost and ease of production of these tests is another advantage of this technology. If the target analyte and necessary antibodies are available, assay development costs can be between $30,000 and $100,000, and once full optimization is achieved, test kits can be manufactured for $0.10–$3.00 per test (Wong & Tse, 2008). Another useful property of LFAs relies on their easy integration with electronic devices, such as scanners or cameras, which permit data to be digitized and interpreted (Koczula & Gallotta, 2016). Potential disadvantages of these assays include lot-to-lot reproducibility, restriction to qualitative or semi-quantitative readout and unclear patent situation, in some instances (Koczula & Gallotta, 2016).

Currently no LFA for (lipid) oxidation products exists, so there is potentially a commercial opportunity for deployment of anti-HNE antibodies, namely the enriched antiserum described in previous chapters, in rapid and simple diagnostic lateral flow assays for detection of HNE adducts in serum, and consequently assessment of oxidative-stress levels.

4.1.2. Principles of Lateral Flow Assays

In LFAs, a specified volume (10-100 µL) of aqueous sample is applied at one of the extremities of the test strip to a sample well and, due to capillary forces, it moves towards different components of the test, where antibody reagents are dried and immobilized.

Depending on the antibody reagents used, it is capable of reacting with specific analytes within the sample. The flow ceases when either there is no more sample left to flow into the strip or when the absorbent pad (also known as the sump) located at the other extremity of the assay becomes saturated (Berli & Kler, 2016).

These assays are typically composed of four elements: a sample pad, a conjugate pad, a nitrocellulose lateral flow membrane, and an absorbent pad (**Figure IV.1**).

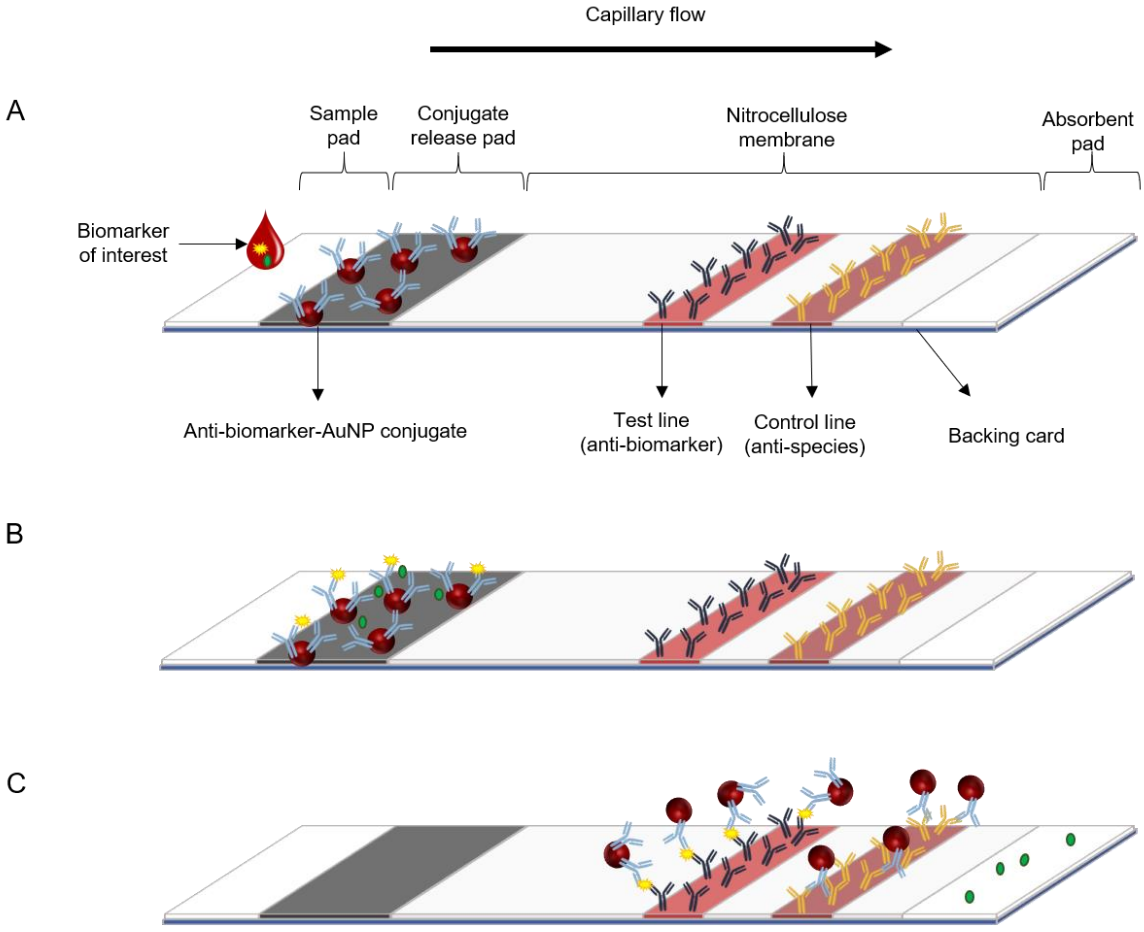

Figure IV.1. Schematic representation of a lateral flow immunoassay test strip. LFA devices are usually composed of a sample pad, conjugate release pad, membrane with immobilized antibodies and an adsorbent pad. The components of the strip may be fixed to an inert backing material and encased in a thermoplastic case with inlet ports and a viewing window over the test and control lines. The sample is applied to the sample pad (A) and it migrates towards the conjugate release pad (B) where the conjugated antibodies bind the biomarker and migrate to the test line (C), where the bound biomarker is captured.

The sample pad, as indicated by its name, is where the sample is applied, and its most important tasks are to promote the even distribution of the sample and control the rate at which the liquid enters the device. Then, as the sample penetrates the pad, it migrates to the conjugate release pad which is where specific labelled reagents (usually antibodies) are dried.

The most common label used for LFAs is in the form of gold nanoparticles (AuNP), to which the antibodies or other reagents can be adsorbed in such a way that a sufficient proportion of them can still retain their antigen binding properties. This pad is responsible not only for holding the dried detector molecules, but also to ensure their release occurs as soon as the liquid touches the pad. Once released, both the sample and the detection molecules flow together into the nitrocellulose test membrane, which is where specific capture reagents (again, typically antibodies) are pre-immobilized as invisible transverse line. In a conventional LFA, this membrane has two different immobilized antibodies in two different areas named as the test line and the control line. If the target analyte is present in the sample, the test line will become coloured, the intensity of colour being proportional to the concentration of the analyte, between predefined concentrations. In contrast, the control line is designed to develop a standard colour every time, simply indicating that the test sample had flowed properly through the strip. This membrane is usually made of nitrocellulose (NC), which has very high protein binding affinity and an ideal pore structure/size to support capillary flow. This combination enables the process of capillary flow to take place in a matrix in which localized antibody deposition provides a capture line for specific molecular detection. Lastly, once all the liquid has flowed through both reaction lines, it migrates into the absorbent pad, or sump. This pad is very important for the function and performance of the assay as it is for the means by which increased sample volumes can be applied and processed through the capture line. With larger volumes of sample, more analyte can be captured, thus increasing sensitivity. In addition, the capacity to cope with larger volumes of liquid allows for the use of “chase” or rinse fluids to wash away unbound detection antibodies, which can lower the background signal to enable greater sensitivity (improving the signal to noise ratio) (Koczula & Gallotta, 2016).

4.1.3. Gold Nanoparticles (AuNP) as Detection Label in LFA

The result of a lateral flow assay, in the end, depends entirely on the labelled reagent released from the conjugate pad, that upon deposition on test and/or control lines of the nitrocellulose membrane, exhibits a detectable signal. Ideally, a signalling label should be easy to conjugate to any target molecule without losing its biological integrity and activity and, of course, to be as sensitive as possible without compromising the results. Labels are expected to possess minimal specific binding characteristics and to be stable under various chemical conditions and temperatures (Sajid, Kawde, & Daud, 2015).

The most commonly used visualisation labels include gold nanoparticles (AuNP) (Bailes, Mayoss, Teale, & Soloviev, 2012; Christopher, Robinson, & Shaw, 2007; Ngom, Guo,

Wang, & Bi, 2010), latex nanoparticles (5,266,497, 1993), magnetic particles (Huang, Wu, Hung, Wang, & Chang, 2018), carbon particles (van Amerongen et al., 1993), selenium particles (Wang et al., 2014), silver nanoparticles (Anfossi et al., 2019), quantum dots (Xie et al., 2019), up converting phosphors (Corstjens et al., 2001), enzymes and liposomes (Sajid et al., 2015). Latex nanoparticles were among the earliest used. They can be synthesized in different colours, which is ideal for multiplexing, are fairly inexpensive to synthesize, and easy to prepare and conjugate. However, they have a natural tendency to aggregate after conjugation to the ligands, which is not desired in rapid tests. Inert particulates such as gold, silver and carbon are much less prone to aggregation and therefore have been extensively used in many different applications (Christopher et al., 2007).

Colloidal gold nanoparticles (AuNP) are, perhaps, the most widely used label in LFA. These particles are synthesized by reduction of the chemical reduction of chloroauric anions ($AuCl^-_4$) as the gold precursor. They can be synthesized in a variety of sizes from 5 to 100 nm, with the most appropriate diameters for LFA detection being between 40 and 80 nm. Below 10 nm AuNPs start losing their bright and intense colour, and above 40 nm start to aggregate (López-Lorente, 2014). Although very easy to synthesize, the manufacture of high-quality AuNPs with consistent reproducibility is a hard task to achieve. Irregular morphologies in the particles make them prone to aggregate and compromise the distribution and availability of the conjugated ligand (Christopher et al., 2007). Nevertheless, their intense colour poses a great benefit, as direct visualization can be achieved without any requirement for further development steps. Another advantage of gold nanoparticles is their negatively charged surface, which makes them ionically attracted towards positively charged biomolecules, such as antibodies at high pH values, making them easy to be conjugated. Besides ionic attraction, the interaction between antibodies and gold nanoparticles can also be achieved via hydrophobic attraction between the antibody and the gold surface and/or dative binding between the gold conducting electrons and amino acid sulphur atoms of the antibody (Jazayeri, Amani, Pourfatollah, Pazoki-Toroudi, & Sedighimoghaddam, 2016). In all cases, antibody conjugation to AuNPs is a very sensitive procedure that requires a controlled pH buffer environment and a suitable concentration of both antibodies and particles (Cvak, Pum, Molinelli, & Krska, 2012).

Regarding effective LFA detection limits, conventional AuNPs-based LFA have been constrained to limits of detection of ~1-10 ng/mL (Fernández-Sánchez et al., 2005; Lai, Fung, Yang, Renrong, & Xiong, 2009). The sensitivity obtained with carbon or silver nanoparticles that can reach sensitivities of low pg/mL. Nevertheless, sensitivity-

enhancement methods have been developed such as silver deposition, NH_2OH-HCl enlargement, and signal amplification of large AuNP (M. Chen et al., 2015).

4.1.4. LFA Formats

LFAs, like ELISAs, can be operated as direct (sandwich) assays or as competitive assays. In a sandwich LFA, the target analyte is captured between two complementary antibodies, the detection antibody, that is conjugated to detection reagent and is dried on the conjugate pad, and the capture antibody that is immobilized on the test line. The intensity of the colour developed by the deposition of detection reagent on the test line will be indicative of the amount of analyte present in the sample, making the LFA a quantitative assay (Wong & Tse, 2008).

In competitive LFAs, labelled antigen is immobilized at the test line and if the same analyte is present in the sample it will bind to the detection antibody, dried in the conjugate pad, which will be unable to bind to the antigen on the test line. Therefore, the lower the signal, the higher the amount of analyte present in the tested sample. This format is usually applied to small analytes, that have a single epitope of interest, and therefore cannot bind to two antibodies simultaneously (Sajid et al., 2015).

In order to improve efficiency and achieve high-throughput detection, LFAs can be designed to detect multiple analytes in a single sample simultaneously. These assays, known as multiplexed assays, are a derivatization of the aforementioned direct (sandwich) assays, with the difference of extra reaction lines on test strip. As a rule, LFAs include two reaction sites, the test and the control lines, which develop independently from each other, but the addition of further reaction sites along the test strip allows the assay to be multiplexed. However the spatial separation of multiple detection sites needs to be very well studied as reading the results is not as simple as with a conventional single parameter assay (Anfossi, Di Nardo, Cavalera, Giovannoli, & Baggiani, 2018).

4.1.5. Chapter IV Aims

The aim of the work described in this chapter was to assess the applicability of the in-house SA369 enriched anti-HNE pAb (generated by sheep immunization with HSA-HNE adducts) and the commercial anti-HNE pAb (generated by animal immunization KLH-HNE) in the development of a novel lateral flow immunoassay for detection of HNE adducts on proteins.

For the development of the LFA, several buffers were optimised, namely buffers used for conjugation of antibodies to gold nanoparticles, and buffers used for drying the conjugates to the conjugate release pad. Different HNE-modified proteins were tested, at different concentrations, and, for sensitivity, different HNE:protein molar ratios were investigated.

4.2. Reagents

Human serum albumin (A1653), bovine serum albumin (A7906) and albumin from chicken egg white (A5503) were obtained from Sigma-Aldrich (UK). 4-hydroxynonenal diethyl acetal (HNE-DEA) was generously supplied by Prof. Giancarlo Aldini from University of Milan. Tween 20, BES (N,N-*bis*(2-hydroxyethyl)-2-aminoethanesulfonic acid), MES (2-(N-morpholino) ethane sulfonic acid), TES (2-[(2-hydroxy-1,1-*bis*(hydroxymethyl)ethyl)amino]ethane sulfonic acid), TAPS (N-[tris(hydroxymethyl)methyl]-3-aminopropanesulfonic acid), boric acid and sodium tetraborate decahydrate were acquired from Sigma Aldrich (UK). Sucrose and PBS tablets were purchased from Fisher scientific (UK), hydrochloric acid and sodium hydroxide from VWR (UK) and sodium chloride from Sigma-Aldrich (UK). Colloid gold nanoparticles 40 nm were purchased from BBI solutions (UK). Commercial goat polyclonal antibody anti-HNE (Ab46544) was purchased from Abcam (UK). All solvents were of LC-MS grade and all solutions were prepared using Milli-Q water. Backing card (60 mm) was purchased from Lohmann Technologies (UK), Nitrocellulose 140 (25 mm) from Sartorius Stedim Biotech GmbH (Germany), Sink pad (22 mm) and conjugate pad (17 mm) from Ahlstrom-Munksjö Germany GmbH Germany), sample pad FR1 from MDI Advanced Microdevices Pvt, Ltd (India), and universal LFA housing cassettes from Adreco Plastics (UK).

4.3. Material and Methods

4.3.1. Preparation of HNE-modified HSA, OVA and KLH Standards

HNE adducts on HSA, OVA and KLH proteins were prepared as stated in **2.3.4. Generation of HNE Adducts on HSA, HSA Peptides**.

4.3.2. Buffer Optimization for Antibody-gold Conjugation

Abcam anti-HNE and SA369 enriched anti-HNE antibodies were diluted separately in different buffers (20 mM BES pH 6.3, 20 mM MES pH 6.7, 20 mM TES pH 7.1, 20 mM TES pH 7.5, 20 mM BES pH 7.8, 20 mM TAPS pH 8.5, 20 mM Borate pH 8.5, 25 mM Borate pH 8.5, 20 mM Borate pH 9.3 and 25 mM Borate pH 9.3) to concentrations ranging from 0 to 5 µL/mL.

A 96-well plate was loaded with 20 µL of each solution, to which 200 µL of colloid gold 40 nm OD1 was added and left to incubate for 10 min with shaking (150 rpm). To induce aggregation, 40 µL of 10% (w/v) NaCl were added to each antibody-gold solution and the absorbance was measured 10 min later at 550 nm and 600 nm. The aggregation ratio was calculated using **Equation 1**.

$$\text{Aggregation ratio} = \frac{\text{Abs}_{600\text{ nm}}}{\text{Abs}_{550\text{ nm}}} \quad \text{(Equation 1)}$$

4.3.3. Deposition of SA369 Enriched anti-HNE pAb onto Nitrocellulose

An antibody solution at a concentration of 1 mg/mL in PBS with 1% (w/v) sucrose was prepared and dispensed across a 30 cm nitrocellulose (NC140) membrane, 7 mm away from the top edge, using the IsoFlow™ flatbed dispenser (Imagene Technology, USA) at a dispenser rate of 0.1 µL/mm. The band was then dried at 60 ºC, at 10 mm/sec using the Drying Tunnel Type BT3 Conveyor Oven (Hedinair, UK).

4.3.4. Atomization of Abcam anti-HNE pAb-gold Conjugate onto the Conjugate Pad

The pAb-gold conjugates were prepared by incubating 5 µg/mL of Abcam anti-HNE pAb prepared in 25 mM sodium tetraborate pH 9.3 with 100 µL of gold nanoparticles 40 nm. The solution was incubated for 10 min before blocking with 1 µL of BSA (200 µg/mL) for 30 min at RT. For rapid optimization protocols, the assays were first tested under the “wet assay” format, i.e., by adding the pAb-gold conjugate solution in a microplate well and dipping the strip test on it. For the “dry form” of the LFA, the pAb-gold solution was atomized in a 30 cm non-woven glass fibre conjugate pad (17 mm), using the IsoFlow™ flatbed dispenser (Imagene Technology, USA) at a dispenser rate of 0.8 µL/mm. The band was dried at 60ºC, at 5 mm/sec using the Drying Tunnel Type BT3 Conveyor Oven, (Hedinair, UK).

4.3.5. Device Assembly and Running

The nitrocellulose membrane with immobilised capture Ab, the sink pad, the gold conjugate pad and the sample pad were mounted on a plastic backing card, in this specific order, at 20 mm, 0 mm, 43 mm and 55 mm, respectively, counting from the top of the backing card, using a lateral flow strip laminator from Cambridge Systems Engineering, Ltd (Cambridge, UK).

The mounted band was then cut in 5 mm strips using the Matrix 2360 Programmable Shear from Kinematic Automation, Inc (CA, USA) and each individual strip was then assembled within plastic cassettes that were closed using a cassette closure roller from Point A Technologies, Inc (CA, USA). The cassettes were packed in foil pouches with desiccant sachets and stored at room temperature. Schematic representations of the assembling of the different assay bands and of the final device is shown in **Appendix 12**.

The lateral flow device was run by pipetting 80 µL of sample/standard to the sample pad of the device and the strength of the test line signal was read at 20 minutes using a lateral flow device reader, also known as Cube reader (opTricon GmbH, Germany). Further details on the use of the electronic reader are given in **Appendix 13.**

4.4. Results

4.4.1. Antibody Conjugation to Gold Nanoparticles (AuNP)

In order to select the most suitable buffer for the conjugation of both anti-HNE antibodies to AuNPs, the aggregation of different of Ab-AuNPs conjugates, prepared using different amounts of antibody in different buffer compositions, was induced by adding NaCl solution, which is known to destabilize the gold and induce particle aggregation. When aggregated, conjugation to proteins is diminished, and this can be observed by a change in AuNP colour from bright red to purple, which shifts their maximum peak of absorption from ~550 nm to ~600 nm. The aggregation ratio for each buffer and each antibody concentration was then calculated by dividing the Abs value measured at 600 nm by the Abs value measured at 550 nm, and the results are depicted in **Table IV.1 A** and **Table IV.1 B**, respectively for the conjugation of the in-house SA369 pAb and the commercial anti-HNE pAb. The data shown in **Table IV.1 A** and **B** indicate that, regardless of the type of antibody, particle aggregation is inversely proportional to the concentration of antibody, i.e. higher the concentration of antibody conjugated, the lower the aggregation ratio. Therefore, the most suitable concentration of antibody for conjugation to AuNPs appeared to be 5 µg/mL. In terms of the

buffer composition, the results did not differ much between the two antibodies, although slightly lower aggregation values were achieved for the commercial anti-HNE pAb. Generally, the lower aggregation ratios were noticed when using 20 mM MES and TES at pH 6.7 and 7.1, respectively, and borate salts at the concentration of 20 and 25 mM and pH values of 8.5 and 9.3.

Table IV.1. Aggregation ratios of AuNP-SA369 enriched pAb conjugates (A) and AuNP-Abcam anti-HNE pAb conjugates (B) using different conjugation buffers and antibody concentrations. Although not included in the tables, the aggregation ratio obtained for unconjugated colloid gold nanoparticles, in water, was 0.24, and all the values are coloured in a gradient from red to green in comparison to that value, where the most similar values are represented in green.

A

[SA369 pAb] (µg/mL)	20 mM BES 6.3	20 mM MES 6.7	20 mM TES 7.1	20 mM TES 7.5	20 mM BES 7.8	20 mM TAPS 8.5	20 mM Borate 7.0	20 mM Borate 8.5	25 mM Borate 8.5	20 mM Borate 9.3	25 mM Borate 9.3
0	0.76	0.79	0.81	0.80	0.81	0.83	0.81	0.82	0.84	0.80	0.83
1	0.75	0.93	0.89	0.90	0.89	0.90	0.89	0.91	0.90	0.92	0.91
2	0.89	0.94	0.90	0.93	0.92	0.91	0.96	0.93	0.94	0.96	0.95
2.5	0.97	0.98	0.96	0.97	0.95	0.95	0.95	0.94	0.96	0.93	0.95
3	0.98	0.88	0.95	0.96	0.97	0.96	0.86	0.66	0.93	0.78	0.81
3.5	0.92	0.81	0.70	0.75	0.67	0.83	0.70	0.62	0.72	0.60	0.57
4	0.42	0.38	0.36	0.52	0.40	0.50	0.60	0.48	0.40	0.43	0.38
5	0.39	0.34	0.35	0.36	0.36	0.37	0.58	0.46	0.31	0.38	0.33

B

[Abcam pAb] (µg/mL)	20 mM BES 6.3	20 mM MES 6.7	20 mM TES 7.1	20 mM TES 7.5	20 mM BES 7.8	20 mM TAPS 8.5	20 mM Borate 7.0	20 mM Borate 8.5	25 mM Borate 8.5	20 mM Borate 9.3	25 mM Borate 9.3
0	0.81	0.83	0.83	0.81	0.80	0.83	0.83	0.81	0.84	0.82	0.82
1	0.90	0.88	0.90	0.89	0.90	0.90	0.93	0.94	0.92	0.95	1.02
2	0.90	0.89	0.91	0.93	0.94	0.94	0.98	0.99	0.96	0.99	1.03
2.5	0.98	0.94	0.97	0.95	0.97	1.00	1.01	1.03	1.00	1.05	0.60
3	1.02	1.00	1.02	0.98	1.04	1.04	1.03	0.84	1.04	1.00	0.94
3.5	1.05	1.05	1.06	1.02	1.04	1.05	0.93	0.39	0.93	0.47	0.61
4	1.03	0.90	0.75	1.03	0.83	0.67	0.38	0.29	0.40	0.30	0.29
5	0.45	0.36	0.31	0.69	0.37	0.33	0.30	0.29	0.29	0.28	0.27

4.4.2. Strip Performance using Commercial anti-HNE pAb-gold Conjugate in Solution (Wet testing)

Before the development of the final lateral flow assay, where all the components previously mentioned are assembled, the feasibility of the assay was tested by leaving the AuNP-

Abcam anti-HNE pAb conjugate in solution, together with the antigen, and dipping the NC strip (with SA369 enriched anti-HNE previously adsorbed), into the solution.

As the most promising conjugation buffers did not differ much in terms of salt concentration nor pH values, the first investigation of the assay was performed with AuNP-Abcam anti-HNE pAb conjugates prepared in buffers of 20 mM borate pH 8.5 and 25 mM borate pH 9.3, separately, and adding to them HNE modified HSA, KLH and OVA protein standards at a concentration of 50 µg/mL. The intensity of the test bands was measured using the cube reader after 20 min of sample application and the values were plotted together with their corresponding negative controls (**Figure IV.2**). The data show no substantial differences between the two tested conjugation buffers in terms of the detection of HNE adducts. It is worth noting, though, that without any previous optimization, the strip was able to differentiate between non-modified and modified proteins, indicating the two anti-HNE antibodies might form a good pair for LFA.

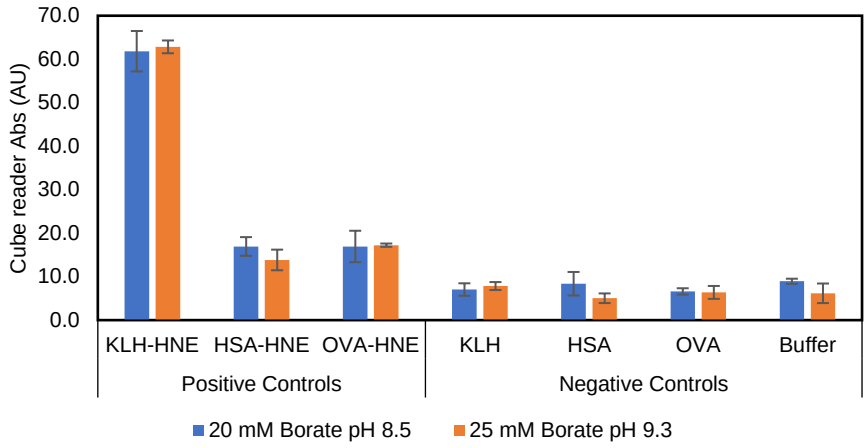

Figure IV.2. AuNP-antibody buffer conjugation effect on strip performance. Anti-HNE pAb was conjugated to AuNPs under the same conditions with 20 mM Borate buffer pH 8.5 and 25 mM borate buffer pH 9.3, separately, and the detection of HNE adducts was assessed by dipping the strips on each Au-NP conjugate solution containing HNE-modified and non-modified HSA, OVA and KLH at 50 µg/mL. The intensity of the test lines was measured after 20 min after sample application and for each standard sample. The assays were performed in triplicate (n=3) and data is presented as mean ± SEM.

Of the three tested HNE modified proteins, KLH-HNE gave the stronger response as seen by the higher intensity of the test line, and regarding HSA and OVA they both seem to have the same level detection. Distinction between the negative controls and HSA-HNE and OVA-HNE was anyhow clear by eye (data not shown), which as a starting experiment was very promising. The 25 mM borate buffer at pH 9.3 was selected for further experiments.

The second optimization under solution conditions related to the antigen concentration used for testing. In the previous experiment the performance of the strip was tested by adding the antigens at a concentration of 50 µg/mL but in **Figure IV.3** a range of concentrations between 1.56 and 100 µg/mL was tested.

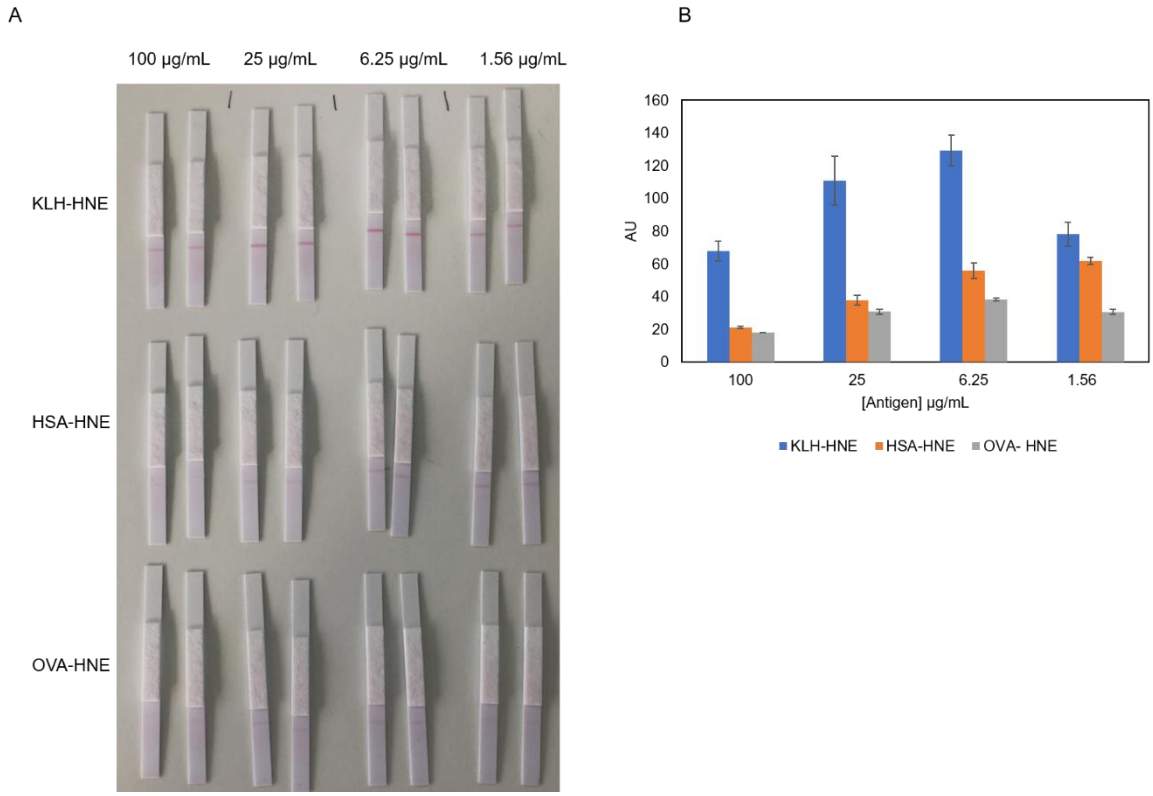

Figure IV.3. Antigen concentration effect on strip performance (wet testing). NC strips previously plotted with SA369 anti-HNE pAb were dipped in AuNP-Abcam anti-HNE pAb conjugate solution containing HNE-modified HSA, OVA and KLH at 1.56, 6.25, 25 and 100 µg/mL and KLH-HNE tested strips were photographed 20 min after sample application (B). The intensity of the test lines was measured with a cube reader after a 20 min incubation (A). The assays were performed in duplicate (n=2) and data is presented as mean ± SEM.

Data shown in **Figure IV.3** indicates that, surprisingly, the intensity of the test line is not directly proportional to the concentration of antigen added, within this range of tested concentrations. In fact, from 1.56 µg/mL to 6.25 µg/mL there is an increment of the test lines intensity, for all the three HNE-modified proteins, but from 6.25 µg/mL to 100 µg/mL the intensity of the signal starts to decrease, suggesting saturation of the antibodies. As the highest signals were achieved using antigen concentrations of 6.25 µg/mL, that value was fixed for further experiments.

4.4.3. Assay Performance (Dry testing)

For dry testing LFA, strip tests composed of sample pad, conjugate pad, NC membrane and absorbent pad – the four elements of a conventional LFA – were assembled as depicted in **Appendix 12**. In the conjugate pad, AuNP-Abcam Anti-HNE pAb was dried at a concentration of 25 µg/mL and in the NC membrane the SA369 enriched pAb was plotted at a concentration of 1 mg/mL.

The first tests performed in genuine assay conditions consisted in the assessment of the effect of the running and drying buffer compositions, which are, respectively, the buffers in which the antigen solutions, and AuNP-SA369 anti-HNE pAb conjugates were prepared **Figure IV.4**.

Three different running buffers were tested against three different drying buffers, the compositions of which mainly varied in the concentration of Tween 20, BSA and sucrose – components that play an important role in assay sensitivity. In order to simplify the visualization and interpretation of the results, the intensity of the lines was analysed with the cube reader **Figure IV.4 D.**

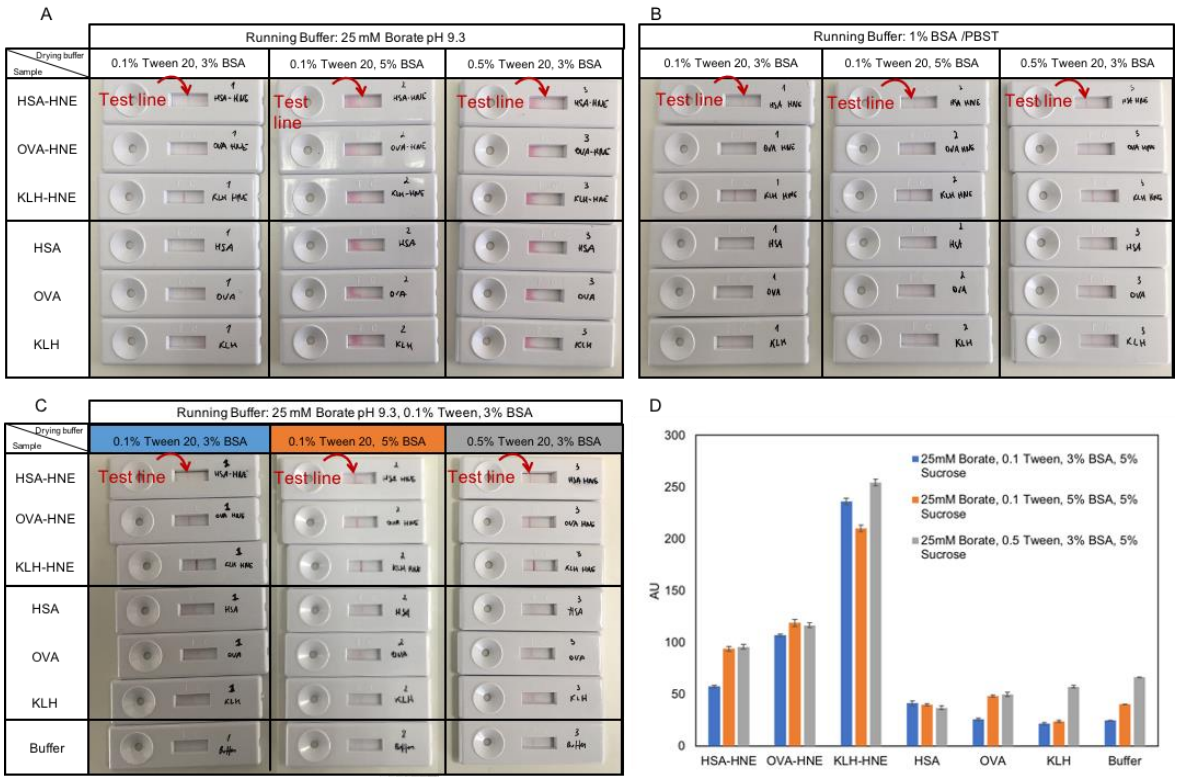

Figure IV.4. Effect of different running and drying buffers composition in assay performance. HNE-modified and non-modified antigen solutions were prepared similarly in running buffers: 25 mM borate buffer pH 9.3 (A), 1% (w/v) BSA/PBST (0.1% (v/v) Tween 20) (B) and 25 mM borate buffer pH 9.3 containing 0.1% (v/v) Tween 20 and 3% (w/v) BSA (C). For each of these running buffers, the detection of HNE adducts was compared by preparing the AuNP-SA369 anti-HNE pAb conjugates in either (a) 25 mM Borate pH 9.3, 0.1% (v/v) Tween 20, 3% (w/v) BSA; 5% (w/v) Sucrose, (b) 25 mM Borate pH 9.3, 0.1% (v/v) Tween 20, 5% (v/v) BSA; 5% (v/v) Sucrose or (c) 25 mM Borate pH 9.3, 0.5% (v/v) Tween 20, 3% (w/v) BSA; 5% (w/v) Sucrose. An 80-µL aliquot of each HNE-modified and non-modified standard solution (6.25 µg/mL) was added into the sample pad and the picture was taken after a 20 min incubation. The assays were performed in triplicate (n=3) and data is presented as mean ± SEM.

The results observed in **Figure IV.4** reveal that the concentrations of detergents and blocking agents, in both running and drying buffers, play a critical role not only in the performance but also in the sensitivity of the assay.

When preparing the protein standards in 25 mM borate buffer, pH 9.3 (**Figure IV.4 A**), one can see that Tween 20 and BSA are needed in the drying buffer at specific concentrations so the optimal flow of AuNP-pAb conjugate along NC membrane is achieved. For concentrations above 0.1% (v/v) and 3% (w/v), respectively for Tween 20 and BSA, as it is the case of drying buffers (b) and (c), irregular flow is observed preventing the sample from running properly and form of a thin test line. Therefore, when neither Tween 20 or BSA are present in the running buffer, 0.1% (v/v) Tween 20 and 3% (w/v) BSA seem to be the most

suitable for composition (drying buffer (a)). Nevertheless, the intensity of test lines regarding HSA-HNE and OVA-HNE are somehow very weak.

Regarding **Figure IV.4 B,** when preparing the standards in 1% BSA/PBST, no obvious difference in between the three drying buffers was observed. For all the three, the liquid flow seemed to be constant and no dragged lines were observed. Again, test lines for HSA-HNE and OVA-HNE were very weak and the AuNP-pAb conjugate seemed to deposit correctly on the test line. Drying buffer (c) showed the highest non-specific binding, as seen for the negative controls.

Finally, when combining all the elements of the two previously tested running buffers to form running buffer 25 mM Borate, pH 9.3 containing 0.1% (v/v) Tween 20 and 3% (w/v) BSA (**Figure IV.4 C**), the sensitivity of the assays seemed to be considerably improved. For all of the tested drying buffers, a normal liquid flow was observed, and once again higher non-specific binding was noticed when using drying buffer (c) that contains 0.5% Tween 20. Although no replicas were performed in these experiments, according to **Figure IV.4 D,** drying buffer (b) seems to offer the best compromise between assay sensitivity and low non-specific binding. Thus, for further experiments 25 mM borate buffer, pH 9.3 containing 0.1% of Tween 20 and 3% (w/v) BSA was used as running buffer and 25 mM Borate, pH 9.3, containing 0.1% of Tween 20, 5% BSA and 5% of sucrose was used as drying buffer.

4.4.4. Detection of HNE Adducts on KLH and HSA (Calibration Curves)

Once the most important assay parameters were optimized, the linearity of the LFA in the detection of HNE adducts in HNE-modified KLH and HSA standard solutions was assessed through the performance of a calibration curve ranging from 0 to 20 μg/mL (in triplicate) (**Figure IV.5**). Both HNE-modified and non-modified protein standard were prepared in 25 mM borate buffer, pH 9.3 containing 0.1% of Tween 20, and 80-μL aliquot of each standard were added to three devices.

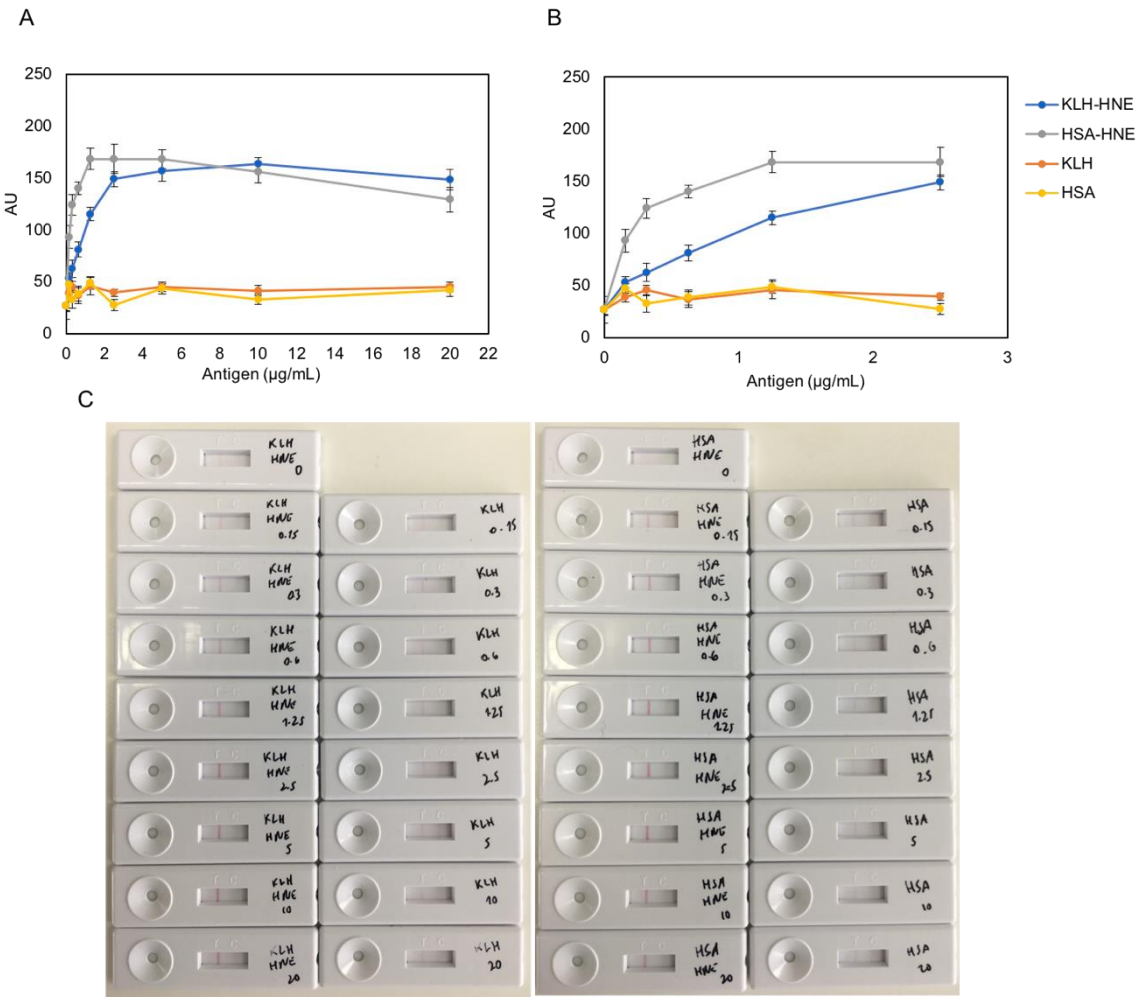

Figure IV.5. Calibration curves represented in standard linear scale obtained from triplicate assays tested with HNE-modified and non-modified HSA and KLH standard solutions (A). As the signal is seen to saturate around the antigen concentration of 2 µg/mL, the range 0-0.25 was investigated in more detail (B) so the differences within the range of 0-2.5 µg/mL can be seen in greater detail. All the devices were photographed 20 min after sample running where the increment in intensity of the test lines can be observed for the increasing concentrations of HNE modified KLH and HSA (C). The assays were performed in triplicate (n=3) and data is presented as mean ± SEM.

The calibration curves depicted above (**Figure IV.5 A**) show that the developed LFA was able to detect HNE modifications in two different proteins (HSA and KLH), and was capable of distinguishing between HNE-modified proteins and non-modified proteins. Nevertheless, the dynamic range of the assay was relatively low, as the signal for both HNE-modified proteins appear to be saturated at around 1-2 µg/mL. The devices showed a very high background signal as well when testing non-modified proteins (around 40 of absorbance), which might be related to the cross-reactivity of the SA369 pAb or the high optical density of the gold used in the assay. When curves were only plotted for the range of concentrations

between 0-2.5 μg/mL (**Figure IV.5 B)**, the increment in signal can be seen in greater detail. For the same concentrations, HSA was shown to be more HNE-modified than KLH.

4.4.5. Detection of HNE Adducts on HSA Standards Treated with HNE Concentrations

The developed LFA was tested extensively for the detection of HNE adducts on HSA protein standards treated with different concentrations of HNE. The devices in **Figure IV.6** show calibration curves ranging from 0.625 to 10 μg/mL obtained for HSA protein standards treated with HNE at molar ratios of 1:0, 1:10, 1:20, 1:40, 1:100 and 1:200.

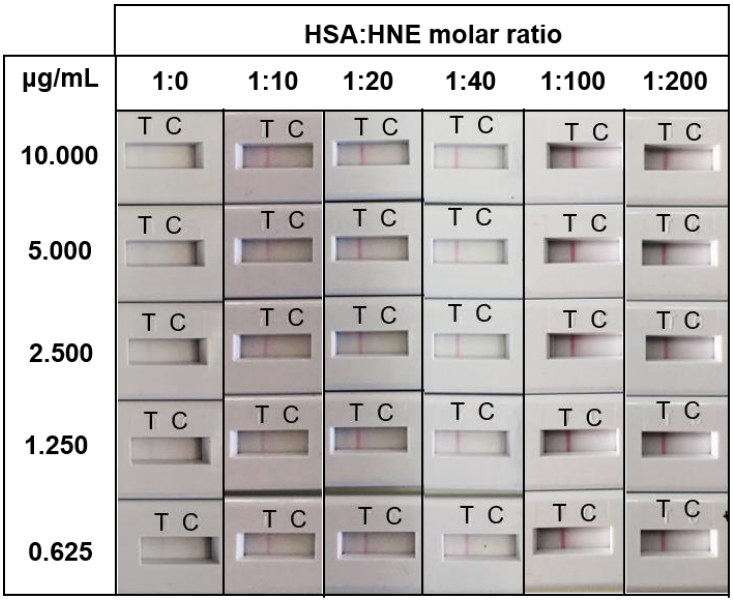

Figure IV.6. HSA-HNE detection on LFA devices. In each device concentrations from 0.625 (bottom assays) to 10 μg/mL (top assays) of HSA proteins standard treated with HNE at molar ratios 1:0, 1:10, 1:20, 1:40, 1:100 and 1:200 (left to right) were tested. The letter T on top of the window of each device stands for test line, which is where the capture antibody is immobilised and the gold-conjugated Ab binds if HNE is present in the sample. All the deviced were photographed 20 min after HSA-HNE samples were applied. These devices were only performed once (n=1).

Although the intensity of the test lines of the assays in **Figure IV.6** was not quantified with the cube reader, the calibration curves regarding the HSA-HNE samples treated with HNE at molar ratios of 1:100 and 1:200 show a considerably different intensity of colour from the HSA-HNE samples treated with HNE at molar ratios of 1:10,1:20 and 1:40. Again, although the distinction between modified and non-modified HSA is clear, the tested range of concentrations seems to be already in the saturation zone which does not allow inferring about the linearity of the signal. Nevertheless, the results suggest that, with further optimization, the LFA developed could be used for semi-quantitative purposes.

4.5. Chapter IV Discussion, Conclusions and Future Work

The work in this chapter describes the deployment of the previously described sheep anti-HNE antibody in a rapid diagnostic lateral flow test for the detection of HNE-protein adducts in clinical samples.

The developed prototype was designed to detect general protein-HNE adducts, by using the Abcam commercial anti-HNE pAb conjugated to gold nanoparticles, as detection reagent, and the in-house SA369 enriched pAb as capture reagent, in the test line. Results showed the devices were able to distinguish between HNE-modified and non-modified protein standards, and sensitivities as low as 1.5 μg/mL were achieved. The assay was shown to be capable of semi-quantifying HNE adducts in HSA as well, by display of different intensities of test lines colours for the same concentration of HSA standards modified at different HSA:HNE molar ratios, which as a proof-of concept is noteworthy. Unfortunately, due to time constraints, the assay was not tested with any biological samples.

When developing an assay, the main aim is to achieve the highest intensity of signal with the lowest non-specific binding, which is directly related to the sensitivity and the specificity, respectively. The optimisation process generally includes testing different antibody pairs, conjugation conditions, sample pad and conjugate pad materials, types of nitrocellulose membranes, antibody concentrations, running buffers, and sample volume (Hsieh et al., 2017); however, due to time constraints only a few of these metrics were tested.

Regarding the antibody pair, the development of this assay was restricted to the use of the in-house anti-HSA-HNE enriched pAb and the commercially available anti-HNE pAb from Abcam. It is always best to start with the highest affinity antibody as the capture reagent, however, since deposition of antibody lines in the NC pad requires large quantities of reagent, because of cost and availability issues, the assay was had to use as detection antibody the commercial anti-HNE from Abcam, and the SA369 enriched pAb as capture antibody, conjugated to gold nanoparticles.

The second critical aspect taken into consideration for the development of the assay was the interaction between the NC membrane and the detection particles, which is what defines the flow of the captured reagent and is, in part, related to the physical space of the nanoparticles in solution. If particles associate in larger aggregates, their flow along the strip will be largely impaired and consequently the detection of analyte will be disturbed (Wong & Tse, 2008). Thus, in order to evaluate the stability of both antibody-gold nanoparticles conjugates, their aggregation levels were determined by using different conjugation buffers and different antibody concentrations. Results showed that, for both the commercial and

the in-house antibody, the aggregation levels decrease with increasing concentrations of antibody and increasing pH values, which can be explained by the different charges present on the surface of both the particles and the antibodies. Typically, conjugation of antibodies occurs via non-covalent interactions such as dative bonding, hydrogen bonding, electrostatic forces, and hydrophobic adsorption (Cvak et al., 2012). Because the isoelectric point of an immunoglobulin is generally around 8, at pH values above 8, antibodies are positively charged and will naturally adsorb to AuNPs, that are negatively charged. However, if the concentration of antibody is not high enough to cover the whole surface of the particle, then antibodies can adsorb to multiple particles through different sites and induce aggregation; which is why for a range from 1-5 μg/mL the lowest aggregation ratios were observed at 5 μg/mL. Another reason for controlling the pH in antibody-AuNPs conjugation protocols is the fact antibodies orient themselves depending on the pH value of the solution where they are in, which affects the direction they bind to a certain particle (Cvak et al., 2012). At low pH values, antibodies were seen to face the surface of AuNPs with their Fab part, which is where the antigen binding regions are located, but at higher pH values, when both the colloid gold and the antibody are negatively charged, the adsorption occurs via hydrophobic interactions through the Fc part of the antibody, leaving the Fab part available for antigen binding (Ruiz, Tripathi, Okyem, & Driskell, 2019).

Based on assays performed in wet conditions, ideal antigen concentrations were seen to be between 1.56 and 6.25 μg/mL, as above 6.25 μg/mL saturation of the signal was observed, generating false negative results. This phenomenon, seen to occur before in Chapter III when screening for sheep antibodies by ELISA, is known as the “hook effect”, and it occurs when the amount of antigen applied is so high that both the capture and detection antibodies become saturated, preventing the detection signal from increasing. In what regards buffer optimisation, the core of all the buffers used in this LFA was kept the same – 25 mM Borate pH 9.3 – as borate was seen in the literature to provide a good buffering capacity (EMD Merk Millipore, 2013) and to work well in different antibody conjugation protocols followed at Mologic. Moreover, because borate has a slight surfactant quality, this buffer seems to be particularly suitable for the re-solubilization of the AuNP. Apart from borate salts, in both running and drying buffers, Tween 20 and BSA were seen to be important, as extra components, in the reduction of non-specific binding of proteins (Wong & Tse, 2008). These are particularly crucial when the capture reagent is dispensed at concentrations lower that 100 μg/mL and the surface of the NC membrane is unlikely to get saturated. The addition of Tween 20 was seen, as well, to promote the flow front stability, which is sometimes an issue due to the presence of surfactants in the capture reagent solution (EMD Merk Millipore, 2013).

Best results were observed when preparing the antigens in 25 mM borate solution, 0.1% (v/v) Tween 20 and 3% (w/v) BSA; however, the optimization of this buffer composition can be subjective, as devices would ideally be used for direct application of whole blood or serum samples, to which very few treatment can be done. Regarding optimisation of the buffer used for drying the Ab-AuNP conjugate, strongest test lines were observed when utilizing 25 mM borate buffer with the 0.5% (v/v) Tween 20, 3% (w/v) BSA and 5% (w/v) sucrose. Concentrations of Tween 20 higher than 0.1% (v/v) were seen to largely increase the background signal of the lines, and the concentration BSA was seen to be best between 3 and 5% (w/v). Sucrose was also added to the drying buffer as it acts as a preservative and a re-solubilization agent. When the detecting particles are dried in the presence of sugar, the sugar molecules form a layer around the particles which helps them to stabilize their biological structures. Sucrose was also added in the detection reagent buffer (EMD Merk Millipore, 2013).

As a proof of concept, calibration curves ranging from 0.15 and 20 μg/mL were performed to assess the linearity of the adducts, and the assay was shown to give a clear distinction between modified and non-modified proteins, achieving sensitivities as low as 1.50 μg/mL. As stated before in ***1.3.1.14-Hydroxynonenal (HNE), the Most Toxic Lipid Peroxidation Product***, levels of HNE in human plasma were reported to be between 0.1-1 μM, i.e., 0.0156-0.156 μg/mL, which is unfortunately 100-10 times below the sensitivity achieved. Nevertheless, transient concentrations of HNE in severe conditions ranging 50-100 μM were seen observed (Q. Liu et al., 2012), which could potentially be detected by this assay.

However, it is worth remarking that the sensitivity of an assay is directly related to the affinity of the antibodies used, specially the on-rate affinity, which dictates how fast an antibody can bind to its target. In order to achieve great sensitivity assays, in the range of picomolar for instance, antibodies with K_D values in the range of 10^{-10}-10^{-12} are needed. In this case, from the sensitivity observed, there is evidence that the antibodies used are of low affinity, limiting, therefore, the sensitivity of this assay.

Regarding non-specific binding, assays also showed quite high background values for non-modified proteins, around ~40 AU cube reader Abs units, when typically, they should not be higher than 10 AU. Due to this high background level, the intensities of the test lines for the first concentrations tested were considerably high (around 90 AU for HSA-HNE and 55 AU for KLH-HNE), impairing the determination of the assay sensitivity. This non-specific binding observed could potentially be related to the cross-reactivity of the SA369 antibody to HSA, as test lines are always stronger to HSA than KLH, and/or due to the gold optical density (OD) used for conjugation. Gold optical densities of 5 and 10, which are commonly

used, were compared (data not shown), being the intensity of the lines considerably higher when using OD 10. However, with the higher intensity of the gold colour comes a higher background signal, which sometimes can be attenuated by modifying other assay parameters. Another issue noticed with this assay was the dynamic range, which was very low. As signals started to become saturated around 1-2 μg/mL, it would have been useful to start the calibration curves at a lower concentration.

The assay also showed potential to be used as a semi quantitative tool as, when testing increasing concentrations of HNE used for generation of adducts, increasing intensities of the test line colours were observed for the different HNE:HSA molar ratios. Nevertheless, there seems to be a threshold in the number of HNE modifications (somewhere between the HSA:HNE molar ratio of 1:40 and 1:100), that is sensed by the antibodies and triggers the signal; however, these results were only assessed by eye which limits further the analysis of the data.

Nevertheless, for a valid application of the assay, the optimization is far from being finished, as the assay presents several issues. The presence of a control line in the assay could have helped not only to confirm the correct functioning of the assay, as it could have helped to decrease the non-specific binding noticed for with negative controls, by promoting unspecific Ab-gold conjugates to flow to the control line. Possible future work could include testing different antibodies specific to serum proteins in the test line, and concerning the optimisation of Ab-AuNP conjugates, testing *in situ*, directly in NC membranes rather than in polystyrene plates, in order to get more accurate and reproducible results.

Regarding the sensitivity and the dynamic range of the assay, these are slightly harder to adjust, as they depend mainly on the antibodies used. Sensitivity could potentially become higher if using a monoclonal Ab specific to HNE adducts in only HSA, rather than using a partially purified polyclonal antibody that cross-reacts with native HSA; however, assuming no changes were allowed in the antibody pair, testing other detection labels, such as latex or cellulose nanoparticles, could be a good follow-up experiment.

In conclusion, the prototype LFA development describer for the detection of HNE adducts in proteins was shown to be successful when using HNE-treated protein standards. Calibration curves presented a clear distinction between HNE-modified and non-modified HSA and KLH proteins, and the use of the assay as a semi quantitative tool is not completely excluded.

This is a promising test for detection of HNE protein adducts and presents the attractive opportunity of a point-of-care test for lipoxidation status, which would allow patients/clinicians to monitoring redox levels using simple, rapid and inexpensive LFA

devices. However, taking a lateral flow test strip from the design stage to final manufacture is very challenging and requires commitment of significant resources in order to achieve a product fit for the market.

CHAPTER V

DEVELOPMENT OF SHEEP Fab AND scFv LIBRARIES for GENERATION OF ANTI-HSA-HNE ANTIBODY FRAGMENTS USING PHAGE DISPLAY TECHNOLOGY

5.1. Introduction

Since polyclonal antibodies generated by immunization represent a mixture of molecules with different affinities and specificities, the development of techniques like hybridoma technology and phage display came to revolutionize completely the market of antibody molecules, by allowing the generation of antibodies from the same parent cell, containing uniform variable regions and thus presenting specificity to a single epitope. Therefore, since the cross-reactivity towards non-modified HSA was not eliminated by downstream processing techniques, phage display technology was applied to this work with the intention of surpassing the limitations of the anti HSA-HNE polyclonal antibodies generated.

5.1.1. Generation of Antibody Phage Display Libraries

The display of peptides and proteins on the surface of bacteriophages allows the construction of antibody libraries of enormous molecular diversity, making the phage display technology a great alternative to the hybridoma technology, regarding the production of mAbs.

Due to limitations in the bacteria folding machinery, efficient expression of full-length antibody molecules is very difficult to achieve, and therefore, phage display of antibody fragments is the most common approach. Single-chain Fv (scFv), Fabs, single-domain antibodies (sdAb) and diabody fragments (**Figure IV.1**) are some examples of different antibody fragment formats that have been expressed successfully on the surface of M13 phages with no apparent loss of the antibody's affinity and specificity (Barbas, Kang, Lerner, & Benkovic, 1991; Davies & Riechmann, 1996; Holliger, Prospero, & Winter, 2006; McCafferty, Griffiths, Winter, & Chiswell, 1990). ScFv fragments consist of a variable domain of the antibody heavy chain (V_H) and a variable domain of the antibody light chain (V_L) connected by a flexible oligopeptide linker. Due to their small size (~25 kDa) are fairly easy to be cloned and be better tolerated by bacteria, however, they have propensity to undergo aggregation and form higher molecular weight species, which can complicate selection and characterization. Fabs, in turn, consist of the variable heavy chain along with its first constant domain (V_HC_H) associated with the whole light chain (V_LC_L). These fragments are bigger in size (~55 kDa), and therefore cause some toxicity for bacteria, but lack the tendency to multimerize.

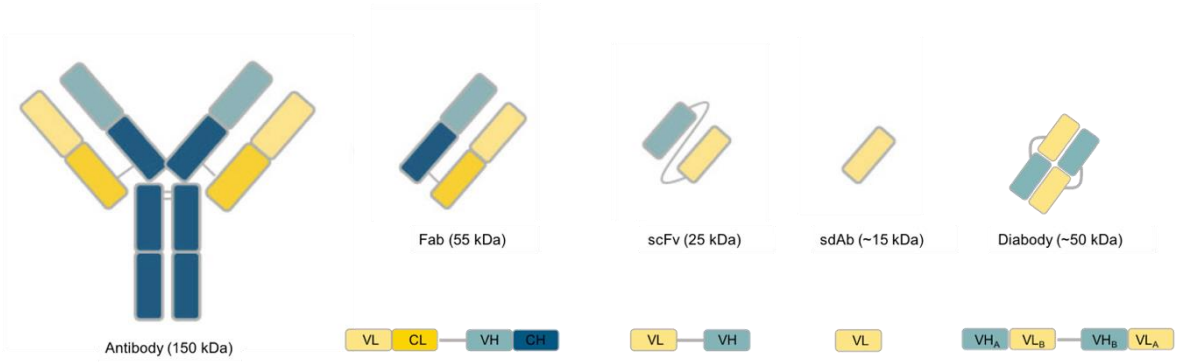

Figure V.1. Schematic illustration of an intact IgG molecule compared to Fab, scFv, sdAb and diabody fragments. For each fragment, their respective gene construct/ domain association for each arrangement of V_H and V_L is depicted.

Nevertheless, notwithstanding the antibody fragment format desired, the achievement of highly specific antibody fragments relies on the construction of large functional antibody libraries with a high degree of genetic diversity (Teixeira & Gonzalez-Pajuelo, 2018). These can be constructed from natural repertoires obtained from immunized animals or naïve B cells, or even from synthetic or semi-synthetic libraries which diversity is introduced with designed synthetic DNA that targets precisely the regions encoding the CDR regions (G. Chen & Sidhu, 2014). In immune libraries, the antibody clones are generated from B cell mRNA, extracted from either the blood or spleen of animals on active immunization with the target immunogen. The mRNA is then reverse transcribed to cDNA, and from this cDNA the V_H and V_L-encoding genes can be amplified by PCR using sets of primers specific to the more conserved regions of the antibody genes. For the construction of naïve libraries, the same procedure is applied, but isolating B cells from diverse lymphoid sources of nonimmunized animals (i.e., healthy human) (Teixeira & Gonzalez-Pajuelo, 2018).

Immune libraries have the advantage of being enriched in antigen-specific antibodies, as the immune system of the immunized animal has already gone through a process of antibody affinity maturation (Berry & Popkov, 2015). Generally, for libraries generated from immune repertoires, a diversity of 10^6-10^7 is sufficient to achieve a high-affinity clone, while when using naïve and synthetic libraries a diversity on the order of at least 10^{10} clones is required (Berry & Popkov, 2015).

The size of a library is mainly limited by the transformation efficiency in bacteria, which depends on both the transformation method applied, usually electroporation, and on the strain of bacteria used. Strategies to achieve larger libraries usually include increasing the number of transformations and/or conjugating different libraries obtained from different donors (Teixeira & Gonzalez-Pajuelo, 2018). This last approach has the added advantage

of allowing recombination of V_H genes from one animal with V_L genes from another, thus increasing the pool of recombined antibodies not seen in the host animals.

However, as the quality of the library functional diversity is achieved from the random combination of the pool of heavy and light chain variable genes, it depends on a larger number of factors. The origin of the V-gene repertoires (immune, naïve and synthetic libraries), the number of donors, the source of the B-cells and the molecular methods for amplifying and engineering the V-genes, which encompasses the primer sets used for synthesis of cDNA and the V_H and V_L genes, the used V-genes assembly procedure and phagemid vectors, are all important factors to consider (Tohidkia, Barar, Asadi, & Omidi, 2012).

Yet, standard transformation efficiencies obtained for bacterial cells are far away of reaching the natural human antibody diversity, that is at least 10^{11} clones (Murphy & Weaver, 2017). Typical transformation efficiencies for *E. coli* TG-1 cells when using a ligated vector with insert are $1\text{-}10\times10^7$ transformants per μg of vector (du Plessis & Jordaan, 1996). However, not all the antibody clones represented in a library will be displayed. Low expression of antibody fragments has been associated with toxicity effects, intracellular degradation, aggregation and inefficient translocation, which result in only a small percentage of phage particles displaying the antibody fragment (Kulmala, Huovinen, & Lamminmäki, 2017).

To the date, construction of antibody libraries from a variety of species including mouse, human, chicken, rabbit, sheep, camel and shark have been reported (Brien et al., 2002; Leow et al., 2018; Palliyil, Downham, Broadbent, Charlton, & Porter, 2014); however, not much work in the field of lipid oxidation biomarkers has been done resorting phage display technology. Interestingly, in 2015 a group from Aarhus University applied this technique to identify antibody fragments specific to HNE adducts on the α7 subunit of the 20S proteasome using a naïve scFv phage library. Results were, unfortunately, very inconclusive due to the instability of the adduct, and not many data on the antibody were achieved (Just et al., 2015).

5.1.2. Vectors used in Phage Display

There is currently a wide selection of vectors available for expression of antibody fragments on the surface of bacteriophages. However, before constructing or selecting a vector, understanding the diversity and organization of the immunoglobulin genetics is very important. Regarding sheep, its V_H loci includes a total of 9 genes whereas the VL loci

includes 100 V_λ genes and 6 V_κ genes (K. A. Charlton et al., 2018), which reveals that the large diversity of the sheep immunoglobulins arises mostly from the light chain genes. Moreover, sheep was seen to preferential express the λ light chains over the κ light chains, presenting a λ/κ ratio of 20:1 (Sajadi et al., 2016), which is the reason why the Ig κ genes were not amplified or used in this work. Interestingly, studies have also shown that the diversity in both the V_H and V_λ genes in sheep does not a result from the classic V(D)J recombination mechanism mentioned before in **1.6.3 Antibody Variability**, as occurs in humans, but from post-rearrangements diversification strategies of somatic hypermutation that occur in an organ known as the ileal Peyer's patch (Jenne et al., 2006). Hypermutation mechanisms were seen to be particularly targeted on sequences encoding CDRs, and not so much on the frame work regions, which suggests this mechanism increases selectively the diversity in the antigen binding regions and preserves the structural properties of the antibody molecule (Jenne et al., 2006).

The vector used in this work, currently used at Mologic and named pSFD (vector map showed in **Figure V.2 A**), is a 5547 bp bicistronic plasmid that allows the simultaneous expression of the heavy and light chain gene sequences protein using a single promotor. This co-expression is achieved by the presence of two ribosome binding site (RBS) sequences, each upstream each antibody chain genes, allowing each RNA transcript to be translated separately by multiple ribosomes. Besides this feature, this plasmid carries (1) a gene sequence that encodes for the pIII protein of the phage capsid, where the antibody fragment will be displayed, (2) an antibiotic resistance gene for ampicillin (amp^R), that will be further used as selectable marker for cells containing the plasmid, (3) an origin of replication sequence for replication in bacteria and an (4) the origin of replication sequence for replication in bacteriophages, (5) a DNA sequence that encodes for the catabolite activator protein (CAP) binding site, responsible for the activation of the transcription of the operon when glucose levels are low, and (6) the sequences for the lac promoter and lac operator, required for the expression of Fabs in bacteria. Downstream these sequences, there is, as well, (7) a sequence for the binding of the reverse M13 primer, (8) sequences encoding the ribosome binding sites (for protein translation) and (9) DNA stuffer sequences encoding the variable and constant regions of the heavy and λ light chains of a "control" Fab, that were removed and substituted by the sheep SA369 derived VH-CH and Vλ-Cλ encoding sequences, leading to the generation of the final a construct of a final construct of 5930 bp depicted in **Figure V.2 B**. Upstream the light λ and the heavy chain sequences are the signal sequences of the proteins OmpA and PelB, respectively, that are responsible for leading the chains to the periplasmic space, during protein expression. Downstream the

heavy chain sequences, the vector carries, as well, the sequences encoding for a myc tag and a 6xHis tag, for enabling further analysis and purification of the Fab fragment.

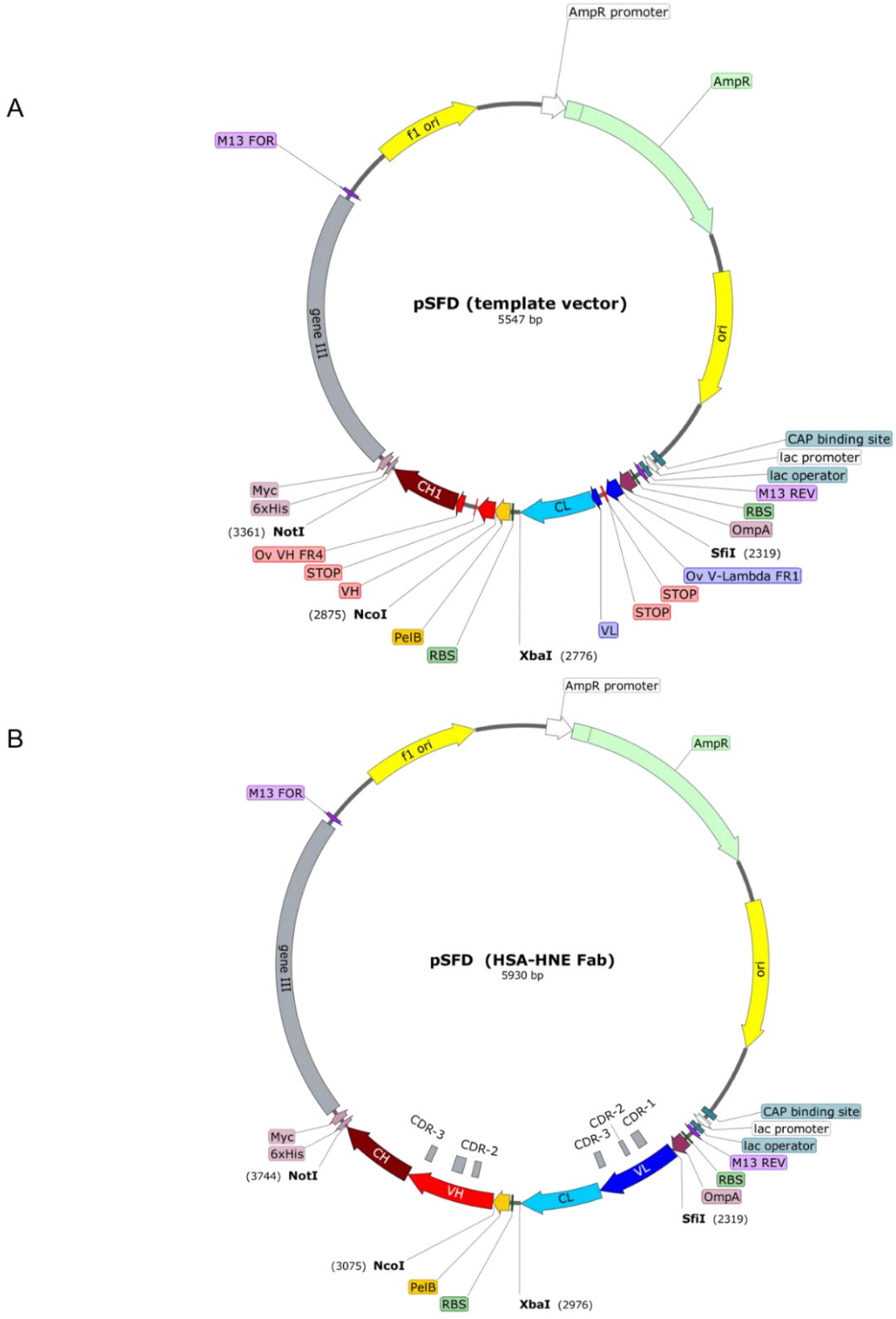

Figure V.2. Illustration of phage display vector pSFD used in this work for the expression of anti-HSA-HNE Fab fragments. The map had, originally, a stuffer fragment of a control Fab (A), that was removed and substituted by the V_HC_H-V_LC_L genes amplified from sheep SA369 B cells, yield a vector of 5930 pb (B).

5.1.3. Selection of Antibody Phage Display Libraries

Once an antibody library is generated, the enrichment of a subpopulation of specific phage antibody fragments is performed by a process known as biopanning, which involves repetitive cycles of antigen binding, washing and elution. During the first round of biopanning, the whole library is exposed to the specific antigen, which might be immobilized by passive adsorption to a 96-well microplate or an immunotube. After a few hours of phage incubation, unbound background phage antibodies are washed away by using non-ionic detergents, and the specific bound antibody phages can afterwards be eluted by applying a pH-gradient. When antibodies specific to post-translational modifications are desired, which is the case of this work, competition strategies with the non-modified antigen are usually applied for depletion of antibodies specific to the native molecules. In the case of HNE-modified HSA, prior to the incubation with HSA-HNE, phages were pre-incubated with non-modified HSA, so phages displaying anti-HSA antibodies could be eliminated. The eluted antibody-phage are then recovered for subsequently amplification by infecting bacteria, and this whole process is repeated, usually 3 to 4 times, until sufficient enrichment is accomplished (Kretzschmar & Von Rüden, 2002; Pande, Szewczyk, & Grover, 2010).

The success of each selection round can be assessed by determining the phage titers before and after elution and by testing the pool of eluted polyclonal antibody-phages by ELISA assay against the specific antigen. Even though it is believed the outcome of the selection process is largely dependent of the quality of the library, the biopanning strategy applied can affect the properties of the enriched antibody clones as well. For example, increasing the stringency of the selections by adjusting the antigen concentration, the time of phage incubation and the number of washing steps results in the selection of a narrow panel of antigen-specific phage binders, potentially with lower off-rates and/or higher on-rates. Moreover, the addition of subtraction/depletion steps before selections or the counterselection with a possible cross-reactive molecule during phage-antigen incubation are strategies very often used to eliminate antibody cross-reactivity (Teixeira & Gonzalez-Pajuelo, 2018).

5.1.4. Chapter V Aims

The aim of the work described in this chapter was to generate monoclonal antibody fragments specific to HNE adducts on HSA, in order to eliminate the cross-reactivity towards unmodified HSA observed in Chapter III in the sheep SA369 Anti-HNE polyclonal antibody.

To accomplish this aim, Fab and ScFv antibody libraries were generated by means of the phage display technology and using as starting material RNA extracted from sheep SA369 lymphocytes.

The panning of the libraries was performed using different strategies, by immobilizing HSA-HNE and OVA-HNE on immunotubes and by using biotinylated HSA-HNE and OVA-HNE whose capture was done via magnetic streptavidin microbeads.

5.2. Reagents

The following reagents were purchased by Acros Organics (UK): ethanol, sodium chloride (NaCl), isopropanol and glycerol 99%. 1,4-Dithiothreitol (DTT), hypodermic needles (20 gauge/0.9 mm), magnesium chloride ($MgCl_2$), ampicillin sodium salt, kanamycin, D-(+)-Glucose ≥99.55% (GC), glycine, tween 20, Trizma® (TRIS base), PEG6000, isopropyl β-D-1-thiogalactopyranoside (IPTG) and Corning® Costar® 96-well cell culture plates were purchased from Sigma-Aldrich, UK.

Sheep Fab Primers, RNaseOUT™ recombinant ribonuclease inhibitor, RNase free water, SuperScript™ IV Reverse Transcriptase, phusion high fidelity DNA polymerase, DMSO, SOC media, culture plates, agarose I molecular biology grade, GeneJET gel extraction and DNA clean-up micro kits, 10x TAE buffer, plate spreaders, Nunc™ bioassay plates, DNA gel loading dye 6X, GeneRuler 1 kb DNA ladder, EZ-Link NHS-PEG4 Biotinylation Kit, PBS, Nunc™ Immunotubes Maxisorp 4 mL, Nunc™ 96-well ELISA plates, TMB substrate solution, Dyna M-280 Streptavidin Magnetic beads were ordered from Thermo Fischer Scientific, UK.

Deoxynucleotide (dNTP) Solution Mix (10 mM of dATP, dCTP, dGTP and dTTP), TG-1 Turbo competent *E. coli* cells, restriction enzymes XbaI, SfiI, NotI-HF, NcoI-HF, EcoRI, MfeI, HaeIII, BstNI, MluI and AscI, CutSmart® buffer, and T4 DNA ligase were purchased from New England Biolabs, UK.

The RNeasy minikit (50) was purchased from Qiagen (Germany), the PureLink™ quick gel extraction kit and the 2-YT Broth from Invitrogen (UK), the Zippy™ Plasmid Miniprerp kit from ZymoResearch (UK), agar bacteriological from Oxoid (UK), GenePulser cuvettes (0.1 cm) from BioRad (UK), the hydrochloric acid solution from Fluka (UK), Gelred® Nucleic Acid Gel Stain (10,000X in H_2O) from Biotium/Cambridge Biosciences (UK) and Milk powder from Marvel (UK). Antibodies anti-mycTag antibody and ati-M13 were ordered from Abcam (UK) and Sino Biological (UK), respectively.

5.3. Materials and Methods

To facilitate the comprehension of the approaches followed, a visual representation of the methods followed for generation of both Fab and scFv libraries can be found in **Figure V.3**.

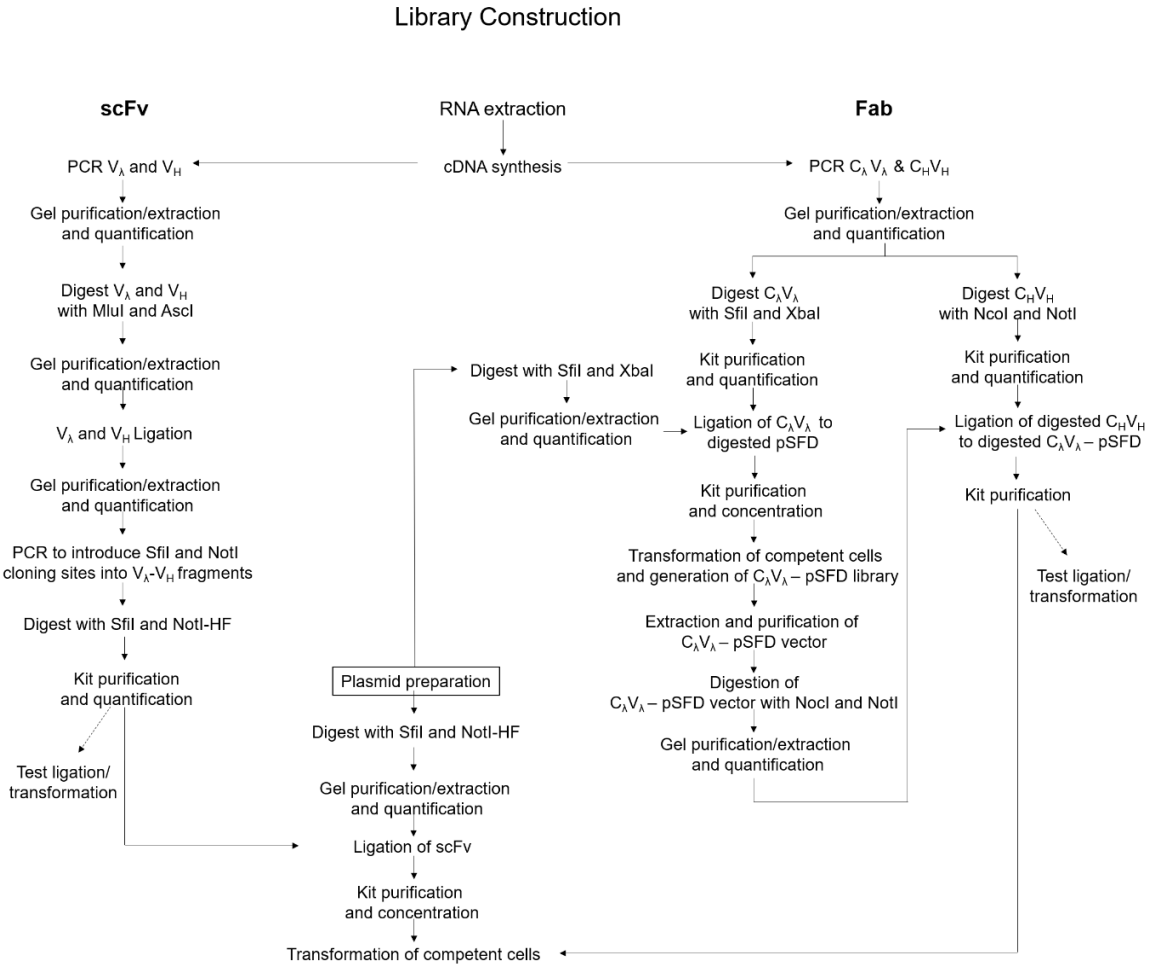

Figure V.3. Flowchart depicting the main steps performed for the generation of antibody single-chain variable fragments (scFv) (left) and antibody Fab fragments (right) libraries.

5.3.1. Construction of Fab Antibody Libraries

5.3.1.1. Preparation of Peripheral Blood Lymphocytes

Peripheral blood lymphocytes (PBLs) from the sheep SA369 were prepared at Orygen Antibodies from approximately 100 mL of whole blood, collected into a blood collection bag containing an acid dextrose solution to prevent coagulation. The blood was diluted in PBS in a 1:1 ratio and loaded into Accuspin tubes with Histopaque 1077 for separation of the lymphocytes by centrifugation at 1000 × g for 10 min. If the PBLs did not form a clear band, or red blood cells remained above the frit, the sample was re-centrifuged at 1500 × g for 15 min. The resulting PBL bands were removed from the tubes, pooled and washed in 10 mL PBS, followed by a centrifugation step at 1000 × g for 10 min. The resulting PBL pellet was re-suspended in 1 mL of RNA stabilization solution RNAlater and shipped to Mologic Ltd, where they were stored at -80^{o}C until further use.

5.3.1.2. RNA Extraction

RNA was extracted from two-200 μL PBL aliquots using the commercial RNeasy MiniKit (Qiagen, Germany), following the manufacturer's instructions. Briefly, cells were pelleted by centrifugation at 300 × g and disrupted by adding buffer RLT. Homogenization was achieved by passing the lysate through a 20-gauge (0.9 mm) needle attached to a sterile plastic syringe at least 5–10 times or until a homogeneous lysate was achieved. One volume of 70% ethanol was added to the homogenized lysate and mixed well before adding the sample to a RNeasy spin column placed in a 2 ml collection tube (supplied). After a 15 s centrifugation at ≥8000 × g, the flow through was removed and 700 μL of buffer RW1 was added to the spin column and centrifuged again for 15 s at ≥8000 × g. Then, column was washed by adding 500 μl of buffer RPE to the RNeasy spin column, centrifuging under the same conditions, and repeating the same wash step with 500 μl Buffer RPE and centrifuging again for 2 min at ≥8000 × g. For elution of RNA, the RNeasy spin column was placed in a new 1.5 mL tube, 50 μL of RNase free water were added directly to the spin column membrane and the column was centrifuged for 1 min at ≥8000 × g. The concentration of the eluted RNA was estimated using a nanodrop (Jenway Genova nano).

5.3.1.3. cDNA Generation

The extracted RNA was used as template to synthesise the first strand of cDNA using primers specific for the ovine antibody heavy and light chain constant region of interest. Primers OvCH1 3'-Hinge- For and OvCL-3'For1 were used for the Fab library, respectively for the heavy and the lambda light chains. The kappa (κ) light chain was not synthesised nor inserted into the vector, as the λ/κ ratio in a sheep IgG molecule is 20:1 and therefore the variability derived from the kappa light chain is not particularly relevant for the process (Sajadi et al., 2016). All the primer sequences used for the generation of the Fab libraries were kindly provided by Prof. Keith Charlon to Mologic Lltd under a non-disclosure agreement.

For cDNA synthesis, per 1 μg of RNA, 1 μL of the primer mix (2 pmol/μL of each primer), 1μL of dNTP mix (containing dATP, dCTP, dGTP and dTTP) and RNAse-free water to a final volume of 13 μL were added and the mixture was incubated on a thermocycler at 65ºC for 5 min. Afterwards, it was quenched for at least 1 min on ice, to allow the annealing of the primers to the RNA chain. Each cDNA mix (13 μL) was further added to a reverse transcriptase mix (7 μL) containing 1 μl of Superscript™ IV reverse transcriptase enzyme, 4 μl of 5x Superscript™ IV buffer, 1 μl of RnaseOUT™ recombinant ribonuclease inhibitor and 1 μl of 0.1M DTT. The mixes (20 μl) were incubated for 55°C for 15 min, followed by heat inactivation at 80°C for 10 min. The generated cDNA was stored in the freezer until further use.

5.3.1.4. PCR Amplification of IgG Heavy and λ Light Constant and Variable Gene Segments

The amplification of the ovine heavy and light λ chains was done by PCR using a unique set of forward and reverse specific primers designed by Keith Charlton, Scotia Biological (detailed sequences not shared).For the amplification of the heavy chain, PCR reactions were set up by using the following primer pairs:

- H1 – OvCH1 hinge-Not-FOR and mixture of OvVH1-Ufab-Nco-REV, OvVH2-Ufab-Nco-REV and OvVH3-Ufab-Nco-REV
- H2 – OvCH1 hinge-Not-FOR and mixture of OvVH4-Ufab-Nco-REV, OvVH5-Ufab-Nco-REV and OvVH6-Ufab-Nco-REV
- H3 – OvCH1 hinge-Not-FOR and mixture of OvVH7-Ufab-Nco-REV, OvVH8-Ufab-Nco-REV and OvVH9-Ufab-Nco-REV

For the amplification of the light λ chain, PCR reactions were set up by using the following primer pairs:

- L1 – OvCL-3-Xba-FOR and mixture of OvVL1 fab-SFi-REV, OvVL2 fab-SFi-REV, OvVL3 fab-SFi-REV, OvVL4 fab-SFi-REV and OvVL5 fab-SFi-REV
- L2 – OvCL-3-Xba-FOR and mixture of and OvVL6 fab-SFi-REV, OvVL7 fab-SFi-REV, OvVL8 fab-SFi-REV, OvVL9 fab-SFi-REV and OvVL12 fab-SFi-REV
- L3 – OvCL-3-Xba-FOR and mixture of OvVL13 fab-SFi-REV, OvVL14 fab-SFi-REV, OvVL15 fab-SFi-REV, OvVL16 fab-SFi-REV and OvVL17 fab-SFi-REV
- L4 – OvCL-3-Xba-FOR and mixture of OvVL18 fab-SFi-REV, OvVL19 fab-SFi-REV, OvVL20 fab-SFi-REV, OvVL21 fab-SFi-REV and OvVL22 fab-SFi-REV

PCR reactions for each chain were set up individually by mixing 5 μL of cDNA with 45 μL of a Master mix containing 10 μL of 5x Phusion buffer (GC), 1 μL of Phusion polymerase, 1.25 μL forward primer (20 pmol/μL), 1.25 μL of reverse primer set (20 pmol/μL), 2 μL dNTPs, 1.5 μL of DMSO and RNase-free water up to 45 μL. The PCR mixes were incubated for 2 min at 98°C, then subjected to 35 cycles of 98°C for 10 seconds, 58°C for 30 seconds and 72°C for 40 seconds, and finally incubated at 72°C for 10 min. Tubes were incubated at 4°C until further use.

5.3.1.5. Agarose Gel Electrophoresis and DNA Extraction

The heavy and light chain DNA PCR products were loaded, separately, into a 1% (w/v) agarose gel for purification. Agarose was melted in 1x TAE buffer (40 mM Tris, 20 mM acetic acid and 1 mM EDTA) for a few minutes in a microwave, allowed to cool down for 15 min and before pouring the gel into the cast, 1x gel red Stock was added for DNA staining. Samples were mixed with 1x DNA gel loading buffer before being loaded. The gel was run at 150 V in 1x TAE buffer until the sample reached the bottom of the gel, to ensure a good separation between the desired PCR products and the background PCR sub-products.

The bands corresponding to the heavy and light chains (~400 bp) were excised from the gel using a scalpel, and the DNA was extracted from the gel bands using the PureLink™ quick gel extraction kit and following the manufacturer's instructions. Briefly, to each gel slice containing the DNA fragment, gel solubilization buffer L3 was added in a gel weight: buffer volume proportion of 1:3, and the mixture was placed in a 50°C water bath for a 10-minute incubation, for gel dissolution. Once dissolved, 1 gel volume of isopropanol was added to the solution and the DNA was purified by attaching the quick gel extraction columns to a vacuum manifold. The dissolved gel mixture was pipetted onto the centre of

the column and vacuum was applied until all the liquid passed through the column. For washing the column, 700 μL of buffer W1 were added to the column and, again, vacuum was applied until all the liquid passed through the column. To remove any traces of ethanol, the column was centrifuged at maximum speed for 5 minutes, and the flow-through was discarded. Elution was achieved by adding 50 μL of elution buffer (E5), leaving the buffer to incubate for 5 min at room temperature and centrifuging the tube at >12,000 × g for 1 minute. The concentration of both heavy and light chains was estimated using a nanodrop (Jenway Genova Nano).

5.3.1.6. Generation of Stock pSFD Phagemid Vector

The template vector used for the development of both Fab scFv antibody libraries was the pSFD, kindly provided by Professor Keith Charlton's group from Aberdeen University. The pSFD phagemid plasmid (Amp^{RES}) was transformed into turbo competent *E. coli* cells by heat shock transformation. Cells (50 μL aliquots) were thaw on ice for 10 min, before 1 μL of phagemid DNA was added. The mixture was placed on ice for 30 min, then incubated at 42°C for 30 s and placed back on ice for 5 min. For cell recovery, 950 μL of SOC media (super optimal broth with catabolite repression: 2% Tryptone, 0.5% Yeast Extract, 10 mM NaCl, 2.5 mM KCl, 10 mM $MgCl_2$, 10 mM $MgSO_4$ and 20 mM glucose) was added to each transformation and the cells were incubated at 37°C for 1 h with shaking (250 rpm). Cell were mixed, 10-fold serial dilutions were performed in SOC media, and 100 μL of each dilution was spread onto 2-YT plates with 1% glucose/100 μg/mL ampicillin (2-YT/glu/amp). Plates were incubated overnight at 37°C. Single pSFD-Turbo cell colonies were picked using a pipette tip and added to lysogeny broth media supplemented with 100 μg/mL ampicillin (LB/Amp) for growth overnight at 37°C with shaking (250 rpm). The phagemid was purified using Zippy™ plasmid midiprep kit by initially centrifuging the cell culture for 3 min at max speed (>10,000 rpm), removing the supernatant, and resuspending the cell pellet in 600 μL of RNAse free water. For cell lysis, 100 μL of 7x Lysis Buffer were added to the culture and mixed by inverting the tubes 4-6 times. Once the colour of the solution has changed from opaque to clear blue, 350 μL of cold neutralization buffer were added to the tube and mixed thoroughly. Tubes were centrifuged for 4 minutes at 11,000 × g, supernatant was transferred into a Zymo-Spin μL IIN column, and placed for centrifugation for 15 seconds at 11,000 × g. The flow-through was discarded, the column was placed in the same collection tube, and 200 μL of Endo-Wash buffer were added to the column. The columns were centrifuged for 30 seconds at 11,000 × g. For the washing step, 400 μL of the Zyppy™ Wash buffer were added to the column and centrifuged for 1 minute at 11,000

× g. The column was then transferred into a clean 1.5 mL tube, 30 µL of the Zyppy™ Elution buffer were applied directly into the centre of the column matrix and left to incubate for 5 minutes at room temperature. The column was then centrifuged for 30 seconds at 11,000 × g to elute the plasmid DNA. The concentration of the eluted DNA was estimated using a nanodrop (Jenway Genova Nano).

5.3.1.7. Restriction Enzyme Digestion of the pSFD Phagemid and of the Heavy and λ Light Chain Fragments

The insertion of the heavy and light lambda chain fragments into the pSFD phagemid was performed sequentially by two restriction cuts and respective ligations. The restriction sites of the enzymes used are located strategically in the vector to, as well, remove the already existing stuffer heavy and light chain fragments. The cloning strategy applied is described below in **Figure V.4**.

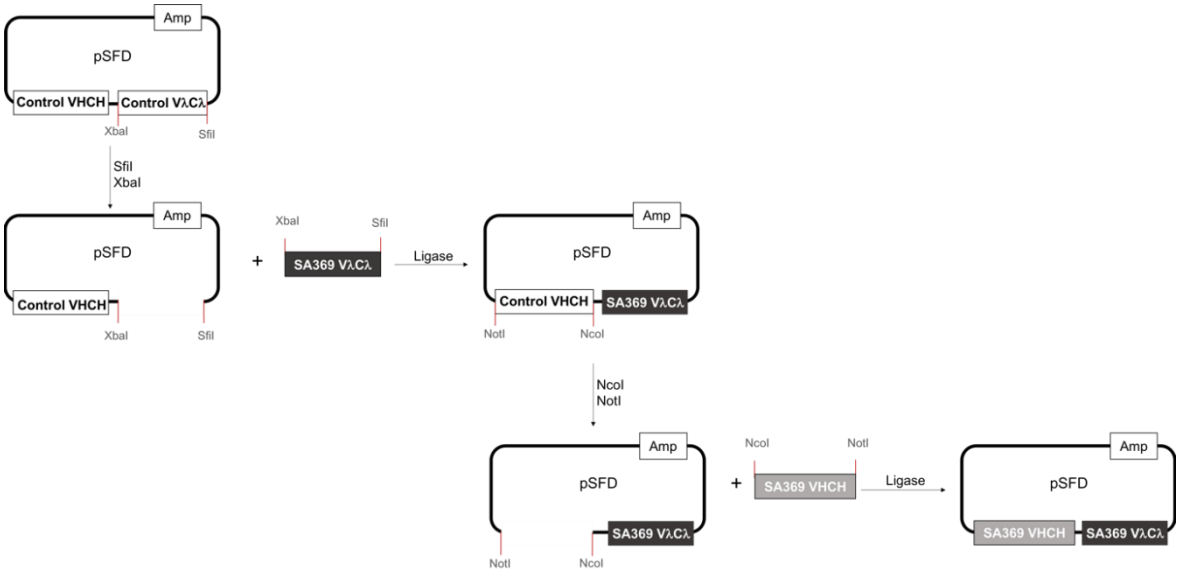

Figure V.4. Cloning strategy for the insertion of the heavy and light λ chain gene fragments into the pSFD phagemid. The insertion of the λ chain into the vector was performed first by digesting both the vector and the λ chain genes, separately, with SfiI and XbaI restriction enzymes. After purification, both the vector and the λ chain fragments were ligated via the action of ligase, and the resulting ligation mix was transformed into *E. coli*. Cells were grown and plated, single colonies were picked for extraction and purification of the λ chain containing phagemid (pSFD-Lλ), and subsequently the insertion of the heavy chain into the pSFD-Lλ vector was performed. Both the pSFD-Lλ and variable heavy chain fragment were digested, separately, with NotI and NocI restriction enzymes, and again, after purification, the ligation of the fragments was performed using the enzyme ligase. The vector was further transformed, cells were grown and plated, and the library containing the final vector (pSFD-Lλ-H) was generated.

For the first digestion, a reaction mix was prepared by mixing the phagemid (~50 μg) with the SfiI enzyme (50 μL, i.e.20 units per 1 μg of phagemid DNA),10x CutSmart® buffer and nuclease free water. The whole mix was split in 40 PCR tubes (49 μL each) and incubated at 50°C for 20h in the thermocycler. Once the digestion with SfiI was finished, 1 μL of XbaI enzyme was added to each PCR tube and left to incubate for further 20h at 37°C.

After the digestion with XbaI was completed, the digested pSFD phagemid was loaded onto a 1% agarose gel for purification, from which a band corresponding to the digested phagemid (~5000 bp) was excised and purified using the PureLink™ quick gel extraction kit.

The λ light chain fragment was also digested with the enzymes XbaI and SfiI following the same protocol, but the digested fragments were purified using the PureLink™ quick PCR purification kit.

The digestion of the heavy chain fragments with NocI-HF and NotI-HF enzymes was performed at the same time by mixing 1 μL of each enzyme. The tubes were incubated at 37°C for 20 h and further inactivation was done at 65°C for 20 min. Digested heavy chains were purified using Invitrogen PureLink™ quick PCR purification kit and stored at 4°C until further use.

5.3.1.8. Ligation of the λ Light Chain to the pSFD vector

The λ light chain was inserted onto the digested plasmid by setting up a 400 μL ligation mix containing the 2 μg of XbaI-SfiI digested pSFD vector, 2 μg of XbaI-SfiI digested light chain insert (equal amounts of L1, L2, L3 and L4), 40 μL of T4 DNA ligase buffer, 20 μL of T4 DNA ligase enzyme and nuclease free water. The mix was split in 8 PCR tubes, which were incubated in a thermocycler at 16°C for 16 h and then heat inactivated at 65°C for 10 min.

The ligation products were further cleaned up using the GeneJET gel extraction and DNA clean-up micro kit (following the manufacturer's instructions) before transformation by electroporation into TG-1 cells.

5.3.1.9. Electroporation into TG-1 Cells

The total volume of ligation mix was split into 1 μL aliquots and multiples electroporations were performed by adding 1 μL of ligation mix into a 30 μL-aliquot of Lucigen TG-1 electrocompetent cells. Before initiating the transformation, the DNA/cell mix was allowed

to chill on ice for further 15-20 min together with the required number of electroporation cuvettes and microcentrifuge tubes. The electropulser was set up to deliver an electrical pulse of 1.8 kV, the DNA/cell mixture was pipetted into the electroporation cuvette and once the pulse is released, 1 ml of recovery SOC medium at room temperature is added to the cuvette. Transformed cultures were grown at 37°C for 1 h with shaking (225 RPM), from which 20 µL of cells were collected and serially diluted tenfold in 2-YT medium to be plated onto 2-YT plates containing 1% (w/v) glucose and 100 µg/mL Ampicillin (2-YT/Glu/Amp). The plates were incubated at 37°C overnight and the size of the library is calculated from the titer obtained from serial dilution plates according **Equation 2**. The remaining culture is plated onto large 2-YT/Glu/Amp bioassay plates and incubated overnight at 30°C.

$$\text{Size of library } \left(\frac{\text{colonies}}{\text{mL}}\right) = \frac{\text{No colonies } \times \text{ Serial dilution } (1 \times 10^{x})}{\text{Volume inoculated (mL)}} \times \text{Volume of transformations (mL)}$$

Where x stands for the dilution applied. (Equation 2)

5.3.1.10. Preparation of the pSFD-Lλ vector

The pSFD-Lλ library was recovered from the bioassay plate by pipetting ~2 mL of 15% (v/v) glycerol in 2-YT media and using a cell spreader to gently loosen the cells. A 500 µL-aliquot of the resuspended λ chain-PSFD library was used to purify the phagemid, while the remaining of the library was aliquoted and stored at -80°C.

The genetic material was extracted by using the Zippy™ Plasmid Miniprep kit, following the instructions of the kit.

5.3.1.11. Colony PCR

Single colonies were picked from the serial dilution plates and used as source of template DNA in colony PCR to confirm the library has the correct insert. A PCR reaction mix was set up by mixing 12.5 µL of DreamTaq Green Master Mix, 1 µL of forward primer (OvCH1 hinge Not For), 1 µL of reverse primer (M13 Rev) and 10.5 µL of nuclease free water, to which a single colony was added. The PCR mixes were incubated at 95ºC for 5 min, followed by 35 cycles of incubation at 95°C for 30 seconds, 58°C for 30 seconds and 72°C for 60 seconds, and a last step at 72°C for 10 min. The PCR products (5 µL) were run on 1% (w/v) agarose gel in 1x TAE buffer, as previously described, to analyse the presence of the insert (~650 bp).

5.3.1.12. Restriction Digest for Cloning the Heavy Chain

For the insertion of the variable heavy chain fragment, the pSFD-Lλ was digested using the restriction enzymes NotI-HF and NcoI-HF. Several digestion mixes were prepared by mixing 1 µg of pSFD-Lλ with 1 µL NotI-HF, 1 µL of NcoI-HF, 5 µL of 10x CutSmart® buffer and nuclease free water up to 50 µL. The tubes were incubated at 37°C for 20h and at 65°C for 20 min for inactivation of the enzymes. The digested vector was run on 1% (w/v) Agarose gel in 1x TAE for purification and the DNA was extracted from the gel bands using the Purelink™ quick gel extraction kit., as described before. DNA concentration was estimated using a nanodrop by measurement of the absorbance at 260 nm.

5.3.1.13. Ligation of the Heavy Chain to the pSFD-Lλ and Transformation

The insertion of the heavy chain fragment into the pSFD-Lλ was performed by preparing ligation mixes using a molar ratio of 1:3 of vector to insert. For a ligation mix of 400 µL, 2 µg of digested vector were mixed with 0.84 ug of digested heavy chain (equal amounts of H1, H2 and H3), 40 µL ligase buffer, 20 µL of ligase and nuclease free water. The mix was divided into 8 PCR tubes of 50 µL, which were incubated in a thermocycler at 16°C for 16 h and then heat inactivated at 65°C for 10 min. The ligation products were further cleaned up using the GeneJET gel extraction and DNA clean-up micro kit (following the manufacturer's instructions) and transformed by electroporation into TG1 cells. The transformation of the cleaned ligation mix into TG-1 cells was performed by electroporation, as described before, and the library was generated following the same protocol. A colony PCR was as well performed to assess the presence of the correct insert into the vector (~ 1500 bp).

5.3.1.14. Restriction Digestion for Assessment of Clone Diversity

For positive clones, the remaining colony PCR mix was cleaned up using the Purelink™ PCR purification kit for purification of the vector. To assess the diversity of the genetic material, the vector was individually digested with restriction enzymes HaeIII and BstNI, by setting up 40 µL digestion reaction containing, 1 µg of DNA, 10 U of the enzyme, 4 µL of 10x CutSmart® buffer and nuclease free water. Reaction mixes for HaeIII digestion were incubated at 37°C for 90 min and heat inactivate at 80°C for 20 minutes, and reaction mixes for BstNI were incubated at 60°C for 90 min. The DNA products were loaded into 3% agarose gel, and the digestion pattern was assessed.

5.3.2. Construction of scFv Antibody Libraries

5.3.2.1. cDNA Generation

cDNA was synthesised using primers OvCHFOR and OvCLFOR specific for the ovine antibody heavy and light chain, respectively. The kappa light chain, once again for the same reasons stated below, was not synthesised or inserted in the vector. All the primers used for the development of the scFv library are shown in **Appendix 14**.

For cDNA synthesis, per 1 μg of RNA, 1 μL of the primer mix (2 pmol/μL of each primer), 1μL of dNTP mix (containing dATP, dCTP, dGTP and dTTP) and RNAse-free water to a final volume of 13 μL were added and the mix was incubated on a thermocycler at 65ºC for 5 min and quenched for at least 1 min on ice, to allow the annealing of the primers to the RNA chain. Each cDNA mix (13 μL) was further added to a reverse transcriptase mix (7 μL) containing 1 μl of Superscript™ IV reverse transcriptase enzyme, 4 μl of 5x Superscript™ IV buffer, 1 μl of RnaseOUT™ recombinant ribonuclease inhibitor and 1 μl of 0.1M DTT. The mixes (total volume of 20 μl) were incubated for 55°C for 15 min, followed by heat inactivation at 80°C for 10 min. The generated cDNA was stored in the freezer until further use.

5.3.2.2. PCR Amplification of IgG Heavy and λ Light variable Gene Segments

The amplification of the ovine heavy and λ chains was done by PCR using a unique set of forward and reverse specific primers.

For the amplification of the heavy chain, PCR reactions were set up by using the following primer pairs:

- H1 – Mixture of OvJH1LINKFOR, OvJH2LINKFOR, OvJH3LINKFOR and OvJH4LINKFOR, and OvVH1BACK
- H2 – Mixture of OvJH1LINKFOR, OvJH2LINKFOR, OvJH3LINKFOR and OvJH4LINKFOR, and OvVH2BACK
- H3 – Mixture of OvJH1LINKFOR, OvJH2LINKFOR, OvJH3LINKFOR and OvJH4LINKFOR, and MuVH1BACK
- H4 – Mixture of OvJH1LINKFOR, OvJH2LINKFOR, OvJH3LINKFOR and OvJH4LINKFOR, and Hu4aBACK

For the amplification of the λ chain, PCR reactions were set up by using the following primer pairs:

- λ1 – Mixture of OvJL1FOR and OvJL2FOR and OvVL1LINKBACK
- λ2 – Mixture of OvJL1FOR and OvJL2FOR and OvVL2LINKBACK
- λ3 – Mixture of OvJL1FOR and OvJL2FOR and OvVL3LINKBACK
- λ4 – Mixture of OvJL1FOR and OvJL2FOR and OvVL4LINKBACK
- λ5 – Mixture of OvJL1FOR and OvJL2FOR and OvVL5LINKBACK

PCR reactions for each chain were set up individually by mixing 5 μL of cDNA with 45 μL of a Master mix containing 10 μL of 5x Phusion buffer (GC), 1 μL of Phusion polymerase, 1.25 μL forward primer (20 pmol/μL), 1.25 μL of reverse primer set (20 pmol/μL), 2 μL dNTPs, 1.5 μL of DMSO and RNase-free water up to 45 μL. The reaction mixes were heated up to 98°C for 30 s, subjected to a 30 cycle temperature gradient program of denaturation at 98°C for 10 seconds, annealing at gradient temperature of 52-72°C for 30 seconds and polymerization at 72°C for 40 seconds, followed by a final extension at 72°C for 10 min. Tubes were incubated at 4°C until further use.

5.3.2.3. Agarose Gel Electrophoresis and DNA Extraction

The heavy and light DNA PCR products were purified by agarose gel electrophoresis, using a 1% (w/v) agarose gel. Bands corresponding to the heavy and light chains (~350 bp) were excised from the gel using a scalpel, and the DNA was extracted from the gel bands using the Purelink™ quick gel extraction kit, following the manufacturer's instructions. The concentration of both heavy and light chains was estimated using a nanodrop (Jenway Genova Nano).

5.3.2.4. Restriction Enzyme Digestion of the Heavy and λ Light Chain Fragments with MluI and AscI Restriction Enzymes

The primers used for the amplification of the variable heavy (V_H) and lambda light chain (Vλ) from cDNA were designed to incorporate the restriction sites of the enzyme AscI for the heavy chain and restriction sites of the enzyme MluI for the light chain at the linker region, for enabling further cloning processes.

Equal amounts of V_{H1}, V_{H2}, V_{H3}, V_{H4} were individually digested by setting up reaction mixes containing 1 μg of DNA, 1 μL of AscI enzyme (10 U), 5 μL of 10x CutSmart® buffer and nuclease free water up to a final volume of 50 μL, and the same mixes were prepared for the digestion of the Vλ1, Vλ2, Vλ3, Vλ4 and Vλ5 using MluI enzyme instead. The PCR tubes were incubated at 37°C for 3 h. After the digestions are complete, the DNA is purified by agarose gel electrophoresis and extracted from the gel bands using the PureLink™ quick gel extraction kit.

5.3.2.5. Ligation of the Variable Heavy Chain (V_H) and the λ Light Chain ($V_λ$)

A total amount of 1 μg of digested heavy chain (0.25 μg of V_{H1}, V_{H2}, V_{H3}, V_{H4}) was ligated to a total amount of 1 μg of digested λ chain (0.2 μg of $V_{λ1}$, $V_{λ2}$, $V_{λ3}$, $V_{λ4}$ and $V_{λ5}$ by adding 20 μL of T4 DNA ligase and 40 μL of ligase buffer and water to a final volume of 40 μL. The enzymes MluI and AscI (2 μL, i.e. 20 U of each) were as well added to the mix to prevent the formation of VH-VH and Vλ- Vλ products, as successful ligation of V_H-$V_λ$ removes AscI and MluI sites from the linker region. Ligation was performed for 4 h at 37°C, and the ligation products were purified by gel electrophoresis by cutting of a band of ~750 bp, and extracting its DNA using the PureLink™ quick gel extraction kit.

5.3.2.6. Incorporation of SfiI and NotI Cloning sites into V_H-$V_λ$ DNA Fragments

A PCR reaction was performed to include the cloning sites of the restriction enzymes SfiI and NotI into the ligated V_H-$V_λ$, for its later insertion into the phagemid vector. The amplification was performed by adding to a 1 μL of purified V_H-$V_λ$ fragment, 25 pmol of a forward primer mix containing primers OvJL1FOR-Not and OvJL2FOR-Not, 25 pmol of a reverse primer mix containing primers OvVH1BACK-Sfi, OvVH2BACK-Sfi, MuVH1BACK-Sfi and Hu4aBACK-Sfi, 1 μL of Phusion DNA Polymerase, 10 μL of a 5x Phusion buffer GC, 2 μL of a dNTP mix, 1.5 μL of DMSO and nuclease free water to a final volume of 50 μL. The PCR mixes were incubated at 98°C for 30 s and subjected to 2 cycles of denaturation at 98°C for 10 seconds, annealing at 65°C for 30 seconds and polymerization at 72°C for 30 seconds, followed by an extension step at 72°C for 10 min. After 2 cycles of initial amplification, mixes were subjected to further 25 cycles of PCR reactions with 72°C as the annealing temperature. Products were purified by gel electrophoresis and extracted from the gel using the PureLink™ quick gel extraction kit.

5.3.2.7. Restriction Digestion of V_H-V_λ Fragment and Phagemid Vector

For construction of the scFv library both the V_H-V_λ fragments and the vector were digested, individually, with SfiI and NotI-HF. Both DNA products were firstly digested with SfiI by adding to each μg of DNA 2μL of SfiI enzyme (20 U), 5 μL of 5x CutSmart® Buffer and nuclease free water up to 50 μL. The mixes were incubated for 4h at 50°C, and afterwards, 2 μL of NotI-HF were added to each mix. Tubes were again incubated for another 4 h-period at 37°C and 20 min at 65°C for heat inactivation of the enzyme. The digested phagemid was later purified by agarose gel electrophoresis, by excising a band corresponding to ~5000 bp and extracting the DNA using the PureLink™ quick gel extraction kit, while the digested V_H-V_λ fragments were purified using the PureLink™ quick PCR purification kit. DNA product were stored at 4°C until further use.

5.3.2.8. Ligation of the V_H-V_λ Fragment to the Phagemid Vector and Transformation of the Ligation Product

The V_H-V_λ fragment was ligated into the phagemid vector following a 1:3 molar ratio of vector:insert. A ligation mix of 400 μL was prepared by mixing 2 μg of vector with 0.9 μg of insert, 20 μL of T4 ligase, 40 μL ligase buffer and nuclease free water. The mix was split into 8-50μL tubes and the reaction was performed for 16 h at 16°C. The ligated DNA was purified and cleaned up using the GeneJET gel extraction and DNA clean-up micro kit before being transformed into TG-1 cells.

5.3.3. Rescue and Panning of Recombinant Antibody Phage Display Library

5.3.3.1. Rescue of the Phagemid Libraries

Since the infection of bacterial cells by phages is dependent of the interaction between the pIII of the phage particle and the tip of the F conjugative pilus of the bacteria, an aliquot of the bacterial library is grown to mid log phase, so cells start expressing the f-pilus. In order to ensure a good representation of the library, at least a ~10x fold excess of cells to clones in the library was used by inoculating 50 mL 2-YT media supplemented with 100 μg/mL of ampicillin and 2% of glucose (2-YT/glu/amp) to an OD_{600} of 0.1 (or $4x10^9$ cells total)*. Cells were incubated at 37°C with shaking for 1-2 h and allowed to grow until OD_{600} of 0.5 was

reached (mid log phage). For infection with helper phage, 10 mL of the culture were inoculated into a 15 mL falcon tube and infected with helper phage (M13K07), in a 1:20 ratio of helper phage:bacteria, for 30 min in a 37°C water bath. Infected cells were centrifuged at 3300 × g for 10 min, part of the supernatant was discarded, and the pellet was gently resuspended in 2-3 mL of the remaining supernatant. The culture was transferred into 100 mL of 2-YT media containing 100 μg/mL of ampicillin and 50 μg/mL of kanamycin and incubated overnight at 30°C with 220 rpm shaking.

On the next day, phage-antibody particles were harvested by centrifugation and PEG precipitation. The overnight cultures were decanted into two 50-mL tubes, centrifuged for 30 min at 4500 × g and 4°C, and the pellet was discarded. The supernatant was divided into three 50-mL tubes (~35 mL each), and to each $1/5^{th}$ volume of 20% PEG6000 in 2.5 M NaCl was added. Tubes were incubated for 1 h at 4°C, before centrifuging again for 30 min at 4500× g and 4°C. The supernatants were discarded, and the pellets resuspended in ~3 mL of cold deionized water. The three fractions were combined and $1/5^{th}$ volume of 20% PEG 6000 in 2.5 M NaCl was once again added and leave to incubate for 20 min at 4°C. After another centrifugation step (same conditions), the supernatant was discarded and the pellet was resuspended in 1.5 mL of PBS, followed by a centrifugation at 3300 × g for 10 min to remove any residual bacterial debris.

5.3.3.2. Selection of Phage-antibody Libraries by Panning in Immunotubes

Immunotubes were coated with (freshly prepared) HSA-HNE and OVA-HNE antigens overnight 10, 5 and 1 μg/mL, in PBS, respectively for the first, second and third rounds of panning. On the next day, the immunotubes were washed three times with PBS and blocked with 2% of MPBS (skimmed milk powder in PBS) for 2 h at room temperature. After blocked, the immunotube was washed three times with PBS and filled with 1 mL of rescued phage (between 10^{12} to 10^{13} transducing units), 2 mL of 2% MPBS and 1 mL of 4% MPBS. The tube was incubated for 30 min at room temperature rotating continuously on an under-over turntable and for further 90 minutes in a fixed position.

After the incubation step, the non-specific phages were removed by washing the tube 20 times with PBST and 20 times with PBS. The elution of the bound phages was done by adding 1 mL of 100 mM Glycine, pH 3.0 and let the tube incubate for 10 min while rotating. The phages were neutralized by addition of 500 μL of 1 M Tris-HCl pH 7.4. To allow the infection, 1 mL of eluted phage was incubated with 9 mL of exponentially growing culture of TG-1 cells (OD_{600} 0.5), for 30 min in a water bath at 37°C, with no shaking. A 20 μL

aliquot of the infected culture is serially diluted tenfold in 2-YT medium and plated onto 2-YT/Glu/Amp plates and incubated overnight at 37°C. The rest of the culture was centrifuged for 10 min at 3300 rpm for pelleting the cells, which were later resuspended in 1 mL of 2-YT medium and plated onto a large bioassay plate. The plate was incubated overnight at 30°C. The library size was estimated by counting the number of bacterial colonies on the serial dilution plates using **Equation 2**.

The library was recovered from the bioassay plate by loosen the cells, with a spreader, in ~2 mL of filtered 2-YT medium containing 15% glycerol. The bacterial suspension was aliquoted and stored at -80°C as a bacterial stock containing the selected phage from the first round of selection. This panning process was further repeated 2-3 more times, always using the bacterial stock generated from the previous selection as the starting material for the next round of panning.

5.3.3.3. Selection of Phage-Antibody Libraries by Panning with Biotinylated Antigens

Two 100 μL aliquots of Dynabeads™ M-280 Streptavidin were washed three times with PBS and blocked with 2% MPBS for 1h at room temperature with end-over-end mixing. Phages were blocked as well with 2% MPBS for 30 min at 4°C, and if competition is needed for the selections, a 10-fold molar excess of the non-biotinylated competitor molecule was added as well. After 30 min, to the blocked solution of phages 50 nM of biotinylated antigen were added, and left incubating with end-over-end mixing overnight at 4°C.

The phage solution (containing the antigen) was mixed with 100 μL of blocked beads and left incubating for 10 min with end-over-end mixing. For removal of non-specific phages, beads are washed 6 times with MTPBS (PBS containing 2% milk powder and 2% Tween 20), transferred to a new 1.5 mL tube where were washed again 6 times with MTPBS, and transferred one more time to a new 1.5 mL tube, where they were washed twice with PBS.

To elute the antigen bound antibody-phages, beads were resuspended in 1 mL of glycine pH 3 and incubated for 10 min at room temperature with end-over-end mixing. The eluted phages were neutralized by adding 0.5 mL of 0.1 M of Tris-HCl pH 7.4. The total volume of eluted phage was incubated with 10 mL of exponentially growing culture of TG-1 cells (OD_{600} 0.5), for 30 min in a water bath at 37°C, with no shaking. The infected culture was later plated as described before in section 5.3.3.2.

5.3.4. Screening and Expression of Selected Clones

5.3.4.1. Polyclonal Phage ELISA

After each round of panning, an ELISA assay was performed for screening the binding of the eluted antibody phages to assess library enrichment.

A 96-well ELISA plate was coated overnight at 4°C with 100 μL of the antigen (HNE-modified and non-modified antigen) at different concentrations, ranging from 0.001 to 1 μg/mL. The wells were washed three times with PBS and further blocked with 200 μL of 1% BSA in PBS for 2 h at room temperature. Plates were washed again three times with PBS and incubated for 90 min with 100 μL of the harvested phages (diluted 10x in 1% BSA/PBS) from the different generated libraries. Plates were further washed three times with PBST and three times with PBS and incubated for 1 h with 100 μL of 0.1 μg/mL HRP-labelled anti-M13 bacteriophage antibody. TMB substrate solution (100 µL) was used for detection and its reaction was stopped after 15–30 min by addition of 50 µL of stopping solution (1 M HCl). Absorbance was read at 450 nm.

5.3.4.2. Removal of Gene III from Final pSFD-Lλ-H Vector

The genetic material of each final library was extracted using the Zyppy™ mini-prep kit, by following the manufacturer's protocol, and the DNA concentration was measured with the nanodrop.

For each library, 1 μg of DNA was digested with restriction enzymes EcoRI and MfeI by preparing a 50 μL master mix containing 5 μL of 10X CutSmart® Buffer, 1 μL of each enzyme and nuclease free water. Tubes were incubated at 37°C for 1h in a thermocycler, and once finished the reaction, the digested products were run on a 1% agarose gel for purification. A band corresponding to the vector without the gene III was excised (~5000 bp), and the DNA was purified from the gel band using the PureLink™ Quick Gel Extraction Kit.

The vector was later re-ligated by setting up a 400 μL ligation mix, for each vector, containing 2 μg of digested vector, 20 μL of T4 DNA ligase, 40 μL of ligase buffer and nuclease free water, that was split up in 50 μL aliquots over 8 PCR tubes. The ligation reaction was performed at 16°C overnight, and after a heat inactivation step of 15 minutes at 65°C, 0.5 μL aliquots of each ligated vector were electroporated into 30 μL of TG-1 cells, following the same conditions aforementioned. Transformed cultures were grown at 37°C

for 1 h with shaking (225 RPM), a fraction of the cells was collected for serial dilution and plating onto 2-YT/Glu/Amp plates. The plates were incubated at 37°C overnight

5.3.4.3. Fab Expression and Screening

Induction of Colony Cultures

From the dilution plates generated in the previous step, 96 individual colonies were picked and grown individually into 100 μL of 2-YT/Glu/Amp in a 96-well culture plate (plate 1). The plate was left incubating overnight at 30°C with 230 rpm shaking, and on the next day, 2 μL of each well were transferred into a second 96-well plate (plate 2) containing 200 μL of 2-YT/Glu/Amp. Plate 2 was incubated at 37º, with 230 rpm shaking until the OD reaches 0.9 (2-3 h). To generate glycerol stocks of all the clones, 100 μL 2-YT/Glu/Amp + 50% glycerol were added to each well of the plate 1 and the plate was stored at - 80°C.

To induce protein expression, IPTG was added to each well of the plate 2 to a final concentration of 1 mM and left incubating overnight with at 30°C with shaking. On the next day, the plate was centrifuged down at 1800 G for 10 min and the supernatant was discarded. For periplasmic expression of the antibody clones, the pellets were resuspended in 100 μL of ice-cold lysis buffer (20% sucrose, 200 mM Tris-HCl pH 7.5, 1 mM EDTA, 500 μg/mL of lysozyme) and left shaking for 10 min at 4°C with shaking (200 rpm). Magnesium sulfate was added to each well to a final concentration of 5 mM and the incubation with shaking was continued for further 10 minutes. The plate was centrifuged at 1800 × g for 10 min and the periplasmic supernatant was used for assessment by an ELISA assay.

Monoclonal Expression ELISA

ELISA plates were coated overnight with 100 μL of antigen (HSA, HSA-HNE, or other) at 1 μg/mL and blocked with 2% MPBS for 2 h at room temperature. After three washes with PBS, the plates were incubated with 100 μL of the periplasmic fraction (10x diluted) to each corresponding well, for 90 min. After another set of washes, 1 μg/ml of mouse anti-Myc antibody was added to the plates and incubated for more 90 min. Plates were again washed and a secondary anti-mouse-HRP labelled antibody was used for detection. TMB substrate solution (100 μL) was used for detection and its reaction was stopped after 15–30 min by addition of 50 μL of stopping solution (1 M HCl). Absorbance was read at 450 nm.

5.3.4.4. Small Scale Fab Antibody Expression

The best responding clones observed on the monoclonal ELISA were selected for small scale expression. For each clone, a 5 µL aliquot of the monoclonal glycerol stock was inoculated into 10 mL of 2-YT/Glu/Amp and culture were grown overnight with 230 RPM shaking at 30°C. On the next day, an aliquot of the overnight culture was inoculated into 100 mL 2xTY/Amp/0.1%Glu, so initial OD_{600}=0.1, and cultures were grown during the day until OD_{600} reached 1. For induction, IPTG was added to a final concentration of 0.5 mM, and cultures were incubated overnight at 23°C with shaking (230 rpm). On the next day, expression cultures were centrifuged for 10 min at 5000 rpm and 4°C, supernatant was discarded, and the pellet was resuspended in 25 mL of periplasmic lysis buffer. Cultures were incubated in ice for 20 min with shaking until $MgSO_4$ was added to a final concentration of 5 mM, and left incubating in ice for another 20 min period. Cultures centrifuged for 30 min at 5000 rpm, and the supernatant (containing the Fab) was kept for further analysis.

5.3.4.5. Fab Antibody Purification

Expressed Fabs were purified by affinity chromatography using 1 mL of Ni-NTA agarose resin to each Fab. The resin was washed three times with PBS before being incubated with 5 mL of periplasmic fraction for 1h with end-over-end mixing. The unbound fraction was kept for further analysis and the resin was washed three times in washing buffer (50 mM NaH_2PO_4, 300 mM NaCl, 20 mM imidazole pH 8.0). Bound fabs were eluted from the resin by adding 0.5 mL of elution buffer (50 mM NaH_2PO_4, 300 mM NaCl, 250 mM imidazole pH 8.0), and buffer exchanged to PBS overnight by dialysis. The periplasmic, unbound and eluted fractions were analysed by ELISA and SDS PAGE electrophoresis.

5.4. Results

5.4.1. Construction of Sheep Fab Antibodies Libraries

Once the RNA was extracted from the PBL and the cDNA was synthesised by reverse transcriptional PCR, the variable and constant lambda light (Lλ) and heavy (H) chains were amplified by using the specific primers sets. An agarose gel analysis showed that the size of the Lλ (**Figure V.5 A)** and H (**Figure V.5 B**) chains was ~650 bp, as expected, indicating that the quality of the cDNA was adequate for the following library construction. The Lλ amplified fragments and the template vector were further digested with restriction enzymes

SfiI and XbaI, so the chain could be inserted in the pSFD vector. **Figure V.5 C** confirms that the vector was effectively digested, as seen by the presence of a band with the size of ~5000 bp, that corresponds to the size of the digested pSFD vector and a band of ~500 bp, that corresponds to the size of excised stuffer fragment.

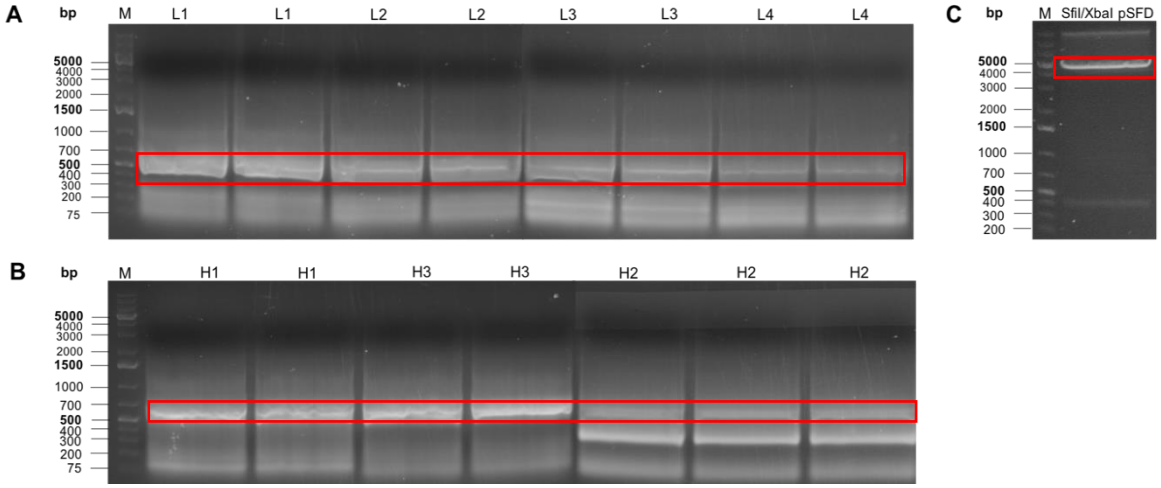

Figure V.5. Agarose gel analysis of the DNA products resulting from the PCR amplification of the lambda chains (L1, L2, L3 and L4) (A) and the heavy chains (H1, H2, and H3) (B), and of the digested pSFD phagemid (C). The DNA bands corresponding to the size of 500 bp in gels depicted in A and B were excised and purified from the gels, and further cloned into the XbaI /SfiI digested phagemid which band (~5000 bp) was as well excised and purified from gel C. DNA bands corresponding to lower sizes in gels A and B, namely ~300 bp and 50-100 bp represent mis-priming PCR products and primers, respectively. Since samples did not fit in a single gel lane, two or more lanes were loaded in order to purify as much DNA as possible. Red oblongs indicate expected band size for an antibody variable and constant chain genes.

The digested vector and digested Lλ fragments were ligated together with T4 DNA ligase and after purification, the ligation mix was subjected to electro-transformation with TG1 cells, so bacteria could incorporate the vector containing the Lλ chain (pSFD-Lλ). The generated library yielded ~$1.3x10^7$ clones, from which 19 randomly picked clones were selected for assessment of the insertion rate of the target fragment. By using primers that amplify the DNA sequence between the SfiI and XbaI specific DNA sequences (i.e. the light chain region), the amplification of a DNA fragment of around 650 bp confirms the correction insertion of the light chain sequence into the vector. From the gel depicted in **Figure V.6,** 4 out of 19 selected single colonies did not have the correct insert, as seen by the presence of bands with size inferior to 650 bp. Therefore, rate of insertion for the light chain was 79%.

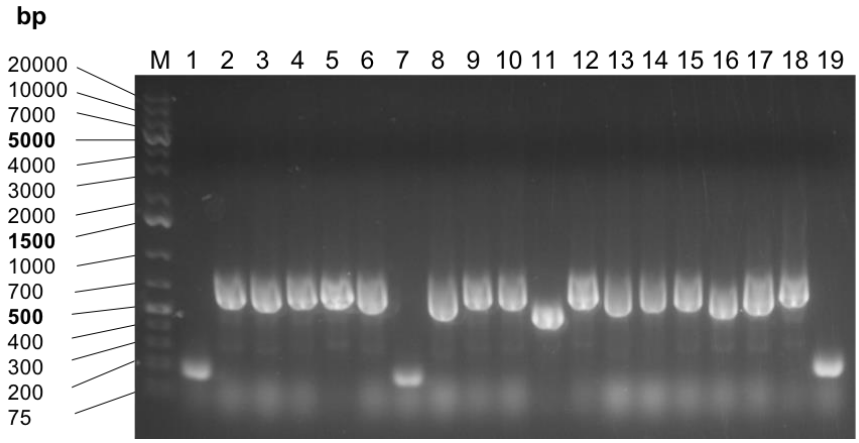

Figure V.6. Agarose gel analysis of colony PCR of 19 randomly selected clones from the pSFD-Lλ library. PCR reactions were performed using primers specific to the light chain region, that should amplify a fragment of around 650 bp if the insertion of the light chain was achieved. Colonies number 1, 7, 11 and 19 do not show the correct size of insert, which by extrapolation suggests that 21% of the library clones does not contain the light chain inserted.

The pSFD-Lλ vector was then extracted from the cells and subjected to a digestion step with the restriction enzymes NocI and NotI, for removal of the heavy stuffer fragment present in the vector and further insertion of the SA369 heavy chain sequence previously PCR amplified. **Figure V.7** confirms again the digestion of the vector was successful, as seen by the presence of a band with the size of ~500 bp that corresponds to the removal of the H stuffer fragment. The H chain amplified fragments were as well digested with the same enzymes, before both digested vector and chain were ligated together with T4 DNA ligase.

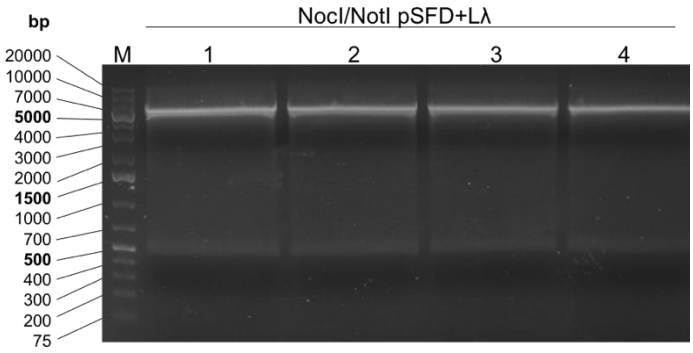

Figure V.7. Agarose gel analysis of the NotI and NocI digested pSFD vector. The bands of around 5000 bp correspond to the digested vector, while the bands of around 500 bp correspond to the removed heavy stuffer fragment. Top bands were excised from the gel and DNA was purified using a commercial kit.

New TG1 bacterial cells were electroporated with the ligation mix for generation of the final Fab library, and again, randomly picked clones were selected for assessment of the insertion rate of the whole Fab gene segment (**Figure V.8 A**) and the library diversity (**Figure V.8 B)**. The antibody diversity was assessed by HaeIII and BstNI fingerprinting of those same individual clones, as these restriction enzymes are seen to cleave in different sites in the antibody's variable regions. Although DNA sequencing is always more advisable for confirming the diversity, DNA fingerprinting with these two restriction enzymes is very often a reliable method.

For the assessment of the insertion rate of the whole Fab gene segment (~1300 bp), primers that bind between the SfiI and NotI and should amplify both the light and heavy chain sequences inserted were used. From 18 single selected clones, only 9 had the correct size of insert (~1300 bp) (**Figure V.8 A**), which suggests a 50% success rate of insertion; however, each of these 9 clones seemed to have a unique sequence, as the digestion pattern observed with both restriction enzymes was different for all of them (**Figure V.8 B**). According to the serial dilution plates generated, the final library had a total size of ~2.4x10^8 clones, from which ~1.2x10^8 clones that have the correct Fab insert.

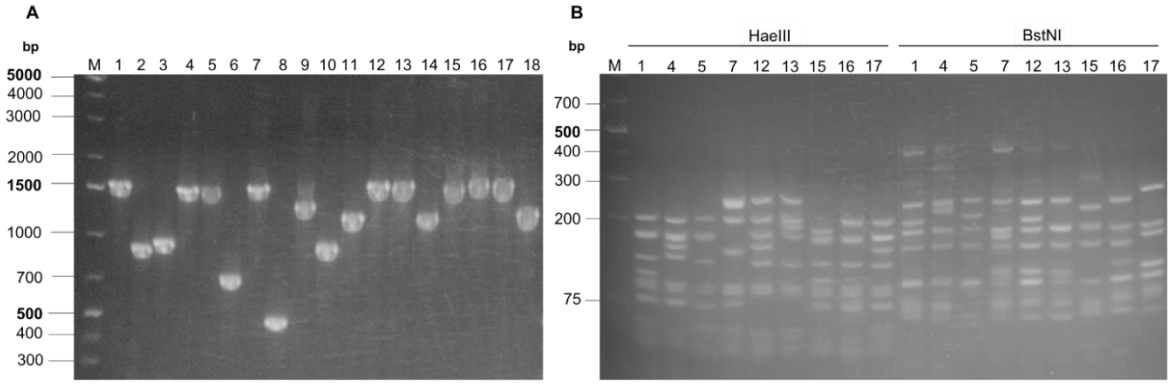

Figure V.8. Agarose gel analysis of colony PCR of 18 randomly selected clones from the pSFD-Lλ library (A) and gel analysis of the diversity of the positive clones (1, 4, 5, 7, 12, 13, 15, 16 and 17), by digestion with restriction enzymes HaeIII and BstNI. PCR reactions run in gel A were performed using primers specific to amplify the light and heavy chain fragments (~1300 bp) allowing the presence of the Fab fragment into the vector to be assessed. Only clones 1, 4, 5, 7, 12, 13, 15, 16 and 17 show the correct size of insert. Each of these positive clones was further digested separately with restriction enzyme HaeIII and BstNI, for assessment of DNA variability. As the digested fragments generated from these enzymatic reactions is different for all the 9 clones, 100% of variability is observed for this pool of 9 clones.

5.4.1.1. Selection of anti-HSA-HNE Fab Fragments

For the selection of specific Fabs against HNE-modified HSA, there rounds of selection/panning (PAN) were performed and adducts were freshly generated on the day before each panning process. For PAN1, 2 and 3 the HNE modified HSA was adsorbed into immunotubes at 10, 5 and 1 μg/mL, respectively. In order to deplete anti-HSA antibodies, after a positive selection in PAN 1 (where no competition with non-modified HSA was performed), PAN 2 and 3 were done alongside with HSA competition. For PAN 2, the competition was carried by incubating the harvested phages with the competitor 1 h after the phages had been incubating with HSA-HNE, i.e., competition in the end (Comp E), but for PAN 3, two different HSA competitions were tested: in the end (Comp E), as performed for PAN 2, and in the beginning (Comp B), by adding HSA at the same time as the phage were incubated with the HSA-HNE. Note that for both PAN 2 and 3, selection with no competition (N comp) was performed as well, for control.

After three rounds of panning, an ELISA assay was performed with the pool of phages harvested before starting any selection (Pre-Pan phages) and after each round of panning (Pan1, Pan 2 N Comp, Pan 2 Comp E, Pan 3 N Comp, Pan 3 Comp B, and Pan 3 Comp E) for assessment of the enrichment of the library towards HSA-HNE (**Figure V.9 A**). Positive enriching against HSA-HNE can be observed in **Figure V.9 A**, by the increasing signal observed along pannings 1, 2 and 3. Before any selection, due to the high amount of unspecific clones, no specific binding to HSA-HNE is observed, and even after a first positive selection against HSA-HNE, the signal is very low. However, after PANs 2 and 3 the binding increases suggesting a good enrichment of the library to the target antigen.

Nevertheless, when comparing the three different eluted pools of phages from the last panning (PAN 3 with no competition, PAN 3 with HSA competition in the beginning and PAN 3 with HSA competition in the end), against different antigens, enrichment for HSA was also seen, which indicates the competition strategies applied were not sufficient to deplete all the anti-HSA clones. Phages eluted from PAN 3 Comp B and PAN 3 Comp E show, on average, a better specificity to HSA-HNE than HSA, than phages eluted from the panning without competition, which might suggest these libraries contain clones with higher specificity to HNE modified HSA. Furthermore, no significant binding to KLH or KLH-HNE is observed, which suggests that the panned antibodies could recognize specifically HSA-HNE adducts.

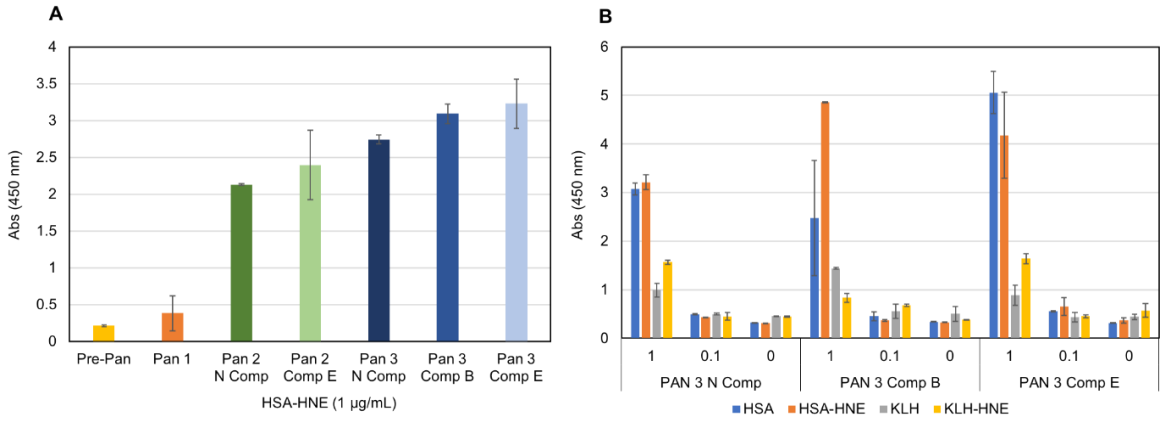

Figure V.9. Polyclonal phage ELISA binding affinity (A) and specificity (B) of the enriched libraries generated after three rounds of panning. In (A) pooled phages harvested before starting any selection (Pre-Pan phages) and after each round of panning (Pan1, Pan 2 N Comp, Pan 2 Comp E, Pan 3 N Comp, Pan 3 Comp B, and Pan 3 Comp E) were added to wells previously coated with 1 µg/mL of HSA-HNE, while in (B), only phages harvested after the three PAN 3 strategies were tested against three different concentrations (1, 0.1 and 0 µg/mL) of HSA-HNE, HSA, KLH-HNE and KLH.

Once the enrichment of the library was confirmed, all the three generated PAN 3 libraries were grown for purification of the genetic material for removal of the gene III sequence of the vector (**Figure V.10**). Since this DNA sequence is responsible for the display of Fab fragments on the protein pIII of the bacteriophage capsid, in order to achieve a successful expression of the Fab clones in bacteria, this gene had to be excised from the expression vector. For ease of reading, libraries generated without HSA competition, with HSA competition in the beginning and with HSA competition in the end were named libraries 3.1, 3.2 and 3.3, respectively. The success of the gene III removal from the vector was evaluated by agarose gel analysis (**Figure V.10**)., from which the digested vector (band of around 5000 bp) was purified before being ligated and transformed back again into TG1 cells. From each transformation performed, 96 randomly picked clones were selected for small scale expression and analysis by monoclonal phage ELISA against HSA and HSA-HNE (**Table V.1**).

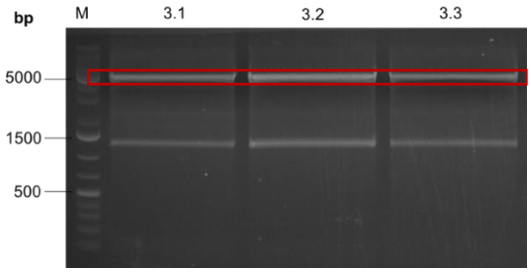

Figure V.10. Agarose gel analysis of the EcoRI and MfeI digestion of the pSFD vector extracted from the three 3rd PAN libraries. The removal of gene III can be observed by the presence of a band corresponding to ~1500 bp that corresponds to the gene III sequence. For ease of reading, libraries generated without HSA competition, with HSA competition in the beginning and with HSA competition in the end were named 3.1, 3.2 and 3.3, respectively. Red oblongs indicate the expected band size for the digested vector.

Table V.1. Monoclonal phage ELISA of 96 random clones selected from PAN 3 library without HSA competition (3.1), with HSA competition in the beginning (3.2) and with HSA competition in the end (3.3), against HSA-HNE (left side tables) and HSA (right side tables) coated plates. Numbers depicted are the absorbance values obtained at 450 nm. The binding intensity was coloured from green to red, where green stands for low binding and red for high binding.

HSA-HNE

3.1

	1	2	3	4	5	6	7	8	9	10	11	12
A	0.63	1.32	6.21	0.43	0.68	5.68	0.48	0.4	0.73	0.5	3.23	0.37
B	0.58	0.34	0.83	0.37	0.32	0.33	1.04	0.45	0.65	0.41	2.82	0.5
C	0.68	0.31	1.47	0.38	0.37	0.89	1.43	0.45	0.76	0.57	0.41	0.53
D	1.33	0.94	0.92	0.35	0.39	1.76	0.64	0.77	1.05	0.68	1	0.66
E	0.43	0.8	0.74	0.73	1.14	0.86	0.5	0.39	1.07	1.25	0.72	0.47
F	0.39	0.67	0.62	0.75	0.33	0.53	0.59	0.46	0.38	0.38	0.6	0.38
G	0.98	0.39	0.47	0.3	0.34	0.54	0.89	0.82	0.49	4.58	0.61	0.44
H	0.51	0.5	0.45	0.71	0.46	0.45	0.54	0.45	0.56	0.49	0.57	1.37

3.2

	1	2	3	4	5	6	7	8	9	10	11	12
A	0.61	0.6	0.39	0.58	0.67	0.7	0.34	0.4	0.36	0.37	0.58	0.43
B	0.4	0.57	0.55	0.59	1.21	0.94	0.74	0.99	0.46	0.68	0.5	0.45
C	0.4	0.48	0.47	0.72	0.61	0.62	0.59	2.52	0.47	0.38	2.21	0.32
D	0.76	0.47	0.67	2.61	0.59	0.63	0.64	0.93	1.02	3.88	3.54	0.6
E	0.38	0.48	0.55	0.72	0.99	0.57	0.43	0.64	0.42	0.47	0.34	0.51
F	0.4	0.62	0.39	0.46	0.41	0.86	0.48	0.53	0.46	0.48	0.34	0.44
G	0.43	0.5	0.76	0.6	0.71	0.62	0.52	0.47	0.55	0.39	0.48	0.39
H	0.41	0.51	0.6	0.43	0.46	0.35	0.37	0.6	0.58	0.34	0.42	3.23

3.3

	1	2	3	4	5	6	7	8	9	10	11	12
A	0.38	0.3	0.41	0.31	0.51	0.3	0.35	0.45	0.31	0.51	0.37	0.3
B	0.39	0.3	0.3	0.36	0.3	3.17	0.49	0.44	0.33	0.4	0.33	0.35
C	0.88	0.46	0.54	0.59	0.42	1	0.36	0.38	0.53	0.37	0.4	0.84
D	0.3	0.41	0.56	0.55	1.09	0.37	0.91	0.29	0.29	0.44	0.31	0.34
E	0.47	0.82	0.28	0.38	0.34	0.45	0.3	0.53	0.25	0.36	0.41	0.36
F	0.5	0.46	0.28	0.3	0.43	0.42	0.28	1.39	0.28	0.37	0.81	0.32
G	0.3	0.31	0.49	0.44	0.29	0.36	0.38	1.33	0.3	0.37	0.63	0.59
H	0.41	0.31	0.35	0.44	0.31	0.29	0.32	0.36	0.37	0.35	0.47	0.57

HSA

3.1

	1	2	3	4	5	6	7	8	9	10	11	12
A	0.33	0.56	4.6	0.33	0.38	3.81	0.59	0.37	0.37	0.38	2.24	0.78
B	0.29	0.39	0.5	0.34	0.31	0.41	0.7	0.41	0.38	0.42	1.67	0.55
C	0.44	0.31	0.93	0.39	0.32	0.64	0.78	0.3	0.45	0.41	0.3	0.94
D	0.69	0.6	0.89	0.29	0.31	1.06	0.71	0.4	0.48	0.33	0.76	0.84
E	0.42	0.55	0.6	0.4	0.54	0.71	0.58	0.35	0.54	0.57	0.57	0.53
F	0.41	0.37	0.4	0.4	0.36	0.37	0.4	0.34	0.39	0.36	0.42	0.35
G	0.43	0.47	0.76	0.42	0.4	0.39	0.64	0.58	0.44	1.68	0.41	0.39
H	0.31	0.47	0.98	0.55	0.43	0.37	0.36	0.33	0.41	0.36	0.44	0.6

3.2

	1	2	3	4	5	6	7	8	9	10	11	12
A	0.52	0.5	0.47	0.64	0.86	0.49	0.57	0.37	0.38	0.42	0.4	0.51
B	0.43	0.53	0.51	0.58	1.32	0.71	0.71	0.61	0.43	0.54	0.43	0.47
C	0.41	0.46	0.64	0.55	0.63	0.46	0.57	1.4	0.51	0.54	1.41	0.4
D	0.56	0.63	0.86	1.55	0.75	0.49	0.77	0.85	0.73	3.1	2.27	0.55
E	0.4	0.53	0.81	0.67	0.9	0.46	0.61	1.22	0.47	0.5	0.54	0.52
F	0.42	0.48	0.48	0.47	0.43	0.6	0.52	0.43	0.4	0.54	0.4	0.45
G	0.38	0.51	0.67	0.47	0.57	0.6	0.54	0.68	0.42	0.5	0.55	0.51
H	0.42	0.56	0.5	0.36	0.4	0.39	0.42	0.63	0.37	0.41	0.45	0.52

3.3

	1	2	3	4	5	6	7	8	9	10	11	12
A	0.38	0.33	0.44	0.36	0.49	0.44	0.36	1.15	0.43	0.4	0.41	0.36
B	0.38	0.36	0.36	0.36	0.43	1.37	0.53	0.37	0.36	0.38	0.32	0.36
C	0.7	0.38	0.43	0.48	0.45	0.59	0.31	0.38	0.51	0.53	0.43	0.86
D	0.39	0.36	0.48	0.41	1.16	0.34	0.58	0.34	0.56	0.35	0.31	0.42
E	0.47	0.57	0.3	0.31	0.3	0.33	0.32	0.42	0.38	0.34	0.4	0.37
F	0.43	0.37	0.33	0.32	0.36	0.68	0.29	0.92	0.3	0.3	0.64	0.41
G	0.35	0.38	0.59	0.41	0.38	0.88	0.35	0.73	0.33	0.32	1.08	0.7
H	0.37	0.36	0.34	0.37	0.4	0.33	0.3	0.31	0.37	0.32	0.41	0.71

The data in **Table V.1** indicates the affinity of 96 individual clones randomly selected from libraries 3.1, 3.2 and 3.3 (a total of 288 different clones) towards HNE modified HSA and native HSA. The presence of clones with higher binding to HSA-HNE than to HSA, such as clones A3, A5 and A11 from library 3.1 might indicate Fab antibody fragments with higher affinity towards the HNE adducts. Therefore, potentially anti-HNE-specific clones (i.e. abs values higher than 2) were selected for further expression, but some clones that showed high binding to non-modified HSA were selected as well, as negative controls.

The selected clones for expression and assessment of diversity were the following: clones A3, A5, A11, B11, C3, C12, D1, D6, G1, G10 and H12 from library 3.1, clones B5, B6, C1, C8, C11, D4, D10, D11, E8, F6 and H11 from library 3.2 and clones A8, B6, C1, C6, C12, D5, D7, F8, G8 and G11 from library 3.3.

All the clones mentioned above were individually subjected to a colony PCR using primers specific to amplify the whole Fab sequence (~1300 bp), for size assessment of the inserted Fab fragment (**Figure V.11 A**) and to a digestion step with BstNI and HaeIII restriction enzymes for diversity evaluation (**Figure V.11 B and C**).

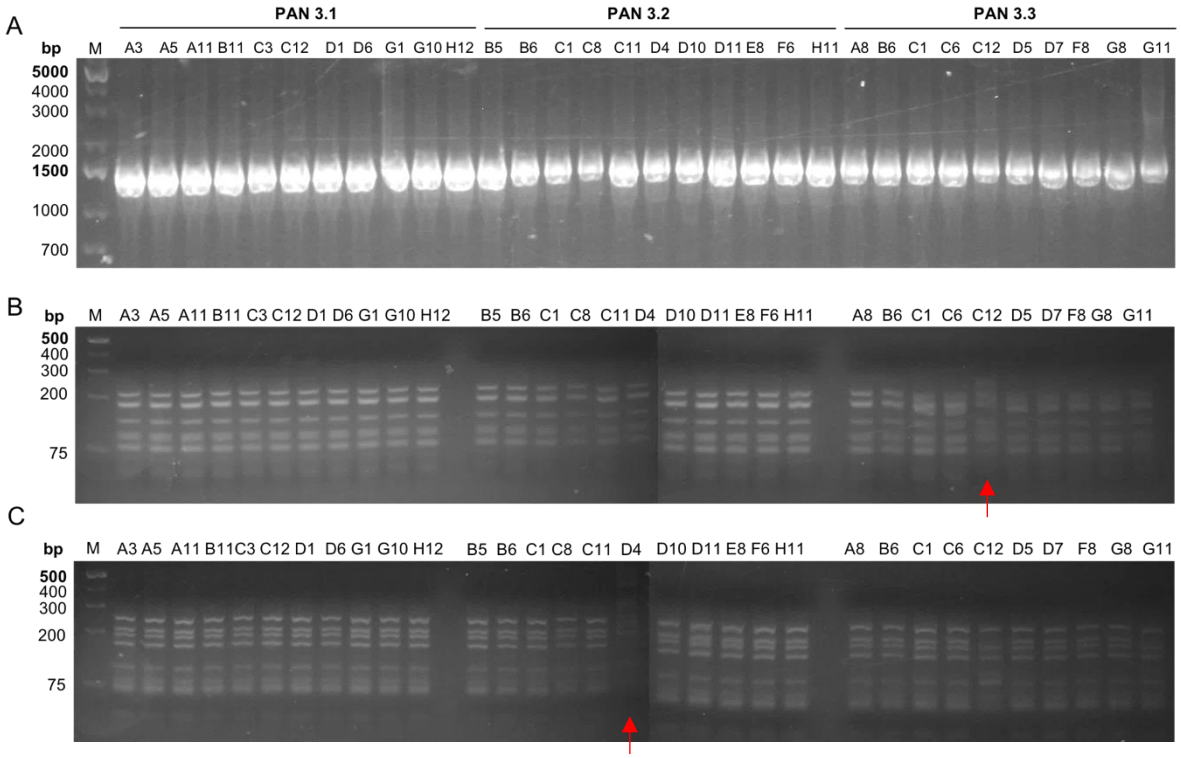

Figure V.11. Gel analysis of colony PCR of 32 clones presenting higher affinities to HNE-modified HSA and native HSA (A) and their respective diversity analysis by digestion with HaeIII (B) and BstNI (C) restriction enzymes. PCR reactions run in gel A were performed using primers specific to amplify the light and heavy chain fragments (~1300 bp) allowing the presence of the Fab fragment into the vector to be assessed. Red arrows indicate clones with different digestion patterns, suggesting, therefore, different nucleotide sequence.

As seen in **Figure V.11 A** all the selected clones contain the correct size of vector (~1300 bp), but from **Figure V.11 B** and **C** only clone D4 from library 3.2 and clone C12 from library 3.3 seem to present a different DNA digestion pattern from all the other 30 clones, which suggests that from a pool of 30 clones, there are only 3 different Fab clones.

To double check the results of the monoclonal phage ELISA, clones G10, A3, A6, D11, H12 and B6 were chosen for large scale expression and purification (**Figure V.12**), but the gel only shows the presence of a single band around ~25 kDa, rather than a double band, which suggests that only the heavy chain was successfully expressed and purified.

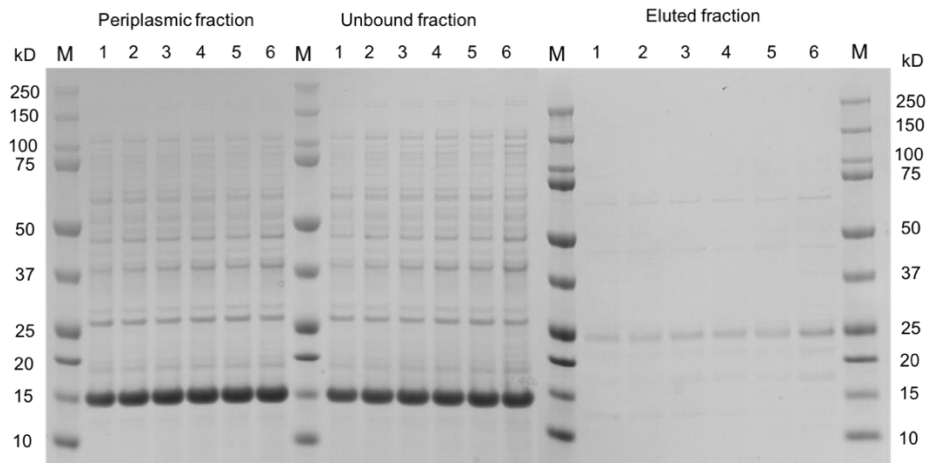

Figure V.12. SDS-PAGE analysis of the periplasmic, unbound and eluted collected fractions during the purification of clones G10, A3, A6, D11, H12 and B6, numbered 1 to 6, respectively. Samples were run on a NuPAGE 12% Bis-Tris protein gel.

Nevertheless, the binding of clone G10 towards HSA, HSA-HNE, OVA and OVA-HNE was assessed by ELISA, using the commercial anti-HNE pAb as a positive control (**Figure V.13**). The results show the absence of binding of clone G10 to any of the proteins, while the commercial pAb binds to HNE-modified HSA and OVA.

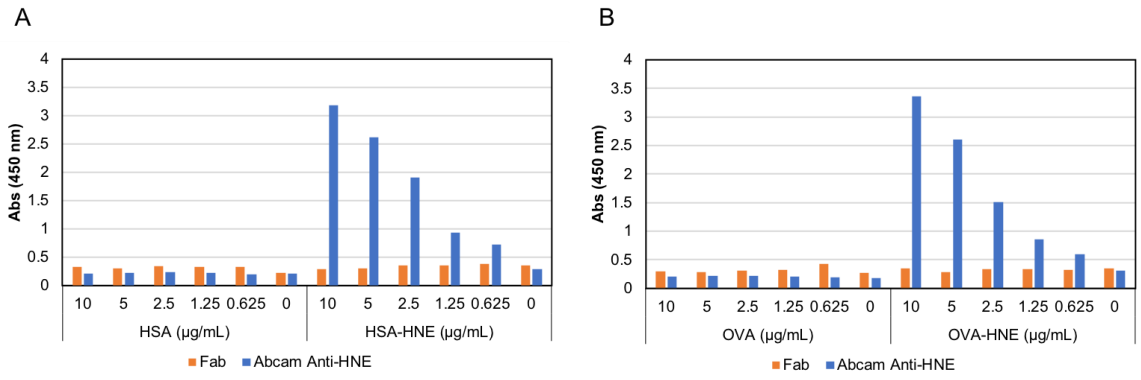

Figure V.13. Binding analysis of Fab G10 clone to HSA and HSA-HNE (A), and OVA and OVA-HNE (B) by direct ELISA. The Abcam anti-HNE pAb was used as positive control. This experiment was done once (n=1) with technical triplicates.

5.4.1.2. Selection of Fab fragments against biotinylated HSA-HNE

As no Fab antibody fragments specific to HSA-HNE adducts were obtained by panning the Fab generated library with HSA-HNE coated immunotubes, a different strategy involving magnetic streptavidin beads and biotinylated HSA-HNE was tested.

HSA was firstly biotinylated using a commercial kit and then aliquots of 1 mg/ mL were freshly modified by HNE before each round of panning. **Figure V.14** shows the commercial anti-HNE pAb recognition of HNE adducts equally on both non-biotinylated and biotinylated HSA-HNE, confirming the present of biotin did not affect the formation of HNE adducts.

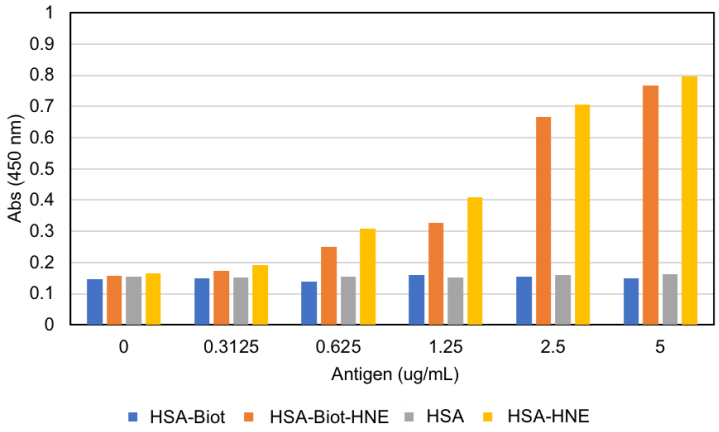

Figure V.14. Direct ELISA assay using the commercial anti-HNE pAb for confirmation of HNE adducts on biotinylated HSA-HNE samples. Biotinylated and non-biotinylated HSA and HSA-HNE were immobilised on a 96-well plate at a concentration range of 0-5 µg/mL and the detection was performed with the Abcam commercial anti-HNE pAb at 1 µg/mL. This experiment was done once (n=1) with technical triplicates.

After a positive selection in PAN 1, with no competition, PAN 2 and 3 were carried out with HSA competition by adding HSA at the same time as the phages were incubated with biotinylated HSA-HNE. After three rounds of panning, the enrichment of libraries was evaluated by a polyclonal phage ELISA (**Figure V.15**), where a positive enrichment against both HSA-HNE and HSA can be observed. The binding of the polyclonal phages to HNE modified HSA seems to be stronger than to HSA.

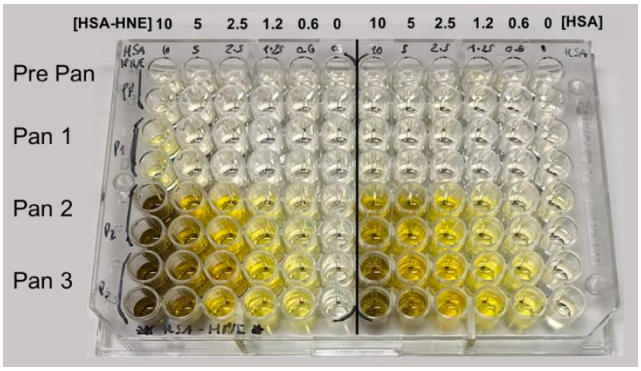

Figure V.15. Polyclonal phage ELISA analysis of the library enrichment after three rounds of panning against biotinylated-HSA-HNE. The plate was coated with HSA-HNE and HSA ate concentrations ranging from 0-10 μg/mL). This experiment was done once (n=1) with technical duplicates.

The library generated from the 3rd PAN was grown overnight for purification of its genetic material; gene III was removed from the vector and, after its ligation, the vector was transformed into grown TG1 cells. A monoclonal phage ELISA was then conducted by selecting 96 random clones to assess their binding to HSA (**Table V.2 A**) and HSA-HNE (**Table V.2 B)**.

Table V.2. Binding assessment of 96 random clones picked from the 3rd PAN by monoclonal phage ELISA against HSA (A) and HSA-HNE (B). Numbers depicted are the absorbance values obtained at 450 nm. The binding intensity was coloured from green to red, where green stands for low binding and red for high binding.

A	**HSA**											
	1	2	3	4	5	6	7	8	9	10	11	12
A	2.257	1.148	0.547	0.533	0.549	0.39	0.369	0.357	0.382	0.199	0.337	0.429
B	0.847	1.333	0.49	0.624	0.403	0.326	0.455	0.343	0.408	0.28	0.36	0.341
C	0.875	0.485	0.437	0.439	0.418	0.378	0.55	0.363	0.507	0.295	0.349	0.583
D	1.095	1.137	0.497	0.432	0.439	0.369	0.395	0.354	0.602	0.37	0.521	0.226
E	5.067	0.781	0.466	0.412	0.496	0.4	0.492	0.36	0.41	0.384	0.375	0.376
F	1.079	0.829	0.491	0.474	0.415	0.422	0.418	0.364	0.441	0.411	0.362	0.94
G	1.16	1.044	0.735	0.527	0.439	0.421	0.371	0.494	0.47	0.499	0.44	0.417
H	1.187	1.575	0.599	0.236	0.644	0.381	0.572	0.461	0.458	0.51	0.467	0.432

B	**HSA-HNE**											
	1	2	3	4	5	6	7	8	9	10	11	12
A	2.929	1.32	1.298	1.09	1.135	1.011	0.614	0.729	0.79	0.218	0.642	0.717
B	1.266	1.506	1.216	1.228	0.984	0.808	0.884	0.74	0.764	0.69	0.864	0.547
C	1.261	0.654	1.015	0.846	0.841	0.812	1.295	0.785	1.022	0.725	0.702	1.302
D	1.515	1.384	0.994	1.016	1.077	0.856	0.868	0.75	1.012	0.703	0.692	0.235
E	4.12	0.982	1.172	0.953	1.055	0.735	1.242	0.608	0.669	0.748	0.591	0.554
F	1.152	1.067	1.026	1.189	0.86	0.76	0.919	0.806	0.832	0.759	0.625	1.922
G	1.062	1.052	1.017	0.294	0.428	0.877	0.384	1.117	0.742	0.731	0.662	0.628
H	1.62	1.922	1.01	0.224	1.194	0.334	1.053	0.933	0.75	0.779	0.801	0.625

Given the obtained results clones E1, A1, H2, H1, B2, F12, C12, E7, C7, A3, B3 and F4 were selected for colony PCR (**Figure V.16 A**). and diversity assessment (**Figure V.16 B** and **C**). Once again, all the selected clones present the correct size of vector (~1500 kb), but they all seem to be the same clone as their digestion pattern obtained with HaeIII and BstNI is the same.

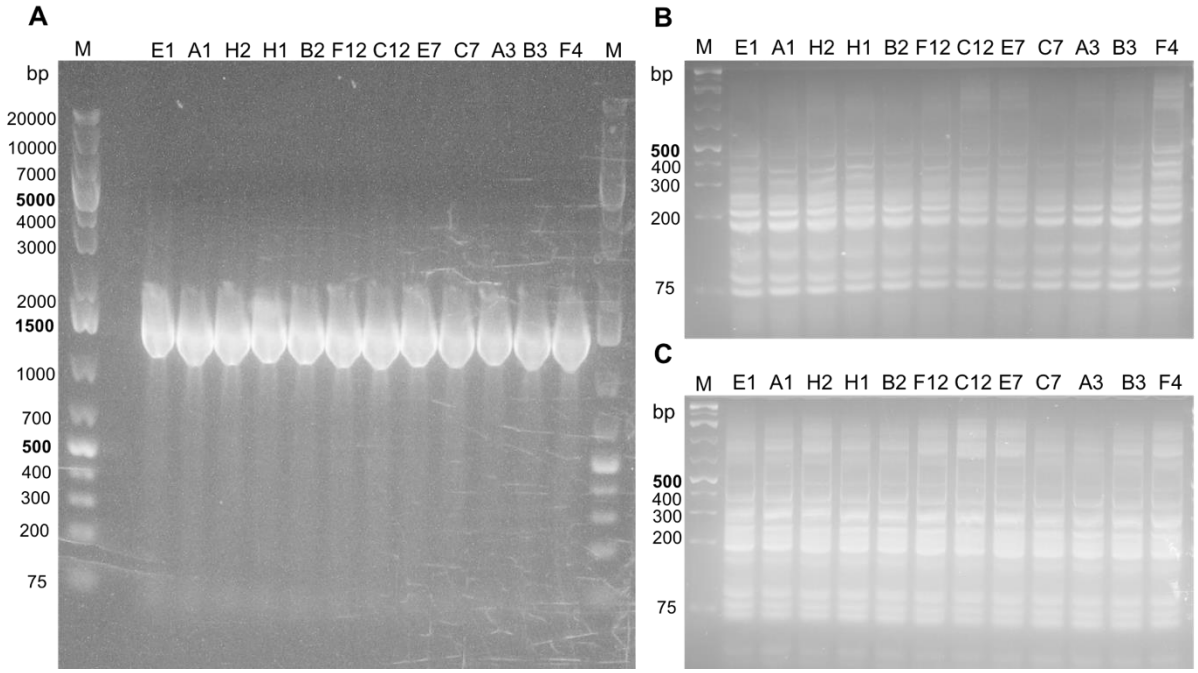

Figure V.16. Agarose gel analysis of colony PCR of the 12 best responding clones (A) and their respective digestion with restriction enzymes HaeIII (B) and BstNI (C). PCR reactions run in gel A were performed using primers specific to amplify the whole light and heavy chain DNA fragment (~1300 bp) allowing the presence of the Fab fragment into the vector to be assessed.

Clone E1 and A1 were selected for large scale production and purification by affinity chromatography using a nickel resin (**Figure V.17**). Purification of Fab E1 did not work as expected, as no band is seen in the elution fraction, but the presence of a double band in the eluted fraction of Fab A1 (**Figure V.17 B)** suggests the clone was expressed and purified from the periplasmic proteins.

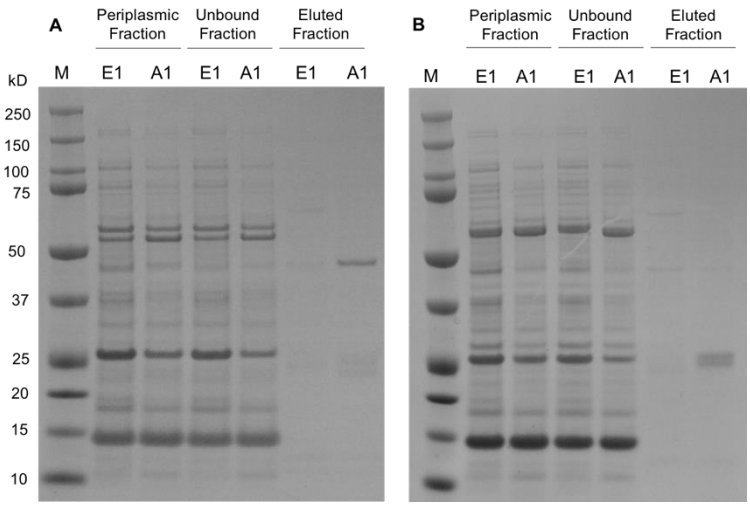

Figure V.17. SDS-PAGE analysis of the periplasmic, flow through and eluted fractions of clones E1 and A1 from their affinity purification. The samples were run under non-reducing (A) and reducing conditions (B).

Clone A1 was then analysed by ELISA for binding assessment towards HSA, HSA-HNE, OVA and OVA-HNE, however the clone did not show binding to any of the antigens (**Figure V.18**).

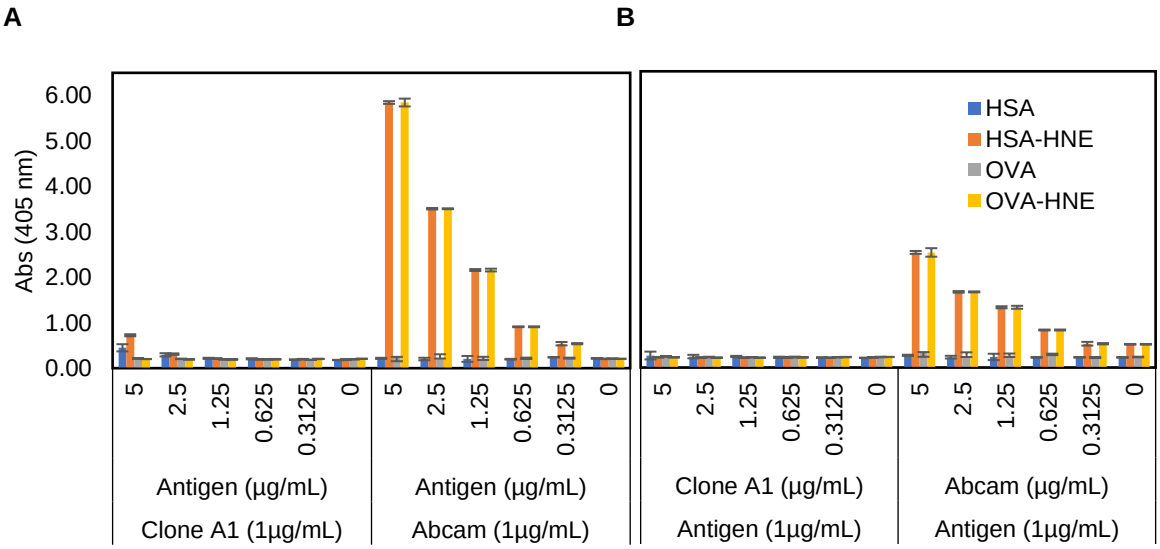

Figure V.18. ELISA analysis comparing the binding of Fab A1 and commercial anti-HNE antibody to HSA, HSA-HNE, OVA and OVA-HNE. In graph A the antigen was coated in a range of concentrations from 0-5 µg/mL and both the Fab A1 and the anti-HNE pAb were incubated at a concentration of 1 µg/mL. In graph B, the concentration of the antigens was fixed at 1 µg/mL while the Fab A1 and the commercial anti-HNE pAb were added in a range of concentrations from 0-5 µg/mL.

4.4.2. Construction of Sheep scFv Antibody Libraries

Given the fact that any of the Fab clones expressed previously showed any binding to HSA or HSA-HNE, a new library was generated for production of a different format of antibody fragment, single chain Fv (scFv) fragments. ScFv fragments, as seen in **Figure V.1,** are actually fusion proteins of the variable regions of the heavy and light chains of immunoglobulins, connected with a short linker peptide, and therefore, the cloning process only requires one insertion step, rather that the two used before for Fabs.

All the primers used for synthesis of the first-strand cDNA, amplification of heavy and light-chain variable-regions and cloning primers with SfiI and NotI restriction sites are given in **Appendix 14**.

Again, once the first strand of cDNA was synthesized, the variable regions of the heavy (H) and lambda light (Lλ) chains were amplified by using the specific primer sets. This time, because only the variable region is being amplified, PCR products or ~350 bb are expected.

As shown in

Figure V.19, the chains have a size of ~350 kb, as expected, confirming the quality of the cDNA was suitable for further construction of the library.

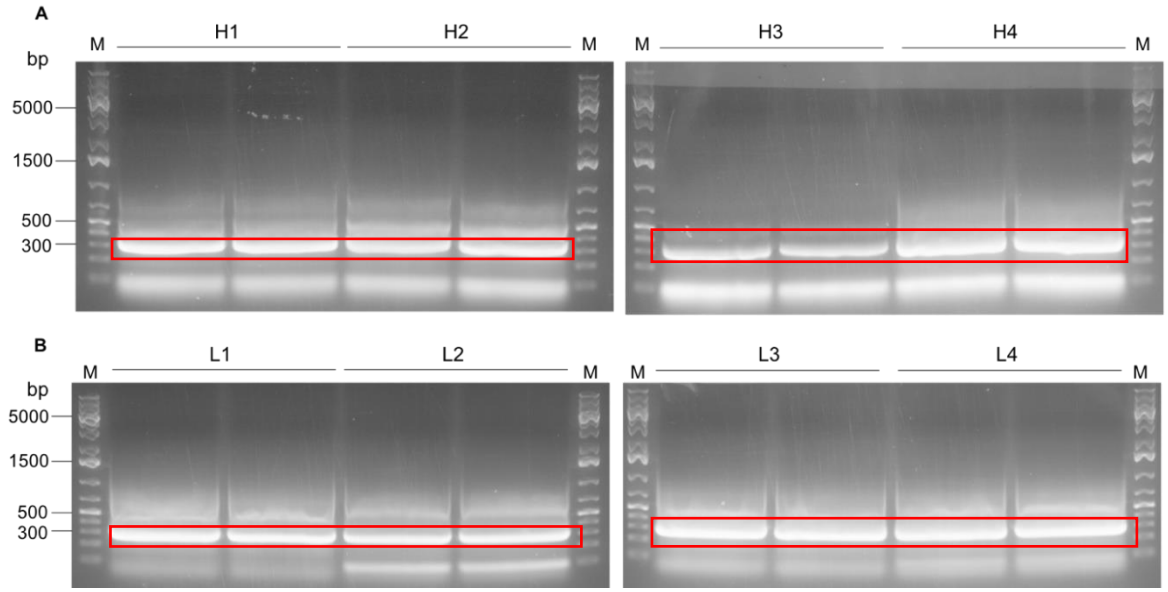

Figure V.19. Agarose gel analysis of the PCR amplified heavy (H1, H2, H3 and H4) chains (A) and lambda light (L1, L2, L3 and L4) chains (B). An extra lambda light chain using primer set L5 was as well PCR amplified and gel purified, however the gel is not included in this figure. DNA bands of ~ 350 bp correspond to the amplified heavy (A) and light (B) chain variable regions, while DNA bands corresponding to lower sizes represent mis-priming PCR products or primers. Since samples did not fit in a single gel lane, two lanes were loaded with each PCR product in order to purify as much DNA as possible. Red oblongs indicate the expected band size for the antibody variable heavy and light chain genes.

After purifying both variable heavy (V_H) and lambda light (V_λ) chains from the agarose gel, both V_H and V_L chains were digested separately with AscI and MluI restriction enzymes, so they could be further ligated to each other with T4 DNA ligase to generate the V_H-V_λ segment. The successful ligation of both chains was confirmed by running the ligation products on a agarose gel (**Figure V.20**), where a fragment of ~700 kb can be observed.

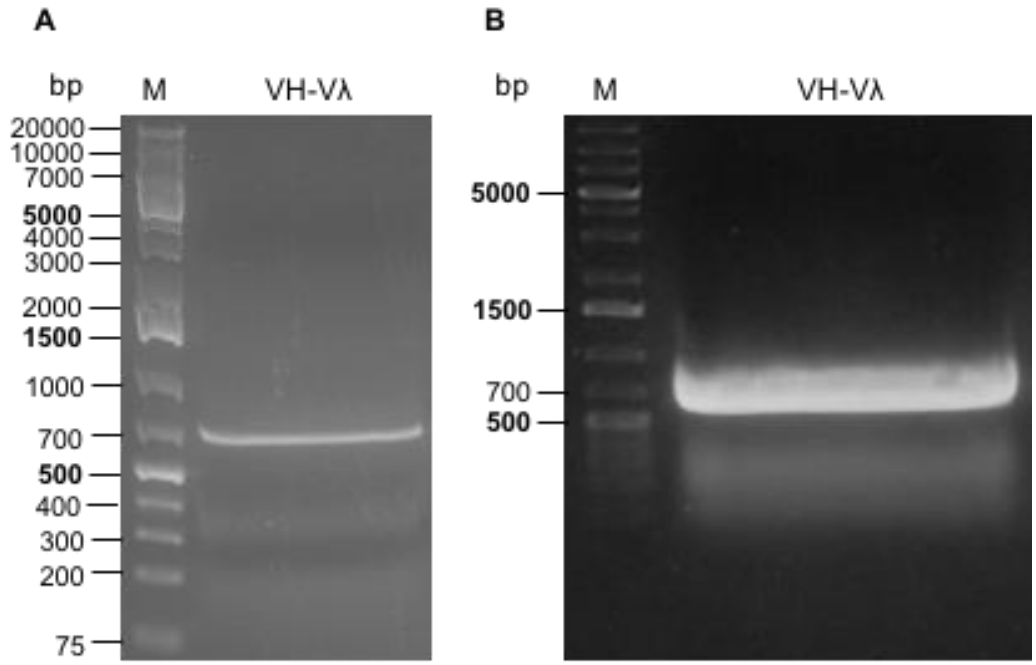

Figure V.20. Agarose gel analysis of the ligated V_H-V_λ fragment (band of ~700 kb) (A) and of its PCR amplification product (B).

The V_H-V_λ ligated fragment and the pSFD vector were further subjected to a digestion with NcoI and NotI restriction enzyme before being ligated with T4 DNA ligase. After purification of the ligation product, the vector was transformed into TG-1 cells and the final scFv library was generated.

To assess the insertion rate of the V_H-V_λ fragment into the vector, 10 randomly picked clones were subjected to a colony PCR using primers specific to the scFV fragment, and the genomic content was analysed on a agarose gel (**Figure V.21**). All the 17 clones contained the correct size of fragment (~700 bp), i.e., a 100% rate of insertion was achieved. The size of the scFv library obtained was $>10^8$ clones.

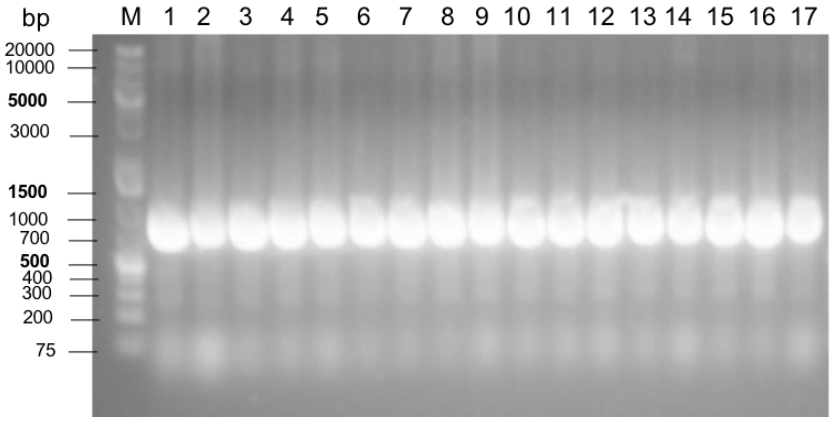

Figure V.21. Agarose gel analysis of colony PCR of 17 randomly selected clones from the scFv library.

4.4.2.1. Selection of anti-HSA-HNE and anti-OVA-HNE scFv Antibody Fragments

The selection of scFv antibody fragments against HNE adducts was done against HNE-modified HSA and HNE-modified OVA, separately, through the use of immunotubes. As for previous panning methods, HNE adducts were prepared freshly on the day the immunotubes were coated and for PAN1, 2 and 3 the immunotubes were coated with 10, 5 and 1 μg/mL of each HNE-modified antigen. Regarding the panning process with HSA-HNE, the first round of panning was done with no competition, for positive selection, and two remaining Pans were done by adding HSA in 5-molar excess. The three OVA-HNE pannings were done with no competition.

The enrichment of the libraries against HSA-HNE and OVA-HNE was again assessed by ELISA, by testing the different eluted pooled antibody-phage fractions against HSA, HSA-HNE, OVA and OVA-HNE**.** Regarding the selection against HSA-HNE (**Figure V.22 A)**, the antibody-phages eluted after PAN 1 seem to show higher specificity to HSA, however, when started to compete with non-modified HSA on the second PAN, that specificity is lost after PAN 2 (green bar). After PAN 3, where a more stringent competition was performed, specificity to HSA but as well to HSA-HNE and OVA-HNE is observed, which may suggest an enrichment of antibody-phages specific to HNE-modified molecules was achieved.

Regarding the selection against OVA-HNE, enrichment towards OVA-HNE and HSA-HNE is only noticed after the third round of panning (**Figure V.22 B)**, with a quite a big difference in the signal between the two modified standards. However, as seen in **Figure V.22 C,** also for the control antibody a considerable difference is observed between HSA-HNE and OVA-HNE, which indicates the ovalbumin standard used for the assay contains more HNE modifications than HSA. Hence, the pooled fraction of antibody-phages collected after PAN 3 may contain promising clones specific to HNE.

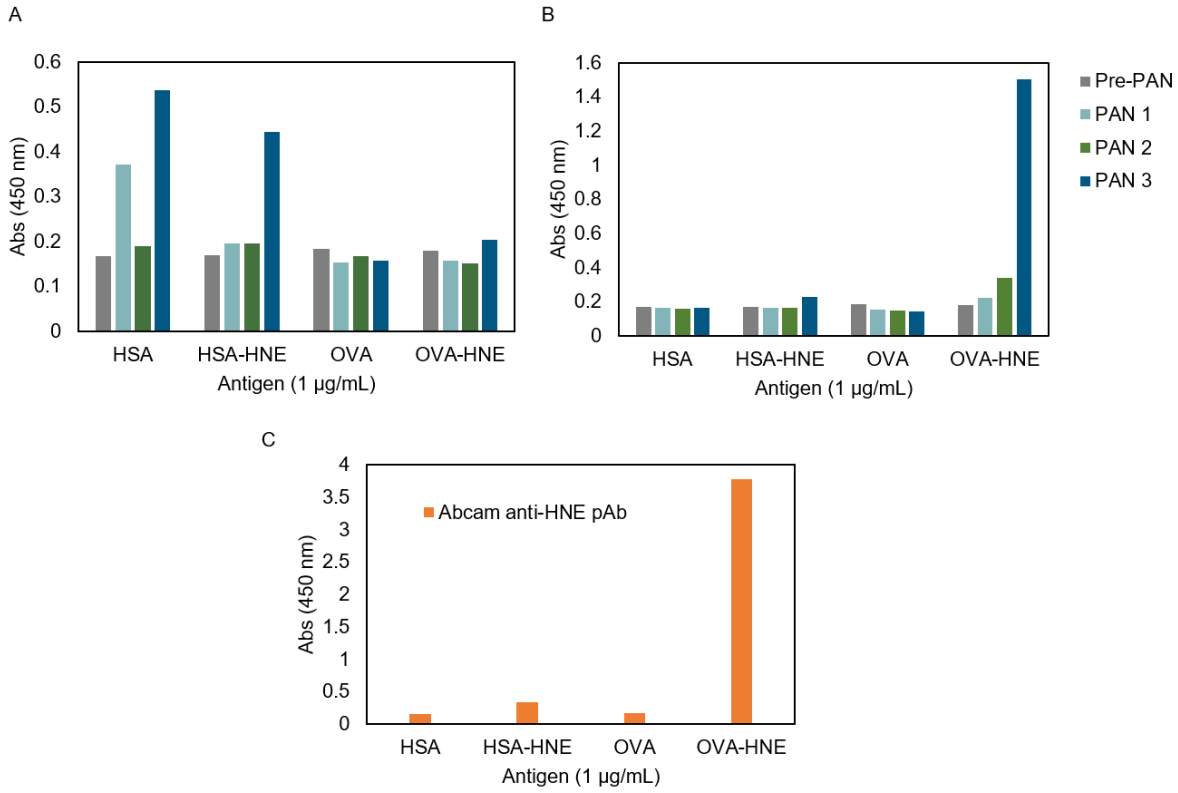

Figure V.22. Polyclonal ELISA assay depicting the enrichment of the scFv library performed against HSA-HNE (A) and OVA-HNE (B) after three rounds of selective biopanning. All the pooled phages collected before (Pre-PAN) and after panning (PAN 1, PAN 2 and PAN 3) were tested on 96-well plates coated with HSA, HSA-HNE, OVA and OVA-HNE at 1 µg/mL. As a control, the assay was as well performed with Abcam anti-HNE pAb at 0.5 µg/mL (C). The assay was performed once (n=1) with technical triplicates.

5.5. Chapter V Discussion, Conclusions and Future Work

In the work described in this chapter, two different antibody fragment libraries were generated for the first time against HNE lipoxidation adducts, by using RNA extracted from B cells of a sheep immunized with HNE-treated HSA. For the construction of both Fab and scFV libraries, the V_H and V_L genes were amplified using sheep specific primers previously designed by Professor Keith Charlton's group, and both the genes were cloned, according to the specific antibody format, into a bicistronic phagemid vector pSFD, as well designed by the same group. One of the most important features of this vector is the presence of the replication origins for both bacteria and bacteriophages, that allows the vector to be replicated in both bacteria and phage particles. Furthermore, this vector does also contain a DNA sequence encoding for the protein pIII, which is one of the five capsid proteins of a phage particle, to which an antibody can be expressed.

For the construction of the Fab vector, the insertion of heavy and light genes was done separately, in two steps, by generating first a large library with the vector containing just the

C_LV_L gene sequences, and later by inserting the heavy chain genes and generating the complete and final C_LV_L - C_HV_H library. The light chain gene was inserted first into the vector, in order to obtain the greatest diversity possible, as sheep IgG possess higher diversity in V_L loci (Berry & Popkov, 2015). The light chain insertion rate obtained was 79%, which is reasonable high; however, when inserting the heavy chain genes for generating the full Fab library, only 50% of the selected the clones appeared to have both the V_LC_L and V_HC_H genes in their genomic DNA. Therefore, from the final library of $2.4x10^8$ clones, only $1.2\ x10^8$ clones contained the complete Fab sequence, while the other $1.2\ x10^8$ clones were just background clones containing only the light chain fragment. This low insertion rate might be explained by the low efficiency of the restrictions enzymes used for the insertion of the genes, as in presence of salts and organic solvents, these enzymes might not reach their maximum activity or be led to cleave in non-specific sites. The DNA purification/washing protocols preformed before each restriction reaction were optimised to remove as much as possible of all the impurities from the PCR reactions; however, it is never easy to guarantee 100% removal. This limitation of the protocol could, however, be overcome in the future by the application of more modern cloning strategies, such as the so-called “seamless” cloning procedures. Both Gibson (Gibson et al., 2009) and Golden Gate (Engler, Kandzia, & Marillonnet, 2008) assembly methods, came to revolutionise the old school molecular engineering methods by allowing sequence-independent and scarless insertion of more than one fragment of DNA into a plasmid vector, at once. Therefore, the heavy and light gene sequences of an antibody could be inserted in a single step without the use of the traditional restriction enzymes, which would not only improve the insertion rate but also diminish the work load, time and resources spent in the generation of both light and light+heavy chain libraries. These seamless strategies were, not applied in this work mainly due to the non-compatibility of the available primers and also the lack of time for optimizing a new cloning system. However, companies like Antibody Design Laboratories™ are already employing these methods.

Although there is no work published regarding the generation of sheep Fab libraries to which we could compare our work with, methodologies for displaying Fab antibody fragments on the surface of phages using human, rabbit and mouse libraries have already been reported (Andris-Widhopf et al., 2011; Nelson & Valadon, 2017; Shen et al., 2007; Thu, Nguyen, Lee, & Shim, 2018). The use of sheep for development of mAbs is not so common within the academic community, as treatment and lodgement of these animals is considerably more complex and expensive than when using smaller animals, like mice. Consequently, a significantly larger amount of research has been done for the development and optimization of cloning and expression methods to be used in small/domestic animals rather than in sheep or goat. On the other hand, companies usually resort to bigger animals from which a larger serum volume can be collected, because they rely on polyclonal sera for the

development of their products; moreover, companies often patent their investigative work than publish it. A good example of a successful Fab library is the one used to select anti-HIV-1 mAbs from human, that had a diversity of $1x10^7$ clones, from which one of the most potent HIV-1 neutralising mAbs, the b12, was achieved (Zwick et al., 2003). In this work, unfortunately, the selection of specific anti-HSA-HNE Fabs was not as successful. In the first antibody panning strategy, where HSA-HNE was used as target, and competition with HSA was performed, phage enrichment after three rounds of panning was observed but the different clones selected for small-scale expression ended up by not presenting much DNA diversity nor specificity towards HSA or HSA-HNE. In fact, clone G10 was later fully expressed and by SDS-PAGE was found to be a single chain molecule, revealing that the formation of the disulphide bridges between the heavy and light chains was not accomplished. It is not clear why the expression of the Fab was not successfully accomplished, but folding problems in *E. coli* have been reported before (Levy, Weiss, Chen, Iverson, & Georgiou, 2001). The second selection approach performed for biopanning the library was based on the use of biotinylated HSA-HNE and magnetic streptavidin beads, which is a strategy typically applied to maximize the number of epitopes in the target antigen, as the antigens are freely in solution and do not suffer type of conformational changes (Teixeira & Gonzalez-Pajuelo, 2018). However, after three rounds of panning, the diversity gel from different colonies showed no sequence diversity and the expressed clones showed no specific binding towards HNE-modified proteins. The fact that both selection approaches failed to provide clones specific even to the carrier protein (HSA) suggests that the vast presence of background phages carrying the wrong size of insert did affect the selection of an anti-HNE specific clone.

Regarding the scFv library, its construction followed the protocol described by Palliyil *et al* (Palliyil, 2018), which relies on the cloning of the V_H and V_λ domains, linked together with a 15 amino acid peptide linker, into a slightly different version of the pSFD vector used previously for the generation of the Fab library (the vector map is depicted in **Appendix 15**). To the date, only Whitelam *et al* (1999) and Charlton *et al* (2001) reported the generation of sheep scFv libraries, with sizes of $4.23\ x10^6$ and $2.8\ x\ 10^7$ clones, respectively (K. Charlton, Harris, & Porter, 2001; Y. Li, Kilpatrick, & Whitelam, 2000), but the construction of scFv antibody libraries from other animals had been described before by the pioneers McCafferty *et al*. (1990), Barbas *et al*., (1991) and Clackson *et al*. (1991) (Barbas et al., 1991; Clackson, Hoogenboom, Griffiths, & WInter, 1991; McCafferty et al., 1990). However, no one has ever attempted the construction of antibody libraries for lipoxidised proteins, which makes this work a novelty. The herein described anti HSA-HNE scFv library presented a considerable large size ($>10^8$ clones) with all the clones, from a sample of 18 clones, expressing the expected size of insert, which was a great success.

The biopanning with immobilized HSA-HNE yielded a significant enrichment towards HSA, HSA-HNE and slightly to OVA-HNE after three rounds panning, but the biopanning with immobilized OVA-HNE seemed very promising, as the pooled phages only bound to HNE-modified proteins. When comparing the signals obtained for both HSA-HNE and OVA-HNE, there seems to be a greater affinity towards OVA-HNE; however, the number of HNE modifications on OVA was seen to be considerably higher than in HSA, which might justify the large difference. Due to time constrains, no further work was done with the enriched scFv library, but the positive enrichment achieved indicates promising clones could be present in the library.

One of the main bottlenecks of this work was, without any doubt, the extremely time-consuming biopanning protocol. When using immunotubes, for a full 3-round panning protocol, a minimum of 3-4 weeks is necessary to confirm the enrichment of the libraries, which limited the number of different panning strategies applied. In order to circumvent this issue, it would be interesting for the future to scale down the protocol and try panning the libraries on 96-microwell plates, where different concentration of antigens and different types of washes can be tested at the same time.

Despite the fact that no specific anti-HNE clones were found, the construction of Fab and scFv libraries is a novelty in the lipid oxidation field, opening the doors for the possibility of developing monoclonal antibody fragments specific to such lipid-protein adducts by phage display. However, the small molecular weight of the lipid oxidation products together with the instability of the adducts makes this work extremely challenging, as biopanning involves the selection of single clones out of millions of phage-displaying antibodies, by immobilisation of the adducts to a surface for several hours. Furthermore, depletion of antibodies specific to the native protein requires pre-incubation of the phages with competing antigens, which is very time consuming. Nonetheless, exploitation of new biopanning strategies could be valuable for the implementation of phage display technology in the development of high affinity antibodies to lipoxidation adducts.

CHAPTER VI

DISCUSSION AND CONCLUSIONS

6.1. Discussion

The consequence of the reactivity of certain lipid peroxidation products towards specific groups of proteins has received particular attention in 1976, when Esterbauer reports lipid peroxidation products such as 4-hydroxynonenal, acrolein and crotonaldehyde to bind to thiol groups of cysteine residues (H. Esterbauer, Ertl, & Scholz, 1976). At the time, it was known that lipid peroxidation yielded a variety of reactive carbonyl species, but the terminology of “lipoxidation products” only emerged years later, in 1996, when Requena *et al* suggested clustering this name for this type of protein-lipid adducts (Requena et al., 1996). Since then, several homologous families of reactive lipid peroxidation products have been identified and their mechanisms of reaction with proteins studied (Kumano-Kuramochi et al., 2012; Requena et al., 1996; Uchida, 2015; Vistoli et al., 2013), but their relationship with the development of chronic pathologies still remains a subject of considerable interest. Lipoxidation adducts have been found in neurodegenerative and inflammatory diseases, such as Alzheimer’s disease, Parkinson’s disease, atherosclerosis, ischemia reperfusion injury (Domingues et al., 2013; Jung, Kang, Lee, & Kim, 2018; McLeod & Sevanian, 1997; Sakamoto, Tsuyoshi Ohnishi, Ohnishi, & Ogawa, 1991), type 2 diabetes mellitus (Inouye, Mio, & Sumino, 1999; Jakus et al., 2000; Lyons & Jenkins, 1997), cancer (Guéraud, 2017; Martín-Sierra et al., 2019; Zhong & Yin, 2015) and cardiovascular diseases (Chavez, Wu, Bisson, & Maier, 2011; Gianazza, Brioschi, Fernandez, & Banfi, 2019; Wu & Stevens, Jan F.; Maier, 2011), which makes these products highly relevant as biomarkers for the diagnosis of oxidative stress related pathologies. HSA-HNE adducts, in particular, are of very great interest as a blood biomarker of oxidative stress, due to the abundance of HSA in blood. Therefore, the work described in this thesis was focussed on the generation of novel anti-HSA-HNE specific antibodies and characterisation of their epitopes. The aim was to build an in-depth understanding of the neo-antigens that result from HSA lipoxidation by HNE, and to reveal the way that the antibodies recognise these epitopes as the foundation on which to translate this important biomarker into the centre-piece of a rapid lipoxidation-based oxidative stress diagnostic test.

By high-resolution tandem MS, eleven HNE modifications were identified *in vitro* on HNE treated HSA standards, suggesting these adducts could, in fact, be used for immunising animals and generating specific polyclonal sera. Moreover, the chemical synthesis of HSA peptide sequences containing key nucleophilic amino acid residues and their treatment with HNE confirmed the reactivity of this aldehyde towards multiple amino acids. This also opened the possibility of generating polyclonal antibodies towards specific HNE adducts by using these synthetic HNE-modified sequences as synthetic immunogens. Analysis by MALDI-TOF MS, direct infusion ESI-MS and immunoassays performed with a commercial anti-HNE pAb also reinforced the results by confirming the formation of HNE adducts on

intact HNE-modified HSA. The data seem to also be in agreement with previous studies in which tandem MS approaches were applied to probe the location of HNE adducts on HSA (Aldini et al., 2006; Q. Liu et al., 2012).

The immunogenicity of different HNE-adducted structures was evaluated by immunisation of different animals, and the resulting antisera were characterised by ELISA. KLH conjugated HSA peptide ^{31}LQQC(HNE)PFE^{37}, containing the only free cysteine of HSA, did not yield any specific antibodies to the HNE structure, either in rabbits or sheep; however, from the immunisation of four sheep with intact HNE-modified HSA, antibodies capable of recognising HNE adducts on different molecules were found. Polyclonal antibodies of interest were partially purified and enriched from remaining antibodies of sheep sera using different affinity chromatography strategies and, after characterisation, were further tested for ELISA applications. However, in order to develop a rapid diagnostic assay with sufficient sensitivity and specificity for application to complex samples, extensive work is required not only in the development of antibodies, but also in the selection of a good antibody pair. Although several anti-HNE antibodies already exist commercially, both polyclonal and monoclonal, most of them were raised against HNE treated proteins and purified by affinity chromatography using different HNE modified proteins, which yields antibodies specific to general HNE adducts rather than specific to a single type of adduct or even a specific type of peptide/protein adduct. Moreover, the development and optimisation of a novel immunoassay requires large amounts of antibody, and therefore it is not practically or economically feasible to rely solely on commercial antibodies.

Since both Michael and Schiff's base adducts are reversible, reduced and non-reduced HSA-HNE adducts were used to immunise in four different sheep to assess the effect of their stability in the triggering of adaptive immune system. Curiously, the only sheep whose immune system responded to HSA-HNE adducts was sheep SA369 which was immunised with non-reduced adducts. No direct correlation could be made between the reduction/stabilisation of adducts and the recognition by B cells, yet the results obtained regarding sheep SA369 showed that non-reduced adducts appeared to be sufficiently stable to stimulate the production of antibodies capable of recognising the HNE moiety of the adducts. These antibodies, however, were shown to be cross-reactive to non-modified HSA, as the larger protein molecular weight also provides numerous molecular structures which can act as immunogenic epitopes for triggering a wide range of antibodies. To circumvent the cross-reactivity and in order to achieve a higher specific pool of polyclonal antibodies, immunisations with KLH conjugated ^{31}LQQC(HNE)PFE^{37} peptide were tested as well, but without any success. Since KLH is not found in mammals and is extremely large it is commonly used as an immune stimulant; however, due to the short length of the peptide and even smaller size of the HNE aldehyde on it, the response to KLH possibly ended up

by diverting the immune response toward its own more immunodominant epitopes, rather than the relatively non provocative adducts. However, over the course of the three immunisations, a small increment in the immune response to HNE modifications was observed, which could suggest more immunisations and time were needed to obtain a sufficient response. However, studies in the literature where synthetic peptides were used in the immunisation of rabbits have shown that 2 to 3 boosts are usually enough to get a substantial production of specific antibodies (Christodoulides, McGuinness, & Heckels, 1993; Ideno et al., 2013). A third immunisation strategy with HNE-treated KLH was tried (data not shown) but again the immune response towards HNE was very low, whereas very high to KLH, supporting the theory that steric hindrance effects might have occurred due to the small molecular weight of HNE compared to the size of KLH protein.

Different affinity chromatography strategies were applied in order to deplete anti-HSA clones from the SA369 pool of antibodies, but cross-reactivity persisted. Epitope characterisation studies with HSA peptide arrays showed that the enriched SA369 anti-HNE pAbs, were still recognising backbone sequences of the native protein, while also binding to the HNE moiety of the adducts, which suggested that the cross-reactivity towards non-modified HSA was inherent to the antibodies and could not be eliminated by downstream processing techniques. It is probable that the epitopes consisted of the adduct as well as some of the neighbouring polypeptide backbone.

Hence, in attempt to eliminate the cross-reactivity observed with the pAbs and work with antibodies that are unique to HSA-HNE and/or HNE, monoclonal antibody fragments were generated, through the construction of Fab and scFV libraries, using RNA extracted from B cells from sheep SA369. Although the Fab library contained a large number of clones (10^7), it was found that only 50% of the clones were carrying the correct size of the insert, which made further enrichment of the library towards HNE-modified antigens very difficult. None of the expressed Fabs was shown to be specific to HNE or HSA, which implied that the library carried too many background clones preventing the selection of the (relatively rare) correct ones. The scFv library constructed, on the other hand, was shown to be of a very large size (10^8), as all the clones in it (from a random selection of 17 clones) were found to be carrying the correct size of fragment. However, there was not enough time to proceed with the expression of scFV clones. Even so, the panning strategies looked promising, suggesting that phage display technology could be successfully applied for the development of lipoxidation-specific antibodies, something that has not previously been attempted. For commercial application, phage display is possibly one of the major approaches employed in the discovery of specific antibodies, stated to be used for enrichment and identification of antibodies with high affinity and specificity from immunised libraries (Bruin, Spelt, Mol, Koes, & Quattrocchio, 1999).

Notwithstanding that limitation, the in-house enriched SA369 pAb was deployed in a lateral flow assay, together with a commercial anti-HNE pAb – as an LFA always requires one antibody for capture and another one for detection – for the detection of HNE adducts on different proteins. Although not tested with biological samples, the assay was capable of detecting HNE adducts on *in vitro* HNE treated solutions of HSA, KLH and OVA, with a sensitivity as low as 1.50 μg/mL, and shown to be capable of displaying different test line intensities for different HNE:protein molar ratios.

For many years, scientists have used the "gold standard methods" of HPLC and GC-MS for studying lipid peroxidation products, but one of the biggest challenges in oxidative research has always been the development of accurate and non-invasive methods for the *in vivo* evaluation of redox status. A rapid multiplex test in which several different lipoxidation biomarkers are detected within a few minutes, by simple application of a single drop of blood, would not only be valuable to guide clinical therapeutics but also in the monitoring of the effectiveness of therapies. In patients with obstructive sleep apnoea, for instance, where hypoxic events were seen to initiate oxidative stress and the formation of lipid peroxidation products has been confirmed, the monitoring of the formation of different lipoxidation products might be extremely valuable to prevent exacerbated cell damage, and consequently, diminish the rate of cardiovascular diseases events and hypertension (Lavie, 2003).

The small size of lipid oxidation products is what makes their detection so challenging, especially when regarding the generation of antibodies. Haptens (molecular weight below 1000 Da) are considered to be invisible to the host immune system unless presented conjugated to carrier proteins, which made the generation of antibodies specific to HNE adducts on HSA (without cross-reacting to the native protein) very challenging. Khan *et al* reported the development of anti-HSA-HNE antibodies by HSA-HNE immunising rabbits, yet, the group states the antibodies were simply purified from the animal sera by using a protein A agarose column, which is just specific to the whole IgG fraction of antibodies (Khan et al., 2016) and not specifically to the anti-immunogen injected.

Immunisation of less frequently used animals such as camelids (llamas, alpacas, dromedaries) or shark, in which immune system only produces heavy-chain antibodies present a possible alternative approach for development of high quality antibodies, as the V_H domains from these animals can (depending on the antigen) present higher affinity and, as a general rule these structures have a good thermostability, good solubility and ease of being genetically engineered (Arbabi-Ghahroudi, 2017). Genetic studies on camelid heavy chain antibodies reported that antibody diversification in these animals relies on gene recombination mechanisms that involve a larger number of unique V_H gene segments recombining with D_H and J_H genes and possibly with additional non-templated nucleotide

insertions leading to longer CDR3 loops (Deschacht et al., 2010). Moreover, involvement of FR2 residues in the antigen binding and in structuring the CD3 loop were reported (Klarenbeek et al., 2015), suggesting the V_H paratopes in these animals acquire more structural complexity, possibly to compensate the lack of V_L domains.

Regarding the prototype LFA, *per se*, in the future it should be refined and tested with biological matrices, such as whole blood or sera, in order to evaluate the behaviour of the assay the presence of such complex biological matrices. The enhancement of the colorimetric response of the strips would probably be required for quantification purposes, which could be achieved by exploring new strategies, such as the inclusion of other materials in the nitrocellulose membrane. A recent study reported the use of nanofibers in the test line can boost the sensitivity of the assay by 40% (Quesada-González et al., 2019).

In conclusion, the studies described in this thesis have helped understanding how lipoxidation adducts act as oxidation-specific epitopes to trigger the immune system to generate antibodies, as exemplified by the generation and characterization of the novel anti-HSA-HNE polyclonal antibodies. The work has also helped in opening the doors to the point-of-care diagnostic market to the oxidative stress/lipoxidation field of research, by demonstrating that antibodies specific to lipid oxidation products, or even to lipoxidation adducts, (as is the case of the SA369 in-house antibody), can be functional in lateral flow assays. Further research on the nature of the neo-antigen epitopes is likely to reveal complex and informative epitopes that provide information not only about the fact that lipoxidation occurred, but also about which proteins or regions of proteins were subject to lipoxidation. A better understanding of how lipoxidation epitopes influence the anti-inflammatory responses and act in the maintenance of redox homeostasis is still very much needed.

CHAPTER VII

REFERENCES

Abbas, A. K., Lichtman, A. H., & Pillai, S. (2007). *Cellular and Molecular Immunology* (6th Editio).

Aćimović, J. M., Jovanović, V. B., Srećković, V. D., Penezić Romanjuk, A. Z., & Mandić, L. M. (2013). Monitoring of the human serum albumin carbonylation level through determination of guanidino group content. *Analytical Biochemistry*, *433*(2), 162–167. https://doi.org/10.1016/j.ab.2012.10.028

Aebersold, R., & Domon, B. (2006). Mass Spectrometry and Protein Analysis. *Science*, *312*(April), 212–217.

Aebersold, R., & Mann, M. (2003). Mass spectrometry-based proteomics. *Nature*, *422*(March).

Afonso, C. B., & Spickett, C. M. (2018). Lipoproteins as targets and markers of lipoxidation. *Redox Biology*, (October), 101066. https://doi.org/10.1016/j.redox.2018.101066

Ahmed, N., Dobler, D., Dean, M., & Thornalley, P. J. (2005). Peptide mapping identifies hotspot site of modification in human serum albumin by methylglyoxal involved in ligand binding and esterase activity. *Journal of Biological Chemistry*, *280*(7), 5724–5732. https://doi.org/10.1074/jbc.M410973200

Aldini, G., Gamberoni, L., Orioli, M., Beretta, G., Regazzoni, L., Facino, R. M., & Carini, M. (2006). Mass spectrometric characterization of covalent modification of human serum albumin by 4-hydroxy-trans-2-nonenal. *Journal of Mass Spectrometry : JMS*, *43*(7), 854–864. https://doi.org/10.1002/jms

Aldini, G., Regazzoni, L., Orioli, M., Rimoldi, I., Facino, R. M., & Carini, M. (2008). A tandem MS precursor-ion scan approach to identify variable covalent modification of albumin Cys34: a new tool for studying vascular carbonylation. *Journal of Mass Spectrometry : JMS*, *43*(7), 854–864. https://doi.org/10.1002/jms.1419 A

Aldini, G., Rosário Domingues, M., Spickett, C. M., Domingues, P., Altomare, A., Sánchez-Gómez, F. J., … Pérez-Sala, D. (2015). Protein lipoxidation: Detection strategies and challenges. *Redox Biology*, *5*, 253–266. https://doi.org/10.1016/j.redox.2015.05.003

Aldini, G., Vistoli, G., Regazzoni, L., Gamberoni, L., Facino, R. M., Yamaguchi, S., … Carini, M. (2008). Albumin is the main nucleophilic target of human plasma: A protective role against pro-atherogenic electrophilic reactive carbonyl species? *Chemical Research in Toxicology*, *21*(4), 824–835. https://doi.org/10.1021/tx700349r

Andris-Widhopf, J., Steinberger, P., Fuller, R., Rader, C., Barbas, C. F., & Iii, C. F. B. (2011). Generation of human Fab antibody libraries: PCR amplification and assembly of light- and heavy-chain coding sequences. *Cold Spring Harbor Protocols*, *6*(9), 1151–1165. https://doi.org/10.1101/pdb.prot065565

Anfossi, L., Di Nardo, F., Cavalera, S., Giovannoli, C., & Baggiani, C. (2018). Multiplex lateral flow immunoassay: An overview of strategies towards high-throughput point-of-need testing. *Biosensors*, *9*(1). https://doi.org/10.3390/bios9010002

Anfossi, L., Di Nardo, F., Russo, A., Cavalera, S., Giovannoli, C., Spano, G., … Baggiani, C. (2019). Silver and gold nanoparticles as multi-chromatic lateral flow assay probes for the detection of food allergens. *Analytical and Bioanalytical Chemistry*, *411*(9), 1905–1913. https://doi.org/10.1007/s00216-018-1451-6

Anguizola, J., Matsuda, R., Barnaby, O. S., Hoy, K. S., Wa, C., DeBolt, E., … Hage, D. S. (2013). Review: Glycation of human serum albumin. *Clinica Chimica Acta*, *425*, 64–76. https://doi.org/10.1016/j.cca.2013.07.013

Annibal, A., Colombo, G., Milzani, A., Dalle-Donne, I., Fedorova, M., & Hoffmann, R.

(2016). Identification of dityrosine cross-linked sites in oxidized human serum albumin. *Journal of Chromatography B: Analytical Technologies in the Biomedical and Life Sciences*, *1019*, 147–155. https://doi.org/10.1016/j.jchromb.2015.12.022

Anraku, M., Chuang, V. T. G., Maruyama, T., & Otagiri, M. (2013). Redox properties of serum albumin. *Biochimica et Biophysica Acta*, *1830*(12), 5465–5472. https://doi.org/10.1016/j.bbagen.2013.04.036

Arbabi-Ghahroudi, M. (2017). Camelid single-domain antibodies: Historical perspective and future outlook. *Frontiers in Immunology*, *8*(NOV), 1–8. https://doi.org/10.3389/fimmu.2017.01589

Aruoma, O. (1998). Free Radicals, Oxidative Stress, and Antioxidants in Human Health and Disease. *Journal of the Siena Academy of Sciences*, *75*(2), 199–212.

Ayala, A., Munoz, M. F., Arguelles, S., Muñoz, M. F., Argüelles, S., Munoz, M. F., & Arguelles, S. (2014). Lipid peroxidation: Production, metabolism, and signaling mechanisms of malondialdehyde and 4-hydroxy-2-nonenal. *Oxidative Medicine and Cellular Longevity*, *2014*. https://doi.org/10.1155/2014/360438

Bailes, J., Mayoss, S., Teale, P., & Soloviev, M. (2012). Gold Nanoparticle Antibody Conjugates for Use in Competitive Lateral Flow Assays. In *Nanoparticles in Biology and Medicine* (Vol. 906). https://doi.org/10.1007/978-1-61779-953-2

Baird, C. L., Fischer, C. J., Pefaur, N. B., Miller, K. D., Kagan, J., Srivastava, S., & Rodland, K. D. (2009). Developing recombinant antibodies for biomarker detection. *Cancer Biomarkers*, *6*(5–6), 271–279. https://doi.org/10.3233/CBM-2009-0144

Baraibar, M. A., & Friguet, B. (2013). Oxidative proteome modifications target specific cellular pathways during oxidative stress, cellular senescence and aging. *EXG*, *48*(7), 620–625. https://doi.org/10.1016/j.exger.2012.10.007

Barbas, C. F., Kang, A. S., Lerner, R. A., & Benkovic, S. J. (1991). Assembly of combinatorial antibody libraries on phage surfaces: the gene III site. *Proceedings of the National Academy of Sciences*, *88*(18), 7978–7982. https://doi.org/10.1073/pnas.88.18.7978

Barrera, G., Pizzimenti, S., Ciamporcero, E. S., Daga, M., Ullio, C., Arcaro, A., … Gentile, F. (2014). Role of 4-Hydroxynonenal-Protein Adducts in Human Diseases. *Antioxidants & Redox Signaling*, *22*(18), 150127063122000–150127063122000. https://doi.org/10.1089/ars.2014.6166

Baynes, J. W., & Thorpe, S. R. (1996). The role of oxidative stress in diabetic complications. *Current Opinion in Endocrinology and Diabetes*, *3*(4), 277–284. https://doi.org/10.1097/00060793-199608000-00001

Baynes, J. W., & Thorpe, S. R. (2000). Glycoxidation and lipoxidation in atherogenesis, *28*(12), 1708–1716.

Behrendt, R., White, P., & Offer, J. (2016). Advances in Fmoc solid-phase peptide synthesis. *Journal of Peptide Science*, *22*(1), 4–27. https://doi.org/10.1002/psc.2836

Benedetti, A., Comporti, M., & Esterbauer, H. (1980). Identification of 4-hydroxynonenal as a cytotoxic product originating from the peroxidation of liver mircrosomal lipids. *Biochimica et Biophysica Acta*, *620*, 281–296. Retrieved from http://weekly.cnbnews.com/news/article.html?no=124000

Bengmark, S. (2007). Advanced Glycation and Lipoxidation End Products-Amplifiers of Inflammation: The Role of Food. *Journal of Parenteral and Enteral Nutrition*, *31*(5), 430–440. https://doi.org/10.1177/0148607107031005430

Benjamin, D. C., Berzo, J. A., Sk, !, East3, J., Gurd4, F. R. N., Hannum5, C., … Wilsonl, A. C. (1984). The Antigenic Structure of Proteins: a Reappraisal. *Ann. Rev. Immuno{*,

2, 67–101.

Berli, C. L. A., & Kler, P. A. (2016). A quantitative model for lateral flow assays. *Microfluidics and Nanofluidics*, *20*(7). https://doi.org/10.1007/s10404-016-1771-9

Berry, J. D., & Popkov, M. (2015). Antibody libraries from immunized repertoires. *Phage Display in Biotechnology and Drug Discovery, Second Edition*, (June), 373–453. https://doi.org/10.1201/b18196

Binder, C. J., Papac-Milicevic, N., & Witztum, J. L. (2016). Innate sensing of oxidation-specific epitopes in health and disease. *Nature Reviews Immunology*. https://doi.org/10.1038/nri.2016.63

Birben, E., Murat, U., Md, S., Sackesen, C., Erzurum, S., & Kalayci, O. (2012). Oxidative Stress and Antioxidant Defense. *WAO Journal*, *5*(January), 9–19. https://doi.org/10.1097/WOX.0b013e3182439613

Boisvert, M. R., Koski, K. G., & Skinner, C. D. (2010). Increased oxidative modifications of amniotic fluid albumin in pregnancies associated with gestational diabetes mellitus. *Analytical Chemistry*, *82*(3), 1133–1137. https://doi.org/10.1021/ac902322w

Bollineni, R. C., Hoffmann, R., & Fedorova, M. (2011). Identification of protein carbonylation sites by two-dimensional liquid chromatography in combination with MALDI- and ESI-MS. *Journal of Proteomics*, *74*(11), 2338–2350. https://doi.org/10.1016/j.jprot.2011.07.002

Borovic, S., Rabuzin, F., Waeg, G., & Zarkovic, N. (2006). Enzyme-linked immunosorbent assay for 4-hydroxynonenal-histidine conjugates. *Free Radical Research*, *40*(8), 809–820. https://doi.org/10.1080/10715760600693422

Brien, P. M. O., Aitken, R., Chames, P., Hoogenboom, H. R., & Henderikx, P. (2002). *Antibody Phage Display Methods and Protocols*. (J. M. Walker, Ed.) (Vol. 178). Humana Press. https://doi.org/10.1542/neo.17-4-e203

Bruin, R. de, Spelt, K., Mol, J., Koes, R., & Quattrocchio, F. (1999). Selection of high-affinity phage antibodies from phage display libraries Successful screening of phage display libraries will lead to more efficient ,. *Nature Biotechnology*, *17*, 397–399.

Burdon, R. H., & van Knippenberg, P. H. (1988). Immunization with peptides. In *Laboratory Techniques in Biochemistry and Molecular Biology* (Vol. 19, pp. 131–144). https://doi.org/10.1016/S0075-7535(08)70008-1

Castro, J. P., Jung, T., Grune, T., & Siems, W. (2017). 4-Hydroxynonenal (HNE) modified proteins in metabolic diseases. *Free Radical Biology and Medicine*, *111*(October), 309–315. https://doi.org/10.1016/j.freeradbiomed.2016.10.497

Chapple, S. J., Cheng, X., & Mann, G. E. (2013). Effects of 4-hydroxynonenal on vascular endothelial and smooth muscle cell redox signaling and function in health and disease. *Redox Biology*, *1*(1), 319–331. https://doi.org/10.1016/j.redox.2013.04.001

Charlton, K. A., Moyle, S., Porter, A. J. R., Harris, W. J., Charlton, K. A., Moyle, S., … Harris, W. J. (2018). Analysis of the Diversity of a Sheep Antibody Repertoire as Revealed from a Bacteriophage Display Library. https://doi.org/10.4049/jimmunol.164.12.6221

Charlton, K., Harris, W. J., & Porter, A. J. (2001). The isolation of super-sensitive anti-hapten antibodies from combinatorial antibody libraries derived from sheep, *16*, 639–646.

Chavakis, T., Bierhaus, A., & Nawroth, P. P. (2004). RAGE (receptor for advanced glycation end products): A central player in the inflammatory response. *Microbes and Infection*, *6*(13), 1219–1225. https://doi.org/10.1016/j.micinf.2004.08.004

Chavez, J. D., Wu, J., Bisson, W., & Maier, C. S. (2011). Site-specific proteomic analysis of lipoxidation adducts in cardiac mitochondria reveals chemical diversity of 2-alkenal adduction. *Journal of Proteomics*, *74*(11), 2417–2429. https://doi.org/10.1016/j.jprot.2011.03.031

Chen, G., & Sidhu, S. S. (2014). Design and Generation of Synthetic Antibody Libraries for Phage Display. In V. Ossipow & N. Fischer (Eds.), *Monoclonal Antibodies: Methods and Protocols, Methods in Molecular Biology* (Vol. 1131, pp. 71–95). New York: Springer Science. https://doi.org/10.1016/B978-0-444-63660-7.00004-8

Chen, M., Yu, Z., Liu, D., Peng, T., Liu, K., Wang, S., … Lai, W. (2015). Dual gold nanoparticle lateflow immunoassay for sensitive detection of Escherichia coli O157:H7. *Analytica Chimica Acta*, *876*, 71–76. https://doi.org/10.1016/j.aca.2015.03.023

Christodoulides, M., McGuinness, B. T., & Heckels, J. E. (1993). Immunization with synthetic peptides containing epitopes of the class 1 outer-membrane protein of Neisseria meningitidis: Production of bactericidal antibodies on immunization with a cyclic peptide. *Journal of General Microbiology*, *139*(8), 1729–1738. https://doi.org/10.1099/00221287-139-8-1729

Christopher, P., Robinson, N., & Shaw, M. K. (2007). Antibody-Label Conjugates in Lateral-Flow Assays. *Drugs of Abuse*, 87–98. https://doi.org/10.1007/978-1-59259-951-6_5

Clackson, T., Hoogenboom, H. R. ., Griffiths, A. D. ., & WInter, G. (1991). Making antibody fragments using phage display libraries. *Nature*, *352*.

Corstjens, P., Zuiderwijk, M., Brink, A., Li, S., Feindt, H., Niedbala, R. S., & Tanke, H. T. (2001). Use of up-converting phosphor reporters in lateral-flow assays to detect specific nucleic acid sequences: A rapid, sensitive DNA test to identify human papillomavirus type 16 infection. *Clinical Chemistry*, *47*(10), 1885–1893.

Csala, M., Kardon, T., Legeza, B., Lizák, B., Mandl, J., Margittai, É., … Bánhegyi, G. (2015). On the role of 4-hydroxynonenal in health and disease. *Biochimica et Biophysica Acta - Molecular Basis of Disease*, *1852*(5), 826–838. https://doi.org/10.1016/j.bbadis.2015.01.015

Cvak, B., Pum, D., Molinelli, A., & Krska, R. (2012). Synthesis and characterization of colloidal gold particles as labels for antibodies as used in lateral flow devices. *Analyst*, *137*(8), 1882–1887. https://doi.org/10.1039/c2an16108g

D'souza, A., Kurien, B. T., Rodgers, R., Shenoi, J., Kurono, S., Matsumoto, H., … Scofield, R. H. (2008). Detection of Catalase as a major protein target of the lipid peroxidation product 4-HNE and the lack of its genetic association as a risk factor in SLE. *BMC Medical Genetics*, *9*, 1–8. https://doi.org/10.1186/1471-2350-9-62

Dahlgren, C., & Karlsson, A. (1999). Respiratory burst in human neutrophils. *Journal of Immunological Methods*, *232*(1–2), 3–14. https://doi.org/10.1016/S0022-1759(99)00146-5

Davies, J., & Riechmann, L. (1996). Single antibody domains as small recognition units: design and in vitro antigen selection of camelized, human VH domains with improved protein stability. *Protein Engineering*, *9*(6), 531–537. https://doi.org/10.1093/protein/9.6.531

Deen, A. J., Sihvola, V., Härkönen, J., Patinen, T., Adinolfi, S., & Levonen, A. L. (2018). Regulation of stress signaling pathways by nitro-fatty acids. *Nitric Oxide - Biology and Chemistry*. https://doi.org/10.1016/j.niox.2018.03.012

Deschacht, N., De Groeve, K., Vincke, C., Raes, G., De Baetselier, P., & Muyldermans, S. (2010). A Novel Promiscuous Class of Camelid Single-Domain Antibody Contributes

to the Antigen-Binding Repertoire. *The Journal of Immunology*, *184*(10), 5696–5704. https://doi.org/10.4049/jimmunol.0903722

Domingues, R. M., Domingues, P., Melo, T., Pérez-Sala, D., Reis, A., & Spickett, C. M. (2013). Lipoxidation adducts with peptides and proteins: Deleterious modifications or signaling mechanisms? *Journal of Proteomics*. https://doi.org/10.1016/j.jprot.2013.06.004

Dröge, W. (2002). Free radicals in the physiological control of cell function. *Physiological Reviews*, *82*(1), 47–95. https://doi.org/10.1152/physrev.00018.2001

du Plessis, D. H., & Jordaan, F. (1996). *Phage Display of Peptides and Proteins*. (B. K. Kay, J. WInter, & J. McCafferty, Eds.), *Phage Display of Peptides and Proteins*. Academic Press. https://doi.org/10.1016/B978-012402380-2/50011-3

EMD Merk Millipore. (2013). Rapid Lateral Flow Test Strips: Considerations for Product Development.

Engler, C., Kandzia, R., & Marillonnet, S. (2008). A one pot, one step, precision cloning method with high throughput capability. *PLoS ONE*, *3*(11). https://doi.org/10.1371/journal.pone.0003647

Era, S., Kuwata, K., Imai, H., Hayashi, T., & Masaru, S. (1995). Age-related change in redox state of human serum albumin. *Biochimica et Biophysica Acta*, *1247*, 12–16.

Esterbauer, H., Ertl, A., & Scholz, N. (1976). The reaction of cysteine with α,β-unsaturated aldehydes. *Tetrahedron*, *32*(2), 285–289. https://doi.org/10.1016/0040-4020(76)87015-9

Esterbauer, Hermann, Schaur, R. J., & Zollner, H. (1991). Chemistry and biochemistry of 4-hydroxynonenal, malonaldehyde and related aldehydes. *Free Radical Biology and Medicine*, *11*(1), 81–128. https://doi.org/10.1016/0891-5849(91)90192-6

Fanali, G., Di Masi, A., Trezza, V., Marino, M., Fasano, M., & Ascenzi, P. (2012). Human serum albumin: From bench to bedside. *Molecular Aspects of Medicine*, *33*(3), 209–290. https://doi.org/10.1016/j.mam.2011.12.002

Fernández-Sánchez, C., McNeil, C. J., Rawson, K., Nilsson, O., Leung, H. Y., & Gnanapragasam, V. (2005). One-step immunostrip test for the simultaneous detection of free and total prostate specific antigen in serum. *Journal of Immunological Methods*, *307*(1–2), 1–12. https://doi.org/10.1016/j.jim.2005.08.014

Foell, D., Wittkowski, H., & Roth, J. (2007). Mechanisms of Disease: A “DAMP” view of inflammatory arthritis. *Nature Clinical Practice Rheumatology*, *3*(7), 382–390. https://doi.org/10.1038/ncprheum0531

Forsström, B., Axnäs, B. B., Stengele, K.-P., Bühler, J., Albert, T. J., Richmond, T. A., … Uhlen, M. (2014). Proteome-wide Epitope Mapping of Antibodies Using Ultra-dense Peptide Arrays. *Molecular & Cellular Proteomics*, *13*(6), 1585–1597. https://doi.org/10.1074/mcp.M113.033308

Gianazza, E., Brioschi, M., Fernandez, A. M., & Banfi, C. (2019). Lipoxidation in cardiovascular diseases. *Redox Biology*, (January). https://doi.org/10.1016/j.redox.2019.101119

Gibson, D. G., Young, L., Chuang, R., Venter, J. C., Iii, C. A. H., & Smith, H. O. (2009). Enzymatic assembly of DNA molecules up to several hundred kilobases, (May). https://doi.org/10.1038/nmeth.1318

Grönwall, C., Clancy, R. M., Getu, L., Lloyd, K. A., Siegel, D. L., Reed, J. H., … Silverman, G. J. (2016). Modulation of natural IgM autoantibodies to oxidative stress-related neo-epitopes on apoptotic cells in newborns of mothers with anti-Ro autoimmunity. *Journal of Autoimmunity*, *73*, 30–41.

https://doi.org/10.1016/j.jaut.2016.05.014

Grune, T., Michel, P., Sitte, N., Eggert, W., Albrecht-Nebe, H., Esterbauer, H., & Siems, W. G. (1997). Increased levels of 4-hydroxynonenal modified proteins in plasma of children with autoimmune diseases. *Free Radical Biology and Medicine*, *23*(3), 357–360. https://doi.org/10.1016/S0891-5849(96)00586-2

Guéraud, F. (2017). 4-Hydroxynonenal metabolites and adducts in pre-carcinogenic conditions and cancer. *Free Radical Biology and Medicine*, *111*(December 2016), 196–208. https://doi.org/10.1016/j.freeradbiomed.2016.12.025

Gundry, R. L., Fu, Q., Jelinek, C. A., Van Eyk, J. E., & Cotter, R. J. (2007). Investigation of an albumin-enriched fraction of human serum and its albuminome. *Proteomics - Clinical Applications*, *1*(1), 73–88. https://doi.org/10.1002/prca.200600276

Haberland, M. E., Fong, D., & Cheng, L. (1988). Malondialdehyde-altered protein occurs in atheroma of Watanabe heritable hyperlipidemic rabbits. *Science (New York, N.Y.)*, *241*(4862), 215–218. https://doi.org/10.1126/science.2455346

Halliwell, B., & Gutteridge, J. M. C. (2015). *Free Radicals in Biology and Medicine*. (B. Halliwell & J. M. C. Gutteridge, Eds.) (Fifth Edit). Oxford Press University.

Harlow, E., & Lane, D. (1988). *Antibodies: A Laboratory Manual*. (E. Harlow & D. Lane, Eds.). Cold Spring Harbor Laboratory.

Hartley, D. P., Kroll, D. J., & Petersen, D. R. (1997). Prooxidant-Initiated Lipid Peroxidation in Isolated Rat Hepatocytes : Detection of 4-Hydroxynonenal- and Malondialdehyde-Protein Adducts, (96), 895–905.

Heesters, B. A., Myers, R. C., & Carroll, M. C. (2014). Follicular dendritic cells: Dynamic antigen libraries. *Nature Reviews Immunology*, *14*(7), 495–504. https://doi.org/10.1038/nri3689

Hermeling, S., Crommelin, D. J. A., Schellekens, H., & Jiskoot, W. (2004). Structure-Immunogenicity Relationships of Therapeutic Proteins, *21*(6).

Hilpert, K., Winkler, D. F. H., & Hancock, R. E. W. (2007). Peptide arrays on cellulose support: SPOT synthesis, a time and cost efficient method for synthesis of large numbers of peptides in a parallel and addressable fashion. *Nature Protocols*, *2*(6), 1333–1349. https://doi.org/10.1038/nprot.2007.160

Hofmann, M. A., Drury, S., Fu, C., Qu, W., Taguchi, A., Lu, Y., … Schmidt, A. M. (1999). RAGE Mediates a Novel Proinflammatory Axis: A Central Cell Surface Receptor for S100/Calgranulin Polypeptides. *Cell*, *97*, 889–901.

Höhn, A., König, J., & Grune, T. (2013). Protein oxidation in aging and the removal of oxidized proteins. *Journal of Proteomics*, *92*, 132–159. https://doi.org/10.1016/j.jprot.2013.01.004

Holliger, P., Prospero, T., & Winter, G. (2006). “Diabodies”: small bivalent and bispecific antibody fragments. *Proceedings of the National Academy of Sciences*, *90*(14), 6444–6448. https://doi.org/10.1073/pnas.90.14.6444

Holt, L. J., Enever, C., Wildt, R. M. T. De, & Tomlinson, I. M. (2000). The use of recombinant antibodies in proteomics, 445–449.

Hori, O., Brett, J., Slattery, T., Cao, R., Zhang, J., Chen, J. X., … Schmid, A. M. (1995). The receptor for advanced glycation end products (RAGE) is a cellular binding site for amphoterin. *Journal of Biological Chemistry*, *270*(43), 25752–25761. https://doi.org/10.1074/jbc.270.43.25752

Hörkkö, S., Palinski, W., Witztum, J. L., Hörkkö, S., Bird, D. A., Miller, E., … Witztum, J. L. (1999). Monoclonal autoantibodies specific for oxidized phospholipids or oxidized

phospholipid – protein adducts inhibit macrophage uptake of oxidized low-density lipoproteins. *The Journal of Clinical Investigation*, *103*, 117–128.

Hsieh, H. V, Dantzler, J. L., & Weigl, B. H. (2017). Analytical Tools to Improve Optimization Procedures for Lateral Flow Assays. *Diagnostics*, *7*(2), 29. https://doi.org/10.3390/diagnostics7020029

Huang, W.-C., Wu, K.-H., Hung, H.-C., Wang, J.-C., & Chang, S.-C. (2018). Magnetic Nanoparticle-Based Lateral Flow Immunochromatographic Strip as a Reporter for Rapid Detection of Melamine. *Journal of Nanoscience and Nanotechnology*, *18*(10), 7190–7196. https://doi.org/10.1166/jnn.2018.16020

Hust, M., & Lim, T. S. (Eds.). (2002). *Phage Display: Methods and Protocols.* (Vol. 178). Humana Press. https://doi.org/10.1007/978-1-4939-7447-4

Ideno, S., Sakai, K., Yunoki, M., Kubota-Koketsu, R., Inoue, Y., Nakamura, S., … Ikuta, K. (2013). Immunization of rabbits with synthetic peptides derived from a highly conserved β-sheet epitope region underneath the receptor binding site of influenza A virus. *Biologics: Targets and Therapy*, *7*(1), 233–241. https://doi.org/10.2147/BTT.S50870

Imai Senzo, M., Yoshiko Kouda, T., Toru Nishihara, K., & Masahiko Kinoshita, S. (1993). *5,266,497*. Japan.

Inouye, M., Mio, T., & Sumino, K. (1999). Link between glycation and lipoxidation in red blood cells in diabetes. *Clinica Chimica Acta*, *285*(1–2), 35–44. https://doi.org/10.1016/S0009-8981(99)00065-0

Jakus, V., Bauerova, K., Michalkova, D., & Carsky, J. (2000). Values of markers of early and advanced glycation and lipoxidation in serum proteins of children with diabetes mellitus. *Bratisl Lek Listy*, *101*(9), 484–489.

Jazayeri, M. H., Amani, H., Pourfatollah, A. A., Pazoki-Toroudi, H., & Sedighimoghaddam, B. (2016). Various methods of gold nanoparticles (GNPs) conjugation to antibodies. *Sensing and Bio-Sensing Research*, *9*, 17–22. https://doi.org/10.1016/j.sbsr.2016.04.002

Jenne, C. N., Kennedy, L. J., & Reynolds, J. D. (2006). Antibody repertoire development in the sheep. *Developmental and Comparative Immunology*, *30*(1–2), 165–174. https://doi.org/10.1016/j.dci.2005.06.009

Jung, G. B., Kang, S. W., Lee, G. J., & Kim, D. (2018). Biochemical Characterization of the Brain Hippocampal Areas after Cerebral Ischemia-Reperfusion Using Raman Spectroscopy. *Applied Spectroscopy*, *72*(10), 1479–1486. https://doi.org/10.1177/0003702818776627

Jurgens, G., Ashy, A., & Esterbauer, H. (1990). Detection of new epitopes formed upon oxidation of low-density lipoprotein , lipoprotein (a) and very-low-density lipoprotein. *Biochemical Journal*, *265*, 605–608.

Just, J., Jung, T., Friis, N. A., Lykkemark, S., Drasbek, K., Siboska, G., … Kristensen, P. (2015). Identification of an unstable 4-hydroxynoneal modification on the 20S proteasome subunit α7 by recombinant antibody technology. *Free Radical Biology and Medicine*, *89*, 786–792. https://doi.org/10.1016/j.freeradbiomed.2015.10.405

Kaneko, K., Kimata, T., Tsuji, S., Ohashi, A., Imai, Y., Sudo, H., & Kitamura, N. (1970). Measurement of urinary 8-oxo-7,8-dihydro-2-deoxyguanosine in a novel point-of-care testing device to assess oxidative stress in children. *Clinica Chimica Acta*, *413*(23–24), 1822–1826. https://doi.org/10.1016/j.cca.2012.07.009

Kansanen, E., Kuosmanen, S. M., Leinonen, H., & Levonenn, A. L. (2013). The Keap1-Nrf2 pathway: Mechanisms of activation and dysregulation in cancer. *Redox Biology*,

1(1), 45–49. https://doi.org/10.1016/j.redox.2012.10.001

Khan, F., Moinuddin, Mir, A. R., Isalma, S., & Alam, Khursheed, Ali, A. (2016). Immunochemical studies on HNE-modified HSA: Anti-HNE-HSA antibodies as a probe for HNE damaged albumin in SLE. *International Journal of Biological Macromolecules*, *86*, 145–154. https://doi.org/10.1016/j.ijbiomac.2016.01.053

Khansari, N., Shakiba, Y., & Mahmoudi, M. (2009). Chronic inflammation and oxidative stress as a major cause of age-related diseases and cancer. *Recent Patents on Inflammation & Allergy Drug Discovery*, *3*, 73–80. https://doi.org/10.2174/187221309787158371

Khatoon, F., Moinuddin, Alam, K., & Ali, A. (2012). Physicochemical and immunological studies on 4-hydroxynonenal modified HSA: Implications of protein damage by lipid peroxidation products in the etiopathogenesis of SLE. *Human Immunology*, *73*(11), 1132–1139. https://doi.org/10.1016/j.humimm.2012.08.011

Klarenbeek, A., Mazouari, K. El, Desmyter, A., Blanchetot, C., Hultberg, A., Jonge, N. De, … Achour, I. (2015). Camelid Ig V genes reveal significant human homology not seen in therapeutic target genes , providing for a powerful therapeutic antibody platform, (August), 693–706.

Koczula, K. M., & Gallotta, A. (2016). Lateral flow assays. *Essays in Biochemistry*, *60*(June), 111–120. https://doi.org/10.1042/EBC20150012

Köhler, G., & Milstein, C. (1975). Continuous cultures of fused cells secreting antibody of predefined specificity. *Nature*, *256*, 495–497.

Kretzschmar, T., & Von Rüden, T. (2002). Antibody discovery: Phage display. *Current Opinion in Biotechnology*, *13*(6), 598–602. https://doi.org/10.1016/S0958-1669(02)00380-4

Kulmala, A., Huovinen, T., & Lamminmäki, U. (2017). Effect of DNA sequence of Fab fragment on yield characteristics and cell growth of E. coli. *Scientific Reports*, *7*(1), 1–10. https://doi.org/10.1038/s41598-017-03957-6

Kumano-Kuramochi, M., Shimozu, Y., Wakita, C., Ohnishi-Kameyama, M., Shibata, T., Matsunaga, S., … Machida, S. (2012). Identification of 4-hydroxy-2-nonenal–histidine adducts that serve as ligands for human lectin-like oxidized LDL receptor-1. *Biochemical Journal*, *442*(1), 171–180. https://doi.org/10.1042/BJ20111029

Kumar Maurya, P., & Chandra, P. (2017). *Oxidative Stress: Diagnostic Methods and Applications in Medical Science*. (P. Kumar Maurya & P. Chandra, Eds.). Retrieved from https://link.springer.com/content/pdf/10.1007%2F978-981-10-4711-4.pdf

Kurien, B. T., Hensley, K., Bachmann, M., & Scofield, R. H. (2006). Oxidatively modified autoantigens in autoimmune diseases. *Free Radical Biology and Medicine*, *41*(4), 549–556. https://doi.org/10.1016/j.freeradbiomed.2006.05.020

Laffly, E., & Sodoyer, R. (2005). Monoclonal and recombinant antibodies, 30 years after. *Human Antibodies*, *14*, 33–55. Retrieved from http://iospress.metapress.com/index/d9etwg9vvj1t51ep.pdf

Lai, W., Fung, D. Y. C., Yang, X., Renrong, L., & Xiong, Y. (2009). Development of a colloidal gold strip for rapid detection of ochratoxin A with mimotope peptide. *Food Control*, *20*(9), 791–795. https://doi.org/10.1016/j.foodcont.2008.10.007

Lam, P. T., Leung, M. W., & Tse, C. Y. (2007). Identifying prognostic factors for survival in advanced cancer patients: A prospective study. *Hong Kong Medical Journal*, *13*(6), 453–459.

Lambeth, J. D. (2004). NOX enzymes and the biology of reactive oxygen. *Nature Reviews Immunology*, *4*(3), 181–189. https://doi.org/10.1038/nri1312

Lavie, L. (2003). Obstructive sleep apnoea syndrome - An oxidative stress disorder. *Sleep Medicine Reviews*, *7*(1), 35–51. https://doi.org/10.1053/smrv.2002.0261

Leenaars, M., & Hendriksen, C. F. M. (2005). Critical Steps in the Production of Polyclonal and Monoclonal Antibodies: Evaluation and Recommendation. *Ilar Journal*, *46*(3), 269–279. https://doi.org/10.1093/ilar.46.3.269

Leibundgut, G., Witztum, J. L., & Tsimikas, S. (2013). Oxidation-specific epitopes and immunological responses: Translational biotheranostic implications for atherosclerosis. *Curr Opin Pharmacol.*, *13*(2), 233–236. https://doi.org/10.1038/mp.2011.182.doi

Leonarduzzi, G., Robbesyn, F., & Poli, G. (2004). Signaling kinases modulated by 4-hydroxynonenal. *Free Radical Biology and Medicine*, *37*(11), 1694–1702. https://doi.org/10.1016/j.freeradbiomed.2004.08.027

Leow, C. H., Fischer, K., Leow, C. Y., Braet, K., Cheng, Q., & McCarthy, J. (2018). Isolation and characterization of malaria PfHRP2 specific V NAR antibody fragments from immunized shark phage display library. *Malaria Journal*, *17*(1), 1–15. https://doi.org/10.1186/s12936-018-2531-y

Levonen, A.-L., Landar, A., Ramachandran, A., Ceaser, E. K., Dickinson, D. A., Zanoni, G., … Darley-Usmar, V. M. (2004). Cellular mechanisms of redox cell signalling: role of cysteine modification in controlling antioxidant defences in response to electrophilic lipid oxidation products. *Biochemical Journal*, *378*(2), 373–382. https://doi.org/10.1042/bj20031049

Levy, R., Weiss, R., Chen, G., Iverson, B. L., & Georgiou, G. (2001). Production of correctly folded fab antibody fragment in the cytoplasm of Escherichia coli trxB gor mutants via the coexpression of molecular chaperones. *Protein Expression and Purification*, *23*(2), 338–347. https://doi.org/10.1006/prep.2001.1520

Li, Y., Kilpatrick, J., & Whitelam, G. C. (2000). Sheep monoclonal antibody fragments generated using a phage display system. *J Immunol Methods*, *236*(1–2), 133–146. https://doi.org/10.1016/s0022-1759(99)00227-6

Li, Z., Woo, C. J., Iglesias-Ussel, M. D., Ronai, D., & Scharff, M. D. (2004). The generation of antibody diversity through somatic hypermutation and class switch recombination. *Genes and Development*, *18*(1), 1–11. https://doi.org/10.1101/gad.1161904

Lipman, N. S., Jackson, L. R., Trudel, L. J., & Weis-Garcia, F. (2005). Monoclonal versus polyclonal antibodies: distinguishing characteristics, applications, and information resources. *ILAR Journal / National Research Council, Institute of Laboratory Animal Resources*, *46*(3), 258–268. Retrieved from http://www.ncbi.nlm.nih.gov/pubmed/15953833

Liu, H. F., Ma, J., Winter, C., & Bayer, R. (2010). Recovery and purification process development for monoclonal antibody production. *MAbs*, *2*(5), 480–499. https://doi.org/10.4161/mabs.2.5.12645

Liu, Q., Simpson, D. C., & Gronert, S. (2012). The reactivity of human serum albumin toward trans-4-hydroxy-2-nonenal. *Journal of Mass Spectrometry*, *47*(4), 411–424. https://doi.org/10.1002/jms.2037

Liyasova, M. S., Schopfer, L. M., & Lockridge, O. (2010). Reaction of human albumin with aspirin in vitro: Mass spectrometric identification of acetylated lysines 199, 402, 519, and 545. *Biochemical Pharmacology*, *79*(5), 784–791. https://doi.org/10.1016/j.bcp.2009.10.007

Loizides-Mangold, U. (2013). On the future of mass-spectrometry-based lipidomics. *FEBS Journal*, *280*(12), 2817–2829. https://doi.org/10.1111/febs.12202

López-Lorente, Á. I. (2014). *Gold Nanoparticles in Analytical Chemistry*. *Comprehensive Analytical Chemistry* (Vol. 66). https://doi.org/10.1016/B978-0-444-63285-2.00001-8

Lyons, T. J., & Jenkins, A. J. (1997). Glycation, oxidation, and lipoxidation in the development of the complications of diabetes: a carbonyl stress hypothesis. *Diabetes Rev (Alex)*, *5*(4), 365–391. https://doi.org/10.1007/s12671-013-0269-8.Moving

Martín-Sierra, C., Laranjeira, P., Domingues, M. R., & Paiva, A. (2019). Lipoxidation and cancer immunity. *Redox Biology*, (January), 101103. https://doi.org/10.1016/j.redox.2019.101103

Martínez-Riaño, A., Bovolenta, E. R., Mendoza, P., Oeste, C. L., Martín-bermejo, M. J., Bovolenta, P., … Alarcón, B. (2018). Antigen phagocytosis by B cells is required for a potent humoral response, 1–15. https://doi.org/10.15252/embr.201846016

McCafferty, J., Griffiths, A. D., Winter, G., & Chiswell, D. J. (1990). Phage antibodies: filamentous phage displaying antibody variable domains. *Nature*. https://doi.org/10.1038/348552a0

McLeod, L. L., & Sevanian, A. (1997). Lipid peroxidation and modification of lipid composition in an endothelial cell model of ischemia and reperfusion. *Free Radical Biology and Medicine*, *23*(4), 680–694. https://doi.org/10.1016/S0891-5849(97)00055-5

Milic, I., Griesser, E., Vemula, V., Ieda, N., Nakagawa, H., Miyata, N., … Fedorova, M. (2015). Profiling and relative quantification of multiply nitrated and oxidized fatty acids. *Analytical and Bioanalytical Chemistry*, *407*(19), 5587–5602. https://doi.org/10.1007/s00216-015-8766-3

Miller, Y. I., Choi, S., Wiesner, P., Fang, L., Harkewicz, R., Hartvigsen, K., … Witztum, L. (2012). Oxidation-specific epitopes are danger associated molecular patterns recognized by pattern recognition receptors of innate immunity. *Circulation Research*, *108*(2), 235–248. https://doi.org/10.1161/CIRCRESAHA.110.223875.Oxidation-Specific

Milstein, C. (1999). The hybridoma revolution : an offshoot of basic research. *BioEssays*, *21*, 966–973.

Murphy, K., & Weaver, C. (2017). *Janeway's Immunology*. (K. Murphy & C. Weaver, Eds.) (9th Editio). Garland Science, Taylor & Francis Group.

Musante, L., Candiano, G., Petretto, A., Bruschi, M., Dimasi, N., Caridi, G., … Ghiggeri, G. M. (2007). Active Focal Segmental Glomerulosclerosis Is Associated with Massive Oxidation of Plasma Albumin. *Journal of the American Society of Nephrology*, *18*(3), 799–810. https://doi.org/10.1681/asn.2006090965

Nagumo, K., Tanaka, M., Chuang, V. T. G., Setoyama, H., Watanabe, H., Yamada, N., … Maruyama, T. (2014). Cys34-cysteinylated human serum albumin is a sensitive plasma marker in oxidative stress-related chronic diseases. *PLoS ONE*, *9*(1). https://doi.org/10.1371/journal.pone.0085216

Nakashima, I., Liu, W., Akhand, A. A., Takeda, K., Kawamoto, Y., Kato, M., & Suzuki, H. (2003). 4-Hydroxynonenal triggers multistep signal transduction cascades for suppression of cellular functions. *Molecular Aspects of Medicine*, *24*(4–5), 231–238. https://doi.org/10.1016/S0098-2997(03)00018-9

Negre-Salvayre, A., Coatrieux, C., Ingueneau, C., & Salvayre, R. (2008). Advanced lipid peroxidation end products in oxidative damage to proteins. Potential role in diseases and therapeutic prospects for the inhibitors. *British Journal of Pharmacology*, *153*(1), 6–20. https://doi.org/10.1038/sj.bjp.0707395

Nelson, R. S., & Valadon, P. (2017). A universal phage display system for the seamless

construction of Fab libraries. *Journal of Immunological Methods*, *450*(April), 41–49. https://doi.org/10.1016/j.jim.2017.07.011

Ngom, B., Guo, Y., Wang, X., & Bi, D. (2010). Development and application of lateral flow test strip technology for detection of infectious agents and chemical contaminants: A review. *Analytical and Bioanalytical Chemistry*, *397*(3), 1113–1135. https://doi.org/10.1007/s00216-010-3661-4

Noiri, E., & Tsukahara, H. (2005). Parameters for Measurement of Oxidative Stress in Diabetes Mellitus: Applicability of Enzyme-Linked Immunosorbent Assay for Clinical Evaluation. *Journal of Investigative Medicine*, *53*(4), 167–175. https://doi.org/10.2310/6650.2005.00403

Oettl, K., Birner-Gruenberger, R., Spindelboeck, W., Stueger, H. P., Dorn, L., Stadlbauer, V., … Stauber, R. E. (2013). Oxidative albumin damage in chronic liver failure: Relation to albumin binding capacity, liver dysfunction and survival. *Journal of Hepatology*, *59*(5), 978–983. https://doi.org/10.1016/j.jhep.2013.06.013

Otagiri, M., & Giam Chuang, V. T. (2016). *Albumin in medicine: Pathological and clinical applications*. (M. Otagiri & V. T. Giam Chuang, Eds.), *Albumin in Medicine: Pathological and Clinical Applications*. Springer Nature. https://doi.org/10.1007/978-981-10-2116-9

Palinski, W., Rosenfeld, M. E., Ylä-Herttuala, S., Gurtner, G. C., Socher, S. S., Butler, S. W., … Witztum, J. L. (1989). Low density lipoprotein undergoes oxidative modification in vivo. *Proceedings of the National Academy of Sciences of the United States of America*, *86*(4), 1372–1376. https://doi.org/10.1073/pnas.86.4.1372

Palliyil, S. (2018). Generation of High-Sensitivity Monoclonal Antibodies Specific for Homoserine Lactones. In L. Leoni & G. Rampioni (Eds.), *Quorum Sensing: Methods and Protocols* (Vol. 1673, pp. 325–352).

Palliyil, S., Downham, C., Broadbent, I., Charlton, K., & Porter, J. (2014). High-Sensitivity Monoclonal Antibodies Specific for Homoserine Lactones Protect Mice from Lethal Pseudomonas aeruginosa Infections, *80*(2), 462–469. https://doi.org/10.1128/AEM.02912-13

Palmieri, B., & Sblendorio, V. (2007). Oxidative stress tests : overview on Part II. *European Review for Medical and Pharmacological Sciences*, *11*, 383–399.

Pande, J., Szewczyk, M. M., & Grover, A. K. (2010). Phage display: Concept, innovations, applications and future. *Biotechnology Advances*, *28*(6), 849–858. https://doi.org/10.1016/j.biotechadv.2010.07.004

Pandey, K. B., & Rizvi, S. I. (2011). Biomarkers of oxidative stress in red blood cells. *Biomedical Papers*, *155*(2), 131–136. https://doi.org/10.5507/bp.2011.027

Patterson, E., Wall, R., Fitzgerald, G. F., Ross, R. P., & Stanton, C. (2012). Health Implications ofHigh DietaryOmega-6 Polyunsaturated FattyAcids. *Journal of Nutrition and Metabolism*, *2011*(11). https://doi.org/10.1155/2012/539426

Pavlatou, M. G., Papastamataki, M., Apostolakou, F., Papassotiriou, I., & Tentolouris, N. (2009). FORT and FORD: two simple and rapid assays in the evaluation of oxidative stress in patients with type 2 diabetes mellitus. *Metabolism: Clinical and Experimental*, *58*(11), 1657–1662. https://doi.org/10.1016/j.metabol.2009.05.022

Peled, J. U., Kuang, F. L., Iglesias-Ussel, M. D., Roa, S., Kalis, S. L., Goodman, M. F., & Scharff, M. D. (2008). The Biochemistry of Somatic Hypermutation. *Annual Review of Immunology*, *26*(1), 481–511. https://doi.org/10.1146/annurev.immunol.26.021607.090236

Petersen, C. E., Ha, C. E., Harohalli, K., Feix, J. B., & Bhagavan, N. V. (2000). A dynamic

model for bilirubin binding to human serum albumin. *Journal of Biological Chemistry*, *275*(28), 20985–20995. https://doi.org/10.1074/jbc.M001038200

Pham-Huy, L. A., He, H., & Pham-Huy, C. (2008). Free Radicals, Antioxidants in Disease and Health. *Www.Ijbs.Org Int J Biomed Sci*, *4*(2).

Phaniendra, A., Jestadi, D. B., & Periyasamy, L. (2015). Free Radicals: Properties, Sources, Targets, and Their Implication in Various Diseases. *Indian Journal of Clinical Biochemistry*, *30*(1), 11–26. https://doi.org/10.1007/s12291-014-0446-0

Pitt, A. R. (1998). Application of electrospray mass spectrometry in biology. *Natural Product Reports*, *15*(1), 59. https://doi.org/10.1039/a815059y

Poli, G., Biasi, F., & Leonarduzzi, G. (2008). 4-Hydroxynonenal-protein adducts: A reliable biomarker of lipid oxidation in liver diseases. *Molecular Aspects of Medicine*. https://doi.org/10.1016/j.mam.2007.09.016

Quesada-González, D., Stefani, C., González, I., de la Escosura-Muñiz, A., Domingo, N., Mutjé, P., & Merkoçi, A. (2019). Signal enhancement on gold nanoparticle-based lateral flow tests using cellulose nanofibers. *Biosensors and Bioelectronics*, *141*(May), 111407. https://doi.org/10.1016/j.bios.2019.111407

Reed, T. T., Pierce, W. M., Markesbery, W. R., & Butterfield, D. A. (2009). Proteomic identification of HNE-bound proteins in early Alzheimer disease: Insights into the role of lipid peroxidation in the progression of AD. *Brain Research*, *1274*, 66–76. https://doi.org/10.1016/j.brainres.2009.04.009

Reis, A., & Spickett, C. M. (2012). Chemistry of phospholipid oxidation. *Biochimica et Biophysica Acta - Biomembranes*, *1818*(10), 2374–2387. https://doi.org/10.1016/j.bbamem.2012.02.002

Requena, J., Fu, M.-X., Ahmed, M. U., Jenkins, A. J., Lyons, T. J., & Thorpe, S. R. (1996). Lipoxidation products as biomarkers of oxidative damage to proteins during lipid peroxidation reactions. *Nephrology Dialysis Transplantation*, (11), 48–53.

Reynaud, C. A., Garcia, C., Hein, W. R., & Weill, J. C. (1995). Hypermutation generating the sheep immunoglobulin repertoire is an antigen-independent process. *Cell*, *80*(1), 115–125. https://doi.org/10.1016/0092-8674(95)90456-5

Rippe, B., Kamiva, A., & Folkow, B. (1979). Transcapillary passage of albumin, effects of tissue cooling and of increases in filtration and plasma colloid osmotic pressure. *Acta Physiologica Scandinavica*, *105*(2), 171–187. https://doi.org/10.1111/j.1748-1716.1979.tb06329.x

Rossi, R., Colombo, R., Carini, M., Milzani, A., & Dalle-donne, I. (2010). Water-Soluble a,b-Unsaturated Aldehydes of Cigarette Smoke Induce Carbonylation of Human Serum Albumin, *12*(3), 349–364.

Ruiz, G., Tripathi, K., Okyem, S., & Driskell, J. D. (2019). pH Impacts the Orientation of Antibody Adsorbed onto Gold Nanoparticles. *Bioconjugate Chemistry*, *30*(4), 1182–1191. https://doi.org/10.1021/acs.bioconjchem.9b00123

Sajadi, M. M., Farshidpour, M., Brown, E. P., Ouyang, X., Seaman, M. S., Pazgier, M., … Lewis, G. K. (2016). λ light chain bias associated with enhanced binding and function of anti-HIV Env glycoprotein antibodies. *Journal of Infectious Diseases*, *213*(1), 156–164. https://doi.org/10.1093/infdis/jiv448

Sajid, M., Kawde, A. N., & Daud, M. (2015). Designs, formats and applications of lateral flow assay: A literature review. *Journal of Saudi Chemical Society*, *19*(6), 689–705. https://doi.org/10.1016/j.jscs.2014.09.001

Sakamoto, A., Tsuyoshi Ohnishi, S., Ohnishi, T., & Ogawa, R. (1991). Relationship between free radical production and lipid peroxidation during ischemia-reperfusion

injury in the rat brain. *Brain Research*, *554*(1–2), 186–192. https://doi.org/10.1016/0006-8993(91)90187-Z

Satoh, K., Yamada, S., Koike, Y., Igarashi, Y., Toyokuni, S., Kumano, T., … Uchida, K. (1999). A 1-Hour Enzyme-Linked Immunosorbent Assay for Quantitation of Acrolein- and Hydroxynonenal-Modified Proteins by Epitope-Bound Casein Matrix Method• 1. *Analytical Biochemistry*, *270*(2), 323–328. Retrieved from http://linkinghub.elsevier.com/retrieve/pii/S0003269799940733

Schaur, R. J. (2003). Basic aspects of the biochemical reactivity of 4-hydroxynonenal. *Molecular Aspects of Medicine*, *24*(4–5), 149–159. https://doi.org/10.1016/S0098-2997(03)00009-8

Schmitt, F. J., Renger, G., Friedrich, T., Kreslavski, V. D., Zharmukhamedov, S. K., Los, D. A., … Allakhverdiev, S. I. (2014). Reactive oxygen species: Re-evaluation of generation, monitoring and role in stress-signaling in phototrophic organisms. *Biochimica et Biophysica Acta - Bioenergetics*, *1837*(6), 835–848. https://doi.org/10.1016/j.bbabio.2014.02.005

Schroeder Jr, H. W., & Cavacini, L. (2010). Structure and Function of Immunoglobulins. *J Allergy Clin Immunol.*, *125*, 41–52. https://doi.org/10.1016/j.jaci.2009.09.046.Structure

Sevilla, C. L., Mahle, N. H., Eliezer, N., Uzieblo, A., O'Hara, S. M., Nokubo, M., … Marnett, L. J. (1997). Development of monoclonal antibodies to the malondialdehyde- deoxyguanosine adduct, pyrimidopurinone. *Chemical Research in Toxicology*, *10*(2), 172–180. https://doi.org/10.1021/tx960120d

Shamim i. Ahmad. (2016). *Reactive oxygen species in biology and human health*. CRC Press.

Shen, Y., Yang, X., Dong, N., Xie, X., Bai, X., & Shi, Y. (2007). Generation and selection of immunized Fab phage display library against human B cell lymphoma. *Cell Research*, *17*(7), 650–660. https://doi.org/10.1038/cr.2007.57

Shibata, T., Shimizu;, K., Hirano;, K., Nakashima;, F., Kikuchi;, R., Matsushita;, T., … Uchida, K. (2017). Adductome-based identification of biomarkers for lipid peroxidation. *Journal of Biological Chemistry*, *292*(20), 8223–8235. https://doi.org/10.1074/jbc.M116.762609

Shoeb, M., Ansari, N., Srivastava, S., & Ramana, K. (2013). 4-Hydroxynonenal in the Pathogenesis and Progression of Human Diseases. *Current Medicinal Chemistry*, *21*(2), 230–237. https://doi.org/10.2174/0929867311320999018 1

Sies, H. (1985). *Oxidative stress*. *Academic Press* (Vol. 36). https://doi.org/10.1177/0148607111434963

Sies, H. (1993). Strategies of antioxidant defense. *European Journal of Biochemistry*, *219*, v. 215, n. 2, pp. 213–219.

Sifniotis, V., Cruz, E., Eroglu, B., & Kayser, V. (2019). Current Advancements in Addressing Key Challenges of Therapeutic Antibody Design, Manufacture, and Formulation. *Antibodies*, *8*(2), 36. https://doi.org/10.3390/antib8020036

Smith, G. P. . (1985). Filamentous Fusion Phage : Novel Expression Vectors that Display Cloned Antigens on the Virion Surface. *Science*, *228*(4705), 1315–1317.

Sousa, B. C., Pitt, A. R., & Spickett, C. M. (2017). Chemistry and analysis of HNE and other prominent carbonyl-containing lipid oxidation compounds. *Free Radical Biology and Medicine*, *111*(January), 294–308. https://doi.org/10.1016/j.freeradbiomed.2017.02.003

Spickett, C. M. (2013). The lipid peroxidation product 4-hydroxy-2-nonenal: Advances in

chemistry and analysis. *Redox Biology*, *1*(1), 145–152. https://doi.org/10.1016/j.redox.2013.01.007

St John, A., & Price, C. P. (2014). Existing and Emerging Technologies for Point-of-Care Testing. *The Clinical Biochemist. Reviews / Australian Association of Clinical Biochemists*, *35*(3), 155–167. Retrieved from http://www.pubmedcentral.nih.gov/articlerender.fcgi?artid=4204237&tool=pmcentrez&rendertype=abstract

Sun, Y., Liu, Z., Ren, L., Wei, Z., Wang, P., Li, N., & Zhao, Y. (2012). Immunoglobulin genes and diversity: what we have learned from domestic animals, *3*(1), 1. https://doi.org/10.1186/2049-1891-3-18

Surh, Y.-J., & Packer, L. (2005). *Oxidative Stress, Inflammation, and Health*. (Y.-J. Surh & L. Packer, Eds.). CRC Press.

Szapacs, M. E., Riggins, J. N., Zimmerman, L. J., & Liebler, D. C. (2006). Covalent Adduction of Human Serum Albumin by 4-Hydroxy-2-Nonenal : Kinetic Analysis of Competing Alkylation Reactions †, 10521–10528.

Teixeira, D., & Gonzalez-Pajuelo, M. (2018). *Phage Display Technology for Selection of Antibody Fragments*. *Biomedical Applications of Functionalized Nanomaterials*. Elsevier Inc. https://doi.org/10.1016/B978-0-323-50878-0.00003-3

Temple, A., Yen, T. Y., & Gronert, S. (2006). Identification of Specific Protein Carbonylation Sites in Model Oxidations of Human Serum Albumin. *Journal of the American Society for Mass Spectrometry*, *17*(8), 1172–1180. https://doi.org/10.1016/j.jasms.2006.04.030

Thu, T., Nguyen, H., Lee, J. S., & Shim, H. (2018). Construction of Rabbit Immune Antibody Libraries. In *Phage Display: Methods and Protocols, Methods in Molecular Biology* (Vol. 1701, pp. 133–146). https://doi.org/10.1007/978-1-4939-7447-4

Tohidkia, M. R., Barar, J., Asadi, F., & Omidi, Y. (2012). Molecular considerations for development of phage antibody libraries. *Journal of Drug Targeting*, *20*(3), 195–208. https://doi.org/10.3109/1061186X.2011.611517

Touyz, R. M., Briones, A. M., Sedeek, M., Burger, D., & Montezano, A. C. (2011). NOX isoforms and reactive oxygen species in vascular health. *Molecular Interventions*, *11*(1), 27–35. https://doi.org/10.1124/mi.11.1.5

Toyokuni, S., Miyake, N., Hiai, H., Hagiwara, M., Kawakishi, S., Osawa, T., & Uchida, K. (1995). The monoclonal antibody specific for the 4-hydroxy-2-nonenal histidine adduct. *FEBS Letters*, *359*(2–3), 189–191. https://doi.org/10.1016/0014-5793(95)00033-6

Toyokuni, S., Yamad, S., Kashima, M., Ihara, Y., Yamada, Y., Tanaka, T., … Uchida, K. (2000). Serum 4-Hydroxy-2-Nonenal-Modified Albumin Is Elevated in Patients with Type 2 Diabetes Mellitus. *Antioxidants & Redox Signaling*, *2*(4), 681–685.

Tsukahara, H., & Kaneko, K. (2014). *Studies on Pediatric Disorders*. https://doi.org/10.1007/978-1-4939-0679-6

Turell, L., Botti, H., Carballal, S., Radi, R., & Alvarez, B. (2009). Sulfenic acid-A key intermediate in albumin thiol oxidation. *Journal of Chromatography B: Analytical Technologies in the Biomedical and Life Sciences*, *877*(28), 3384–3392. https://doi.org/10.1016/j.jchromb.2009.03.035

Turell, L., Radi, R., & Alvarez, B. (2013). The thiol pool in human plasma: The central contribution of albumin to redox processes. *Free Radical Biology and Medicine*, *65*, 244–253. https://doi.org/10.1016/j.freeradbiomed.2013.05.050

Uchida, K. (2003a). 4-Hydroxy-2-nonenal: A product and mediator of oxidative stress.

Progress in Lipid Research, *42*(4), 318–343. https://doi.org/10.1016/S0163-7827(03)00014-6

Uchida, K. (2003b). Histidine and lysine as targets of oxidative modification. *Amino Acids*, *25*(3–4), 249–257. https://doi.org/10.1007/s00726-003-0015-y

Uchida, K. (2007). Lipid peroxidation and redox-sensitive signaling pathways. *Current Atherosclerosis Reports*, *9*(3), 216–221. https://doi.org/10.1007/s11883-007-0022-7

Uchida, K. (2013). Redox-derived damage-associated molecular patterns: Ligand function of lipid peroxidation adducts. *Redox Biology*, *1*(1), 94–96. https://doi.org/10.1016/j.redox.2012.12.005

Uchida, K. (2015). Aldehyde adducts generated during lipid peroxidation modification of proteins. *Free Radical Research*, *49*(7), 896–904. https://doi.org/10.3109/10715762.2015.1036052

Uchida, K., Itakura, K., Kawakishi, S., Hiai, H., Toyokuni, S., & Stadtman, E. R. (1995). Characterization of epitopes recognized by 4-Hydroxy-2-nonenal specific antibodies. *Archives of Biochemistry and Biophysics*, *324*(2), 241–248. https://doi.org/10.1006/abbi.1995.0036

Uchida, K., Kanematsu, M., Sakai, K., Matsuda, T., Hattori, N., Mizuno, Y., … Osawa, T. (1998). Protein-bound acrolein : Potential markers for oxidative stress. *Proceedings of the National Academy of Sciences of the United States of America*, *95*, 4882–4887.

Uchida, K., Osawa, T., Hiai, H., & Toyokuni, S. (1995). 4-Hydroxy-2-nonenal-trapping elisa: Direct evidence for the release of a cytotoxic aldehyde from oxidized low density lipoproteins. *Biochemical and Biophysical Research Communications*. https://doi.org/10.1006/bbrc.1995.2078

Uchida, K., Szweda, L. I., Chae, H. Z., & Stadtman, E. R. (1993). Immunochemical detection of 4-hydroxynonenal protein adducts in oxidized hepatocytes. *Proceedings of the National Academy of Sciences of the United States of America*, *90*(18), 8742–8746.

Ursini, F., Maiorino, M., & Forman, H. J. (2016). Redox homeostasis: The Golden Mean of healthy living. *Redox Biology*, *8*, 205–215. https://doi.org/10.1016/j.redox.2016.01.010

van Amerongen, A., Wichers, J. H., Berendsen, L. B. J. M., Timmermans, A. J. M., Keizer, G. D., van Doorn, A. W. J., … van Gelder, W. M. J. (1993). Colloidal carbon particles as a new label for rapid immunochemical test methods: Quantitative computer image analysis of results. *Journal of Biotechnology*, *30*(2), 185–195. https://doi.org/10.1016/0168-1656(93)90112-Z

Vasil'ev, Y. V, Tzeng, S.-C., Huang, L., & Maier, C. S. (2014). Protein modifications by electrophilic lipoxidation products: adduct formation, chemical strategies and tandem mass spectrometry for their detection and identification. *Mass Spectrometry Reviews*, *33*(3), 157–182.

Verrastro, I., Pasha, S., Jensen, K., Pitt, A., & Spickett, C. M. (2015). Mass Spectrometry-Based Methods for Identifying Oxidized Proteins in Disease: Advances and Challenges. *Biomolecules*, *5*(2), 378–411. https://doi.org/10.3390/biom5020378

Vistoli, G., De Maddis, D., Cipak, A., Zarkovic, N., Carini, M., & Aldini, G. (2013). Advanced glycoxidation and lipoxidation end products (AGEs and ALEs): an overview of their mechanisms of formation. *Free Radical Research*, *47 Suppl 1*(August), 3–27. https://doi.org/10.3109/10715762.2013.815348

Waeg, G., Dimsity, G., & Esterbauer, H. (1996). Monoclonal antibodies for detection of 4-

hydroxynonenal modified proteins. *Free Radic. Res.*, *25*(2), 149–159.

Wang, Z., Zhao, Y., Ru, Y., Li, H., Zhi, D., Zhang, H., & Wang, X. (2014). Lateral flow test strip based on colloidal selenium immunoassay for rapid detection of melamine in milk, milk powder, and animal feed. *International Journal of Nanomedicine*, *9*(1), 1699–1707. https://doi.org/10.2147/IJN.S58942

Weber, D., Milkovic, L., Bennett, S. J., Griffiths, H. R., Zarkovic, N., & Grune, T. (2013). Measurement of HNE-protein adducts in human plasma and serum by ELISA-Comparison of two primary antibodies. *Redox Biology*, *1*(1), 226–233. https://doi.org/10.1016/j.redox.2013.01.012

Weismann, D., & Binder, C. J. (2012). The innate immune response to products of phospholipid peroxidation. *Biochimica et Biophysica Acta - Biomembranes*, *1818*(10), 2465–2475. https://doi.org/10.1016/j.bbamem.2012.01.018

Wild, A. C., Moinova, H. R., & Mulcahy, R. T. (1999). Regulation of γ-glutamylcysteine synthetase subunit gene expression by the transcription factor Nrf2. *Journal of Biological Chemistry*, *274*(47), 33627–33636. https://doi.org/10.1074/jbc.274.47.33627

Wild, D., John, R., & Sheehan, C. (2013). *The Immunoassay Handbook Theory and applications of ligand binding , Edited by David Wild*. *The Immunoassay Handbook*. https://doi.org/10.1016/B978-0-08-097037-0.01001-0

Wojciech, Ł., & Agnieszka, G. (2017). Antioxidants and HNE in redox homeostasis. *Free Radical Biology and Medicine*, *111*(November 2016), 87–101. https://doi.org/10.1016/j.freeradbiomed.2016.11.033

Wong, R., & Tse, H. (2008). *Lateral Flow Immunoassay*. Retrieved from http://books.google.ch/books?id=D4-capuCoRUC

Wu, J., & Stevens, Jan F.; Maier, C. S. (2011). Mass spectrometry-based quantification of myocardial protein adducts with acrolein in an in vivo model of oxidative stress. *Mol Nutr Food Res*, *4*(164), 1401–1410. https://doi.org/10.1126/scisignal.2001449.Engineering

Xiao, M., Zhong, H., Xia, L., Tao, Y., & Yin, H. (2017). Pathophysiology of mitochondrial lipid oxidation: Role of 4-hydroxynonenal (4-HNE) and other bioactive lipids in mitochondria. *Free Radical Biology and Medicine*, *111*, 316–327. https://doi.org/10.1016/j.freeradbiomed.2017.04.363

Xie, S., Wen, K., Wang, S., Wang, J., Peng, T., Mari, G. M., … Jiang, H. (2019). Quantitative and rapid detection of amantadine and chloramphenicol based on various quantum dots with the same excitations. *Analytical and Bioanalytical Chemistry*, *411*(10), 2131–2140. https://doi.org/10.1007/s00216-019-01643-2

Yamada, S., Funada, T., Shibata, N., Kobayashi, M., Kawai, Y., Tatsuda, E., … Uchida, K. (2004). Protein-bound 4-hydroxy-2-hexenal as a marker of oxidized n-3 polyunsaturated fatty acids, *45*. https://doi.org/10.1194/jlr.M300376-JLR200

Zarkovic, K., Jakovcevic, A., & Zarkovic, N. (2017). Contribution of the HNE-immunohistochemistry to modern pathological concepts of major human diseases. *Free Radical Biology and Medicine*, *111*(October 2016), 110–126. https://doi.org/10.1016/j.freeradbiomed.2016.12.009

Zhang, H., & Forman, H. J. (2017). 4-hydroxynonenal-mediated signaling and aging. *Free Radical Biology and Medicine*, *111*, 219–225. https://doi.org/10.1016/j.freeradbiomed.2016.11.032

Zhong, H., & Yin, H. (2015). Role of lipid peroxidation derived 4-hydroxynonenal (4-HNE) in cancer: Focusing on mitochondria. *Redox Biology*, *4*, 193–199.

https://doi.org/10.1016/j.redox.2014.12.011

Zwick, M. B., Parren, P. W. H. I., Saphire, E. O., Church, S., Wang, M., Scott, J. K., … Burton, D. R. (2003). Molecular Features of the Broadly Neutralizing Immunoglobulin G1 b12 Required for Recognition of Human Immunodeficiency Virus Type 1 gp120. *Journal of Virology*, *77*(10), 5863–5876. https://doi.org/10.1128/jvi.77.10.5863-5876.2003

APPENDIX

Appendix 1. Nomenclature of reactive species (Halliwell & Gutteridge, 2015)**.**

Appendix 2. Usage report for synthesis of peptide MOL 663 ^{31}LQQCPFE^{37} generated by Liberty Pepdriver Software.

Usage Report

Amino acid concentration: 0.2 M

Liberty Methods Included

Method	Quantity
MOL 663	1

Required Reagent Amounts

Reagent	Volume (mL)	Mass (g)
Cysteine	3	0.36
Glutamine	11	1.35
Glutamate	3	0.26
Leucine	6	0.43
Phenylalanine	6	0.47
Proline	6	0.41
Main Wash (DMF)	415	390.11
Deprotection (Piperidine)	84	
Activator (HOBt monohydrate)	26	
Activator Base (DIC)	13	

Total waste volume: 573 mL

Worst-Case (UV) Reagent Amounts

Reagent	Volume (mL)	Mass (g)
Main Wash (DMF)	516	485.05
Deprotection (Piperidine)	126	

Total waste volume (worst-case): 716 mL

Reported: 3/1/2017 8:41:57 AM Page 1 of 1

Appendix 3. Usage report for synthesis of peptide MOL 664 ^{141}EIARRHPYFYAPEL^{154} generated by Liberty Pepdriver Software.

Usage Report

Amino acid concentration: 0.2 M

Liberty Methods Included

Method	Quantity
MOL 664	1

Required Reagent Amounts

Reagent	Volume (mL)	Mass (g)
Alanine	11	0.69
Arginine	11	1.43
Glutamate	6	0.52
Histidine	3	0.29
Isoleucine	6	0.43
Leucine	3	0.22
Phenylalanine	6	0.47
Proline	6	0.41
Tyrosine	11	1.02
Main Wash (DMF)	770	723.8
Deprotection (Piperidine)	158	
Activator (HOBt monohydrate)	47	
Activator Base (DIC)	24	

Total waste volume: 1062 mL

Worst-Case (UV) Reagent Amounts

Reagent	Volume (mL)	Mass (g)
Main Wash (DMF)	959	901.47
Deprotection (Piperidine)	237	

Total waste volume (worst-case): 1330 mL

Reported: 12/13/2016 1:58:14 PM Page 1 of 1

Appendix 4. Usage report for synthesis of peptide MOL 665 ^{198}LKCASLQK^{205}generated by Liberty Pepdriver Software.

Usage Report

Amino acid concentration: 0.2 M

Liberty Methods Included

Method	Quantity
MOL 665	1

Required Reagent Amounts

Reagent	Volume (mL)	Mass (g)
Alanine	6	0.38
Cysteine	3	0.36
Glutamine	3	0.37
Leucine	11	0.78
Lysine	6	0.57
Serine	3	0.24
Main Wash (DMF)	455	427.71
Deprotection (Piperidine)	95	
Activator (HOBt monohydrate)	24	
Activator Base (DIC)	12	

Total waste volume: 618 mL

Worst-Case (UV) Reagent Amounts

Reagent	Volume (mL)	Mass (g)
Main Wash (DMF)	569	534.86
Deprotection (Piperidine)	142	

Total waste volume (worst-case): 779 mL

Reported: 12/13/2016 1:58:55 PM Page 1 of 1

Appendix 5. List of the human serum albumin (UniProt ID: P02768) peptides synthesized on the arrays. The sequence includes both the signal peptide (1-18) and pro-peptide (19-24) of HSA.

Positional Reference	Peptide sequence	Positional Reference	Peptide sequence
A1	Blank	B26	G-E-M-A-D-C-C-A-K-Q-E-P-E-R-N
A2	M-K-W-V-T-F-I-S-L-L-F-L-F-S-S	B27	M-A-D-C-C-A-K-Q-E-P-E-R-N-E-C
A3	W-V-T-F-I-S-L-L-F-L-F-S-S-A-Y	B28	D-C-C-A-K-Q-E-P-E-R-N-E-C-F-L
A4	T-F-I-S-L-L-F-L-F-S-S-A-Y-S-R	B29	C-A-K-Q-E-P-E-R-N-E-C-F-L-Q-H
A5	I-S-L-L-F-L-F-S-S-A-Y-S-R-G-V	B30	K-Q-E-P-E-R-N-E-C-F-L-Q-H-K-D
A6	L-L-F-L-F-S-S-A-Y-S-R-G-V-F-R	C1	E-P-E-R-N-E-C-F-L-Q-H-K-D-D-N
A7	F-L-F-S-S-A-Y-S-R-G-V-F-R-R-D	C2	E-R-N-E-C-F-L-Q-H-K-D-D-N-P-N
A8	F-S-S-A-Y-S-R-G-V-F-R-R-D-A-H	C3	N-E-C-F-L-Q-H-K-D-D-N-P-N-L-P
A9	S-A-Y-S-R-G-V-F-R-R-D-A-H-K-S	C4	C-F-L-Q-H-K-D-D-N-P-N-L-P-R-L
A10	Y-S-R-G-V-F-R-R-D-A-H-K-S-E-V	C5	L-Q-H-K-D-D-N-P-N-L-P-R-L-V-R
A11	R-G-V-F-R-R-D-A-H-K-S-E-V-A-H	C6	H-K-D-D-N-P-N-L-P-R-L-V-R-P-E
A12	V-F-R-R-D-A-H-K-S-E-V-A-H-R-F	C7	D-D-N-P-N-L-P-R-L-V-R-P-E-V-D
A13	R-R-D-A-H-K-S-E-V-A-H-R-F-K-D	C8	N-P-N-L-P-R-L-V-R-P-E-V-D-V-M
A14	D-A-H-K-S-E-V-A-H-R-F-K-D-L-G	C9	N-L-P-R-L-V-R-P-E-V-D-V-M-C-T
A15	H-K-S-E-V-A-H-R-F-K-D-L-G-E-E	C10	P-R-L-V-R-P-E-V-D-V-M-C-T-A-F
A16	S-E-V-A-H-R-F-K-D-L-G-E-E-N-F	C11	L-V-R-P-E-V-D-V-M-C-T-A-F-H-D
A17	V-A-H-R-F-K-D-L-G-E-E-N-F-K-A	C12	R-P-E-V-D-V-M-C-T-A-F-H-D-N-E
A18	H-R-F-K-D-L-G-E-E-N-F-K-A-L-V	C13	E-V-D-V-M-C-T-A-F-H-D-N-E-E-T
A19	F-K-D-L-G-E-E-N-F-K-A-L-V-L-I	C14	D-V-M-C-T-A-F-H-D-N-E-E-T-F-L
A20	D-L-G-E-E-N-F-K-A-L-V-L-I-A-F	C15	M-C-T-A-F-H-D-N-E-E-T-F-L-K-K
A21	G-E-E-N-F-K-A-L-V-L-I-A-F-A-Q	C16	T-A-F-H-D-N-E-E-T-F-L-K-K-Y-L
A22	E-N-F-K-A-L-V-L-I-A-F-A-Q-Y-L	C17	F-H-D-N-E-E-T-F-L-K-K-Y-L-Y-E
A23	F-K-A-L-V-L-I-A-F-A-Q-Y-L-Q-Q	C18	D-N-E-E-T-F-L-K-K-Y-L-Y-E-I-A
A24	A-L-V-L-I-A-F-A-Q-Y-L-Q-Q-C-P	C19	E-E-T-F-L-K-K-Y-L-Y-E-I-A-R-R
A25	V-L-I-A-F-A-Q-Y-L-Q-Q-C-P-F-E	C20	T-F-L-K-K-Y-L-Y-E-I-A-R-R-H-P
A26	I-A-F-A-Q-Y-L-Q-Q-C-P-F-E-D-H	C21	L-K-K-Y-L-Y-E-I-A-R-R-H-P-Y-F
A27	F-A-Q-Y-L-Q-Q-C-P-F-E-D-H-V-K	C22	K-Y-L-Y-E-I-A-R-R-H-P-Y-F-Y-A
A28	Q-Y-L-Q-Q-C-P-F-E-D-H-V-K-L-V	C23	L-Y-E-I-A-R-R-H-P-Y-F-Y-A-P-E
A29	L-Q-Q-C-P-F-E-D-H-V-K-L-V-N-E	C24	E-I-A-R-R-H-P-Y-F-Y-A-P-E-L-L
A30	Q-C-P-F-E-D-H-V-K-L-V-N-E-V-T	C25	A-R-R-H-P-Y-F-Y-A-P-E-L-L-F-F
B1	P-F-E-D-H-V-K-L-V-N-E-V-T-E-F	C26	R-H-P-Y-F-Y-A-P-E-L-L-F-F-A-K
B2	E-D-H-V-K-L-V-N-E-V-T-E-F-A-K	C27	P-Y-F-Y-A-P-E-L-L-F-F-A-K-R-Y
B3	H-V-K-L-V-N-E-V-T-E-F-A-K-T-C	C28	F-Y-A-P-E-L-L-F-F-A-K-R-Y-K-A
B4	K-L-V-N-E-V-T-E-F-A-K-T-C-V-A	C29	A-P-E-L-L-F-F-A-K-R-Y-K-A-A-F
B5	V-N-E-V-T-E-F-A-K-T-C-V-A-D-E	C30	E-L-L-F-F-A-K-R-Y-K-A-A-F-T-E
B6	E-V-T-E-F-A-K-T-C-V-A-D-E-S-A	D1	L-F-F-A-K-R-Y-K-A-A-F-T-E-C-C
B7	T-E-F-A-K-T-C-V-A-D-E-S-A-E-N	D2	F-A-K-R-Y-K-A-A-F-T-E-C-C-Q-A
B8	F-A-K-T-C-V-A-D-E-S-A-E-N-C-D	D3	K-R-Y-K-A-A-F-T-E-C-C-Q-A-A-D
B9	K-T-C-V-A-D-E-S-A-E-N-C-D-K-S	D4	Y-K-A-A-F-T-E-C-C-Q-A-A-D-K-A
B10	C-V-A-D-E-S-A-E-N-C-D-K-S-L-H	D5	A-A-F-T-E-C-C-Q-A-A-D-K-A-A-C
B11	A-D-E-S-A-E-N-C-D-K-S-L-H-T-L	D6	F-T-E-C-C-Q-A-A-D-K-A-A-C-L-L
B12	E-S-A-E-N-C-D-K-S-L-H-T-L-F-G	D7	E-C-C-Q-A-A-D-K-A-A-C-L-L-P-K
B13	A-E-N-C-D-K-S-L-H-T-L-F-G-D-K	D8	C-Q-A-A-D-K-A-A-C-L-L-P-K-L-D
B14	N-C-D-K-S-L-H-T-L-F-G-D-K-L-C	D9	A-A-D-K-A-A-C-L-L-P-K-L-D-E-L
B15	D-K-S-L-H-T-L-F-G-D-K-L-C-T-V	D10	D-K-A-A-C-L-L-P-K-L-D-E-L-R-D
B16	S-L-H-T-L-F-G-D-K-L-C-T-V-A-T	D11	A-A-C-L-L-P-K-L-D-E-L-R-D-E-G
B17	H-T-L-F-G-D-K-L-C-T-V-A-T-L-R	D12	C-L-L-P-K-L-D-E-L-R-D-E-G-K-A
B18	L-F-G-D-K-L-C-T-V-A-T-L-R-E-T	D13	L-P-K-L-D-E-L-R-D-E-G-K-A-S-S
B19	G-D-K-L-C-T-V-A-T-L-R-E-T-Y-G	D14	K-L-D-E-L-R-D-E-G-K-A-S-S-A-K
B20	K-L-C-T-V-A-T-L-R-E-T-Y-G-E-M	D15	D-E-L-R-D-E-G-K-A-S-S-A-K-Q-R
B21	C-T-V-A-T-L-R-E-T-Y-G-E-M-A-D	D16	L-R-D-E-G-K-A-S-S-A-K-Q-R-L-K
B22	V-A-T-L-R-E-T-Y-G-E-M-A-D-C-C	D17	D-E-G-K-A-S-S-A-K-Q-R-L-K-C-A
B23	T-L-R-E-T-Y-G-E-M-A-D-C-C-A-K	D18	G-K-A-S-S-A-K-Q-R-L-K-C-A-S-L
B24	R-E-T-Y-G-E-M-A-D-C-C-A-K-Q-E	D19	A-S-S-A-K-Q-R-L-K-C-A-S-L-Q-K
B25	T-Y-G-E-M-A-D-C-C-A-K-Q-E-P-E	D20	S-A-K-Q-R-L-K-C-A-S-L-Q-K-F-G

Positional Reference	Peptide sequence	Positional Reference	Peptide sequence
D21	K-Q-R-L-K-C-A-S-L-Q-K-F-G-E-R	F16	L-A-A-D-F-V-E-S-K-D-V-C-K-N-Y
D22	R-L-K-C-A-S-L-Q-K-F-G-E-R-A-F	F17	A-D-F-V-E-S-K-D-V-C-K-N-Y-A-E
D23	K-C-A-S-L-Q-K-F-G-E-R-A-F-K-A	F18	F-V-E-S-K-D-V-C-K-N-Y-A-E-A-K
D24	A-S-L-Q-K-F-G-E-R-A-F-K-A-W-A	F19	E-S-K-D-V-C-K-N-Y-A-E-A-K-D-V
D25	L-Q-K-F-G-E-R-A-F-K-A-W-A-V-A	F20	K-D-V-C-K-N-Y-A-E-A-K-D-V-F-L
D26	K-F-G-E-R-A-F-K-A-W-A-V-A-R-L	F21	V-C-K-N-Y-A-E-A-K-D-V-F-L-G-M
D27	G-E-R-A-F-K-A-W-A-V-A-R-L-S-Q	F22	K-N-Y-A-E-A-K-D-V-F-L-G-M-F-L
D28	R-A-F-K-A-W-A-V-A-R-L-S-Q-R-F	F23	Y-A-E-A-K-D-V-F-L-G-M-F-L-Y-E
D29	F-K-A-W-A-V-A-R-L-S-Q-R-F-P-K	F24	E-A-K-D-V-F-L-G-M-F-L-Y-E-Y-A
D30	A-W-A-V-A-R-L-S-Q-R-F-P-K-A-E	F25	K-D-V-F-L-G-M-F-L-Y-E-Y-A-R-R
E1	A-V-A-R-L-S-Q-R-F-P-K-A-E-F-A	F26	V-F-L-G-M-F-L-Y-E-Y-A-R-R-H-P
E2	A-R-L-S-Q-R-F-P-K-A-E-F-A-E-V	F27	L-G-M-F-L-Y-E-Y-A-R-R-H-P-D-Y
E3	L-S-Q-R-F-P-K-A-E-F-A-E-V-S-K	F28	M-F-L-Y-E-Y-A-R-R-H-P-D-Y-S-V
E4	Q-R-F-P-K-A-E-F-A-E-V-S-K-L-V	F29	L-Y-E-Y-A-R-R-H-P-D-Y-S-V-V-L
E5	F-P-K-A-E-F-A-E-V-S-K-L-V-T-D	F30	E-Y-A-R-R-H-P-D-Y-S-V-V-L-L-L
E6	K-A-E-F-A-E-V-S-K-L-V-T-D-L-T	G1	A-R-R-H-P-D-Y-S-V-V-L-L-L-R-L
E7	E-F-A-E-V-S-K-L-V-T-D-L-T-K-V	G2	R-H-P-D-Y-S-V-V-L-L-L-R-L-A-K
E8	A-E-V-S-K-L-V-T-D-L-T-K-V-H-T	G3	P-D-Y-S-V-V-L-L-L-R-L-A-K-T-Y
E9	V-S-K-L-V-T-D-L-T-K-V-H-T-E-C	G4	Y-S-V-V-L-L-L-R-L-A-K-T-Y-E-T
E10	K-L-V-T-D-L-T-K-V-H-T-E-C-C-H	G5	V-V-L-L-L-R-L-A-K-T-Y-E-T-T-L
E11	V-T-D-L-T-K-V-H-T-E-C-C-H-G-D	G6	L-L-L-R-L-A-K-T-Y-E-T-T-L-E-K
E12	D-L-T-K-V-H-T-E-C-C-H-G-D-L-L	G7	L-R-L-A-K-T-Y-E-T-T-L-E-K-C-C
E13	T-K-V-H-T-E-C-C-H-G-D-L-L-E-C	G8	L-A-K-T-Y-E-T-T-L-E-K-C-C-A-A
E14	V-H-T-E-C-C-H-G-D-L-L-E-C-A-D	G9	K-T-Y-E-T-T-L-E-K-C-C-A-A-A-D
E15	T-E-C-C-H-G-D-L-L-E-C-A-D-D-R	G10	Y-E-T-T-L-E-K-C-C-A-A-A-D-P-H
E16	C-C-H-G-D-L-L-E-C-A-D-D-R-A-D	G11	T-T-L-E-K-C-C-A-A-A-D-P-H-E-C
E17	H-G-D-L-L-E-C-A-D-D-R-A-D-L-A	G12	L-E-K-C-C-A-A-A-D-P-H-E-C-Y-A
E18	D-L-L-E-C-A-D-D-R-A-D-L-A-K-Y	G13	K-C-C-A-A-A-D-P-H-E-C-Y-A-K-V
E19	L-E-C-A-D-D-R-A-D-L-A-K-Y-I-C	G14	C-A-A-A-D-P-H-E-C-Y-A-K-V-F-D
E20	C-A-D-D-R-A-D-L-A-K-Y-I-C-E-N	G15	A-A-D-P-H-E-C-Y-A-K-V-F-D-E-F
E21	D-D-R-A-D-L-A-K-Y-I-C-E-N-Q-D	G16	D-P-H-E-C-Y-A-K-V-F-D-E-F-K-P
E22	R-A-D-L-A-K-Y-I-C-E-N-Q-D-S-I	G17	H-E-C-Y-A-K-V-F-D-E-F-K-P-L-V
E23	D-L-A-K-Y-I-C-E-N-Q-D-S-I-S-S	G18	C-Y-A-K-V-F-D-E-F-K-P-L-V-E-E
E24	A-K-Y-I-C-E-N-Q-D-S-I-S-S-K-L	G19	A-K-V-F-D-E-F-K-P-L-V-E-E-P-Q
E25	Y-I-C-E-N-Q-D-S-I-S-S-K-L-K-E	G20	V-F-D-E-F-K-P-L-V-E-E-P-Q-N-L
E26	C-E-N-Q-D-S-I-S-S-K-L-K-E-C-C	G21	D-E-F-K-P-L-V-E-E-P-Q-N-L-I-K
E27	N-Q-D-S-I-S-S-K-L-K-E-C-C-E-K	G22	F-K-P-L-V-E-E-P-Q-N-L-I-K-Q-N
E28	D-S-I-S-S-K-L-K-E-C-C-E-K-P-L	G23	P-L-V-E-E-P-Q-N-L-I-K-Q-N-C-E
E29	I-S-S-K-L-K-E-C-C-E-K-P-L-L-E	G24	V-E-E-P-Q-N-L-I-K-Q-N-C-E-L-F
E30	S-K-L-K-E-C-C-E-K-P-L-L-E-K-S	G25	E-P-Q-N-L-I-K-Q-N-C-E-L-F-E-Q
F1	L-K-E-C-C-E-K-P-L-L-E-K-S-H-C	G26	Q-N-L-I-K-Q-N-C-E-L-F-E-Q-L-G
F2	E-C-C-E-K-P-L-L-E-K-S-H-C-I-A	G27	L-I-K-Q-N-C-E-L-F-E-Q-L-G-E-Y
F3	C-E-K-P-L-L-E-K-S-H-C-I-A-E-V	G28	K-Q-N-C-E-L-F-E-Q-L-G-E-Y-K-F
F4	K-P-L-L-E-K-S-H-C-I-A-E-V-E-N	G29	N-C-E-L-F-E-Q-L-G-E-Y-K-F-Q-N
F5	L-L-E-K-S-H-C-I-A-E-V-E-N-D-E	G30	E-L-F-E-Q-L-G-E-Y-K-F-Q-N-A-L
F6	E-K-S-H-C-I-A-E-V-E-N-D-E-M-P	H1	F-E-Q-L-G-E-Y-K-F-Q-N-A-L-L-V
F7	S-H-C-I-A-E-V-E-N-D-E-M-P-A-D	H2	Q-L-G-E-Y-K-F-Q-N-A-L-L-V-R-Y
F8	C-I-A-E-V-E-N-D-E-M-P-A-D-L-P	H3	G-E-Y-K-F-Q-N-A-L-L-V-R-Y-T-K
F9	A-E-V-E-N-D-E-M-P-A-D-L-P-S-L	H4	Y-K-F-Q-N-A-L-L-V-R-Y-T-K-K-V
F10	V-E-N-D-E-M-P-A-D-L-P-S-L-A-A	H5	F-Q-N-A-L-L-V-R-Y-T-K-K-V-P-Q
F11	N-D-E-M-P-A-D-L-P-S-L-A-A-D-F	H6	N-A-L-L-V-R-Y-T-K-K-V-P-Q-V-S
F12	E-M-P-A-D-L-P-S-L-A-A-D-F-V-E	H7	L-L-V-R-Y-T-K-K-V-P-Q-V-S-T-P
F13	P-A-D-L-P-S-L-A-A-D-F-V-E-S-K	H8	V-R-Y-T-K-K-V-P-Q-V-S-T-P-T-L
F14	D-L-P-S-L-A-A-D-F-V-E-S-K-D-V	H9	Y-T-K-K-V-P-Q-V-S-T-P-T-L-V-E
F15	P-S-L-A-A-D-F-V-E-S-K-D-V-C-K	H10	K-K-V-P-Q-V-S-T-P-T-L-V-E-V-S

Positional Reference	Peptide sequence	Positional Reference	Peptide sequence
H11	V-P-Q-V-S-T-P-T-L-V-E-V-S-R-N	J6	K-Q-T-A-L-V-E-L-V-K-H-K-P-K-A
H12	Q-V-S-T-P-T-L-V-E-V-S-R-N-L-G	J7	T-A-L-V-E-L-V-K-H-K-P-K-A-T-K

H13	S-T-P-T-L-V-E-V-S-R-N-L-G-K-V	J8	L-V-E-L-V-K-H-K-P-K-A-T-K-E-Q
H14	P-T-L-V-E-V-S-R-N-L-G-K-V-G-S	J9	E-L-V-K-H-K-P-K-A-T-K-E-Q-L-K
H15	L-V-E-V-S-R-N-L-G-K-V-G-S-K-C	J10	V-K-H-K-P-K-A-T-K-E-Q-L-K-A-V
H16	E-V-S-R-N-L-G-K-V-G-S-K-C-C-K	J11	H-K-P-K-A-T-K-E-Q-L-K-A-V-M-D
H17	S-R-N-L-G-K-V-G-S-K-C-C-K-H-P	J12	P-K-A-T-K-E-Q-L-K-A-V-M-D-D-F
H18	N-L-G-K-V-G-S-K-C-C-K-H-P-E-A	J13	A-T-K-E-Q-L-K-A-V-M-D-D-F-A-A
H19	G-K-V-G-S-K-C-C-K-H-P-E-A-K-R	J14	K-E-Q-L-K-A-V-M-D-D-F-A-A-F-V
H20	V-G-S-K-C-C-K-H-P-E-A-K-R-M-P	J15	Q-L-K-A-V-M-D-D-F-A-A-F-V-E-K
H21	S-K-C-C-K-H-P-E-A-K-R-M-P-C-A	J16	K-A-V-M-D-D-F-A-A-F-V-E-K-C-C
H22	C-C-K-H-P-E-A-K-R-M-P-C-A-E-D	J17	V-M-D-D-F-A-A-F-V-E-K-C-C-K-A
H23	K-H-P-E-A-K-R-M-P-C-A-E-D-Y-L	J18	D-D-F-A-A-F-V-E-K-C-C-K-A-D-D
H24	P-E-A-K-R-M-P-C-A-E-D-Y-L-S-V	J19	F-A-A-F-V-E-K-C-C-K-A-D-D-K-E
H25	A-K-R-M-P-C-A-E-D-Y-L-S-V-V-L	J20	A-F-V-E-K-C-C-K-A-D-D-K-E-T-C
H26	R-M-P-C-A-E-D-Y-L-S-V-V-L-N-Q	J21	V-E-K-C-C-K-A-D-D-K-E-T-C-F-A
H27	P-C-A-E-D-Y-L-S-V-V-L-N-Q-L-C	J22	K-C-C-K-A-D-D-K-E-T-C-F-A-E-E
H28	A-E-D-Y-L-S-V-V-L-N-Q-L-C-V-L	J23	C-K-A-D-D-K-E-T-C-F-A-E-E-G-K
H29	D-Y-L-S-V-V-L-N-Q-L-C-V-L-H-E	J24	A-D-D-K-E-T-C-F-A-E-E-G-K-K-L
H30	L-S-V-V-L-N-Q-L-C-V-L-H-E-K-T	J25	D-K-E-T-C-F-A-E-E-G-K-K-L-V-A
I1	V-V-L-N-Q-L-C-V-L-H-E-K-T-P-V	J26	E-T-C-F-A-E-E-G-K-K-L-V-A-A-S
I2	L-N-Q-L-C-V-L-H-E-K-T-P-V-S-D	J27	C-F-A-E-E-G-K-K-L-V-A-A-S-Q-A
I3	Q-L-C-V-L-H-E-K-T-P-V-S-D-R-V	J28	A-E-E-G-K-K-L-V-A-A-S-Q-A-A-L
I4	C-V-L-H-E-K-T-P-V-S-D-R-V-T-K	J29	E-G-K-K-L-V-A-A-S-Q-A-A-L-G-L
I5	L-H-E-K-T-P-V-S-D-R-V-T-K-C-C	J30	Blank
I6	E-K-T-P-V-S-D-R-V-T-K-C-C-T-E		
I7	T-P-V-S-D-R-V-T-K-C-C-T-E-S-L		
I8	V-S-D-R-V-T-K-C-C-T-E-S-L-V-N		
I9	D-R-V-T-K-C-C-T-E-S-L-V-N-R-R		
I10	V-T-K-C-C-T-E-S-L-V-N-R-R-P-C		
I11	K-C-C-T-E-S-L-V-N-R-R-P-C-F-S		
I12	C-T-E-S-L-V-N-R-R-P-C-F-S-A-L		
I13	E-S-L-V-N-R-R-P-C-F-S-A-L-E-V		
I14	L-V-N-R-R-P-C-F-S-A-L-E-V-D-E		
I15	N-R-R-P-C-F-S-A-L-E-V-D-E-T-Y		
I16	R-P-C-F-S-A-L-E-V-D-E-T-Y-V-P		
I17	C-F-S-A-L-E-V-D-E-T-Y-V-P-K-E		
I18	S-A-L-E-V-D-E-T-Y-V-P-K-E-F-N		
I19	L-E-V-D-E-T-Y-V-P-K-E-F-N-A-E		
I20	V-D-E-T-Y-V-P-K-E-F-N-A-E-T-F		
I21	E-T-Y-V-P-K-E-F-N-A-E-T-F-T-F		
I22	Y-V-P-K-E-F-N-A-E-T-F-T-F-H-A		
I23	P-K-E-F-N-A-E-T-F-T-F-H-A-D-I		
I24	E-F-N-A-E-T-F-T-F-H-A-D-I-C-T		
I25	N-A-E-T-F-T-F-H-A-D-I-C-T-L-S		
I26	E-T-F-T-F-H-A-D-I-C-T-L-S-E-K		
I27	F-T-F-H-A-D-I-C-T-L-S-E-K-E-R		
I28	F-H-A-D-I-C-T-L-S-E-K-E-R-Q-I		
I29	A-D-I-C-T-L-S-E-K-E-R-Q-I-K-K		
I30	I-C-T-L-S-E-K-E-R-Q-I-K-K-Q-T		
J1	T-L-S-E-K-E-R-Q-I-K-K-Q-T-A-L		
J2	S-E-K-E-R-Q-I-K-K-Q-T-A-L-V-E		
J3	K-E-R-Q-I-K-K-Q-T-A-L-V-E-L-V		
J4	R-Q-I-K-K-Q-T-A-L-V-E-L-V-K-H		
J5	I-K-K-Q-T-A-L-V-E-L-V-K-H-K-P		

Appendix 6. List of the ovalbumin (UniProt ID: P01012) 15-mer peptides synthesized on the arrays.

	Peptide sequence	Positional Reference	Peptide sequence
A1	Blank	B26	E-E-R-Y-P-I-L-P-E-Y-L-Q-C-V-K
A2	M-G-S-I-G-A-A-S-M-E-F-C-F-D-V	B27	R-Y-P-I-L-P-E-Y-L-Q-C-V-K-E-L
A3	S-I-G-A-A-S-M-E-F-C-F-D-V-F-K	B28	P-I-L-P-E-Y-L-Q-C-V-K-E-L-Y-R
A4	G-A-A-S-M-E-F-C-F-D-V-F-K-E-L	B29	L-P-E-Y-L-Q-C-V-K-E-L-Y-R-G-G
A5	A-S-M-E-F-C-F-D-V-F-K-E-L-K-V	B30	E-Y-L-Q-C-V-K-E-L-Y-R-G-G-L-E
A6	M-E-F-C-F-D-V-F-K-E-L-K-V-H-H	C1	L-Q-C-V-K-E-L-Y-R-G-G-L-E-P-I
A7	F-C-F-D-V-F-K-E-L-K-V-H-H-A-N	C2	C-V-K-E-L-Y-R-G-G-L-E-P-I-N-F
A8	F-D-V-F-K-E-L-K-V-H-H-A-N-E-N	C3	K-E-L-Y-R-G-G-L-E-P-I-N-F-Q-T
A9	V-F-K-E-L-K-V-H-H-A-N-E-N-I-F	C4	L-Y-R-G-G-L-E-P-I-N-F-Q-T-A-A
A10	K-E-L-K-V-H-H-A-N-E-N-I-F-Y-C	C5	R-G-G-L-E-P-I-N-F-Q-T-A-A-D-Q
A11	L-K-V-H-H-A-N-E-N-I-F-Y-C-P-I	C6	G-L-E-P-I-N-F-Q-T-A-A-D-Q-A-R
A12	V-H-H-A-N-E-N-I-F-Y-C-P-I-A-I	C7	E-P-I-N-F-Q-T-A-A-D-Q-A-R-E-L
A13	H-A-N-E-N-I-F-Y-C-P-I-A-I-M-S	C8	I-N-F-Q-T-A-A-D-Q-A-R-E-L-I-N
A14	N-E-N-I-F-Y-C-P-I-A-I-M-S-A-L	C9	F-Q-T-A-A-D-Q-A-R-E-L-I-N-S-W
A15	N-I-F-Y-C-P-I-A-I-M-S-A-L-A-M	C10	T-A-A-D-Q-A-R-E-L-I-N-S-W-V-E
A16	F-Y-C-P-I-A-I-M-S-A-L-A-M-V-Y	C11	A-D-Q-A-R-E-L-I-N-S-W-V-E-S-Q
A17	C-P-I-A-I-M-S-A-L-A-M-V-Y-L-G	C12	Q-A-R-E-L-I-N-S-W-V-E-S-Q-T-N
A18	I-A-I-M-S-A-L-A-M-V-Y-L-G-A-K	C13	R-E-L-I-N-S-W-V-E-S-Q-T-N-G-I
A19	I-M-S-A-L-A-M-V-Y-L-G-A-K-D-S	C14	L-I-N-S-W-V-E-S-Q-T-N-G-I-I-R
A20	S-A-L-A-M-V-Y-L-G-A-K-D-S-T-R	C15	N-S-W-V-E-S-Q-T-N-G-I-I-R-N-V
A21	L-A-M-V-Y-L-G-A-K-D-S-T-R-T-Q	C16	W-V-E-S-Q-T-N-G-I-I-R-N-V-L-Q
A22	M-V-Y-L-G-A-K-D-S-T-R-T-Q-I-N	C17	E-S-Q-T-N-G-I-I-R-N-V-L-Q-P-S
A23	Y-L-G-A-K-D-S-T-R-T-Q-I-N-K-V	C18	Q-T-N-G-I-I-R-N-V-L-Q-P-S-S-V
A24	G-A-K-D-S-T-R-T-Q-I-N-K-V-V-R	C19	N-G-I-I-R-N-V-L-Q-P-S-S-V-D-S
A25	K-D-S-T-R-T-Q-I-N-K-V-V-R-F-D	C20	I-I-R-N-V-L-Q-P-S-S-V-D-S-Q-T
A26	S-T-R-T-Q-I-N-K-V-V-R-F-D-K-L	C21	R-N-V-L-Q-P-S-S-V-D-S-Q-T-A-M
A27	R-T-Q-I-N-K-V-V-R-F-D-K-L-P-G	C22	V-L-Q-P-S-S-V-D-S-Q-T-A-M-V-L
A28	Q-I-N-K-V-V-R-F-D-K-L-P-G-F-G	C23	Q-P-S-S-V-D-S-Q-T-A-M-V-L-V-N
A29	N-K-V-V-R-F-D-K-L-P-G-F-G-D-S	C24	S-S-V-D-S-Q-T-A-M-V-L-V-N-A-I
A30	V-V-R-F-D-K-L-P-G-F-G-D-S-I-E	C25	V-D-S-Q-T-A-M-V-L-V-N-A-I-V-F
B1	R-F-D-K-L-P-G-F-G-D-S-I-E-A-Q	C26	S-Q-T-A-M-V-L-V-N-A-I-V-F-K-G
B2	D-K-L-P-G-F-G-D-S-I-E-A-Q-C-G	C27	T-A-M-V-L-V-N-A-I-V-F-K-G-L-W
B3	L-P-G-F-G-D-S-I-E-A-Q-C-G-T-S	C28	M-V-L-V-N-A-I-V-F-K-G-L-W-E-K
B4	G-F-G-D-S-I-E-A-Q-C-G-T-S-V-N	C29	L-V-N-A-I-V-F-K-G-L-W-E-K-A-F
B5	G-D-S-I-E-A-Q-C-G-T-S-V-N-V-H	C30	N-A-I-V-F-K-G-L-W-E-K-A-F-K-D
B6	S-I-E-A-Q-C-G-T-S-V-N-V-H-S-S	D1	I-V-F-K-G-L-W-E-K-A-F-K-D-E-D
B7	E-A-Q-C-G-T-S-V-N-V-H-S-S-L-R	D2	F-K-G-L-W-E-K-A-F-K-D-E-D-T-Q
B8	Q-C-G-T-S-V-N-V-H-S-S-L-R-D-I	D3	G-L-W-E-K-A-F-K-D-E-D-T-Q-A-M
B9	G-T-S-V-N-V-H-S-S-L-R-D-I-L-N	D4	W-E-K-A-F-K-D-E-D-T-Q-A-M-P-F
B10	S-V-N-V-H-S-S-L-R-D-I-L-N-Q-I	D5	K-A-F-K-D-E-D-T-Q-A-M-P-F-R-V
B11	N-V-H-S-S-L-R-D-I-L-N-Q-I-T-K	D6	F-K-D-E-D-T-Q-A-M-P-F-R-V-T-E
B12	H-S-S-L-R-D-I-L-N-Q-I-T-K-P-N	D7	D-E-D-T-Q-A-M-P-F-R-V-T-E-Q-E
B13	S-L-R-D-I-L-N-Q-I-T-K-P-N-D-V	D8	D-T-Q-A-M-P-F-R-V-T-E-Q-E-S-K
B14	R-D-I-L-N-Q-I-T-K-P-N-D-V-Y-S	D9	Q-A-M-P-F-R-V-T-E-Q-E-S-K-P-V
B15	I-L-N-Q-I-T-K-P-N-D-V-Y-S-F-S	D10	M-P-F-R-V-T-E-Q-E-S-K-P-V-Q-M
B16	N-Q-I-T-K-P-N-D-V-Y-S-F-S-L-A	D11	F-R-V-T-E-Q-E-S-K-P-V-Q-M-M-Y
B17	I-T-K-P-N-D-V-Y-S-F-S-L-A-S-R	D12	V-T-E-Q-E-S-K-P-V-Q-M-M-Y-Q-I
B18	K-P-N-D-V-Y-S-F-S-L-A-S-R-L-Y	D13	E-Q-E-S-K-P-V-Q-M-M-Y-Q-I-G-L
B19	N-D-V-Y-S-F-S-L-A-S-R-L-Y-A-E	D14	E-S-K-P-V-Q-M-M-Y-Q-I-G-L-F-R
B20	V-Y-S-F-S-L-A-S-R-L-Y-A-E-E-R	D15	K-P-V-Q-M-M-Y-Q-I-G-L-F-R-V-A
B21	S-F-S-L-A-S-R-L-Y-A-E-E-R-Y-P	D16	V-Q-M-M-Y-Q-I-G-L-F-R-V-A-S-M
B22	S-L-A-S-R-L-Y-A-E-E-R-Y-P-I-L	D17	M-M-Y-Q-I-G-L-F-R-V-A-S-M-A-S
B23	A-S-R-L-Y-A-E-E-R-Y-P-I-L-P-E	D18	Y-Q-I-G-L-F-R-V-A-S-M-A-S-E-K
B24	R-L-Y-A-E-E-R-Y-P-I-L-P-E-Y-L	D19	I-G-L-F-R-V-A-S-M-A-S-E-K-M-K
B25	Y-A-E-E-R-Y-P-I-L-P-E-Y-L-Q-C	D20	L-F-R-V-A-S-M-A-S-E-K-M-K-I-L

Positional Reference	Peptide sequence	Positional Reference	Peptide sequence
D21	R-V-A-S-M-A-S-E-K-M-K-I-L-E-L	F16	H-A-A-H-A-E-I-N-E-A-G-R-E-V-V
D22	A-S-M-A-S-E-K-M-K-I-L-E-L-P-F	F17	A-H-A-E-I-N-E-A-G-R-E-V-V-G-S
D23	M-A-S-E-K-M-K-I-L-E-L-P-F-A-S	F18	A-E-I-N-E-A-G-R-E-V-V-G-S-A-E
D24	S-E-K-M-K-I-L-E-L-P-F-A-S-G-T	F19	I-N-E-A-G-R-E-V-V-G-S-A-E-A-G
D25	K-M-K-I-L-E-L-P-F-A-S-G-T-M-S	F20	E-A-G-R-E-V-V-G-S-A-E-A-G-V-D
D26	K-I-L-E-L-P-F-A-S-G-T-M-S-M-L	F21	G-R-E-V-V-G-S-A-E-A-G-V-D-A-A
D27	L-E-L-P-F-A-S-G-T-M-S-M-L-V-L	F22	E-V-V-G-S-A-E-A-G-V-D-A-A-S-V
D28	L-P-F-A-S-G-T-M-S-M-L-V-L-L-P	F23	V-G-S-A-E-A-G-V-D-A-A-S-V-S-E
D29	F-A-S-G-T-M-S-M-L-V-L-L-P-D-E	F24	S-A-E-A-G-V-D-A-A-S-V-S-E-E-F
D30	S-G-T-M-S-M-L-V-L-L-P-D-E-V-S	F25	E-A-G-V-D-A-A-S-V-S-E-E-F-R-A
E1	T-M-S-M-L-V-L-L-P-D-E-V-S-G-L	F26	G-V-D-A-A-S-V-S-E-E-F-R-A-D-H
E2	S-M-L-V-L-L-P-D-E-V-S-G-L-E-Q	F27	D-A-A-S-V-S-E-E-F-R-A-D-H-P-F
E3	L-V-L-L-P-D-E-V-S-G-L-E-Q-L-E	F28	A-S-V-S-E-E-F-R-A-D-H-P-F-L-F
E4	L-L-P-D-E-V-S-G-L-E-Q-L-E-S-I	F29	V-S-E-E-F-R-A-D-H-P-F-L-F-C-I
E5	P-D-E-V-S-G-L-E-Q-L-E-S-I-I-N	F30	E-E-F-R-A-D-H-P-F-L-F-C-I-K-H
E6	E-V-S-G-L-E-Q-L-E-S-I-I-N-F-E	G1	F-R-A-D-H-P-F-L-F-C-I-K-H-I-A
E7	S-G-L-E-Q-L-E-S-I-I-N-F-E-K-L	G2	A-D-H-P-F-L-F-C-I-K-H-I-A-T-N
E8	L-E-Q-L-E-S-I-I-N-F-E-K-L-T-E	G3	H-P-F-L-F-C-I-K-H-I-A-T-N-A-V
E9	Q-L-E-S-I-I-N-F-E-K-L-T-E-W-T	G4	F-L-F-C-I-K-H-I-A-T-N-A-V-L-F
E10	E-S-I-I-N-F-E-K-L-T-E-W-T-S-S	G5	F-C-I-K-H-I-A-T-N-A-V-L-F-F-G
E11	I-I-N-F-E-K-L-T-E-W-T-S-S-N-V	G6	I-K-H-I-A-T-N-A-V-L-F-F-G-R-C
E12	N-F-E-K-L-T-E-W-T-S-S-N-V-M-E	G7	H-I-A-T-N-A-V-L-F-F-G-R-C-V-S
E13	E-K-L-T-E-W-T-S-S-N-V-M-E-E-R	G8	A-T-N-A-V-L-F-F-G-R-C-V-S-P
E14	L-T-E-W-T-S-S-N-V-M-E-E-R-K-I		
E15	E-W-T-S-S-N-V-M-E-E-R-K-I-K-V		
E16	T-S-S-N-V-M-E-E-R-K-I-K-V-Y-L		
E17	S-N-V-M-E-E-R-K-I-K-V-Y-L-P-R		
E18	V-M-E-E-R-K-I-K-V-Y-L-P-R-M-K		
E19	E-E-R-K-I-K-V-Y-L-P-R-M-K-M-E		
E20	R-K-I-K-V-Y-L-P-R-M-K-M-E-E-K		
E21	I-K-V-Y-L-P-R-M-K-M-E-E-K-Y-N		
E22	V-Y-L-P-R-M-K-M-E-E-K-Y-N-L-T		
E23	L-P-R-M-K-M-E-E-K-Y-N-L-T-S-V		
E24	R-M-K-M-E-E-K-Y-N-L-T-S-V-L-M		
E25	K-M-E-E-K-Y-N-L-T-S-V-L-M-A-M		
E26	E-E-K-Y-N-L-T-S-V-L-M-A-M-G-I		
E27	K-Y-N-L-T-S-V-L-M-A-M-G-I-T-D		
E28	N-L-T-S-V-L-M-A-M-G-I-T-D-V-F		
E29	T-S-V-L-M-A-M-G-I-T-D-V-F-S-S		
E30	V-L-M-A-M-G-I-T-D-V-F-S-S-S-A		
F1	M-A-M-G-I-T-D-V-F-S-S-S-A-N-L		
F2	M-G-I-T-D-V-F-S-S-S-A-N-L-S-G		
F3	I-T-D-V-F-S-S-S-A-N-L-S-G-I-S		
F4	D-V-F-S-S-S-A-N-L-S-G-I-S-S-A		
F5	F-S-S-S-A-N-L-S-G-I-S-S-A-E-S		
F6	S-S-A-N-L-S-G-I-S-S-A-E-S-L-K		
F7	A-N-L-S-G-I-S-S-A-E-S-L-K-I-S		
F8	L-S-G-I-S-S-A-E-S-L-K-I-S-Q-A		
F9	G-I-S-S-A-E-S-L-K-I-S-Q-A-V-H		
F10	S-S-A-E-S-L-K-I-S-Q-A-V-H-A-A		
F11	A-E-S-L-K-I-S-Q-A-V-H-A-A-H-A		
F12	S-L-K-I-S-Q-A-V-H-A-A-H-A-E-I		
F13	K-I-S-Q-A-V-H-A-A-H-A-E-I-N-E		
F14	S-Q-A-V-H-A-A-H-A-E-I-N-E-A-G		
F15	A-V-H-A-A-H-A-E-I-N-E-A-G-R-E		

Appendix 7. Usage report for synthesis of peptide ^{365}DPHECYAKVFDEFKPLV^{381} generated by Liberty Pepdriver Software.

Usage Report

Amino acid concentration: 0.2 M

Liberty Methods Included

Method	Quantity
MOL 671	1

Required Reagent Amounts

Reagent	Volume (mL)	Mass (g)
Alanine	3	0.19
Aspartate	6	0.5
Cysteine	3	0.36
Glutamate	6	0.52
Histidine	3	0.29
Leucine	3	0.22
Lysine	6	0.57
Phenylalanine	6	0.47
Proline	6	0.41
Tyrosine	3	0.28
Valine	6	0.41
Main Wash (DMF)	877	824.39
Deprotection (Piperidine)	189	
Activator (HOBt monohydrate)	36	
Activator Base (DIC)	18	

Total waste volume: 1171 mL

Worst-Case (UV) Reagent Amounts

Reagent	Volume (mL)	Mass (g)
Main Wash (DMF)	1236	1161.84
Deprotection (Piperidine)	284	

Total waste volume (worst-case): 1625 mL

Reported: 7/10/2019 9:43:31 AM Page 1 of 1

Appendix 8. Statistical analysis obtained for data depicted in Figure II.14. The two data sets were also represented individually, and their respective ANOVA statistical analysis was performed (A). Statistical analysis for the combined data represented in Figure II.14 was also performed using the Kruskal-Wallis rank sum test (B), and the Dunn test (C).

A

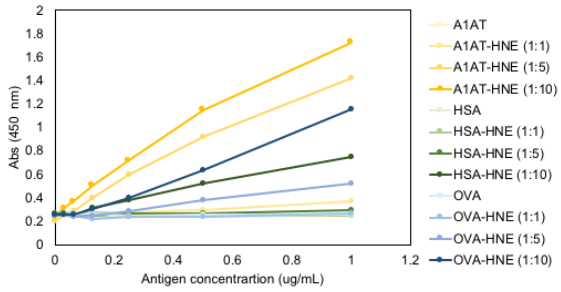

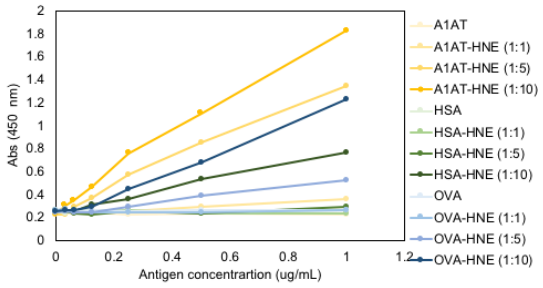

A1AT-HNE 1

Anova: Single Factor

SUMMARY

Groups	Count	Sum	Average	Variance
1:0	7	1.934	0.24175	3.3357E-05
1:1	7	2.482	0.31025	0.01008164
1:5	7	6.086	0.76075	0.42337879
1:10	7	7.459	0.932375	0.62612827

ANOVA

Source of Variation	SS	df	MS	F	P-value	F crit
Between Groups	2.74092209	3	0.9136407	3.44893047	0.02988326	2.94668527
Within Groups	7.41735438	28	0.26490551			
Total	10.1582765	31				

A1AT-HNE 2

Anova: Single Factor

SUMMARY

Groups	Count	Sum	Average	Variance
1:0	7	1.907	0.238375	8.7125E-05
1:1	7	2.375	0.296875	0.00885355
1:5	7	5.748	0.7185	0.35850514
1:10	7	7.305	0.913125	0.58440441

ANOVA

Source of Variati	SS	df	MS	F	P-value	F crit
Between Gro	2.56928084	3	0.85642695	3.59899875	0.02569541	2.94668527
Within Group	6.66295163	28	0.23796256			
Total	9.23223247	31				

HSA-HNE 1

Anova: Single Factor

SUMMARY

Groups	Count	Sum	Average	Variance
1:0	7	2	0.25	4.3714E-05
1:1	7	2.126	0.26575	7.4214E-05
1:5	7	2.271	0.283875	0.00312298
1:10	7	3.71	0.46375	0.0756825

ANOVA

Source of Variation	SS	df	MS	F	P-value	F crit
Between Groups	0.23794434	3	0.07931478	4.01983546	0.01694307	2.94668527
Within Groups	0.55246388	28	0.01973085			
Total	0.79040822	31				

OVA- HNE 1

Anova: Single Factor

SUMMARY

Groups	Count	Sum	Average	Variance
1:0	7	2.033	0.254125	5.0411E-05
1:1	7	2.028	0.2535	0.00069743
1:5	7	2.876	0.3595	0.02709457
1:10	7	4.7609	0.5951125	0.22779376

ANOVA

Source of Variati	SS	df	MS	F	P-value	F crit
Between Gro	0.62165021	3	0.20721674	3.24236963	0.03686452	2.94668527
Within Group	1.78945318	28	0.06390904			
Total	2.4111034	31				

HSA-HNE 2

Anova: Single Factor

SUMMARY

Groups	Count	Sum	Average	Variance
1:0	7	2.039	0.254875	9.8411E-05
1:1	7	2.016	0.252	0.00021286
1:5	7	2.15	0.26875	0.00312993
1:10	7	3.657	0.457125	0.06866527

ANOVA

Source of Variation	SS	df	MS	F	P-value	F crit
Between Groups	0.23789563	3	0.07929854	4.39896991	0.01174479	2.94668527
Within Groups	0.50474525	28	0.01802662			
Total	0.74264088	31				

OVA- HNE 2

Anova: Single Factor

SUMMARY

Groups	Count	Sum	Average	Variance
1:0	7	2.05	0.25625	2.5071E-05
1:1	7	2.073	0.259125	0.0003527
1:5	7	2.866	0.35825	0.02548707
1:10	7	5.025	0.628125	0.26131127

ANOVA

Source of Variati	SS	df	MS	F	P-value	F crit
Between Gro	0.73504513	3	0.24501504	3.41274968	0.03099716	2.94668527
Within Group	2.01023275	28	0.07179403			
Total	2.74527788	31				

B

Protein	*p* value from Kruskal-Wallis test
A1AT vs 1:1 vs 1:5 vs 1:10	0.01535
HSA vs 1:1 vs 1:5 vs 1:10	0.1051
OVA vs 1:1 vs 1:5 vs 1:10	0.02606

C

Comparison <fctr>	Z <dbl>	P.unadj <dbl>
A1AT - A1AT-HNE (1:1)	-1.4924050	0.135593001
A1AT - A1AT-HNE (1:10)	-3.0381102	0.002380669
A1AT-HNE (1:1) - A1AT-HNE (1:10)	-1.5457052	0.122175782
A1AT - A1AT-HNE (1:5)	-2.3985081	0.016462014
A1AT-HNE (1:1) - A1AT-HNE (1:5)	-0.9061030	0.364881314
A1AT-HNE (1:10) - A1AT-HNE (1:5)	0.6396021	0.522431285

Comparison <fctr>	Z <dbl>	P.unadj <dbl>
OVA - OVA-HNE (1:1)	0.4265187	0.669729917
OVA - OVA-HNE (1:10)	-2.3858390	0.017040208
OVA-HNE (1:1) - OVA-HNE (1:10)	-2.8123577	0.004917977
OVA - OVA-HNE (1:5)	-0.8663661	0.386289412
OVA-HNE (1:1) - OVA-HNE (1:5)	-1.2928848	0.196050891
OVA-HNE (1:10) - OVA-HNE (1:5)	1.5194729	0.128643503

Appendix 9. Statistical analysis obtained for data depicted in Figure III.14 A using a Student's t-Test.

t-Test: Paired Two Sample for Means

	KLH (5 ug/mL)	KLH-HNE (5 ug/mL)
Mean	0.36	5.586
Variance	0.005299	0.117883
Observations	3	3
Pearson Correlation	0.892221277	
Hypothesized Mean Difference	0	
df	2	
t Stat	-32.28982791	
P(T<=t) one-tail	0.000478866	
t Critical one-tail	2.91998558	
P(T<=t) two-tail	0.000957733	
t Critical two-tail	4.30265273	

t-Test: Paired Two Sample for Means

	KLH (2.5 ug/mL)	KLH-HNE (2.5 ug/mL)
Mean	0.243833333	5.283333333
Variance	0.001978083	0.052295583
Observations	3	3
Pearson Correlation	0.824218788	
Hypothesized Mean Difference	0	
df	2	
t Stat	-45.0700013	
P(T<=t) one-tail	0.000245966	
t Critical one-tail	2.91998558	
P(T<=t) two-tail	0.000491931	
t Critical two-tail	4.30265273	

t-Test: Paired Two Sample for Means

	KLH (1.25 ug/mL)	KLH-HNE (1.25 ug/mL)
Mean	0.162133333	4.120166667
Variance	0.000927203	0.045735083
Observations	3	3
Pearson Correlation	0.526414118	
Hypothesized Mean Difference	0	
df	2	
t Stat	-34.36086994	
P(T<=t) one-tail	0.000422951	
t Critical one-tail	2.91998558	
P(T<=t) two-tail	0.000845903	
t Critical two-tail	4.30265273	

t-Test: Paired Two Sample for Means

	KLH (0.625 ug/mL)	KLH-HNE (0.625 ug/mL)
Mean	0.104666667	2.062833333
Variance	0.000196333	0.009654083
Observations	3	3
Pearson Correlation	0.966169934	
Hypothesized Mean Difference	0	
df	2	
t Stat	-39.99846444	
P(T<=t) one-tail	0.000312231	
t Critical one-tail	2.91998558	
P(T<=t) two-tail	0.000624463	
t Critical two-tail	4.30265273	

t-Test: Paired Two Sample for Means

	KLH (0.3125 ug/mL)	KLH-HNE (0.3125 ug/mL)
Mean	0.080033333	0.763
Variance	6.40033E-05	0.017932
Observations	3	3
Pearson Correlation	0.99401552	
Hypothesized Mean Difference	0	
df	2	
t Stat	-9.391254874	
P(T<=t) one-tail	0.005574579	
t Critical one-tail	2.91998558	
P(T<=t) two-tail	0.011149159	
t Critical two-tail	4.30265273	

t-Test: Paired Two Sample for Means

	HSA (5 ug/mL)	HSA-HNE (5 ug/mL)
Mean	0.367166667	1.016833333
Variance	0.002002583	0.026261083
Observations	3	3
Pearson Correlation	0.989350348	
Hypothesized Mean Difference	0	
df	2	
t Stat	-9.539376946	
P(T<=t) one-tail	0.005405581	
t Critical one-tail	2.91998558	
P(T<=t) two-tail	0.010811162	
t Critical two-tail	4.30265273	

t-Test: Paired Two Sample for Means

	HSA (2.5 ug/mL)	HSA-HNE (2.5 ug/mL)
Mean	0.1963	0.6575
Variance	0.02217712	0.02604225
Observations	3	3
Pearson Correlation	0.479096595	
Hypothesized Mean Difference	0	
df	2	
t Stat	-5.032906483	
P(T<=t) one-tail	0.018642352	
t Critical one-tail	2.91998558	
P(T<=t) two-tail	0.037284705	
t Critical two-tail	4.30265273	

t-Test: Paired Two Sample for Means

	HSA (1.25 ug/mL)	HSA-HNE (1.25 ug/mL)
Mean	0.178833333	0.373333333
Variance	0.000496083	0.005792333
Observations	3	3
Pearson Correlation	0.99996998	
Hypothesized Mean Difference	0	
df	2	
t Stat	-6.257665014	
P(T<=t) one-tail	0.012299474	
t Critical one-tail	2.91998558	
P(T<=t) two-tail	0.024598948	

t Critical two-tail	4.30265273

t-Test: Paired Two Sample for Means

	HSA (0.625 ug/mL)	HSA-HNE (0.625 ug/mL)
Mean	0.137833333	0.198066667
Variance	0.001396583	0.000992263
Observations	3	3
Pearson Correlation	0.982713729	
Hypothesized Mean Difference	0	
df	2	
t Stat	-12.03357057	
P(T<=t) one-tail	0.003417516	
t Critical one-tail	2.91998558	
P(T<=t) two-tail	0.006835031	
t Critical two-tail	4.30265273	

t-Test: Paired Two Sample for Means

	HSA (0.3125 ug/mL)	HSA-HNE (0.3125 ug/mL)
Mean	0.104	0.138333333
Variance	0.000361	0.000906333
Observations	3	3
Pearson Correlation	0.999122311	
Hypothesized Mean Difference	0	
df	2	
t Stat	-5.333137843	
P(T<=t) one-tail	0.016703489	
t Critical one-tail	2.91998558	
P(T<=t) two-tail	0.033406978	
t Critical two-tail	4.30265273	

t-Test: Paired Two Sample for Means

	OVA (5 ug/mL)	OVA-HNE (5 ug/mL)
Mean	0.340666667	3.027833333
Variance	1.63333E-05	0.002331583
Observations	3	3
Pearson Correlation	-0.648654812	
Hypothesized Mean Difference	0	
df	2	
t Stat	-91.25950269	
P(T<=t) one-tail	6.00255E-05	
t Critical one-tail	2.91998558	
P(T<=t) two-tail	0.000120051	
t Critical two-tail	4.30265273	

t-Test: Paired Two Sample for Means

	OVA (2.5 ug/mL)	OVA-HNE (2.5 ug/mL)
Mean	0.232	2.27735
Variance	0.001227	0.007356468
Observations	3	3
Pearson Correlation	0.353756819	
Hypothesized Mean Difference	0	
df	2	
t Stat	-44.08444511	
P(T<=t) one-tail	0.000257078	
t Critical one-tail	2.91998558	
P(T<=t) two-tail	0.000514155	
t Critical two-tail	4.30265273	

t-Test: Paired Two Sample for Means

	OVA (1.25 ug/mL)	OVA-HNE (1.25 ug/mL)
Mean	0.140166667	1.371
Variance	0.000282583	0.004791
Observations	3	3
Pearson Correlation	-0.444543375	
Hypothesized Mean Difference	0	
df	2	
t Stat	-27.27767809	
P(T<=t) one-tail	0.000670627	
t Critical one-tail	2.91998558	
P(T<=t) two-tail	0.001341253	
t Critical two-tail	4.30265273	

t-Test: Paired Two Sample for Means

	OVA (0.625 ug/mL)	OVA-HNE (0.625 ug/mL)
Mean	0.115833333	0.6255
Variance	5.30833E-05	0.00468525
Observations	3	3
Pearson Correlation	0.820120807	
Hypothesized Mean Difference	0	
df	2	
t Stat	-14.09890423	
P(T<=t) one-tail	0.002496532	
t Critical one-tail	2.91998558	
P(T<=t) two-tail	0.004993063	
t Critical two-tail	4.30265273	

t-Test: Paired Two Sample for Means

	OVA (0.3125 ug/mL)	OVA-HNE (0.3125 ug/mL)
Mean	0.083	0.3725
Variance	0.000028	0.00428025
Observations	3	3
Pearson Correlation	-0.966234496	
Hypothesized Mean Difference	0	
df	2	
t Stat	-7.107460713	
P(T<=t) one-tail	0.009613324	

t Critical one-tail	2.91998558
P(T<=t) two-tail	0.019226649
t Critical two-tail	4.30265273

Appendix 10. Statistical analysis obtained Figure III.14 B.

Anova: Single Factor

SUMMARY

Groups	*Count*	*Sum*	*Average*	*Variance*
HSA	8	0.540167	0.067521	1.89E-05
HSA-HNE	8	5.401167	0.675146	0.101018

ANOVA

Source of Variation	*SS*	*df*	*MS*	*F*	*P-value*	*F crit*
Between Groups	1.476833	1	1.476833	29.23358	9.25E-05	4.60011
Within Groups	0.707257	14	0.050518			
Total	2.18409	15				

Appendix 11. ELISA assay comparing the binding of the anti-HNE Abcam and the Anti-HSA-HNE SA369 antibodies to recombinant HSA expressed in *Saccharomyces cerevisiae* and standard HSA (the same HSA molecule used for immunization).

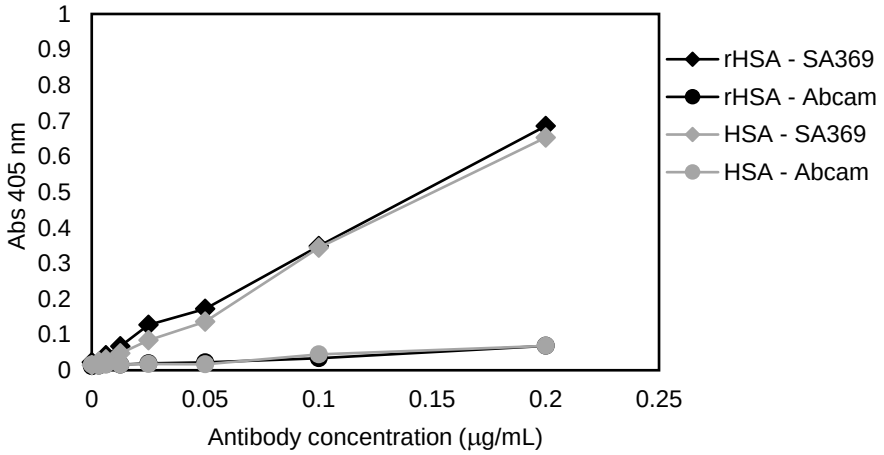

Appendix 12. Schematic representation of the lamination process of the different components of the anti-HNE lateral flow assay. On top of a 30 cm long backing card the nitrocellulose membrane with immobilised capture Ab, the sink pad, the gold conjugate pad and the sample pad were mounted on a plastic backing card, in this specific order, at 20 mm, 0 mm, 43 mm and 55 mm, respectively, counting from the top of the backing card (A). The mounted band is cut in 5 mm strips (B) and gets encased in a plastic cassette (C).

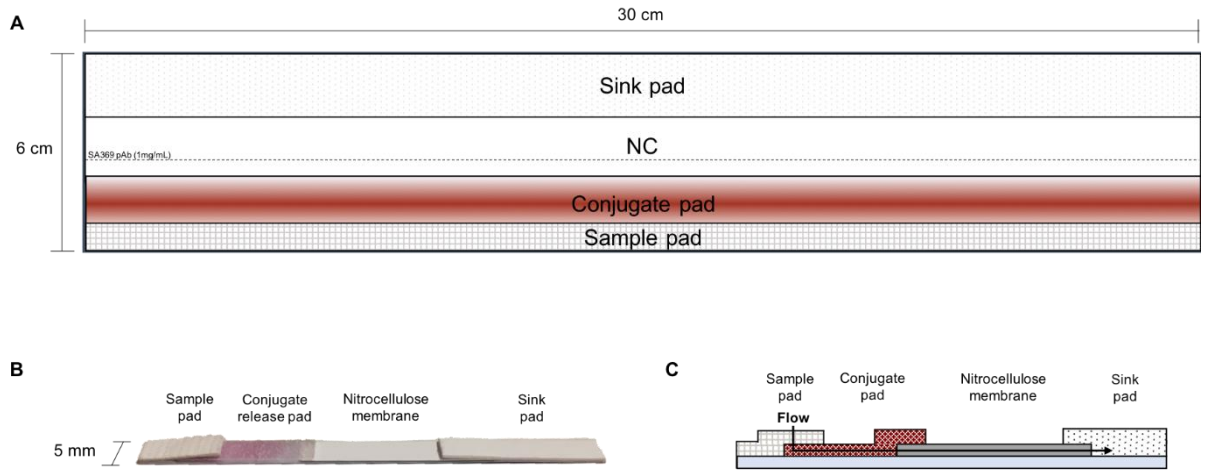

Appendix 13. Flowchart depicting the main followed steps for running and reading a lateral flow assay (LFA). Once all the components of the assay are assembled, each individual strip is encased in a in plastic cassette (A), and only then the sample is applied to the sample pad (B). The liquid will then flow through the conjugate pad, dragging with itself the conjugated reagent to the nitrocellulose membrane (C). For this assay, the device was left for 20 min until all the liquid had been absorbed by the sink pad and the signal of the test line was stable (D). The intensity of the test line was measured using a cube reader which was mounted on top of the cassette (E). This camera reader emits a LED green light within the window area where the test and control lines are shown, which will be reflected back by the gold surface, and measures the absorbance of light (1-transmission). Depending on type of the assay and how many lines exist, the cube can be programmed to integrate the various differences in absorbance seen and calculate their areas (F).

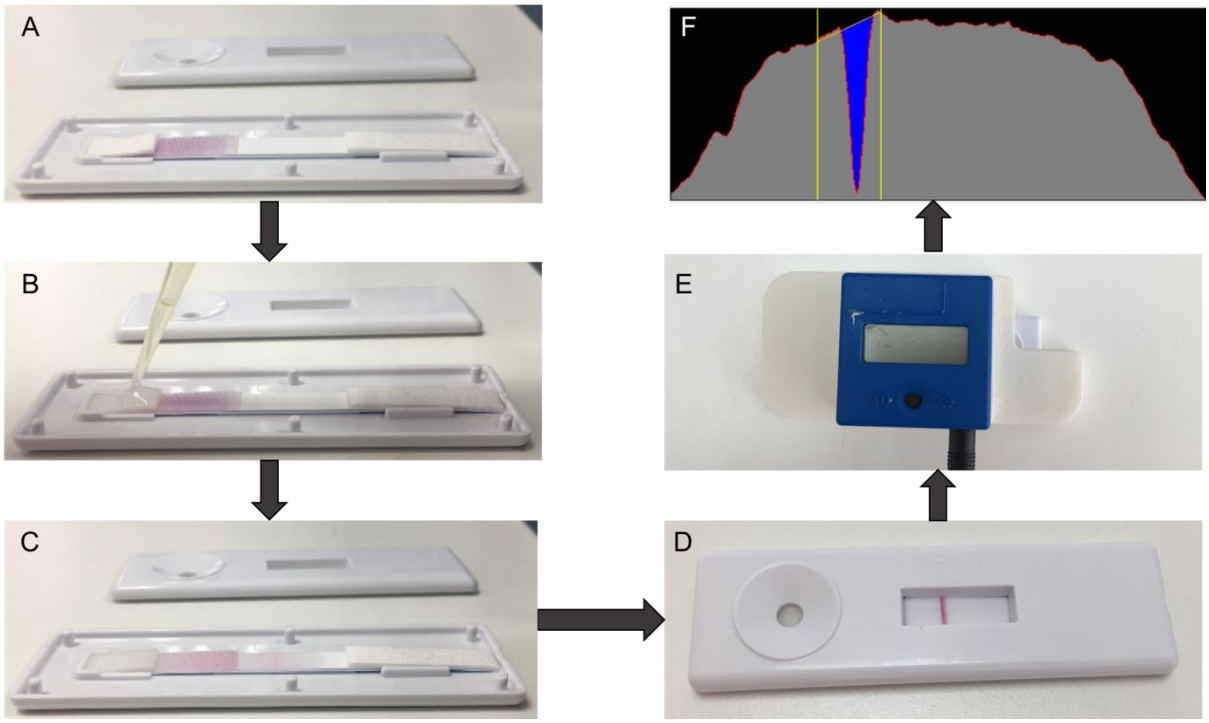

Appendix 14. Sheep Phage Display primers used for construction of the scFv library.

1. Ovine heavy chain constant region 3’ primer.

    (a) OvCHFOR: 5’-GAC TTT CGG GGC TGT GGT GGA GGC-3’.

2. Ovine kappa chain constant region 3’ primer.

    (a) OvCKFOR: 5’-GA TGG TTT GAA GAG GGA GAC GGATGG CTG AGC-3’.

3. Ovine lambda chain constant region 3’ primer.

    (a) OvCLFOR: 5’-A CAG GGT GAC CGAGGG TGC GGA CTT GG-3’.

4. Ovine heavy chain variable region 5’ primers.

    (a) OvVH1BACK: 5’-CAG GTK CRR CTG CAG GRG TCG GG-3’.

    (b) OvVH2BACK: 5’-CAG GTKCAG YTKCAGGAGTCG GG-3’.

    (c) MuVH1BACK: 5’-SAG GTSMARCTGCAGSAGTCW GG-3’.

    (d) Hu4aBACK: 5’-CAG GTG CAG CTG CAG GAG TCG GG-3.

5. Ovine heavy chain variable region 3’ primers.

    (a) OvJH1LINKFOR: 5’-CTC AGA AGG CGC GCC AGA AGA TTT ACC TTC TGA GGA GAC GGT GAC CAG GAG TCC-3’.

    (b) OvJH2LINKFOR: 5’-CTC AGA AGG CGC GCC AGA AGA TTT ACC TTC TGA GGA GRC GGW GAY YAG KAG TCC-3’.

    (c) OvJH3LINKFOR: 5’-CTC AGA AGG CGC GCC AGA AGA TTT ACC TTC TGA GGA GAY RGT RAS CAG GAS TCC-3’.

    (d) OvJH4LINKFOR: 5’-CTC AGA AGG CGC GCC AGA AGA TTT ACC TTC TGA AAG AAC GCT GAT CAG GAG-3’.

6. Ovine lambda chain variable region 5’ primers.

    (a) OvVL1LINKBACK: 5’-AG TCA AAC GCG TCT GGC GAG TCT AAA GTG GAT GAC CAG GCT GTG CTG ACT CAG CCG-3’.

    (b) OvVL2LINKBACK: 5’-AG TCA AAC GCG TCT GGC GAG TCT AAA GTG GAT GAC CAR GCT GTG CTG ACY CAR CYG-3’.

    (c) OvVL3LINKBACK: 5’-AG TCA AAC GCG TCT GGC GAG TCT AAA GTG GAT GAC CAG GCY STG STG ACT CAG CCR-3’.

    (d) OvVL4LINKBACK: 5’-AG TCA AAC GCG TCT GGC GAG TCT AAA GTG GAT GAC MRG GTC RTG CKG ACT CAR CCG-3’.

    (e) OvVL5LINKBACK: 5’-AG TCA AAC GCG TCT GGC GAG TCT AAA GTG GAT GAC CAG KCT GYS CTG ACT CAG CCK-3’.

7. Ovine lambda chain variable region 3’ primers.

(a) OvJL1FOR: 5’-ACC CAG GAC GGT CAG CCT GGT CC-3’.

(b) OvJL2FOR: 5’-ACC CAG GAC GGT CAG YCK RGW CC-3’.

8. Cloning primers (restriction sites underlined).

(a) OvVH1BACK-Sfi:5’-GTC CTC GCA ACT GCG GCC CAG CCG GCC ATG GCC CAG GTKCRRCTG CAG GRG TCG GG-3’.

(b) OvVH2BACK-Sfi:5’-GTC CTC GCA ACT GCG GCC CAG CCG GCC ATG GCC CAG GTKCAG YTKCAG GAG TCG GG-3’.

(c) MuVH1BACK-Sfi:5’-CAT GCC ATG ACT GCG GCC CAG CCG GCC ATG GCC SAG GTS MARCTG CAG SAG TCW GG-3‘.

(d) Hu4aBACK-Sfi:5’-GTC CTC GCA ACT GCG GCC CAG CCG GCC ATG GCC CAG GTG CAG CTG CAG GAG TCG GG-3’.

(e) OvJL1FOR-Not:5’-GAG TCA TTC TCG ACT TGC GGC CGC ACC CAG GAC GGT CAG CCT GGT CC-3’.

(f) OvJL2FOR-Not:5’-GAG TCA TTC TCG ACT TGC GGC CGC ACC CAG GAC GGT CAG YCK RGW CC-3’.

(g) OvJK1FOR-Not:5’-GAG TCA TTC TCG ACT TGC GGC CGC CCG TTT GAT TTC CAC GTT GGT CCC-3’.

(h) OvJK2FOR-Not:5’-GAG TCA TTC TCG ACT TGC GGC CGC CCT TTT GAT CTC TAG TTT GGT TCC-3’.

(i) OvJK3FOR-Not:5’-GAG TCA TTC TCG ACT TGC GGC CGC CCT TTT GAT CTC TAC CTT GGT TCC-3’.

Appendix 15. pSFD vector used for the construction of the SA369 scFV fragment. The fragments in between the restriction sites for enzymes NcoI and NotI were removes and substituted by the V_H-V_λ fragment.

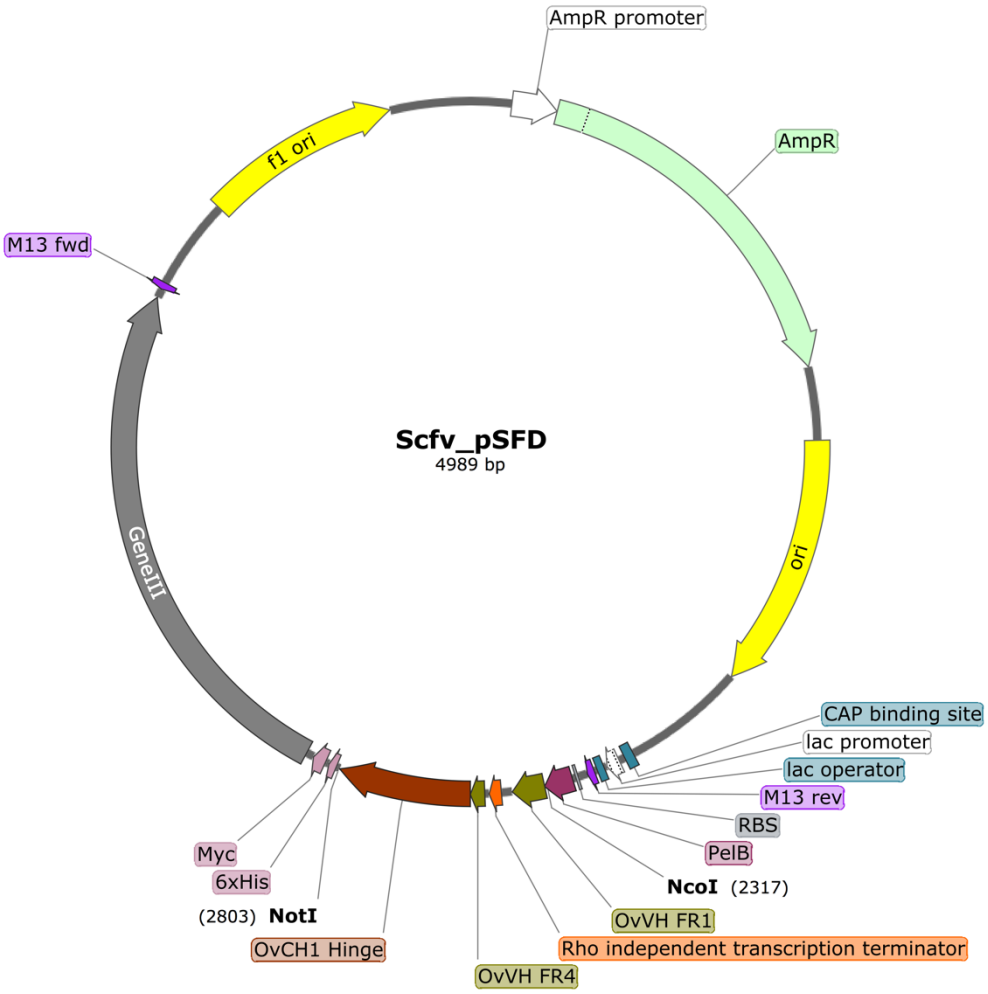

Appendix 16. List of publications

Published articles

- Campos-Pinto, I. *et al.* (2019) 'Epitope mapping and characterization of 4-hydroxy-2-nonenal modified-human serum albumin using two different polyclonal antibodies ⋆', *Free Radical Biology and Medicine*. Elsevier B.V., (March), pp. 1–11. doi: 10.1016/j.freeradbiomed.2019.05.008.

Aston University

Pages removed for copyright restrictions.